Radiobiological Modelling of Non-Small-Cell Lung Cancer: A Tumour Control Probability Perspective

By
Mohammed Ali Alaswad

A thesis submitted in partial fulfilment for the degree of Doctor of Philosophy

Medical Physics Research Cluster
School of Physics
College of Science

Academic supervisors
Dr. Christoph Kleefeld
Dr. Mark Foley

February, 2021

This thesis is dedicated to my lovely parents for the endless support and encouragement.

Abstract

Radiobiology has developed a methodology to evaluate the radiation response of a wide spectrum of cell lines, which can be used to validate a radiation response using mathematical models. The fundamental motivation for this thesis was to examine the ability of a mechanistic TCP model to predict treatment outcomes for a wide range of treatment strategies for NSCLC, such as hypofractionation, standard fractionation, and hyperfractionation. A fully heterogeneous population TCP model based on the linear-quadratic (LQ) cell survival concept combined with the Poisson statistic was established to predict local tumour control after one, two and three years. The TCP model was created using data from 25 publications. The TCP model was fitted to the clinical outcome data using optimised radiosensitivity values produced by the Nelder–Mead simplex algorithm. The statistical analysis for early-stage NSCLC resulted in R^2 values of 0.96, 0.96 and 0.97 and wRMSE values of 3.9%, 5.2% and 5.9% for one-, two- and three-year local tumour control rates, respectively. Based on variations in the TCP with the clonogenic density model, it was estimated that 60% of the dose was sufficient to maintain the TCP after two years for areas with lower clonogenic cell density. The predicted TCP for the T1a vs T1b group after applying 2 Gy in 30 fractions was 48% ± 1.09% vs 43% ± 1.05% according to the 7^{th} edition, and 51.5% ± 0.80% vs 47.8% ± 0.85% according to the 8^{th} edition. Furthermore, the TCP model outcomes for the radiochemotherapy arm exhibited superior TCPs than the radiotherapy alone arm. For the radiochemotherapy arm, TCPs were as high as 75.5%, 50.6% and 41.4% at one-, two- and three-year local tumour control rates, respectively. In contrast to the radiotherapy alone arm results, the model yielded low TCPs values: 51.8%, 38.1% and 33.2% at one-, two- and three-year local tumour control rates, respectively. An important finding of this research is that the T distribution schema of the 7^{th} edition was slightly inferior to that of the 8^{th} edition in terms of specifying the adjacent T subcategories. For instance, the statistical analysis for 3D-CRT resulted in R^2 values of 0.89, 0.95 and 0.93 for the 7^{th} edition and R^2 values of 0.93, 0.95 and 0.94 for the 8^{th} edition. This thesis concludes that the TCP model is appropriate for the analysis and evaluation of radiotherapy treatment plans as well as radiochemotherapy plans.

Contents

List of Figures

List of Tables

Declaration of Authorship

I, Mohammed Ali Alaswad, declare that the research exhibited in this thesis is entirely my own work, and that I have practiced appropriate precautions to ensure that the work is original and does not, to the best of my knowledge, breach any law of copyright and has not been taken from other people's work. In addition, this thesis has not been submitted in whole or in part for any professional qualification or another academic degree. Appropriate credit has been provided where reference is made to others' work.

Signed: **Mohammed Alaswad**

Date: 22/02/2021

Acknowledgment

In an analogy to the traditional African proverb, ‘It takes a village to raise a child’, it also takes an ad-hoc team of supportive and thought-provoking fellow members to facilitate PhD progress, and hence fulfilment of the degree. Thus, this research would have been impossible without the encouragement and advice of numerous individuals who contributed and extended their valuable assistance in the attainment of this thesis.

First, I would like to express my sincere appreciation and gratitude to my supervisors Dr Christoph Kleefeld and Dr Mark Foley for their motivation, patience, enthusiasm and immense knowledge. Their mastery of the smallest details afforded me invaluable supervision and assistance, without which I never would have reached this stage. It has been a great honour and privilege to work with Dr Christoph Kleefeld who always keep the door open and eagerly offer me endless support, valuable advice and a degree of flexibility that I profoundly appreciate. I would like to take this opportunity to thank Professor Alan Hounsell and Professor Brendan McClean for the valuable insight and feedback in the overall PhD direction. I would also like to thank Dr Seán Walsh for the invaluable support with MATLAB technical issues.

A sincere thanks also go to my graduate research committee: Dr Miriam Byrne, Dr Matt Redman, Dr Gary Gillanders and Professor Collin O’Dowd for being regularly available for consultation on any project-related matters. They have been immensely supportive and encouraging throughout this process by closely monitoring my research progress and ensuring I am on the right track with my PhD commitment. Also, I am grateful to all the staff of the School of Physics, in particular; Professor Gerard O'Connor, PJ Walsh, James Nallen and Rebecca Nolan for their assistance, kindness and endless good humour. To all of my incredible PhD colleagues, thanks so much for being there, dealing with my PhD worries, anxiety and stress and reminding me that there is a normal life outside of this thesis. I am grateful for the conversations and nights out. I will not attempt to list names – all of you are equal.

Many thanks also go to the radiotherapy staff at University Hospital Galway, Dr Christoph Kleefeld, Margaret Moore, Dr Gordon Sands, Anyscha Zuchora, Darragh McShane, Sinead Cleary, Louise Fahy, Triona Brosnan, Linda Coleman and James Murphy for their assistance and encouragement throughout the PhD/residency programme. I will be forever grateful for their time and patience.

I would also like to acknowledge the Comprehensive Cancer Centre of King Fahad Medical City for the scholarship that made this project possible. Many thanks also go to the medical physics staff of King Fahad Medical City for their endless encouragement.

A special thanks to my lovely daughters, princess Joory and princess Jody – being your dad has been one of the greatest gifts in my life. Thank you both for the endless humour; you are my source of happiness. I cannot forget the popcorn lady or the burgers safer; you always make me laugh when I even do not want to smile. You fill my days with questions and subjects I never knew a 6- or 8-year-old would ask. You have been always much smarter than me when I was at your age. Princess Joory, the big heart, I am always impressed with how you are willing to share and help others. Princess Jody, I am proud of your hard work, practice and talent that got you on the school stage to sing in front of everyone. You have a nice and pleasant voice, thank you.

Lomi, my lovely wife, my soulmate, my other half, thank you for being there when I needed a shoulder to lean on, for patiently listening to me and helping me deal with my PhD stress. There are so many times where I think about how lucky I am to have you in my life (such a kind, considerate and incredibly gorgeous wife).

Also, I would like to take this opportunity to thank my huge family for the endless support through my MSc, residency training and PhD periods. My sisters Shamah, Fatmah, Khadijah, Safeh and Najat and my brothers Naser, Ahamed and Eisa. Through this process, you have shown me that family is not an important thing, but it is everything. Thank you for the endless support.

Last and most important, thanks to my wonderful parents who have given me so much. I appreciate your love, sacrifice and effort in bringing me up to be a better individual. Mom, thanks for the daily voice messages that remind me to work hard and keep focusing on my PhD efforts to achieve my goals. Dad, thanks for the endless supply of encouragement and words of wisdom, you are my role model. My parents, I owe you everything in life and all the success I have to you.

Dissemination of Research

- **Publications (Peer-reviewed):**

1) **Alaswad M**, Kleefeld C, Foley M. "Optimal tumour control for early-stage non-small cell lung cancer: A radiobiological modelling perspective". Physica Medica. 2019;66:55-65. **(Journal paper).** Citation Indexes: 3. https://twitter.com/ELS_Radiology/status/1181811559175217152

2) **Alaswad M**, Kleefeld C, Moore M, Foley M. "A TCP model for external beam treatment of non-small cell lung cancer". Physica Medica. 2018;52:172. **(Abstract).** Citation Indexes: 3.

3) **Alaswad M**, Kleefeld C, Foley M. "Radiation dose intensity and local tumour control of non-small cell lung cancer: A radiobiological modelling perspective". Journal of Physics: Conference Series: IOP Publishing; 2019. p. 012071. **(Conference paper).** Citation Indexes: 2.

4) **Alaswad M**, Kleefeld C, Foley M. "Comparison of the T descriptor of the 7^{th} and 8^{th} editions of the TNM staging system for non-small cell lung cancer after radiotherapy: An analysis from the TCP modelling perspective". Reports of practical oncology and radiotherapy; 2020; submission ID: RPOR-D-20-00295. **(Journal paper, under review).**

5) **Alaswad M**, Kleefeld C, Foley M. "Radiobiological modelling of concomitant radiochemotherapy for patients with locally advanced non-small cell lung cancer: A tumour control probability perspective". Physics in Medicine & Biology, 2021; **(Journal paper, under preparation).**

6) **Alaswad M**, Kleefeld C, Foley M. "Radiobiological modelling of clonogen distribution, hypoxic fraction and tumour size effects on local tumour control of non-small cell lung cancer". Physica Medica: 2019;67:197. **(Abstract).**

7) **Alaswad M**, Kleefeld C, Foley M. "Comparison of the T descriptor of the 7^{th} and 8^{th} editions of the TNM staging system for non-small cell lung cancer after radiotherapy: An analysis from the TCP modelling perspective". Physica Medica. 2020, submission ID; 392: **(Abstract, accepted).**

8) **Alaswad M**, Kleefeld C, Foley M. "Influence of incorporating radiotherapy and chemotherapy on the tumour control probability of patients with non-small cell lung cancer: A radiobiological modelling study". Physica Medica. 2020, submission ID; 394: **(Abstract, accepted).**

9) **Alaswad M**, Kleefeld C, Foley M. "Internal and external validation of a tumour control probability model for non-small cell lung cancer". Physica Medica. 2020, submission ID; 395: **(Abstract, accepted).**

10) **Alaswad M**, Kleefeld C, Foley M. "Influence of radiotherapy dose uncertainty on local tumour control for locally advanced non-small cell lung cancer". Physica Medica. 2021, submission ID; 477: **(Abstract, accepted).**

11) **Alaswad M**, Kleefeld C, Foley M. "Radiobiological modelling of concomitant radiochemotherapy for patients with locally advanced non-small cell lung cancer: A tumour control probability perspective". Physica Medica. 2021, submission ID; 474: **(Abstract, accepted).**

- **Additional non-thesis related publications during the PhD (Peer-reviewed):**

12) **Alaswad M**, Coleman L. "The sensitivity of patient-specific IMRT QA methods in detecting systematic errors: Field-by-field versus single-gantry-angle composite". Journal of Physics: Conference Series: IOP Publishing; 2019. p. 012063. **(Conference paper).**

13) Kleefeld C, **Alaswad M**, Foley M. "Challenges and opportunities for a CAMPEP-accredited Medical Physics Graduate Program in Galway, Ireland". Journal of Physics: Conference Series: IOP Publishing; 2019. p. 012074. **(Conference paper).**

14) **Alaswad M**, Zuchora A. "A feasibility study to investigate the introduction of HDR intraluminal brachytherapy for oesophageal cancer at University Hospital Galway". Physica Medica: European Journal of Medical Physics. 2019;67:204. **(Abstract).**

15) **Alaswad M,** Coleman L. "Comparison of IMRT QA measurement methodology". Physica Medica. 2017;42:363. **(Abstract).**

- ## Awards

1) Best oral presentation and conference paper (Radiotherapy session). **Alaswad M,** "Optimal tumour control for early-stage non-small-cell lung cancer: A radiobiological modelling perspective", 10th Annual Scientific Meeting of the Irish Association of Physicists in Medicine was held on 23 March 2019 at Croke Park, Dublin, Ireland.

2) Best oral presentation and conference paper (Radiotherapy session). **Alaswad M,** "Radiation dose intensity and local tumour control of non-small cell lung cancer: A radiobiological modelling perspective", 18th Asia-Oceania Congress of Medical Physics (AOCMP) & 16th South-East Asia Congress of Medical Physics (SEACOMP), was held on 11–14 November 2018, Connexion Conference and Event Centre, Nexus, Bangsar South, Kuala Lumpur, Malaysia.

- ## Conference Presentations

1) **Alaswad M**, "Radiobiological modelling of concomitant radiochemotherapy for patients with locally advanced non-small cell lung cancer: A tumour control probability perspective": 3rd European Congress of Medical Physics (ECMP2021) to be held in Torino, Italy, from 16–19 June 2021, **(Poster presentation).**

2) **Alaswad M**, "Influence of radiotherapy dose uncertainty on local tumour control for locally advanced non-small cell lung cancer": 3rd European Congress of Medical Physics (ECMP2021) to be held in Torino, Italy, from 16–19 June 2021, **(Poster presentation).**

3) **Alaswad M**, "Optimal tumour control for early-stage non-small-cell lung cancer: A radiobiological modelling perspective": 10th Annual Scientific Meeting of the Irish Association of Physicists in Medicine was held on 23 March 2019 at Croke Park , Dublin, Ireland **(Oral presentation).**

4) **Alaswad M**, "Radiation dose intensity and local tumour control of non-small cell lung cancer: A radiobiological modelling perspective": 18th Asia-Oceania Congress of Medical Physics (AOCMP) & 16th South-East Asia Congress of Medical Physics (SEACOMP) was held on 11–14 November 2018, Connexion Conference and Event Centre, Nexus, Bangsar South, Kuala Lumpur, Malaysia **(Oral presentation).**

5) **Alaswad M**, "A TCP model for external beam treatment of non-small cell lung cancer": 9th Annual Scientific Meeting of the Irish Association of Physicists in Medicine, was held on 17 February 2018 at the City Hotel Derry, Londonderry, UK. **(Oral presentation).**

6) **Alaswad M**, "Comparison of the T descriptor of the 7th and 8th editions of the TNM staging system for non-small cell lung cancer after radiotherapy: An analysis from the TCP modelling perspective": 11th Annual Scientific Meeting of the Irish Association of Physicists in Medicine, was held on 9–13 November 2020, Galway, Ireland.**(Poster presentation).**

7) **Alaswad M**, "Influence of incorporating radiotherapy and chemotherapy on the tumour control probability of patients with non-small cell lung cancer: A radiobiological modelling study": 11th Annual Scientific Meeting of the Irish Association of Physicists in Medicine, was held on 9–13 November 2020, Galway, Ireland.**(Poster presentation).**

8) **Alaswad M**, "Internal and external validation of a tumour control probability model for non-small cell lung cancer": 11th Annual Scientific Meeting of the Irish Association of Physicists in Medicine, was held on 9–13 November 2020, Galway, Ireland. **(Poster presentation).**

9) **Alaswad M**, "A TCP model for external beam treatment of non-small cell lung cancer": Research day at Galway University Hospital, was held on 21 January 2019. **(Poster presentation).**

10) **Alaswad M**, "Radiation dose intensity and local tumour control of non-small cell lung cancer: A radiobiological modelling perspective": Annual research day at King Fahad Medical City, Saudi Arabia Riyadh, was held on 14 December 2020**. (Poster presentation).**

- **Other achievements**

1) Reviewer for scientific journals

During my PhD, I have been offered the opportunity to contribute to the research activity of the medical physics field through reviewing several manuscripts for the following scientific journals.

I. *International Journal of Radiation Biology* (Taylor and Francis, IJRB)
II. *Journal of Clinical Research and Clinical Oncology* (Springer Nature, J. Cancer Res. Clin. Oncol.).
III. *European Journal of Medical Physics* (Elsevier, Physica Medica),
IV. *Journal of Radiology and Radiation Therapy* (JSciMed Central, JRRT).
V. *Journal of Cancer and Clinical Oncology* (Premier Publishers).

2) Editorial Board Member

A member of the editorial board of the *Artificial Intelligence in Medical Imaging* (AIMI) journal, by the Baishideng Publishing Group (BPG), ISSN; 2644-3260, DOI; 10.35711. Editorial ID number: 05589810.

3) Judge for 11th Annual Scientific Meeting of the Irish Association of Physicists in Medicine

During my PhD, I was offered the opportunity to be a judge for the poster session of 11th Annual Scientific Meeting of the Irish Association of Physicists in Medicine, which was held on 9–13 November 2020, Galway, Ireland.

List of Abbreviation

AAPM	**A**merican **A**ssociation of **P**hysicists in **M**edicine
BED	**B**iologically **e**quivalent **d**ose
CBCT	**C**one-**b**eam **c**omputed **t**omography
CTV	**C**linical **t**arget **v**olume
4D CT	**F**our **d**imensional **c**omputed **t**omography
DNA	**D**eoxyribo**n**ucleic **a**cid
DSB	**D**ouble-**s**trand **b**reak
DTA	**D**istance **t**o **a**greement
DVH	**D**ose-**v**olume **h**istogram
EBRT	**E**xternal **b**eam **r**adiotherapy
EQD2	**E**quivalent **d**ose **m**easured in 2 Gy per **f**raction
GTV	**G**ross **t**umour **v**olume
HDR	**H**igh-**d**ose **r**ate
ICRU	**I**nternational **C**ommission on **R**adiation **U**nits and **M**easurements
IGRT	**I**mage-**g**uided **r**adiation **t**herapy
IMRT	**I**ntensity-**m**odulated **r**adiotherapy
JCOG	**J**apan **C**linical **O**ncology **G**roup
LA-NSCLC	**L**ocally **a**dvanced **n**on–**s**mall **c**ell **l**ung **c**ancer

LD	**L**ethal **d**amage
LDR	**L**ow-**d**ose **r**ate
LET	**L**inear **e**nergy **t**ransfer
Linac	**L**inear **a**ccelerator
LQ	**L**inear-**q**uadratic
MLC	**M**ultileaf **c**ollimator
MRI	**M**agnetic **r**esonance **i**maging
NSCLC	**N**on–**s**mall **c**ell **l**ung **c**ancer
NTCP	**N**ormal **t**issue **c**omplication **p**robability
OAR	**O**rgans **a**t **r**isk
OER	**O**xygen **e**nhancement **r**atio
PE	**P**hotoelectric **e**ffect
PE	**P**lating **e**fficiency
PET	**P**ositron **e**mission **t**omography
PFS	**P**rogression-**f**ree **s**urvival
PLD	**P**otentially **l**ethal **d**ose
PP	**P**air **p**roduction
PSPT	**P**assive **s**cattering **p**roton **t**herapy
PTV	**P**lanning **t**arget **v**olume
QA	**Q**uality **a**ssurance

QUANTEC	**Q**uantitative **A**nalysis of **N**ormal **T**issue **E**ffects in the **C**linic
SABR	**S**tereotactic **a**blative **r**adiotherapy
SCLC	**S**mall-**c**ell **l**ung **c**ancer
SF	**S**urviving **f**raction
SLD	**S**ublethal **d**amage
SSB	**S**ingle-**s**trand **b**reak
TCP	**T**umour **c**ontrol **p**robability
TNM	**T**umour, **n**ode and **m**etastasis
TPS	**T**reatment **p**lanning **s**ystem
VMAT	**V**olumetric-**m**odulated **a**rc **t**herapy

Structure of the thesis

Chapter 1 introduces readers to the overall context of the project by highlighting the fundamental perspectives of radiotherapy physics, including external beam radiotherapy, brachytherapy and radiotherapy treatment planning. This chapter also describes the importance of radiobiological concepts in radiation oncology. Thereafter, the chapter details gaps in the literature that concern TCP modelling of NSCLC. The chapter ends with descriptions of the approaches adopted to fill these gaps.

Chapter 2 presents an in-depth review of the fundamental principle of radiation biology. The review includes the concepts of the cell survival curve, the linear quadratic model and the four (Rs) of radiotherapy.

Chapter 3 describes fundamental components of the TCP model that evolved for NSCLC. A comprehensive meta-analysis of clinical outcomes for a broad spectrum of NSCLC fractionation schemes, such as standard fractionation, hyperfractionation and hypofractionation is also presented. This outcome analysis for clinical radiotherapy of local tumour control for NSCLC has not previously been undertaken or reported by other scholars. Thereafter, the chapter details the novel proposed radiobiological approach for modelling clonogenic cell density, addressing the current limitations of TCP research in the literature using a new mathematical approach. Ultimately, the author introduces the bootstrap statistical procedure, which is used to validate the TCP model.

Chapter 4 explores in depth the main discrepancies between the 7th and 8th editions of the TNM classifications scheme for NSCLC. The chapter also establishes a conceptual TCP framework based on non-quantitative tumour descriptors T in accordance with the recommendations of the 7th and 8th editions of the TNM categorisation schema. New insight is thereby provided into the debate over the superiority of the 8th TNM edition over the 7th within the context of radiobiological modelling of NSCLC.

Chapter 5 compares and analyses clinical outcomes of chemoradiotherapy with radiotherapy alone in patients with histologically verified, locally advanced nonresectable NSCLC. A TCP model then utilises 8 clinical trials to clarify the influence of synergistic chemotherapy with radiotherapy for locally advanced NSCLC patients.

Chapter 6 provides brief sub-conclusions and explains various methodological and findings contributing to the overall thesis objectives. Ultimately, the author discusses the implications of the findings for future research regarding the radiobiological modelling field.

Chapter 1 Introduction

1.1 Thesis aims

This thesis explores three themes from the perspective of the tumour control probability (TCP) modelling of non-small cell lung cancer (NSCLC).

1) The fundamental motivation for this thesis is to examine the ability of a mechanistic TCP model to predict treatment outcomes for a wide range of NSCLC treatment strategies, such as hypofractionation, standard fractionation and hyperfractionation. Variations in the TCP with clonogenic density are further investigated by introducing a new mathematical model to vary the clonogenic cell and radiation dose distribution across the treated volume.

2) Additionally, the central considerations when making medical oncology treatment decisions are disease type and extent, which are described by stage—according to the tumour, node, metastasis (TNM) classification system. Notably, no previous study has developed a model based on the TNM classification system. Thus, one of the aims of this thesis is to incorporate the T descriptor of the TNM classification system into the TCP model.

3) Currently, synergistic cytotoxic chemotherapy with radiotherapy is most prevalent in treating locally advanced NSCLC. Clinical trial experience from multiple references has reported that the risk of locoregional relapse and distant metastasis was less evident for patients treated with concomitant radiochemotherapy than for those treated with radiotherapy alone. Although the influence of radiotherapy alone can be adequately described by the TCP model, the combined impact of concomitant chemotherapy and radiotherapy is still subject to extensive research. Therefore, the

mechanistic TCP model developed in the present thesis will be further extended to assess the effect of synergistic chemotherapy with radiotherapy for locally advanced NSCLC patients.

1.2 Thesis objectives

1) To develop a TCP model that can accurately predict the clinical response of NSCLC to external beam radiotherapy for a variety of fractionation regimens, including conventional fractionation, SABR and CHART.

2) To validate the TCP model using the bootstrap validation approach.

3) To establish a new radiobiological approach for modelling clonogenic density, thereby addressing the current limitations of TCP as reported in the literature.

4) To establish a TCP model based on the non-quantitative tumour descriptors T in accordance with the recommendations of the 7th and 8th editions of the TNM categorisation schema.

5) To extend the TCP model to evaluate the feasibility of quantifying the effect of cytotoxic chemotherapy for locally advanced NSCLC patients.

1.3 Lung cancer statistics

Cancer is identified by the uncontrolled proliferation of cells that have the potential to invade adjacent tissues. Cancer cells can take many forms. Solid tumours grow together forming a solid mass either within or on the surface of a particular organ or tissue.

Other cancers, such as leukaemias and lymphomas, are able to move freely around the body through the blood or the lymphatic system. Untreated cancers have the potential to inhibit and even destroy the function of the host tissue or organ (Zugazagoitia et al., 2016).

Lung cancer remains the most common cause of cancer mortality. In 2020, an estimated two million individuals were diagnosed with lung cancer globally, as depicted in Figure 1.1 (WHO, 2020). Currently, the two primary lung cancer categories are non–small cell lung cancer (NSCLC), which alone accounts for 80% of all lung cancers, and small-cell lung cancer (SCLC), which is designated the remaining 20% (Molina et al., 2008).

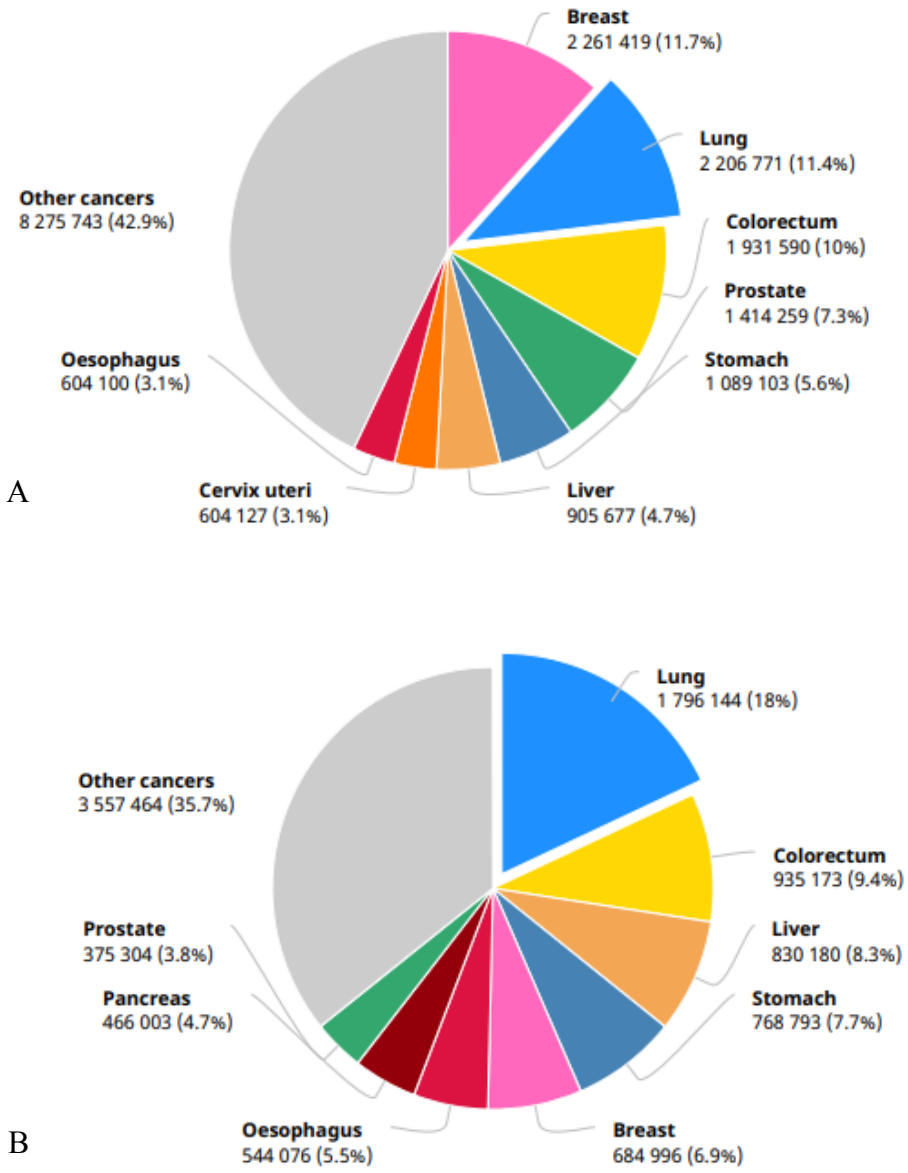

Figure 1.1: Lung cancer incidence (A) and mortality (B) global statistics according to the International Agency for Research of Cancer (IARC), (WHO, 2020) .

1.4 Management of NSCLC cancer

Both the stratification and prognosis of patients diagnosed with NSCLC and other solid cancers are highly contingent on the disease stage. The disease stage of any particular cancer is considered a vital factor through which therapeutic decisions are made. When establishing the stage of NSCLC, there is the need to employ various combinations of radiological, pathological and laboratory examinations (Purandare and Rangarajan, 2015, Koyi et al., 2015).

Presently, the tumour, node and metastasis (TNM) classification scheme is the most commonly accepted cancer staging terminology (Haro et al., 2019). This classification scheme significantly relies on the following three categories:

1. The extent and size of the tumour (T).
2. The extent of tumour spread to lymph nodes (N).
3. The presence of distant metastases (M).

In clinical practice, a category combination consisting of a number and a letter is used to signify the primary tumour size and the extent of its progression. Moreover, this mode of classification is also used to describe the spread of the disease. For instance, tumours that are classified as stage T1a are ones demonstrating the least advanced disease stage which is associated with superior outcomes (see Chapter 4).

In contrast, cancer cells that are classified as stage IV, are ones that have spread (metastasised) to other organs such as the brain or the liver. This classification is elaborated in greater detail in Table 4.1 of Chapter 4. Metastatic cancers are remarkably challenging to cure (Goldstraw et al., 2016).

The aim of cancer therapeutics is the eradication or destruction of the cancer cells and the prevention of further proliferation. The predominant forms of cancer treatments include surgery, which aims to remove the bulk of a tumour, and the application of ionising radiation (radiotherapy) which seeks to destroy the cancer cells. Treatment may also involve the use of cytotoxic drugs (chemotherapy) or the harnessing of the

body's defence mechanisms (immunotherapy). These modalities are employed to both kill and prevent the proliferation of cancer cells (Zappa and Mousa, 2016).

Additionally, these treatment modalities can be employed either alone or in combination. In the context of NSCLC, ensuring optimal management of patients is a complex feat. Not only is the management regimen stage-specific, but it also relies on prior therapies, the patient's age, co-morbidities and functional status (Duma et al., 2019). Surgical resection is typically the treatment of choice for early-stage NSCLC, with an overall survival rate of more than 80% and a local tumour control rate of over 90% after one-year (Kastelijn et al., 2015). Nonetheless, a number of NSCLC patients are considered ineligible for surgical procedures given their long history of smoking and cardiovascular risk factors.

1.5 Radiotherapy

Radiotherapy has consistently been indicated as a fundamental cancer treatment, with approximately half of all cancer patients undergoing radiotherapy at a particular phase during their management (Barton et al., 2006). Ionising radiation can destroy all types of living cells. However, different cells vary in their respective radiosensitivities (Chavaudra et al., 2004).

Accordingly, these differences can be harnessed by altering the radiation dose and ensuring a specific degree of cell destruction is achieved (see Section 2.8). Low dose radiation can be employed in palliative care as a means of attaining partial tumour regression for temporary symptomatic relief rather than for radical or curative intents.

Moreover, radiotherapy can be administered prior to surgery to shrink the tumour, thereby enhancing its resectability (neoadjuvant radiotherapy). Conversely, radiotherapy can also be used following a surgical procedure to destroy any residual tumour cells (adjuvant radiotherapy) (Wang et al., 2018).

It is noteworthy that radiotherapy presents specific practical challenges, including an inability to treat tumour cells in isolation. Any tumour mass would typically be situated close to or within a healthy organ. Thus, of primary concern is the conservation of the organ's functionality following treatment. Additionally, any radiation beam directed at a tumour would have to pass through the healthy structures surrounding it. Accordingly, the primary reason for employing radiotherapy in cancer treatment is for the delivery of a sufficiently high radiation dose to the cancer cells, whilst simultaneously striving to maintain the irradiation of normal tissue at a dose that would not cause a serious complication (morbidity).

Historically, radiotherapy administration has followed two principal routes: internal beam radiotherapy (also termed brachytherapy) and external beam radiotherapy (EBRT). As the most common form of radiotherapy, EBRT is typically performed with photon beams. These beams are high-energy X-rays produced by medical linear accelerators (linacs). Other approaches can also be utilised, including gamma-ray beams from cobalt-60 (^{60}Co) units and lower-energy X-rays in the energy range of 150–500 kVp (orthovoltage). Notably, the use of charged-particle beams, such as protons, has led to the realisation of a significant clinical advantage. This advantage is attributed to the pattern of proton energy deposition, as illustrated in Figure 1.2. For instance, proton beam dose deposition initially exhibits a slow increase in dose with depth, followed by a sharp increase near the end of the range. This peak or sharp rise in dose deposition is termed the *Bragg peak*. Unfortunately, the instalment of proton therapy machinery is associated with prohibitively expensive generating equipment. For instance, the cost of a proton machine can be three to four times greater than that of a typical linac, thus limiting its widespread use (Durante and Flanz, 2019). Note that a state-of-the-art linac such as Varian TrueBeam or Elekta Versa HD costs between €750,000–€1,500,000 (ROS, 2020).

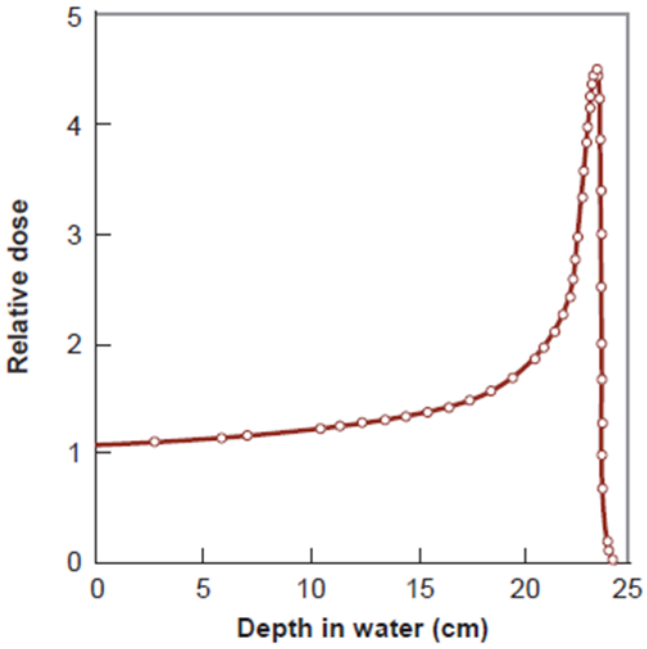

Figure 1.2: Central axis depth dose distribution for a 187-MeV protons beam. The dose reaches a sharp peak well-known as Bragg peak at a depth of approximately 23 cm (Gunderson and Tepper, 2015).

The functional principle governing the use of linacs is their ability to accelerate electrons through a linear tube (waveguide) using a high-frequency electromagnetic wave. The accelerated electrons exit the linac as an electron beam. The electron beam is focused onto a target that possesses a high atomic number, such as tungsten (Z = 64), thereby resulting in a bremsstrahlung interaction that yields photon beams (Greene and Williams, 1997).

Consequently, linacs are considered remarkably versatile machines as they facilitate two separate treatment modes; namely, using photons or electrons. Moreover, they enable the use of a diverse set of energies that can be selected according to the depth of the tumour, as illustrated in Figures 1.3 and 1.4.

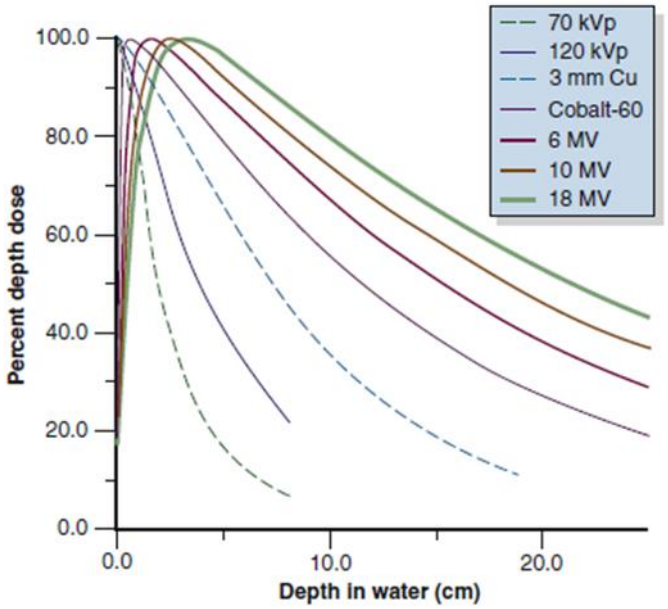

Figure 1.3: Central axis percentage depth dose distribution for varying quality photon beams (Khan and Gibbons, 2014).

Within the radiotherapy framework, photon beams are employed in the treatment of deep-seated tumours such as lung, prostate, brain, bladder or bowel tumours. Conversely, electron beams are utilised in the management of superficial to medium lesions that stretch to a depth of approximately 2–5 cm.

Increasing the beam energy corresponds to a higher beam penetration power, as illustrated in Figures 1.3 and 1.4. The fundamental advantage of the electron treatment mode is the pattern of the percentage depth dose (PDD) curve. Its shape results in a region of relatively uniform dose from the surface to a particular depth, termed as the 'depth of maximum dose' (D_{max}). Beyond D_{max}, the dose drops off rapidly, thereby resulting in minimal irradiation of organs at risk situated beyond the tumour.

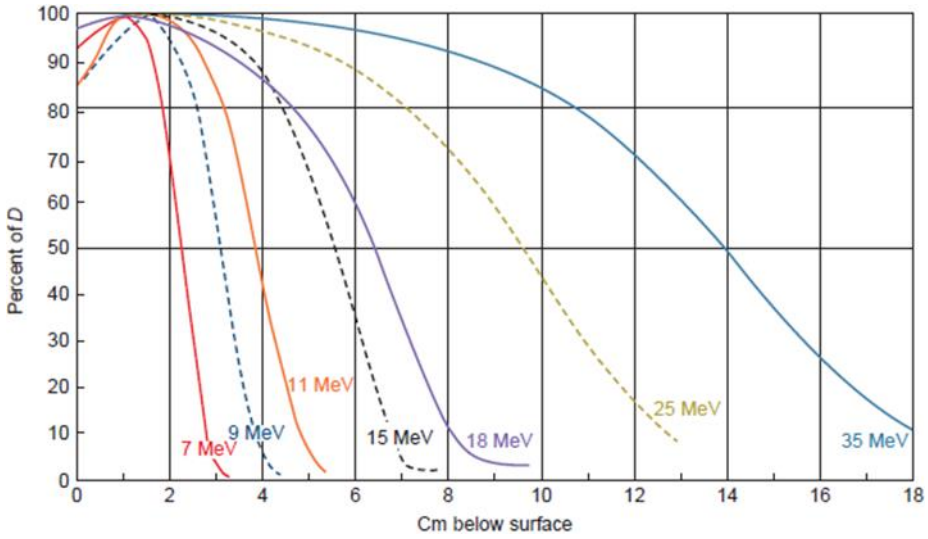

Figure 1.4: Comparison of the percentage depth dose (PDD) curves for different electron beam energies (Khan and Gibbons, 2014).

In comparison, brachytherapy is a treatment modality that utilises sealed radioactive sources placed either within or close to the tumour. Employing brachytherapy allows for the distribution of the radiation dose within the vicinity of the target volume. Thus, this mode of treatment is suited to clinical sites where sources can be placed in close contact with the tumour. This can either be by placing them within an existing body cavity (uterus, vagina, bronchus, oesophagus) or by surgically inserting them into the tissues (breast, rectum, anus, prostate, cheek).

Consequently, this form of therapy opens up the use of various methods of radiation delivery, including intracavitary, interstitial and intraluminal means. Moreover, based on the inverse square law, the falloff in dose as a function of distance from the source in brachytherapy allows the tumour to receive a high dose of radiation while the surrounding normal tissues and organs are only exposed to a minimal radiation dose (Otter et al., 2019).

Traditional radiotherapy protocols prescribe a 1.8–2 Gy of radiation dose to be delivered each day for five days per week, Monday to Friday, for a fixed number of fractions and a predetermined total dose. Note that the lack of weekend radiotherapy sessions is not based on radiobiological notions. Rather, this lack of weekend service is determined based on the logistics of staffing and the funding of radiation oncology centres at weekends. Furthermore, the lack of weekend radiotherapy sessions results in treatment gaps that might adversely affect the level of local tumour control due to the accelerated repopulation of tumour cells. This issue is discussed further in Chapter 2.

Additionally, delivering radiotherapy fractions in several small doses can improve clinical outcomes. This approach led to the initiation of the continuous hyperfractionated accelerated radiotherapy (CHART) regime at Mount Vernon Hospital in January 1985 (Turner et al., 1995). The treatment course was reduced from 40 to 12 days to diminish the likelihood of clonogenic cell proliferation (see Section 2.11). A small dose per fraction of 1.5 Gy was applied to enhance local tumour control and was delivered three times per day, every day – including the weekend – as described in greater depth in Chapter 3.

The last 10 years have seen the development of significant technological advances in radiotherapy. Currently, the management of lung cancer is typically designed to include the use of four-dimensional (4D) computed tomography (CT) scans, through which breathing-related tumour motion can be accounted for in an individualised manner (Brown et al., 2019, Hof et al., 2009). Additionally, volumetric-modulated arc therapy (VMAT) is one technique that is increasingly accepted for various tumour types to yield more conformal dose distribution – and thus, less toxicity to healthy tissue – than the conventional 3D radiotherapy approach. VMAT delivers the radiotherapy prescription doses by modulating photon beam intensities through the continuous variation of dose rates, gantry speeds and multileaf collimator (MLC) positions at each control point (Teoh et al., 2011).

The use of 4D CT allows the tight conformation of the high-dose area to the tumour, thereby facilitating the widespread adoption of stereotactic ablative radiotherapy (SABR). With SABR, very high doses of radiation are delivered over a limited number of fractions. Consequently, this approach allows for significant shortening of the overall treatment times (see Chapter 3). Similarly, the accuracy of the treatment set-up has also been enhanced as a result of the development of image guidance at the point of delivery through the use of the cone-beam computed tomography (CBCT) (Shimohigashi et al., 2016).

1.6 Target volume definitions

To facilitate the accurate, practical and reliable interchange of clinical experience, the use of a common language and concept definitions in radiation therapy is vital. Accordingly, the International Commission on Radiation Units and Measurements (ICRU) has published numerous guidelines aimed at standardising the processes used when prescribing and reporting radiation therapy treatment (Wambersie et al., 1992, Stroom and Heijmen, 2002, Gregoire and Mackie, 2011). These reports provide standard definitions of volumes to be delineated and reported (see Figure 1.5). Therefore, such standardisation allows for clinical outcomes from multiple oncology centres to either be objectively compared or accumulated to provide greater statistical strength. These tumour volume definitions are described briefly in the following subparagraphs.

The gross tumour volume (GTV) is defined as the gross palpable or visible/demonstrable size and location of a tumour at the macroscopic level. GTV might comprise the primary tumour (GTV-T), or metastatic lymphadenopathy (GTV-N) or the distant metastases (GTV-M). The GTV predominantly consists of the malignant growth lesions with the highest tumour cell density. To achieve local tumour control, the radiation dose given to the overall GTV must be sufficiently high to combat the great density of the bulky tumour cells within the GTV.

(A)

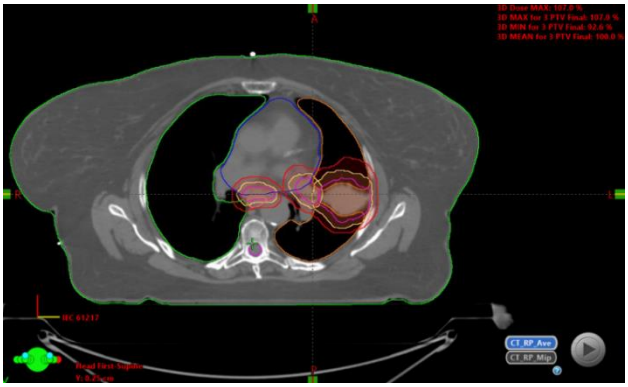

(B)

(C)

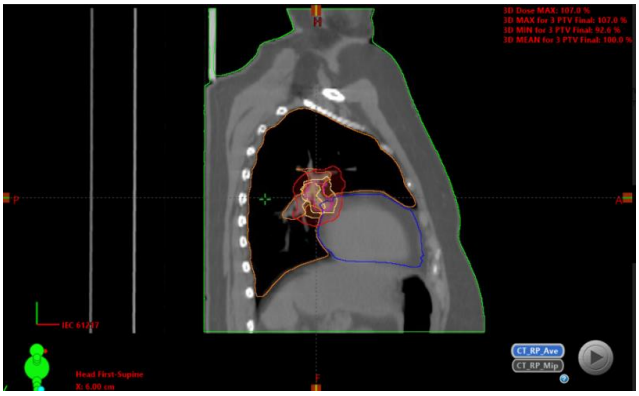

Figure 1.5: Depicts typical delineations of GTV, CTV and PTV, as well as the at-risk organs indicated during radiotherapy treatment planning for an NSCLC patient: (A) axial view of the CT scan, (B) coronal view of the CT scan, and (C) sagittal view of the CT scan. Patient images were adapted anonymously from the treatment planning system of the radiation oncology department at the King Fahad Medical City.

To accomplish this, the GTV is initially delineated on CT images, and then a margin surrounding the GTV is added to account for any spread of the microscopic disease. Together, this diagram yields the clinical target volume (CTV). In the instance of postoperative irradiation, following complete surgical resection, there is no GTV to define. Instead, in such a situation, the delineation only accounts for the CTV (Gregoire and Mackie, 2011).

Subsequently, the CTV is enlarged with a margin for expected random and systematic uncertainties throughout the treatment course. Such uncertainties include the setup uncertainty regarding the position of the patient during treatment. These geometric uncertainties perceive as planning target volume (PTV) (Gregoire and Mackie, 2011).

1.7 Radiotherapy treatment planning

To ensure the fulfilment of the radiation therapy objective, whether seeking palliation or a cure, the treatment plans are designed according to the individual anatomy of the patient. Consequently, the initial phase in the treatment planning procedure is the acquisition of CT images that accurately describe the anatomy and the dimensions of the tumour. The acquired CT images are then exported to the treatment planning system (TPS). Once registered in the TPS, a radiation oncologist manipulates the images by delineating the target volumes described in the previous sections (e.g., GTV, CTV and PTV). The radiation oncologist also delineates the healthy tissues surrounding the tumour that are defined as the organs at risk (OAR).

It is crucial to note that other imaging modalities, including but not limited to positron emission tomography (PET) and magnetic resonance imaging (MRI), are frequently employed to assist in establishing the exact tumour shape and location. Once the target volumes and OARs have been identified, a dosimetrist initiates the process of generating a treatment plan.

Designing a treatment plan involves the selection of suitable radiation beam modes, radiation angles and energy levels. The TPS also benefits from the use of radiation dose calculation algorithms that can estimate the probability of different radiation interactions as it travels through specific tissue densities.

The quality of the treatment plan must also be evaluated. Both the physicists and oncologists continuously assess the plan to fulfil the recommendations set by ICRU report number 83 (ICRU83). This report states that the minimum and maximum coverage of the PTV should be 95% and 107% of the prescribed dose, respectively (Gregoire and Mackie, 2011). The recommendations in this report also ensure that the OARs should not receive more than the recommended tolerance radiation doses as described by the Quantitative Analysis of Normal Tissue Effects in the Clinic (QUANTEC) guidelines (see Table 1.1) (Bentzen et al., 2010).

These guidelines originated from a proposal defined by the Science Council of the American Association of Physicists in Medicine (AAPM) that aimed to review and update recommendations and guidelines published previously by Emami (Emami et al., 1991). Thus, to accomplish these aims, a dose-volume histogram (DVH) which is a graphical display of the radiation dose as a function of volume, must be examined (see Figure 1.6).

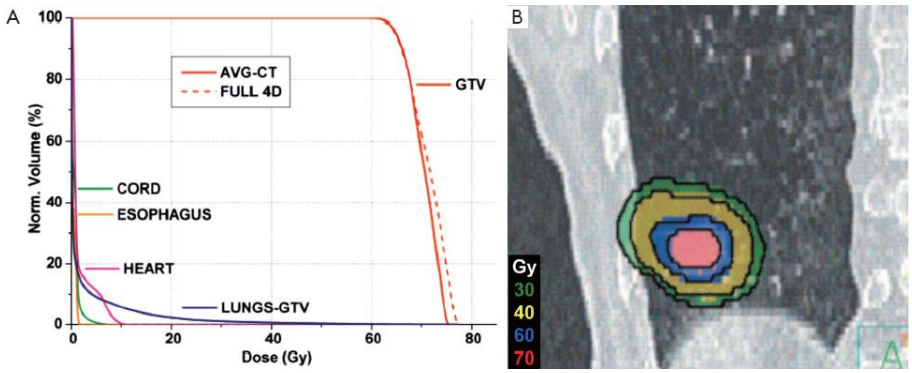

Figure 1.6: An illustration of a typical dose-volume histogram (DVH) for lung cancer case (Glide-Hurst and Chetty, 2014).

Additionally, the typical OARs within the thorax are the lungs, heart, spinal cord and oesophagus. Notably, the radiation dose tolerances of these OARs regulate the daily radiotherapy practice and are adopted in multicentre trials in cooperative groups such as the Radiation Therapy Oncology Group (RTOG) (see Table 1.1).

Table 1.1: Summary of radiation dose tolerances of the common OARs within the thorax; note that V_{20} represents the volume receiving ≥20 Gy and V_{30} represents the volume receiving ≥30 Gy.

Dose limits for OARs	QUANTIC (Marks et al., 2010)	3D-CRT (RTOG 0617) (Bradley et al., 2015)	SABR (RTOG 0618, 18 Gy delivered in 3 fractions) (Timmerman et al., 2013)
Lung	• $V_{20} \leq 30\%$	• Mean lung dose ≤ 20 Gy • $V_{20} \leq 37\%$	• $V_{20} \leq 10\%$
Heart	• Mean dose <26 • V_{30} <46%	• ≤60, ≤45, ≤40 Gy for 1/3, 2/3, 3/3 of heart	• ≤30 Gy (10 Gy/fraction)
Spinal cord (point dose)	• ≤50.0 Gy	• ≤50.0 Gy	• ≤18 Gy (6 Gy/fraction)
Oesophagus	• Mean dose ≤34 Gy	• Mean dose ≤34 Gy	• ≤27 Gy (9 Gy/fraction)

According to the ICRU reports, the OARs can be functionally characterised as parallel, serial or a mixture of both. “Serial” organs are those with functional subunits that are configured in a branching or linear shape. They are designated serial organs as there is interdependence between the subunits of the organ (see Figure 1.7A). In such situations, destruction in one subunit can compromise or damage the entire organ. A good example of a serial organ is depicted by the spinal cord.

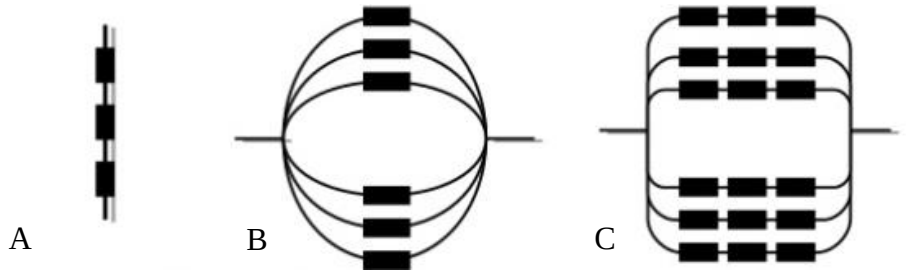

Figure 1.7: Classifications of the organs at risk based on the functional sub unit concepts proposed by the ICRU. (A) Serial organ, (B) parallel organ and (C) a combination of serial and parallel organs (Wambersie et al., 1992, Stroom and Heijmen, 2002, Gregoire and Mackie, 2011).

In contrast, for "parallel" organs, the functional subunits of the organ are independent. Therefore, functional redundancy exists (see Figure 1.7B). Consequently, damage to a particular functional subunit of a parallel organ does not result in damage to the other subunits. Accordingly, the other subunits will remain functioning. Typical parallel functioning organs involve the kidneys, liver and lungs. Some organs are classed as both parallel and serial organs (see Figure 1.7C). The heart is one organ that possesses parallel subunits, such as the myocardium, and serial subunits such as the coronary arteries. Whether an organ is a parallel, serial or a combination organ is a factor that is considered during the evaluation stage of the treatment plan.

1.8 Role of radiobiology in radiation oncology

Radiobiological modelling has been an essential component of radiotherapy for many decades. The need for radiobiological modelling is attributed to how it enhances our understanding of the interaction mechanism taking place between the radiation and the organism.

For instance, a common application of the radiobiological concept is observed in the conversion of a specific physical quantity such as the absorbed dose, to a clinically relevant quantity. Examples of clinically relevant quantities include the equivalent dose estimated in 2 Gy per fraction (EQD2) and the biologically equivalent dose (BED) (Bentzen et al., 2012).

The measurement of these quantities permits optimisation of the treatment plan. In addition to the assessments noted in Sections 1.4 and 1.5, radiobiological modelling has recently been included in the treatment planning system because of its optimisation benefits. When treatment plans are generated in this manner, they are referred to as a biologically based treatment planning system (Barry et al., 2020). Within this framework, the linear-quadratic (LQ) model is employed as the standard practice for describing the influence of the radiation dose on cell survival and tissue responses. The LQ notion is employed to compute the TCP.

Both the TCP and the normal tissue complication probability (NTCP) are presented as sigmoid curves that are frequently used to characterise the radiotherapy principle. Figure 1.8 below illustrates typical sigmoidal curve plots representing the TCP and the NTCP. Due to the steep nature of the TCP curve, a marginal increase in dose can lead to a notable enhancement in the clinical outcomes.

Notwithstanding the preceding, the NTCP curve is also illustrated and it clearly follows a similar distinctive pattern to the TCP curve. Thus, a higher level of risk is demonstrated by the NTCP curve with each increase in dosage. Overall, it is this combination of challenging patterns that led to the establishment of the therapeutic ratio concept.

The therapeutic ratio concept is often used to represent the optimal radiotherapy treatment. In general terms, the therapeutic ratio refers to the ratio of the TCP and the NTCP at a specific level of response. Significantly, the further the NTCP curve is positioned to the right of the TCP curve, the more easily the radiotherapeutic goal can be achieved. In such a situation, the therapeutic ratio would be larger and treatment complications will be less likely, as illustrated in Figure 1.8C.

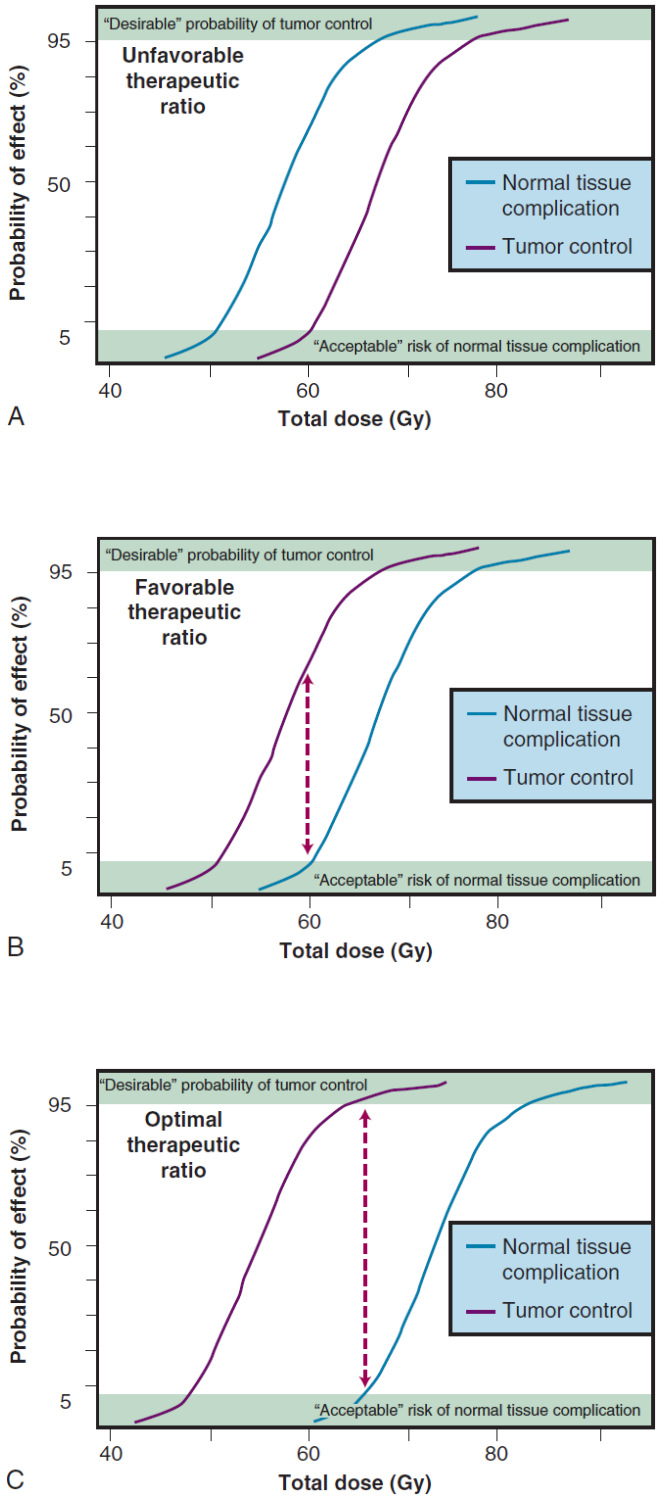

Figure 1.8: Graphical representation of the therapeutic ratio following three scenarios in which the correlation between the tumour control and normal tissue tolerance dose-response curves is (A) undesirable (B), desirable and (C) optimal (Gunderson and Tepper, 2015).

Bio-mathematical modelling of both the TCP and the NTCP can be used to predict the clinical outcome following radiotherapy treatment. The models employed can either be empirical or mechanistic in nature depending on whether they are based on clinical observations or on the cell-kill mechanism. The general theme of the current thesis is to develop a mechanistic TCP model that is highly capable of describing the response of NSCLC to external beam radiotherapy. The following section will outline the gaps in the literature that require further research.

1.9 Overview of the project

Local tumour control is an essential determinant of cancer survival. Moreover, radiotherapy dose escalation is expected to improve long-term outcomes. Research on radiotherapy dose escalation suggests a potential benefit regarding local tumour control when higher radiation doses per fraction are administrated for early-stage NSCLC patients (Guckenberger et al., 2016, Zheng et al., 2014). SABR is one radiotherapy modality employed in dose escalation to tumours while simultaneously avoiding an increase in the dose conveyed to healthy tissues. From this perspective, optimum survival and local tumour control can be managed using SABR rather than the traditional employment of three-dimensional conformal radiation therapy (3D-CRT).

This is particularly true for early-stage NSCLC patients who are frequently considered unsuitable candidates for surgery or who may refuse surgery (Song et al., 2009). SABR also represents a philosophy that differs from other radiotherapy regimens as it delivers very high doses of radiation over a few days. The potential advantage of SABR in the treatment of small tumours is the increased accuracy of delivering high BEDs through the use of respiratory motion management systems such as 4D CT and more precise delivery of multiple radiation beams than other modalities (Boily et al., 2015).

Nevertheless, the central debate remains on whether LQ-based TCP modelling can adequately describe tumour control when observed at a high dose per fraction, as is the case with SABR treatment of NSCLC. The LQ model describes cell responses to radiation and is, therefore, the basis for TCP models (see Chapter 3). For instance Kirkpatrick et al. (2008) argued that the LQ model might be inappropriate for radiotherapy regimens that employ a high dose per fraction. Several researchers have supported this hypothesis by claiming that tumour eradication at a high dose per fraction is governed by biological phenomena that are qualitatively different from those of radiotherapy fractionated schemes. Such schemes include 3D-CRT and CHART, which require a low dose per fraction (Fuks and Kolesnick, 2005).

Additionally, the number of clonogens in the tumours of interest is a fundamental input parameter for TCP modelling. In the case of solid tumours, clonogenic cell density can vary widely, ranging from 10^5-10^9 cm^{-3} (Nahum et al., 2003).The exact value of this number for different tumour types is not known. Moreover, how this number can vary between tumours in different patients is not understood. Within this context, various radiobiological methods have been developed and introduced to calculate TCP (Alaswad et al., 2018, Walsh et al., 2016, Ruggieri et al., 2013, Ruggieri et al., 2010, Baker et al., 2015, Stavreva et al., 2019) .However, the majority of radiobiological research has assumed that the treated volume contains a fixed number of clonogenic cells, which is perceived as one of the major limitations of these models.

Furthermore, the TCP concept is significant for both the clinical and research sides of radiation oncology. Thus, there is a need to apply appropriate statistical methods to assess the reproducibility and generalisability of a TCP model's performance. This process of model evaluation is often termed 'model validation'. Diverse frameworks for validating predictive models have been proposed in the literature (Steyerberg et al., 2003). Validation of TCP models is highly desirable; however, it remains uncommon in practice.

As previously mentioned, accurate prognosis and relevant therapy decisions rely on establishing the accurate staging of NSCLC. The recently proposed 8th edition TNM staging system exhibited significant amendments in the distribution of the T and M descriptors. As noted by Goldstraw et al. (2016), every revision to the TNM classification should contribute to clinical improvement. This is particularly necessary regarding patient stratification, therapy and outcomes.

While several studies reported the superiority of the 8th TNM edition in comparison to the previous 7th TNM edition (Sui et al., 2017, Chansky et al., 2017, Yang et al., 2017) in terms of both the discrimination ability among the various T subgroups and clinical outcomes, others argued against this interpretation (Jung et al., 2018) . Despite these contradictory perspectives, not a single study exists that serves to compare the differences between the 7th and the 8th TNM editions from a TCP modelling perspective.

Regarding the treatment of locally advanced NSCLC, current practice has seen an increase in the application of synergistic cytotoxic chemotherapy with radiotherapy. This approach is believed to offer superior local tumour control (Auperin et al., 2006). Whilst the effect of radiotherapy alone can be well described using a TCP model, the quantification of the combined effect of the concomitant use of chemotherapy and radiotherapy is still subject to intensive research.

Chapter 2 Fundamental principles of radiobiology

2.1 Introduction

Radiobiology as a scientific field concerns the exploration of the impact of radiation on diseased and healthy organs. Through this field, radiation oncologists and medical physicists strive to comprehend the nature and chain of events that arise as a consequence of the absorption of ionising radiation energy. Accordingly, they examine the biological implications of any resulting damage and the mechanisms that enhance, compensate for, or repair the damage.

2.2 Mechanism of biological response to radiation

Irradiation of any biological system produces a sequence of events that vary substantially in their timescale, as illustrated in Figure 2.1. The events that occur can be subdivided into three stages. The first is the physical phase, which encompasses the interaction of charged particles with a tissue's atomic structure. During this stage, an electron primarily interacts with orbital electrons. In doing so, the charged particles raise some electrons to higher energy level within an atom (i.e., excitation) and eject others from the atoms (i.e., ionisation) (Williams, 2019).

The second stage is the chemical stage, in which injured molecules and atoms respond through rapid chemical reactions. The third stage consists of the biological damage that occurs when the energy from the ionising radiation is absorbed by the organs or tissues.

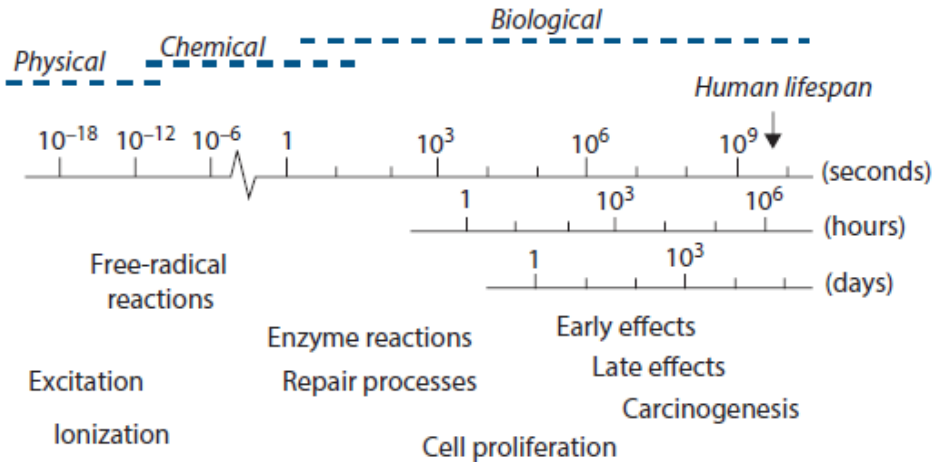

Figure 2.1: Represents the timescales of the effects of radiation exposure on biological systems (Williams, 2019).

A large and growing body of literature has established that the most vulnerable and critical cell component impacted by ionising radiation damage is DNA (Chew et al., 2019a, Willers et al., 2004, Stewart et al., 2011). The most clinically notable radiotherapeutic influences occur as a consequence of irreparable DNA lesions. This, in turn, leads to the proliferative cells' lacking the ability for sustained cell division. Note that a lack of proliferative capability (see Section 2.5) by tumour cells is an essential condition for the realisation of a tumour cure. More precisely, such a lack of proliferation is required for the attainment of local tumour control.

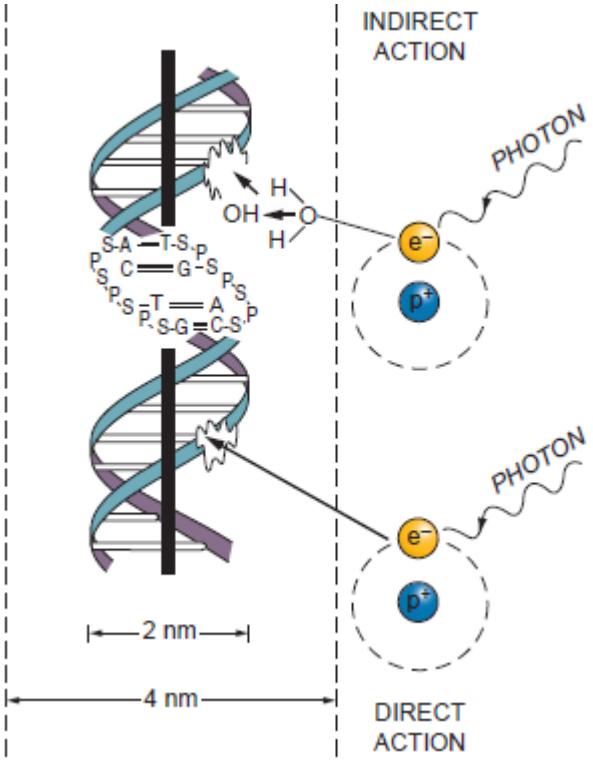

Figure 2.2: Depiction of the structure of DNA. The DNA helix has a diameter of approximately 2mm (20 Å). The figure illustrates the direct and indirect influences of ionising radiation on the biological system. Regarding the direct effect, secondary electrons originating from the absorption of an X-ray photon interact directly with the DNA. Conversely, in the indirect effect, secondary electrons interact with a water molecule to yield a hydroxyl radical group, resulting in DNA damage (Hall and Giaccia, 2012).

Two DNA damage (breakage) mechanisms have been described, that is, consequences from the direct or indirect influence of ionising radiation on the DNA molecule. In the direct mechanism, ionising radiation directly interacts with the DNA molecules, disrupting the molecular structures. Such alterations in structure cause cell damage or even cell death (see Figure 2.2) (Hall and Giaccia, 2012).

Alternatively, in the indirect mechanism, the ionising radiation primarily interacts with water molecules. The likelihood of such an interaction is high, as nearly 80% of a cell is composed of water. The interaction of the radiation with the water yields free radicals, which can diffuse into the cell and damage the critical region within the cell. Thus, the water molecule may become ionised and can be chemically expressed, as noted in Equation (2.1).

$$\mathbf{H_2O = H_2O^+ + e^-} \quad \textbf{(2.1)}$$

Regarding the use of high-energy photons for radiation therapy and imaging purposes, five primary interaction mechanisms exist. These mechanisms include the (1) photoelectric effect (PE), (2) Compton interaction, (3) pair production (PP), (4) Rayleigh (coherent) scatter and (5) photodisintegration. Figure 2.3 exhibits a brief illustration of these interactions.[1]

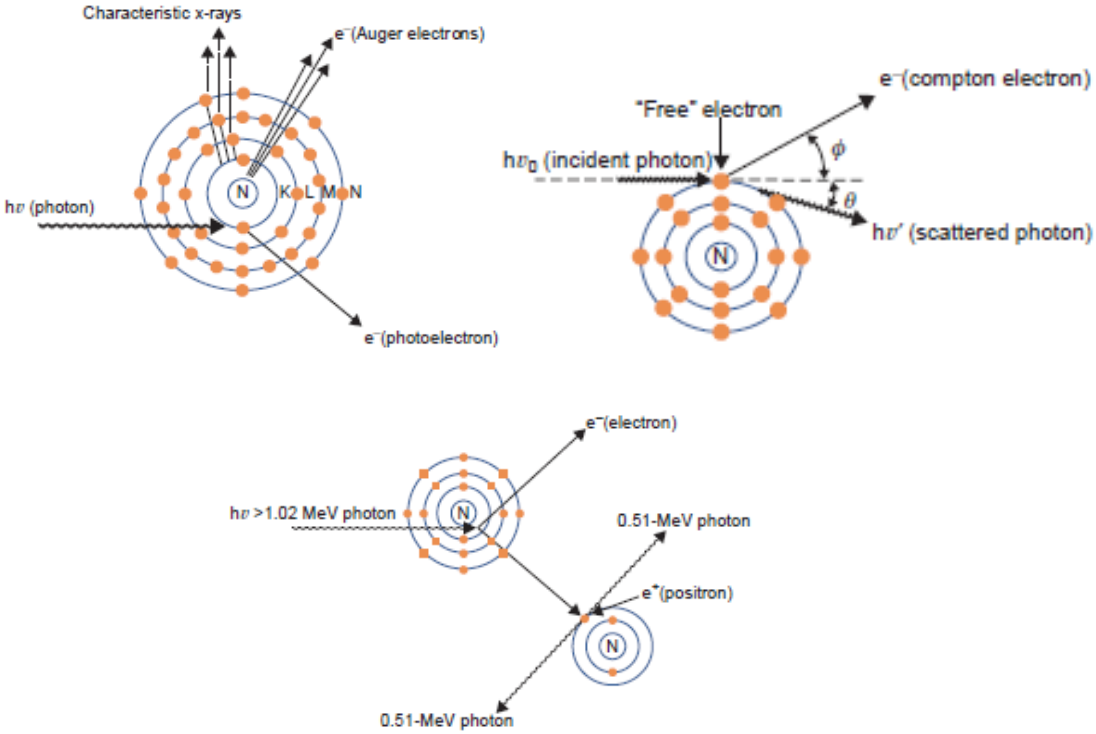

Figure 2.3: Outline of the classical photon interaction mechanisms within a medium. (A) In the photoelectric effect, the incident photon is fully absorbed by the inner shell electrons of the atoms. This interaction is vital for diagnostic imaging. (B) Compton scattering describes the interaction of the photon with the loosely bound electron of the atom. This scattering is important in radiotherapy. (C) pair production is observed where the interaction involves the atom's nuclear field which leads to the emission of an electron and a positron pair, hence the term pair production (Hall and Giaccia, 2012).

[1]For a comprehensive overview, see Halperin et al. (2020), Hendee et al. (2013), Khan and Gibbons (2014) and Mayles et al. (2007).

To further clarify the descriptions of the various mechanisms involved in indirect radiation effects, several concepts must be outlined. An ion is a molecule or an atom that has lost an electron, thus making it electrically charged. Furthermore, a free radical comprises an unpaired electron in the outer shell, causing it to be significantly reactive. Thus, H_2O^+ is a free radical and an ion. Through a sequence of chemical reactions, $H_2O^+$and e^- yield highly reactive free radicals. For instance, the hydroxyl radical (OH) can diffuse through tissue twice the diameter of a DNA double helix. Moreover, OH has a remarkably short lifespan of approximately 10^{-10} seconds. Ultimately, the hydroxyl radical's action can cause both single- and double-strand DNA breaks (see Figure 2.4) (Hall and Giaccia, 2012).

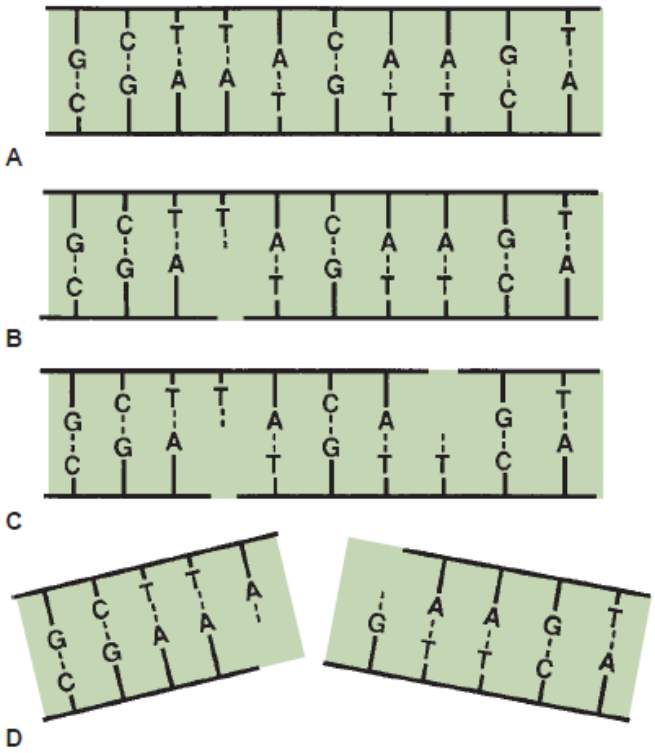

Figure 2.4: Mechanism of DSBs and SSBs induced by ionising radiation: (A) a 2-D sketch of the typical DNA helix. The base pairs carrying the cell's genetic codes are harmonious (i.e., guanine pairs with cytosine and adenine pairs with thymine). (B) Damage in one strand has a minimal effect as the cell can repair it promptly by employing the opposite strand as a template. (C) DSBs are breaks in both strands. If the breaks are widely separated, then they would be repaired as independent breaks. (D) Damages in both strands distanced by a few base pairs. Such breaks result in DSBs (Hall and Giaccia, 2012).

Furthermore, if cells are exposed to a modest dose of ionisation radiation in the range of 1–3 Gy, this could result in 40 double-strand breaks (DSBs) and 1000 single-strand breaks (SSBs). In intact DNA, however, SSBs are of minor biological significance from the standpoint of cell killing because they are smoothly repaired by employing the opposite strand as a template, as displayed in Figure 2.4B. If the strand is mis-repaired, it might lead to a mutation.

In the event that both strands of the DNA are destroyed, and the regions of damage are widely separated (see Figure 2.4C), the damage can still be repaired, as each break would be addressed independently. Conversely, when the damages in the two strands are opposite each other or isolated by only a few base pairs, this might cause a DSB, which leads to the cleavage of chromatin into two sections (see Figure 2.4D).

2.3 Linear energy transfer

Substantial variation is seen in the spatial deposition of the ionising radiation generated by different particles (see Figure 2.5). Consequently, this has led to the development of the linear energy transfer (LET) concept within the context of radiobiology. The LET for a specific radiation type explains the local energy deposition density, which significantly influences the biological radiation effects. The LET can be represented in units of eV or KeV per μm. Additionally, the LET of a charged particle is proportional to the square of the charge and inversely proportional to the particle's kinetic energy (i.e., LET $\propto Q^2/E_k$).

The interaction of photons produces fast electrons, while neutrons give rise to recoiled protons. Additionally, the spatial distribution of ionising events produced by proton beams varies compared to electron beams. Ionising events from photons are minimal, thus, they are referred to as sparsely ionising radiation, or well-known low energy transfer (low-LET) radiation.

As X-rays possess a LET of approximately 0.4 keV μm−1, they are categorised as low-LET radiation. Conversely, the alpha-particles possess a LET of approximately 100 keV μm−1 and are a classical type of high-LET radiation (see Table 2.1). Typically, for a specific absorbed dose, the ionisation paths of high-LET radiation deposit their energy over a considerably shorter range. Thus, they have a greater destructive effect on tumour cells compared to the spare ionisation patterns associated with low LET radiations (Bushberg and Boone, 2011).

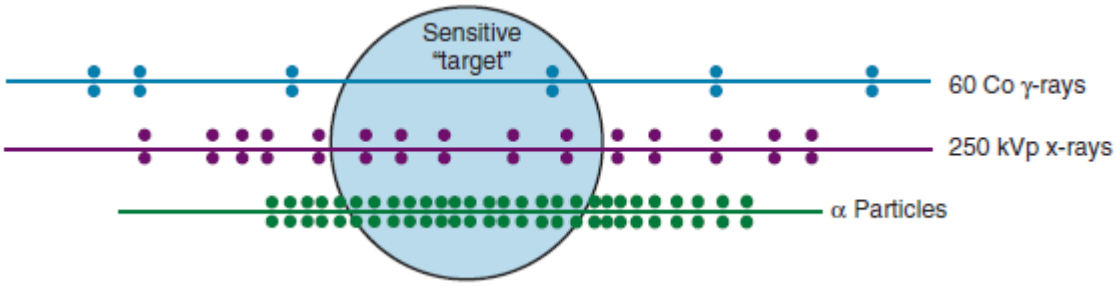

Figure 2.5: Discrepancy in the density of ionising events along an incident particle's path for radiations of diverse values of LET. The more closely spaced the ionising events, the more radiation energy would be imparted in the region of interest. Thus, the radiation nature would be more biologically efficient per unit dose (Gunderson and Tepper, 2015).

In addition to the aforementioned, it is vital to note that ionising radiation is deposited in increasingly energetic packets that are categorised as short tracks (500–5000 eV), blobs (100–500 eV) or spurs (≤100 eV deposited). Each of these yields a few to several dozen ionised atoms along its path (see Figure 2.6). If the clusters of ionising events (thus, either spurs or blobs) have a diameter that approximately equates to the dimension of the DNA (2 nm), it is possible for these ionising events to cause damage to multiple target sites (Gunderson and Tepper, 2015).

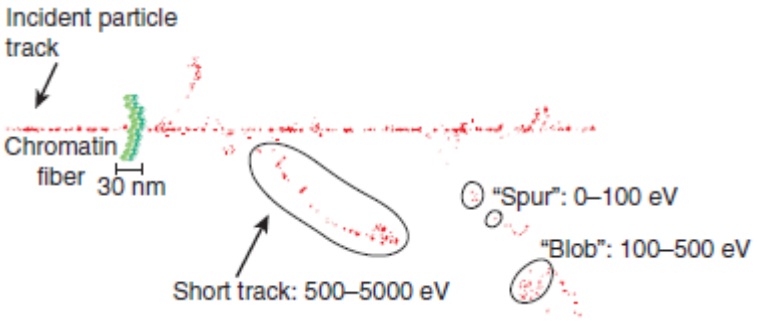

Figure 2.6: Energy deposition events along the particle's path. An individual event is categorised in accordance with the amount of energy deposited locally. Thus, this indicates the number of ionised atoms created (Gunderson and Tepper, 2015).

Table 2.1: Linear energy transfer values for several types of ionising radiation (Murshed, 2019).

Beam quality	LET (KeV/um)
Cobalt-60 (1.17-1.33)	0.2
X-rays (6-15 MeV)	0.4
Beta particle (1 MeV)	0.4
Protons beam (150 MeV)	0.5
Neutrons	0.5–100
Carbon ions	40–90
Alpha particles	50–200

2.4 Deterministic and stochastic effect of radiation

Radiation effects have been assessed in terms of radiation-induced cell death. Most of the body's tissues and organs are uninfluenced by the loss of small amounts of cells. However, the loss of a substantial number of cells will lead to an observable harm, which typically presents as a loss of tissue function. At small radiation doses, the probability of causing harm is negligible. However, once a specific threshold dose is exceeded, the likelihood of harm rises rapidly with the dose – up to 100%. This effect is commonly referred to as deterministic. Figure 2.7 exhibits a schematic representation of the severity of the deterministic influence as a function of the radiation dose. Figure 2.7 also shows the indicated threshold dose. Radiation-induced cataracts are the result of a deterministic effect because there is a threshold dose (McClellan, 2019).

The severity of the effect is associated with the quantity of the radiation dose. Henk et al. (1993) determined that the adult lens can tolerate a total radiotherapy dose of 6 Gy without indicating any symptoms of cataract formation. This study also has revealed that irradiating the lens to dose of 15 Gy or greater would almost invariably result in visual impairment.

If the irradiated cell is viable but modified, then the outcome of irradiation differs substantially. Moreover, such a modification is retained beyond the irradiation period. The delayed effect of such a reaction is carcinogenesis. Thus, the possibility of inducing cancer rises with each dose, but without a threshold dose. Notably, the prognosis of the cancer is not dose related. This implies that a cancer induced by 50 Gy is not more severe than a cancer induced by 0.5 Gy. Such an outcome is perceived as the stochastic effect of radiation (random effect).

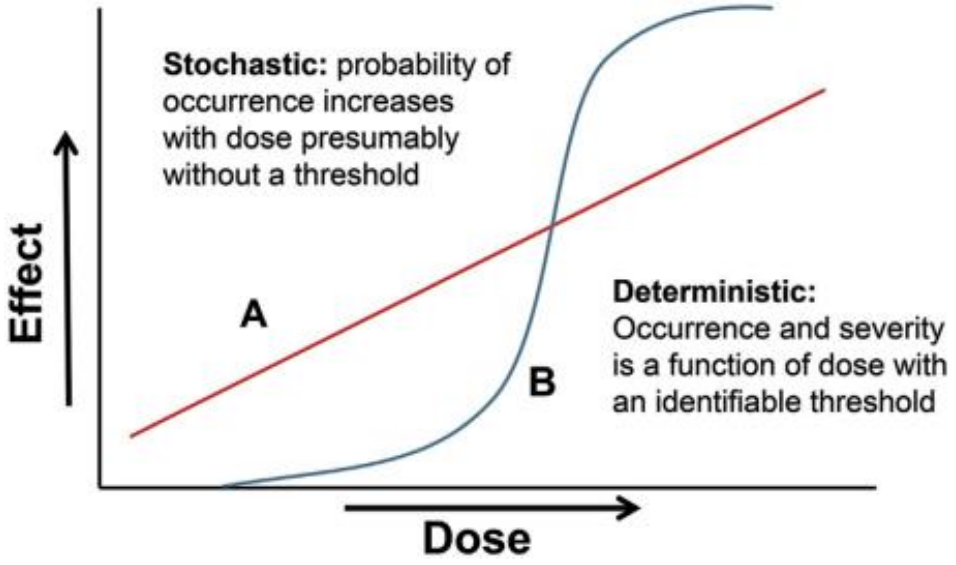

Figure 2.7: Schematic interpretation of two fundamentally distinct radiation dose-effect relations. (A) For a stochastic effect, the likelihood of incidence increases with the received radiation dose, presumably without a dose threshold. (B) The deterministic effect possesses a threshold with the radiation dose, and hence, the severity of the outcome is associated with a specific amount of a radiation dose (McClellan, 2019).

2.5 Cell survival

What is implied by 'survival'? Cells survival, or its inverse, cell death, can be interpreted differently depending upon the context; hence, a specific description is crucial. For instance, for differentiated cells that are incapable of proliferating, such as nerve and muscle cells, death is interpreted as the loss of a particular function (Williams, 2019).

The opposite is true for proliferating cells, such as those of the intestinal epithelium or stem cells in the haematopoietic system. In the latter, the loss of ability for sustained proliferation (also well-known as a loss of reproductive integrity) is a reasonable description. Crucially, this loss of reproductive integrity is often recognised as reproductive death (Williams, 2019).

It is crucial to note that at the physical level, cells might remain physically existing and apparently intact. Moreover, it might also have the ability to make proteins or synthesise DNA.

However, if cells have lost the ability to divide indefinitely and generate a substantial quantity of progeny then according to the definition, cells have not survived (dead). Additionally, surviving cells that have retained their reproductive integrity and are capable of proliferating indefinitely to generate a massive clone or colony are conceived to be clonogenic. Thus, for a tumour to be eradicated, it is only crucial that cells are "killed" within the context that they are rendered incapable to divide. If they are unable to divide then they would not produce additional growth or spread of the malignancy (Douglass, 2018).

Furthermore, the capacity of an individual cell to grow into a large colony that can be clearly perceived with the naked eye is conclusive evidence that such a cell has maintained its reproductive integrity. The loss of this capacity as a function of the radiation dose is characterised by the dose-cell survival curve. A cell survival curve is a plot of the fraction of surviving cells following its exposure to an incremental dose of radiation. The dose-survival curve can be assessed through use of clonogenic assays (see Section 2.6). Additionally, mathematical models such as the single-target model, the single-multivariable target model and the linear-quadratic model are also used to describe the cell survival curve (see Section 2.7).

2.6 Cell survival colongenic assay

Regarding cell death, there is a vital need to recognise how mammalian cell death is defined and quantified following irradiation in vitro and in vivo. The colony-forming assay is the gold standard for examining cell killing by radiation. This procedure involves irradiating tumour cells in a suspension culture. Using modern tissue culture techniques, it is possible to extract a specimen of live cells from diverse species of mammals such as humans, mice or rats.

These tissues are then chopped into small segments and prepared as a single-cell suspension using the enzyme trypsin. These cells are then seeded in a culture dish and maintained at adequate environmental conditions to produce colonies.

Once the mammalian cell colonies consist of approximately 50 cells, they become noticeable to the naked eye, as exhibited in Figure 2.8. Attainment of this cell quantity typically requires an estimated six to seven cell divisions. Cells experiencing fewer or no divisions (invisible) are indicated as dead. The quantity of colonies is counted either with a haemocytometer or an electronic imaging system and compared to the initial quantity of cells that were plated. The plating efficiency (PE) of a cell population can be quantified as the number of colonies observed divided by the number of cells plated (Munshi et al., 2005).

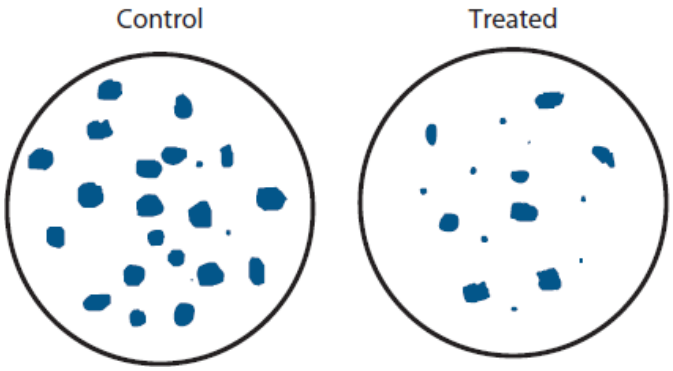

Figure 2.8: The fundamental principle of quantifying a cell surviving fraction. (A) Unirradiated cells and (B) irradiated cells (Williams, 2019).

To study the impact of radiation on the cells, many Petri dishes are plated under the same conditions using genetically identical cells. One set of dishes are not irradiated and are maintained as controls. The remaining Petri dishes are irradiated to various radiation doses. To allow colonies to arise from the surviving cells, both the irradiated cells and the control cells are incubated for a given time (from a few days to a couple of weeks). Such an investigation is termed a 'clonogenic' or a 'survival' assay (see Figure 2.9). The sustained proliferation of a single cell is the assumed mechanism for the formation of a colony. The surviving fraction (SF) for each radiation exposure can be calculated using Equation (2.2).

$$\mathbf{SF} = {}^{\#\ \mathbf{of\ colonies\ perceived}}\Big/\Big(\ \mathbf{\#of\ cells\ seeded} \times \left[\frac{\mathbf{PE}}{\mathbf{100}}\right]\Big) \qquad \mathbf{(2.2)}$$

The preceding process described how an in vitro survival curve could be established. To quantify in vivo cell survival, two clusters of experimental tumours must be employed, which are commonly implanted subcutaneously in mice (Williams, 2019). Once implanted, one tumour group should be exposed to radiation while the other is not irradiated and maintained as a control. A few weeks after irradiation, a cell suspension is prepared from both groups. The cell suspension is then plated out under identical conditions, as previously explained. The discriminating factor in this scenario is the exposure of the cells under in vivo conditions.

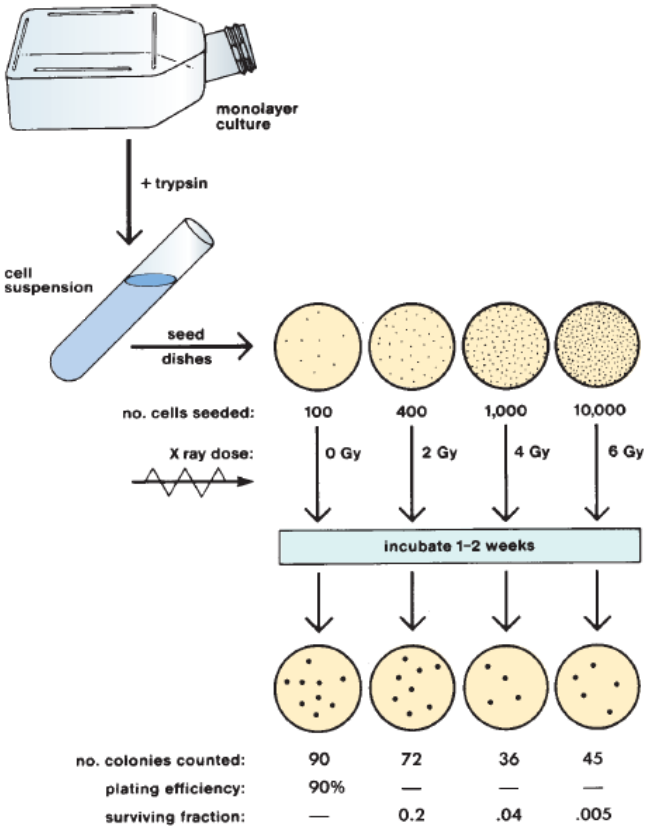

Figure 2.9: Diagram illustrating a typical cell survival experiment (Douglass, 2018).

2.7 Modelling the shape of the survival curve

In radiobiological research, there is an urgent need for predicting the responses of cells to different radiation qualities. The cell survival curve models apply a mathematical formula and statistical concept to describe, quantify and interpret the shape of the cell survival curves. The choice of the cell survival and dose-response model utilised can significantly affect the model outcomes. When characterising cell survival curves, three models are employed to date, each with its own strengths and weaknesses:

1. The single target/single-hit model.
2. The multi-target single-hit model (also termed the two-component model).
3. The linear-quadratic (LQ) model.

These survival curve models are briefly discussed in the following subsections.

2.7.1 Target theory

A simple strategy for modelling the mechanism by which radiation kills cells is based on the notion that specific DNA regions might exist that are critical to retaining the reproductive capability of cell. These sensitive areas are indicated as distinct targets for undertaking radiation damage.

By employing this strategy, the survival of cells following radiation exposure is supposed to be associated with the number of inactivated targets. Regarding definitions of target theory, two interpretations of this fundamental theory have formerly been practised: single hit-target theory and multi-target, single-hit theory.

2.7.1.1 Single hit-target theory

The single-hit target concept evolves from the assumption that a single hit on a single sensitive target within the cell causes cell death. This is also referred to as single-target single-hit inactivation, which results in the shape of the survival curve exhibited in Figure 2.10. The model is mathematically expressed as:

$$SF = \exp\left(\frac{-D}{D_0}\right) \tag{2.3}$$

Where SF is the fraction of cells that survived after receiving radiation dose D, and D_0 is the mean lethal dose. Additionally, the mean lethal dose refers to the dose at which 63% of the cells are killed, or 37% (or 1/e) of the original cell population survived. The value D_0 becomes a measure of the radiosensitivity of a biological specimen. For instance, cells are considered radiosensitive when they display a steep slope or a small D_0. Conversely, the existence of a large D_0 or a gradual slope implies a relatively radio-resistant biological system. It is vital to recognise that D_0 is defined as the dose that diminishes survival from 1 to 0.37 (i.e., to e^{-1}) or from 0.1 to 0.037, and so on (Powers, 1962) .

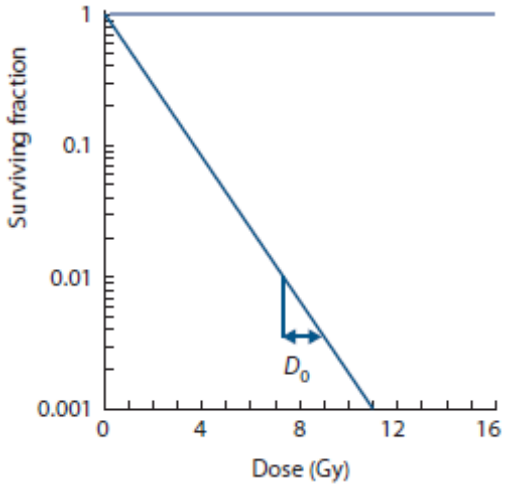

Figure 2.10: Shape of a single-target single-hit inactivation survival curve (Williams, 2019).

Thus, this form of 'single target single-hit' addresses a simplistic scenario where if a single cell receives a specific amount of radiation dose greater than D_0 then it would be damaged, otherwise, it would survive. Crucially, in such a scenario, the cell lacks the opportunity to repair the radiation damage. Thus, this scenario produces a straight survival curve. The single target single-hit notion is suitable for characterising the radiobiological reaction of some highly sensitive human cells (malignant and normal) as well as the reaction to high LET radiations (see Section 2.3) where a straight survival curve is evident.

However, the model cannot explain most scenarios noted through mammalian cell survival data as it does not account for the shoulder portion of the curve at low doses (e.g., repair of sublethal damage, see Section 2.10). Consequently, to address the shoulder portion of the cell curve, a superior comprehensive form of the target principle was introduced; the so-called multi-target single-hit model.

2.7.1.2 Multi-target single-hit theory

In this model, the concept of the *sensitive target within the cell* is extended in such a way that the cell is considered to possess multiple (*n*) sensitive targets rather than just a single target. Moreover, to achieve cell death, a single radiation hit should reach every one of those *n* targets. Thus, Equation 2.3 is modified to address the shoulder observed in the cell survival curve for sparsely ionising radiation, as shown in Figure 2.11. The shoulder portion of the cell curve suggests that there is more than one critical site in a cell, hence the need for the multi-target single-hit model, where a cell is assumed to have *n* targets and all these targets must be inactivated to cause cell death (Little, 1968).

$$SF = 1 - [1\text{-}\exp(-D/D_0)]^n \qquad (2.4)$$

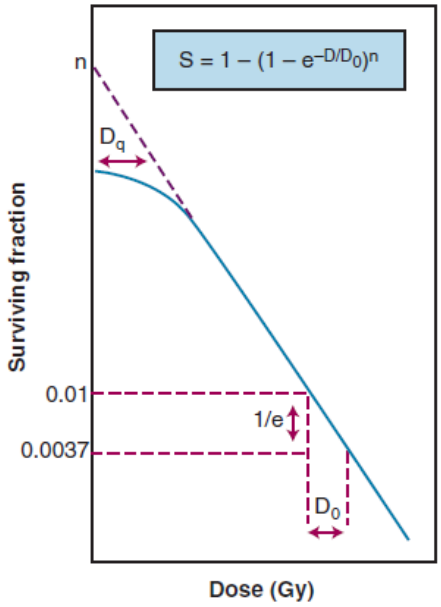

Figure 2.11: Cell survival curve of the multi-target single-hit inactivation model (Gunderson and Tepper, 2015).

In Figure 2.11, the D_q is established by extrapolating the straight part of the curve backward to the point of its intersection with the vertical axis. Thus, it is extrapolated to the point where the surviving fractions equal one. By setting the survival fraction to one, D_q represents a radiation dose below which there is no radiation influence. Thus, D_q is the minimum dose required for the realisation of a radiation effect. Both *n* and D_q are used to describe the width of the shoulder of the curve. If *n* is large, in the range of 10–12, the survival curve is noted to have a broad shoulder. If *n* is small, in the range of 1.5–2.0, then the curve has a narrow shoulder (Nomiya, 2013)

Regarding the radiobiological rationale, the multi-target single-hit theory is an intellectually attractive idea. However, numerous factors have challenged this concept. For instance, the predicted cell survival curve response has an initial slope of zero (a flat response) that corresponds to low radiation doses. Thus, the probability of cell killing would approach zero, a feature that is not supported by experimental data (Nomiya, 2013).

2.7.2 Linear-quadratic model

The linear-quadratic (LQ) model is widely accepted amongst the radiation oncology community. Moreover, this model offers a more detailed explanation of the radiation-induced cell killing. First, it provides a better fit for the initial shoulder region of the cell survival curve. Second, this model can also be applied in both clinical and experimental radiobiology. It commonly performs adequately in representing reactions to radiation through both in vivo and in vitro experiments.

Furthermore, several clinical situations have required the use of LQ principles as powerful clinical tools. The principles have been applied to model almost all the various dose rates and fractionation schemas, such as conventional fractionation, hypofractionation, hyperfractionation, accelerated fractionation, high dose rate brachytherapy, as well as combined brachytherapy and external beam radiotherapy (Qiu et al., 2020, Alaswad et al., 2019a, Guirado et al., 2020).

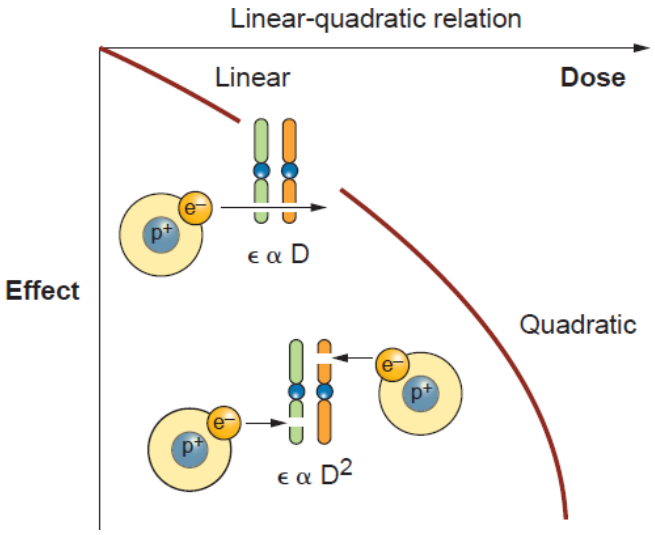

Figure 2.12: Fundamental principles of the LQ model. At low radiation doses, the two DNA damages are the result of a single electron set in motion due to the absorption of ionising radiation. The likelihood of interactions between the damages is proportional to the total radiation dose. At higher doses, the two DNA damages are caused by two separate electrons. In such instances, the likelihood of an event is proportional to the square of the radiation dose (Douglass, 2018).

In the LQ model, two parameters are employed to describe the curved portion of the survival curve, namely α and β. The survival curve is seen to consist of both a linear and a quadratic portion (Douglas and Fowler, 1976, Fowler, 1989, Jones, 1999). A possible explanation of these two contributions to the cell survival curve is that the α portion represents death due to "single-hit" events. Thus, in such cases, the lethal damage (or death) is due to a single incident particle. In contrast, the β expression reflects the "multiple-hit" cell death originating from the DNA damage of two separate ionising events. This notion is depicted in Figure 2.12.

Accordingly, the former linear component that accounts for cell killing due to single hits is described by the following formula:

$$\boldsymbol{SF_1 = \exp(-\alpha D)} \qquad \textbf{(2.5)}$$

Additionally, the β term, which characterises the curving component and has units of inverse dose squared, is that which describes the two-hit survival component. This is represented by the following formula:

$$\boldsymbol{SF_2 = \exp(-\beta D^2)} \qquad \textbf{(2.6)}$$

Assuming that the single-hit and two-hit mechanisms are independent, then the overall expression for the cell survival curve is represented by the following formula:

$$\mathbf{SF = SF_1 . SF_2 = \exp -(\alpha D + \beta D^2)} \qquad \textbf{(2.7)}$$

Of note is that the α/β ratio has units of dose. Moreover, α/β is equal to the dose D at which the linear and quadratic contributions to the survival curve are equal, as described in Figure 2.13 (e.g., α/β = 10 Gy). Crucially, the shoulder width can also be characterised using the α/β ratio. In particular, a higher α/β ratio indicates a narrower shoulder. Conversely, a lower α/β ratio indicates a wider shoulder (see Section 2.8).

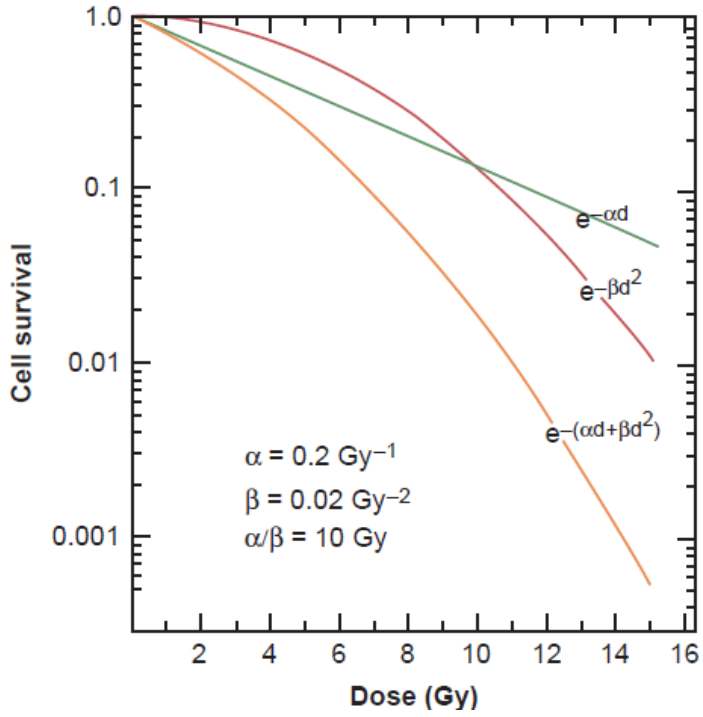

Figure 2.13: Typical LQ cell survival curve. The α/β value is the dose at which both the single- and multi-hit events contribute equitably to cell killing. In this scenario, α/β = 10 Gy, which is a value identical to acutely reacting tissues(Halperin et al., 2020).

2.8 Early and late responding tissues

Different healthy tissues exposed to therapeutic ionising radiation exhibit varying degrees of response. The speed at which reactions evolve differs significantly from one tissue to another. Moreover, the speed of the response tends to profoundly rely on the amount of radiation dose deposited into the tissue.

Accordingly, the impact of radiation on tissues is frequently split into early- and late-reacting tissues. The intestinal epithelium, bone marrow cells and skin, for instance, are all examples of rapidly dividing self-renewing tissues. Thus, these tissues tend to have an early response to the influences of therapeutic ionising radiation. In contrast, the kidneys, lungs and the spinal cord are indicated as late-responding tissues (see Figure 2.4). The early-responding tissues tend to be capable of repopulating between fractions if the number of surviving cells is adequate.

On the contrary, late-responding healthy tissues require further caution because of their poor cell turnover and the unlikely chance of an adequate recovery following substantial radiation damage (Dörr, 2015). Modified fractionation schedules, as described in Chapter 3, consider these distinctions in tissue response to enhance the therapeutic ratio.

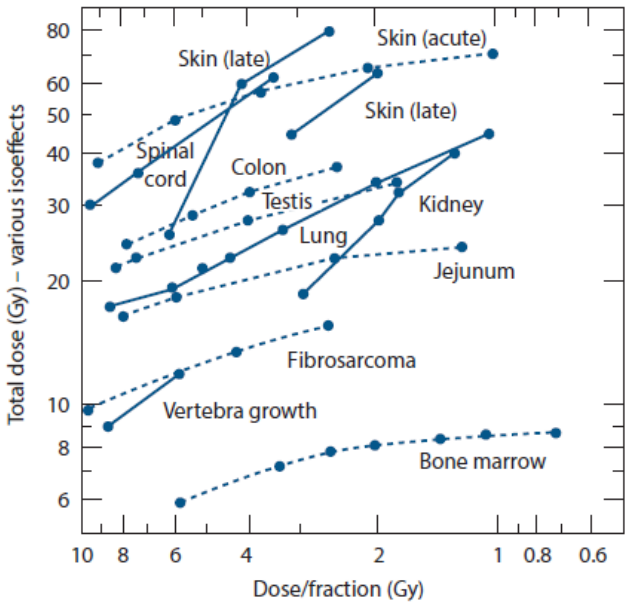

Figure 2.14: Correlation between total radiation dose (D) and dose per fraction (d) across a broad range of healthy tissues in experimental animals. Late-reacting tissues are represented by solid lines and broken lines represent early-reacting tissues. Solid lines clearly are systematically steeper in contrast with the early-reacting tissues (broken lines) (Williams, 2019).

The variation in patterns depicted in the dose-response curves for early- and late-reacting tissues is an explicit distinction in the reaction to radiotherapy fractionation of these two categories of tissues. It is clear from the curves that the late-reacting tissues are more sensitive to alterations in fractionation compared with early-reaction tissues. The overall outcome is indicated in Figures 2.14 and 2.16. Thus, compared to the use of a single acute dose, the application of a fractionated regime to the late-responding normal tissues ensures they are spared more for a specific degree of tumour damage. This raises questions concerning what exactly constitutes “early” or “late” reaction tissues. Using the above descriptions, early-responding tissues would possess a considerable proportion of cycling cells, whereas the late reaction tissues comprise considerable proportions of noncycling cells.

Thus, by employing this rationale, the radiosensitivity parameters α and β are a measure of the radiotherapy fractionation sensitivity of the cells. For instance, cells with a higher α/β, are less sensitive to the sparing effect of fractionation, such as early-responding tissues and tumours (see Figures 2.15 and 2.16). Note that this ratio is remarkably beneficial for estimating likely clinical outcomes. Low α/β ratios (1–5), indicate scenarios where the survival curves are bending rapidly at low radiation doses per fraction. Consequently, within and below the typical clinical radiation dose range (1.5–2.5 Gy per fraction) amendments in fraction size should have a noticeable impact on the isoeffect dose. Conversely, high values of α/β (6–14 Gy) imply a larger predominance of the linear expression α, so that variations in fraction size yield a minor influence on the isoeffect dose (Van Leeuwen et al., 2018, Scheenstra et al., 2014, Chi et al., 2007).

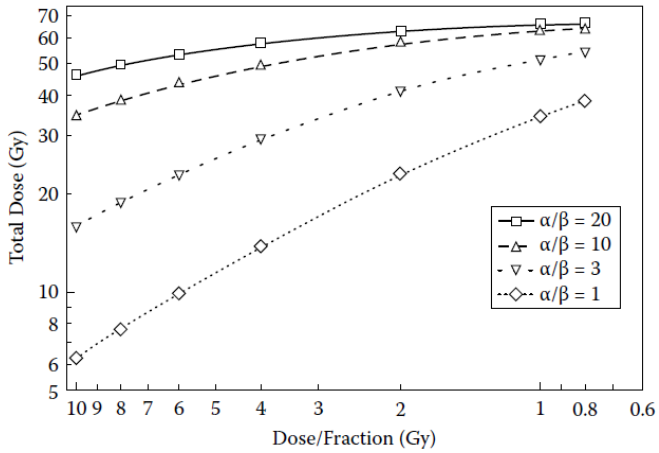

Figure 2.15: Variation of total radiation dose (D) with dose per fraction (d) for different α/β values (Chapman and Nahum, 2016).

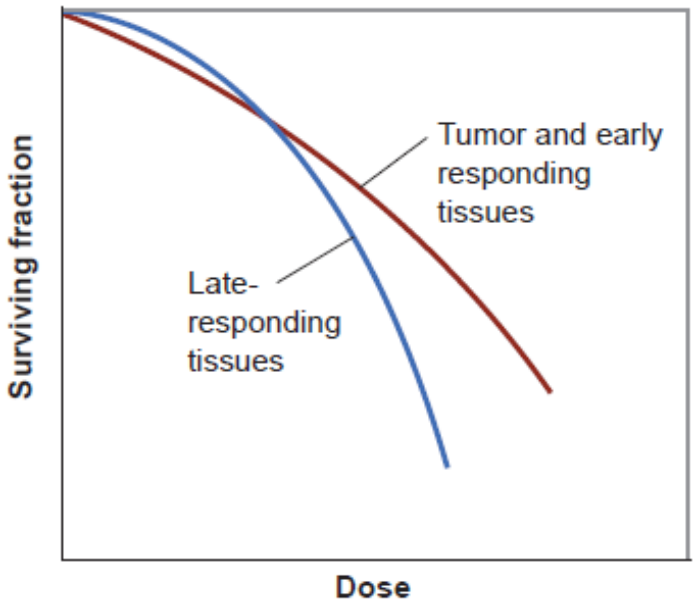

Figure 2.16: LQ survival curves for early- and late-reacting tissues. The cell survival curve for late-reacting tissues depicts a more extensive curvature compared to early-reaction tissues (Barrett et al., 2009).

2.9 Radiotherapy dose fractionation

Radiotherapy dose fractionation constitutes one of the most efficacious radiotherapeutic strategies. The strategy entails a process of delivering a total radiation dose over a period of several weeks rather than as a single acute dose. Fractionation takes advantage of the varying capabilities of normal and malignant cells regarding their ability to recover from DNA damage. Due to this difference, fractionation can enhance the destructive impact on tumour cells while simultaneously diminishing damage to healthy cells.

The fundamental principle of fractionation in radiotherapy can be understood through two simplistic notions. Dividing radiotherapy doses into multiple fractions spares healthy tissues as it enables the repair of sublethal damage (see Section 2.10). Moreover, this division allows for the repopulation of cells if the overall treatment period is adequately long (see Section 2.11).

Similarly, dividing a dose into several fractions enhances damage to the tumour owing to the resultant reoxygenation (see Section 2.12) and reassortment (see Section 2.13) of cells into radiosensitive stages of the cell cycle between radiotherapy dose fractions. It is these process that are often recognised as the four "R's" of radiobiology: repair, repopulation, reoxygenation and reassortment. The following sections describe these radiobiological phenomena in greater detail.

2.10 Repair

DNA damage can either lead to an SSB which is simply rectified, or a DSB, which can result in permanent alterations if the repairs processed are inadequate (such as the incorrect rejoining of chromosomes) or it may lead to cell death. Consequently, according to the level of lethality induced by ionising radiation, damage is subdivided into three types:

(1) Lethal damage (LD), which leads to irreparable cell death.

(2) Sublethal damage (SLD), which typically repairs within a few hours, thereby preventing cellular death.

(3) Potentially lethal damage (PLD), which can potentially damage the cell, but it also can be adjusted to repair the cellular damage under specific physicochemical environments.

All these damage processes are associated in clinical radiotherapy with the efficacy of treatment. Lethal damage is a definite endpoint in treatment, while sublethal damage and potentially lethal damage have variable impacts in the field of radiotherapy.

The predominant cell damage is sublethal, which has the potential to be repaired within hours unless an additional fraction of the radiotherapy dose is delivered. Repair of the DNA damage involves the healing of the radiation-induced damage in the interval between the two fractions of the dose.

However, application of the second dose shortly after the first application reduces the time available for the cell to repair the damage (Barendsen et al., 2001). Consequently, this leads to the cell dying, as indicated in the cell survival curves illustrated in Figure 2.17 (Douglass, 2018) .

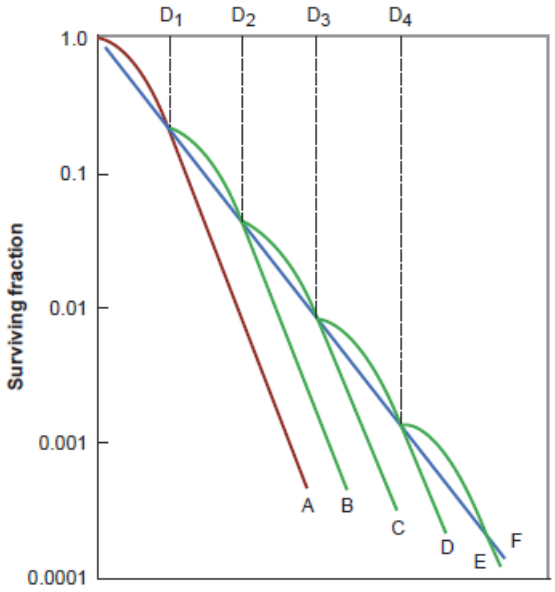

Figure 2.17: Typical cell survival curves exhibiting the influence of radiotherapy fractionation. Curve A is the survival curve for a single acute radiation dose. Curves B to F are survival curves resulting from the delivery of each dose as a sequence of small fractions of D1. Doses are delivered within a time frame between fractions, that is, adequate for the recovery of sublethal damage. Notably, the multi-fraction survival curves are shallower compared to the corresponding single dose curve (Douglass, 2018).

Within this context, healthy cells have an enhanced capacity to recover DNA breaks compared to malignant cells. Thus, splitting the total radiotherapy dose affords healthy cells the opportunity to repair the acquired sublethal damage between fractions. In contrast, the malignant cells with impaired DNA repair pathways have inferior capability to recover from ionising radiation damage to their DNA.

PLD is a type of DNA damage that has the potential to repair the damage if the post-irradiation conditions are suitable, as is the case with cell incubation following irradiation at either a reduced temperature of ≤20°C or treatment with inhibitors of protein synthesis. Moreover, in suboptimal ambiences, such as conditions of reduced temperature, cell survival increases as cell entry into mitosis is delayed. The ensuing delay increases the time cells have to repair radiation-induced DNA damage.

Alternatively stated, the repair mechanism occurs post-irradiation whenever cells are given a sufficient period to repair the damage instead of being allowed to proliferate through to the mitosis phase (Chew et al., 2019b). This type of damage has been observed in both in vitro and in vivo assessments with chemotherapeutic drugs or radiation dosages. Notwithstanding the foregoing, such a drastic treatment condition (e.g., reduced temperature) does not mimic a physiological condition that is ever likely to be perceived during a radiotherapy course. Thus, the importance of PLD to clinical radiation therapy is a subject of debate.

Note that at lower radiotherapy doses, more sublethal damage can be repaired. However, at higher radiotherapy doses, the likelihood of sublethal damage repair diminishes. Additionally, SLD repair relies heavily on the spatial distribution of the ionising events generated by the different particles (e.g., the LET of radiation). For instance, the type of radiation applied governs the broadness of the shoulder observed in acute survival curves, thereby resulting in differences in the amount of SLD repair, as indicated in Figure 2.18. PLD and SLD repair are both observed with low-LET radiations (i.e., the cell survival curves of X-rays and γ-rays have a noticeable broad shoulder) but are absent for high-LET radiations (α-particles).

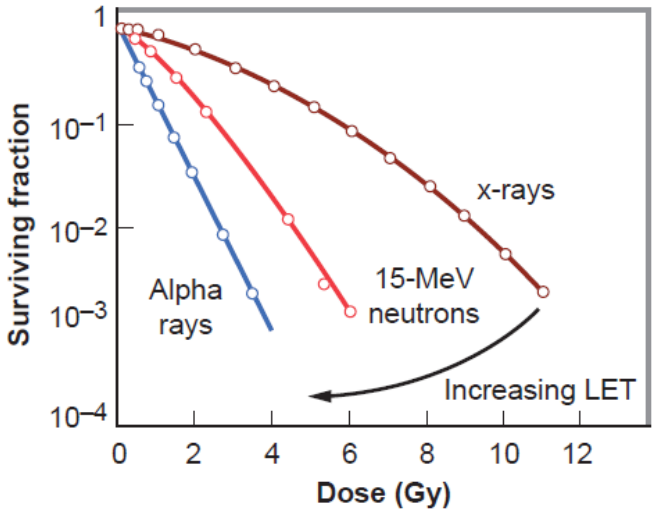

Figure 2.18: LQ survival curves for X-rays, 15-MeV neutrons and alpha particles. Increases in the LET of the ionising radiation result in a steeper survival curve slope and a smaller extension of the initial shoulder.

2.11 Repopulation or re-generation

Both healthy tissues and tumours are able to increase their cell production rate due to radiation-induced cell killing. This attribute is referred to as 'regeneration' or 'repopulation'. A conventional radiotherapy course tends to occur over a period of five to seven weeks. This is considered a sufficient duration to permit considerable cell proliferation to occur. Prolonging a fractionated radiotherapy course has a profound impact on normal tissues. This prolongation diminishes severe side effects as it facilitates recovery from radiation damage (see Section 2.10). However, it can also adversely affect or prevent the attainment of optimum local tumour control to a certain degree.

Additionally, it has been demonstrated that the repopulation paradigm of tumours and healthy tissues after the initiation of irradiation tends to be distinguished by a lag phase (delay) prior to the rapid proliferative response (see Figure 2.19). As soon as the proliferative response becomes noticeable, though, it can be considerably vigorous (Withers et al., 1988). While this progression is distinctly favourable for healthy tissues to recover from radiation damage, rapid proliferation in tumours is evidently undesirable.

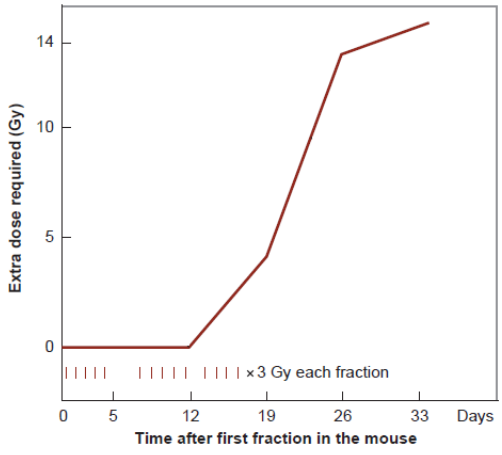

Figure 2.19: Additional dose required to compensate for the proliferation effect in the skin of mice as a function of time following a radiotherapy treatment course of 3 Gy per fraction. A delay (lag-time) followed by a rapid increase in the rate of proliferation is characteristic of time factors in proliferating healthy tissues. In mouse skin, the time delay is approximately two weeks; whereas, in humans, it is approximately four weeks (Fowler, 1984).

The inevitable conclusion from the Withers et al. (1988) study is that radiotherapy, particularly for fast-growing tumours, must be completed as soon after initiation as practicable (see Figures 2.20 and 2.21). It might be preferable to delay the initiation of a radiotherapy course instead of introducing gaps during treatment that result in extending treatment time. Additionally, if the total treatment period is far too long, the efficacy of subsequent radiotherapy dose fractions is compromised owing to the surviving cells in the tumour have been triggered into rapid repopulation.

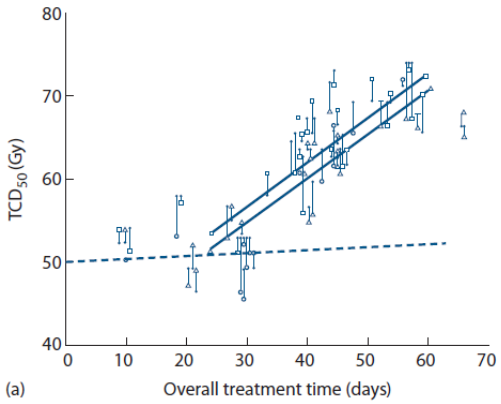

Figure 2.20: Tumour control dose (TCD50) as a function of the total radiotherapy course (Williams, 2019).

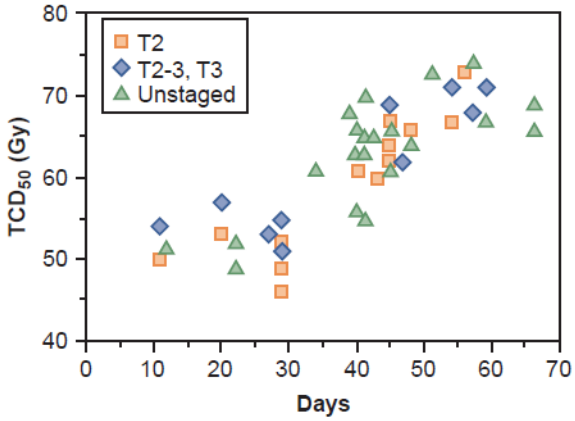

Figure 2.21: Tumour control dose (TCD50) as a function of the total radiotherapy course according to the T descriptor of the tumour node metastasis classification system (Halperin et al., 2020).

Notably, Withers et al. (1988) analysed data for patients who were only treated with a radiotherapy modality. It might be assumed that comparable clinical observations in terms of the repopulating effect are experienced in chemotherapy or in the combination of chemotherapy and radiotherapy regimens. Considering this, evidence from NSCLC demonstrates inferior clinical outcomes from radiotherapy treatment preceded by a course of chemotherapy, in particular, the sequential chemoradiotherapy approach (see Chapter 5). These findings might be explained by the influence of the accelerated tumour repopulation triggered by the induction of chemotherapy.

2.12 Reoxygenation

For healthy tissues to retain viability, they require a regular supply of oxygen and nutrients. This mechanism is managed through a functional blood supply. Solid tumours do not differ from healthy tissue in this respect; they also have the same metabolic requirements. To accomplish this, tumours initially employ the blood supply of the host organ in which the tumour arises. Over time, the blood supply becomes inadequate to satisfy the high demands of the growing tumour mass, thereby leading to areas of hypoxia (Shannon et al., 2003).

Crucially, hypoxic tumours (i.e., exhibiting low oxygen levels) are radioresistant to photon radiation. Therefore, their inactivation requires a higher dosage of radiation. Oxygenated cells are two to three times more sensitive to irradiation compared with hypoxic cells. Consequently, a modest dose of radiation would kill a greater number of oxygenated than hypoxic cells. A typical example of survival curves for mammalian cells irritated to X-rays in the absence and presence of oxygen are displayed in Figure 2.22A (Douglass, 2018).

The ratio of radiation doses delivered under hypoxic to oxic conditions required to attain the same biological outcome is termed the oxygen enhancement ratio (OER). The OER of sparsely ionising radiations (e.g., low-LET), such as X-rays and gamma rays, has a value in the range between 2.0 and 3.0. Moreover, the OER is determined for several biological systems with diverse endpoints, and its value for sparsely ionising radiations always tends to lie within this range.

For densely ionising radiation such as alpha particles, the survival curve has no initial shoulder (see Figure 2.22 C). In this instance, the observed survival curves in the absence or presence of oxygen are identical. Thus, the resultant OER is unified and does not yield an oxygen effect.

Additionally, for radiations of intermediate ionising density such as neutrons, the survival curve exhibits a substantially diminished shoulder. In such instances, the impact of oxygen is noticeable, though less than that observed for X-rays. In the instance displayed in Figure 2.22 B, the OER for neutrons is approximately 1.6 (Douglass, 2018, Brown, 1999). In sum, the oxygen influence is notably substantial in the event of sparsely ionising radiation, such as X-rays, whereas it is negligible for densely ionising radiation.

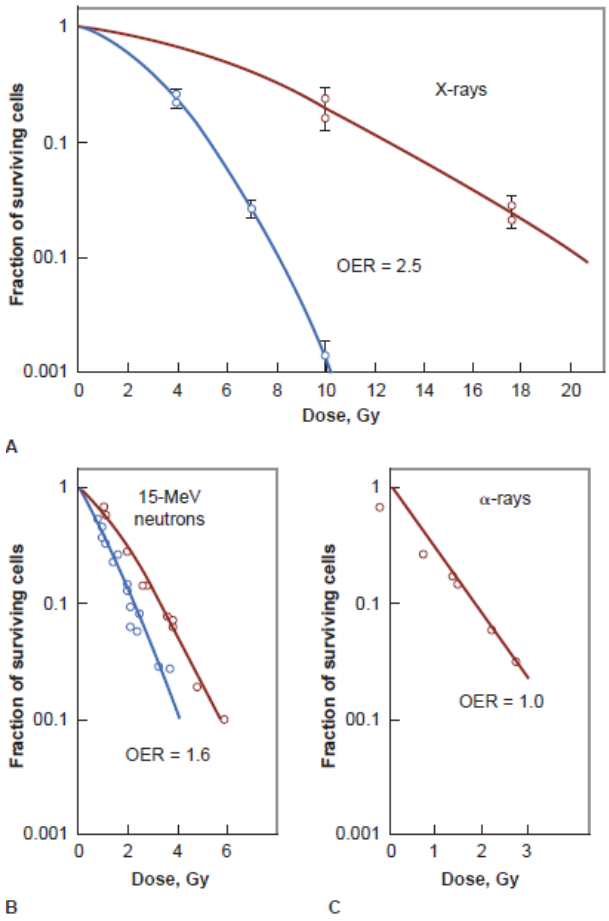

Figure 2.22: OER for different forms of ionising radiation. (A) X-rays display a higher OER of 2.5. (B) Neutrons have an OER of 1.6. (C) α-particles display a unified OER (Douglass, 2018).

The reoxygenation of hypoxic tumour cells is feasible and remarkably productive when radiotherapy dose fractionation is applied. This is attributed to the increased likelihood that the initial radiotherapy dose fraction would eliminate a substantial amount of the well-oxygenated and radiosensitive cells situated in the immediate vicinity of the tumour's blood supply. Subsequent periods between fractions allow the relatively hypoxic cells to increase their supply of oxygen.

Consequently, this leads to the cells increasing in sensitivity during subsequent radiation doses (Hong et al., 2016). This mechanism of radiotherapy reoxygenation is described in Figure 2.23 (i.e., the potential of tumour self-sensitisation is feasible due to reoxygenation).

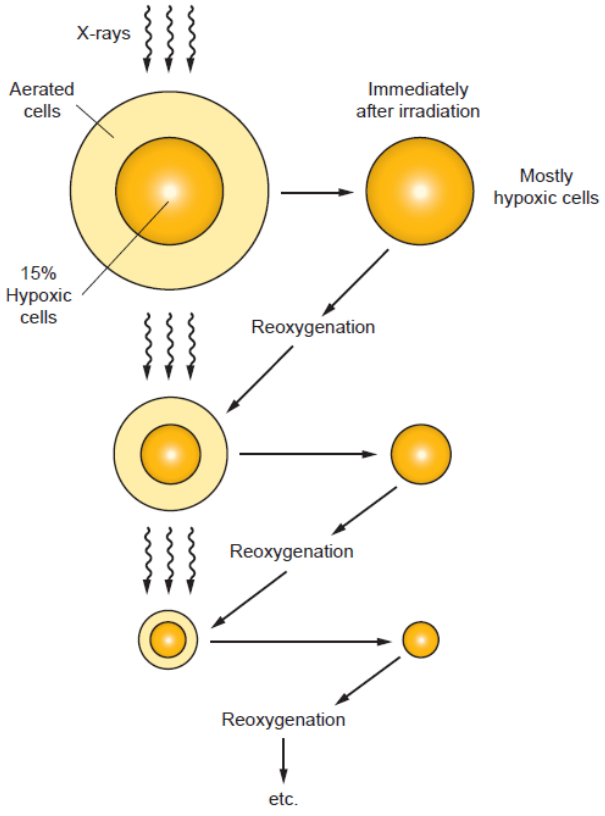

Figure 2.23: Reoxygenation process. Tumours consist of a combination of hypoxic and aerated cells. A radiation dose of X-rays would damage a larger amount of oxic cells compared to hypoxic cells given the increased radiosensitivity of aerated cells. Consequently, immediately following an irradiation dose, most cells in the tumour are hypoxic. However, the reoxygenation of the cells will result in the return of the pre-irradiation pattern. If ionisng radiation is delivered in a sequence of fractions that are sufficiently separated in time for the reoxygenation process to evolve, then the subsequent emergence of hypoxic cells will not have a considerable impact on the tumour control response (Hall and Giaccia, 2012).

In view of the aforementioned findings, the generation of ‘peroxy radicals’ during radiotherapy is the primary reason for describing the killing efficiency of tumour cells. When photon radiation is directed into the body, it interacts with the abundant water molecules present in the body. This interaction generates high energy electrons that lead to the production of hydroxyl free radicals (OH) that are highly reactive and causes damage to the DNA, as described in Section 2.2. However, the resultant damage is potentially repairable, thus enabling the restoration of the damaged DNA and preventing cell lethality. Additionally, if the free radical reacts with oxygen prior to the collision, it produces a different type of radical termed a ‘peroxy radical’. The damage born of the effect of peroxy radicals is challenging and impossible to repair. Consequently, this form of DNA damage is ‘fixed’ into a permanent and irreparable state (West and Slevin, 2019). Thus, this describes the fundamental notion of the influence of oxygen in radiotherapy.

2.13 Reassortment

Reassortment (also referred as redistribution) describes that cells exhibit differential radiation sensitivities during the various cell cycle phases (see Figure 2.24). Each cell’s life cycle consists of four phases that are denoted as follows:

1. Gap1 (G1) phase: the cell growth phase where cells copy organelles and increase in physical size.
2. S phase: the cell synthesis phase involving the complete copying of the DNA in its nucleus.
3. Gap2 (G2) phase: a further growth phase during which a cell produces more organelles and proteins. During this phase, the cell also initiates the restructuring of its contents in preparation for mitosis.
4. Mitotic (M) phase: During the M phase, the cell divides its copied DNA and cytoplasm resulting in the formation of two new daughter cells.

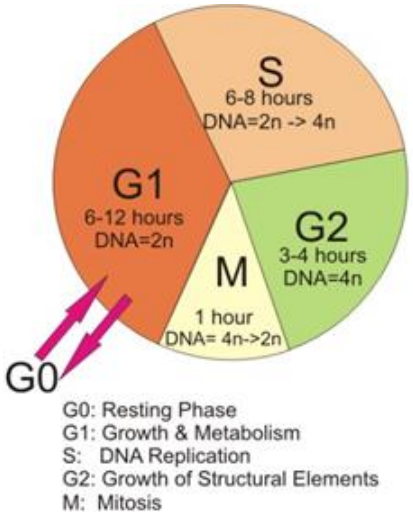

Figure 2.24: Four stages of the cell cycle (Panawala, 2019).

Due to this natural cycling process, the cells display an asynchronous distribution along the cycle. This feature assists fractionated radiotherapy as it causes the cells to develop different radiosensitivities for the different cell-cycle phases. Evidence has shown that cells exhibit the greatest resistance to radiation during the S-phase, and most notably in the final period of the S-phase. In contrast, cells display the greatest levels of sensitivity during the G2 and the mitotic phase. It is during these latter two phases that the cell survival curves display a steeper slope and are, to a large degree, shoulderless (see Figure 2.25).

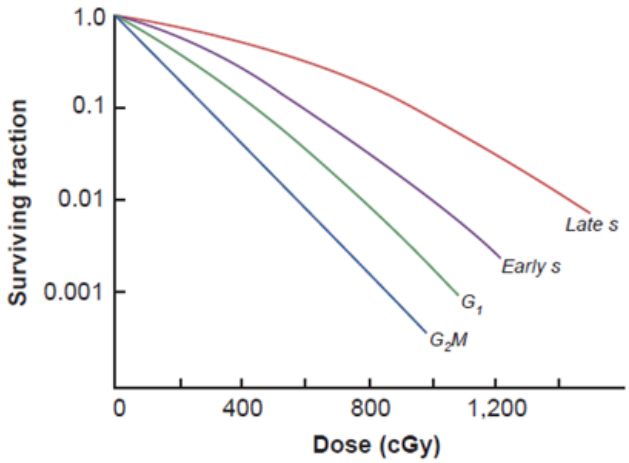

Figure 2.25: Influence of the cell cycle stage on survival curves. Notable variations in survival are observed according to the cell cycle phase (Halperin et al., 2020).

The resistance in S phase is hypothesised to be attributed to the homologous recombination of the chromosomes. This process evolved as a consequence of the increase in the availability of unharmed sister templates in the S phase. Thus, this facilitates the adoption of a sister chromatid as a template for the faithful recreation of the damaged region and the accurate joining of the ends. The sensitivity in the G2 phase potentially arises from the short period available for cells to repair radiation damage before continuing to divide. Furthermore, the time required for the completion of each of the four phases differs. Whilst the DNA synthesis phase takes approximately 8 h to complete, the time a cell takes to complete the mitotic phase is approximately 1 h, the G2-phase is 3 to 5 h and the remainder of the cell cycle, which consists of the G1-phase, is any period from as little as 6 to 12 h. Thus, the G1-phase shows the greatest degree of variability (Schaue and McBride, 2015).

The exposure of an asynchronous population of cells (e.g., different phases during the cell cycles) to a large radiation dose, results in higher number of cells being damaged in the sensitive phases of the cell cycle compared to the resistant phases. Thus, the end result of such an exposure is the production of a cell population that is partially synchronised. These findings imply that the delivery of radiation doses in short time intervals will result in scenarios that may influence the total number of cells killed, and hence, adversely affect local tumour control. If the surviving cells have time to abandon their resistant phase to enter a more sensitive phase, then the impact of a subsequent radiotherapy dose would be more noticeable. This phenomenon is termed redistribution or reassortment (Chapman and Nahum, 2016).

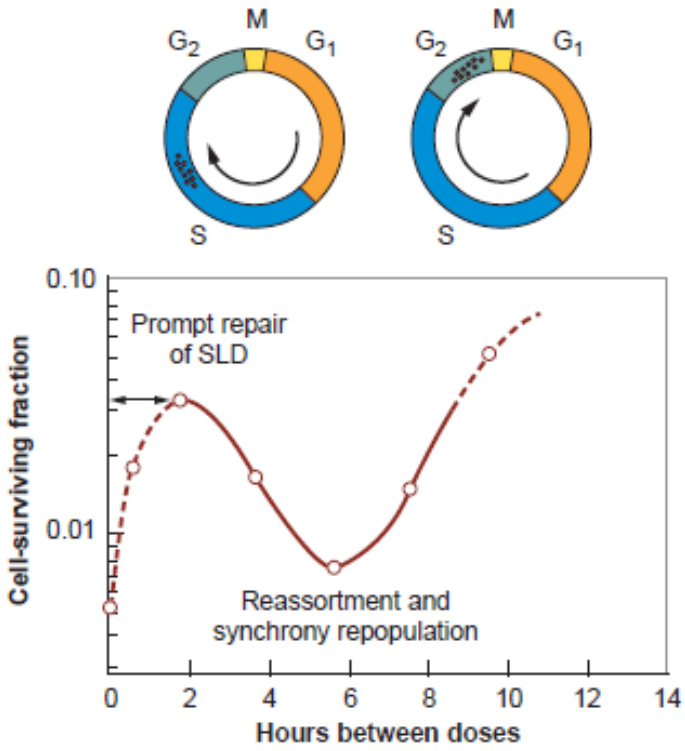

Figure 2.26: Cell survival experiment on Chinese hamsters irradiated with two X-ray fractions over different time frames between two radiation doses. Survivors of the initial radiation dose are predominantly in the resistant (late S) stage of the cycle. If the period between radiation doses is approximately 6 h, then the resistant cells would progress to the more radiation sensitive G2 and M phases (Douglass, 2018).

Notably, the redistribution of cells into the sensitive phases of the cycle is reliant on the capability of the cells to proliferate. For instance, the ordinary non-proliferating tissues, such as connective tissues and the spinal cord, might not be influenced. However, tissues undergoing rapid proliferation, such as tumours, can be more sensitised to redistribution.

Thus, the discrepancy in cell sensitivity is a fundamental factor that must be considered for the delivery of radiation treatment. This is particularly beneficial in the delivery of fractionated doses of ionising radiation as it improves the probability of tumour cells entering a sensitive cell cycle at a certain stage during the treatment regimen, which leads to enhanced tumour cell kill (see Figure 2.26).

Chapter 3 Optimal tumour control for early-stage non-small-cell lung cancer

3.1 Introduction

Radical surgery remains a treatment mainstay for early-stage NSCLC; however, many patients with NSCLC are not candidates for surgery due to comorbidities, such as cardiopulmonary dysfunction, stage I, II or chronic obstructive pulmonary disease or tumour size during stages III and IV (Hatton et al., 2016), or because they refuse surgery altogether. Consequently, curative external-beam radiotherapy is commonly regarded as an alternative therapeutic procedure for early-stage NSCLC (Din et al., 2013).

The conventional fractionation (CF) radiotherapy schedule, as proposed by the Radiation Therapy Oncology Group (RTOG), is 45–70 Gy and includes one treatment per day of 1.8–2.5 Gy per fraction over 6–8 weeks (Taremi et al., 2012). Notably, CF radiotherapy has historically been associated with poor local tumour control (35%, 17% and 9% at one-, two- and three-year follow-ups, respectively) (Baumann et al., 2011). Another fractionation scheme suggested by some institutions in the United Kingdom is continuous hyperfractionated accelerated radiotherapy (CHART), which prescribes radiation doses of 54 Gy via 1.5 Gy per fraction delivered 3 times per day. In the United Kingdom, CHART is recommended as the standard of care for patients undergoing a radiotherapy course for NSCLC. This fractionation scheme has the potential to improve local tumour control up to 66%, 40% and 20% at one-, two- and three-year follow-ups, respectively (Sanganalmath et al., 2018a).

In addition, improved survival and local tumour control can be attained using stereotactic ablative radiotherapy (SABR), a state-of-the-art technique that is considered the optimal treatment for patients with early-stage NSCLC for whom surgical procedures are not appropriate. Several studies and prospective phase II trials have confirmed that the rates of local tumour control are as high as 83–96% (Hamamoto et al., 2012, Andratschke et al., 2011, Takeda et al., 2009, Dunlap et al., 2010, Kopek et al., 2009, Brown et al., 2009), significantly higher than the data reported for three-dimensional conformal radiation therapy (3D-CRT) and CHART. SABR is typically performed at a much greater dose per fraction than either 3D-CRT or CHART, and it has generated outstanding local tumour control in early-stage NSCLC (96%, 89% and 84% at one , two- and three-year follow-ups, respectively) (Hamamoto et al., 2012). The authors of the RTOG 0236 research study recommended that SABR can be regarded as the main therapeutic procedure for patients with early-stage NSCLC (Baumann et al., 2011), and it can be argued that SABR is also preferable to surgery for most patients with early-stage NSCLC.

However, from a radiobiology perspective, the application of the linear-quadratic (LQ) concept at such a high dose per fraction is controversial. Considerable debate exists in the literature regarding the accuracy of LQ-based tumour control probability (TCP) modelling for predicting the clinical outcomes encountered at high dose-per-fraction, such as for SABR treatment of NSCLC. For instance, Kirkpatrick et al. (2008) argued that the LQ model, which expresses the mechanism of the radiation's interaction with and destruction of DNA, and therefore represents a fundamental component of the TCP model, may be inapplicable to radiation therapy protocols that employ a high dose per fraction. A few authors have defended this view by stating that the eradication of tumours using hypofractionated radiotherapy protocols is determined by biological concepts (e.g., vascular and stromal damage) that are more qualitatively complex than those encountered with standard or hyperfractionated radiotherapy protocols. Therefore, these biological phenomena are not accounted for by the LQ model (Brown et al., 2014, Fuks and Kolesnick, 2005, Kocher et al., 2000).

Similar arguments were made by Park et al. (2012) who indicated that radiotherapy treatment courses that apply doses of more than 8.0 Gy/fraction are likely to produce significant vascular damage and injury to the intratumoural microenvironment, thereby leading to indirect tumour cell death; notably, this is not the case for the standard treatment of 2 Gy/fraction.

In response, SABR proponents have argued that its efficacy is due to escalated tumour radiation doses that confer high local tumour control and that its toxicity is limited by the same biological phenomena established for lower radiotherapy fractionation schemes, such as those used for CHART and 3D-CRT; therefore, no new radiobiological concepts are required to describe SABR's clinical outcomes (Brenner, 2008, Brown et al., 2013).

The number of clonogens in the tumours of interest is a fundamental input parameter for TCP modelling. Clonogenic cell density for solid tumours can vary widely, ranging from 10^5–10^9 cm^{-3} (Nahum et al., 2003). The exact value of this number for different tumour types is not known, nor is it understood how this number varies between tumours in different patients. Within this context, various radiobiological methods have been developed and introduced to calculate TCP (Alaswad et al., 2018, Walsh et al., 2016, Ruggieri et al., 2013, Ruggieri et al., 2010, Baker et al., 2015, Stavreva et al., 2019). However, much of this radiobiological research has assumed that the treated volume contains a fixed number of clonogenic cells, which is perceived as one of the major limitations of these models.

Notably, a few researchers have indicated that the likelihood of clonogenic cell density decreases from the centre of the gross tumour volume (GTV) towards the edge and that these decreases also occur within the clinical target volume (CTV) (Giraud et al., 2000, Chao et al., 2003). In these situations, lower clonogenic cell densities can be destroyed with a relatively lower radiation dose than is usually required to eliminate tumours, while a higher radiation dose would be required to eliminate a tumour with a higher clonogenic cell density. Following these plans, the optimal TCP and normal tissue complication probabilities can be attained.

Additionally, the ICRU report 71 provides a conceptual, theoretical framework (see Figure 3.1) to describe the variation of cancer cell density within the GTV and CTV (Gahbauer et al., 2004). For instance, Figure 3.1a exhibit a classical example of tumour definitions (see Section 1.4) of a sole GTV (dark red) and the corresponding CTV (light red).

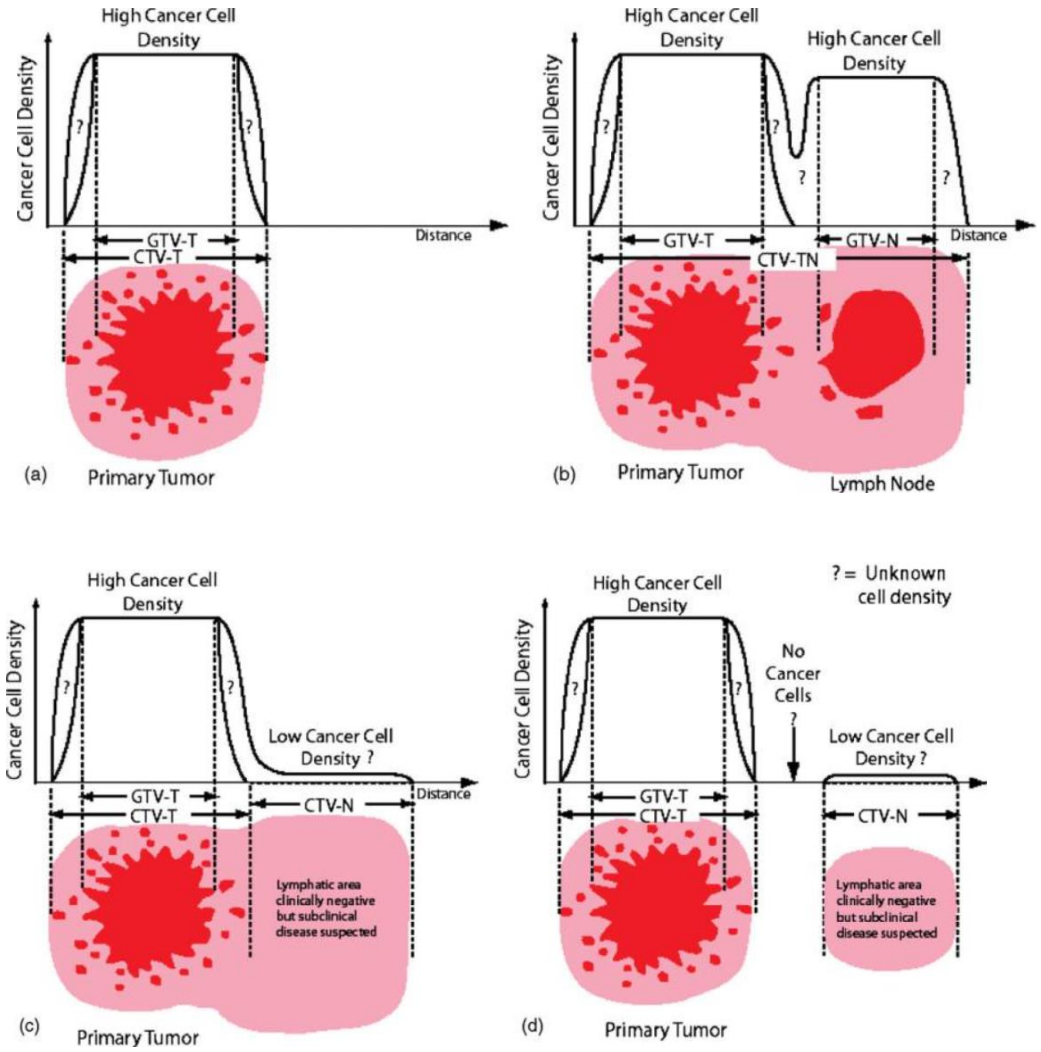

Figure 3.1: Schematic illustration describes the discrepancy of cancer cell density within the GTV and CTV for four different clinical scenarios (Gahbauer et al. 2004).

In this clinical scenario, The GTV incorporates predominantly those regions of the malignant growth where the quantity of cancer density is the maximum (approximately 10^6 cells/mm^3), but might have a slight degree of heterogeneous density distribution due to necrosis. Figure 3.1 demonstrates that the cancer cell density diminishes markedly between the border of the GTV (dark red) and the outer limit of the CTV (light red). Nevertheless, the reduction pattern of the cancer density as a function of the distance has not been quantitatively established (Gahbauer et al., 2004, Berthelsen et al., 2007, Barrett et al., 2009).

The objectives of this chapter were fivefold: (1) to explore the accuracy of a mechanistic TCP model to describe the clinical outcomes of a broad spectrum of NSCLC fractionation schemes, such as standard fractionation, hyperfractionation and hypofractionation; (2) to determine whether SABR's tumouricidal mechanisms are the same as those of 3D-CRT and CHART; (3) to examine the association between radiation dose prescription and TCP for NSCLCs; (4) to develop a new radiobiological approach for modelling clonogenic density, addressing the current limitations of TCP research in the literature by using a new mathematical approach; and (5) to introduce the concept of a GTV–CTV margin into the TCP model.

3.2 Methodology

3.2.1 Patient eligibility

TCP models were fitted to a list of early-stage NSCLC patient data collected from the literature. To identify studies that described clinical outcomes of early-stage NSCLC, a systematic review analysis was conducted using Google Scholar, PubMed and Science Direct databases (see Figure 3.2). This systematic review was conducted using the Preferred Reporting Items for Systematic Reviews and Meta-Analyses (PRISMA) guidelines (Moher et al., 2010). The search included papers that had been published or accepted for publication or that appeared as meeting abstracts between June 1989 and September 2018.

The full articles were accessed when their abstracts were deemed pertinent. The bibliographies of relevant publications were also explored to locate additional related studies. From each article, detailed clinical outcome information was extracted for model analysis and simulation; this information included the number of patients, the total dose, the number of fractions, the dose per fraction, the radiotherapy modality, the prescription dose and local tumour control. Further inclusion criteria were that patients had to have been treated using one of three external-beam radiation therapy approaches: 3D-CRT, SABR or CHART. The studies also had to report local tumour control details at one-, two- and three-year follow-ups. These inclusion criteria had previously been utilised in radiobiological modelling research conducted by Alaswad et al. (2019b).

In the first phase of the systematic review, 2,034 published articles were identified across the three electronic databases, of which 1,910 remained after eliminating all duplicates. EndNote X8.2 software (Thomson Reuters, USA) was used to manage and sort the articles. The article titles and abstracts were then comprehensively screened for the inclusion criteria; 1,857 studies were determined to be ineligible, leaving 53 articles that were relevant to the research question.

After assessing these full-length articles, 16 studies containing a total of 2,713 patients met the inclusion criteria. Articles were excluded for several reasons, including but not limited to imprecise descriptions of radiotherapy dosages or the lack of a detailed quantitative presentation of clinical outcomes. A PRISMA flow chart detailing the process of study identification, inclusion and exclusion is shown in Figure 3.2. Table 3.1 summarises patient dosimetric characteristics and clinical outcomes.

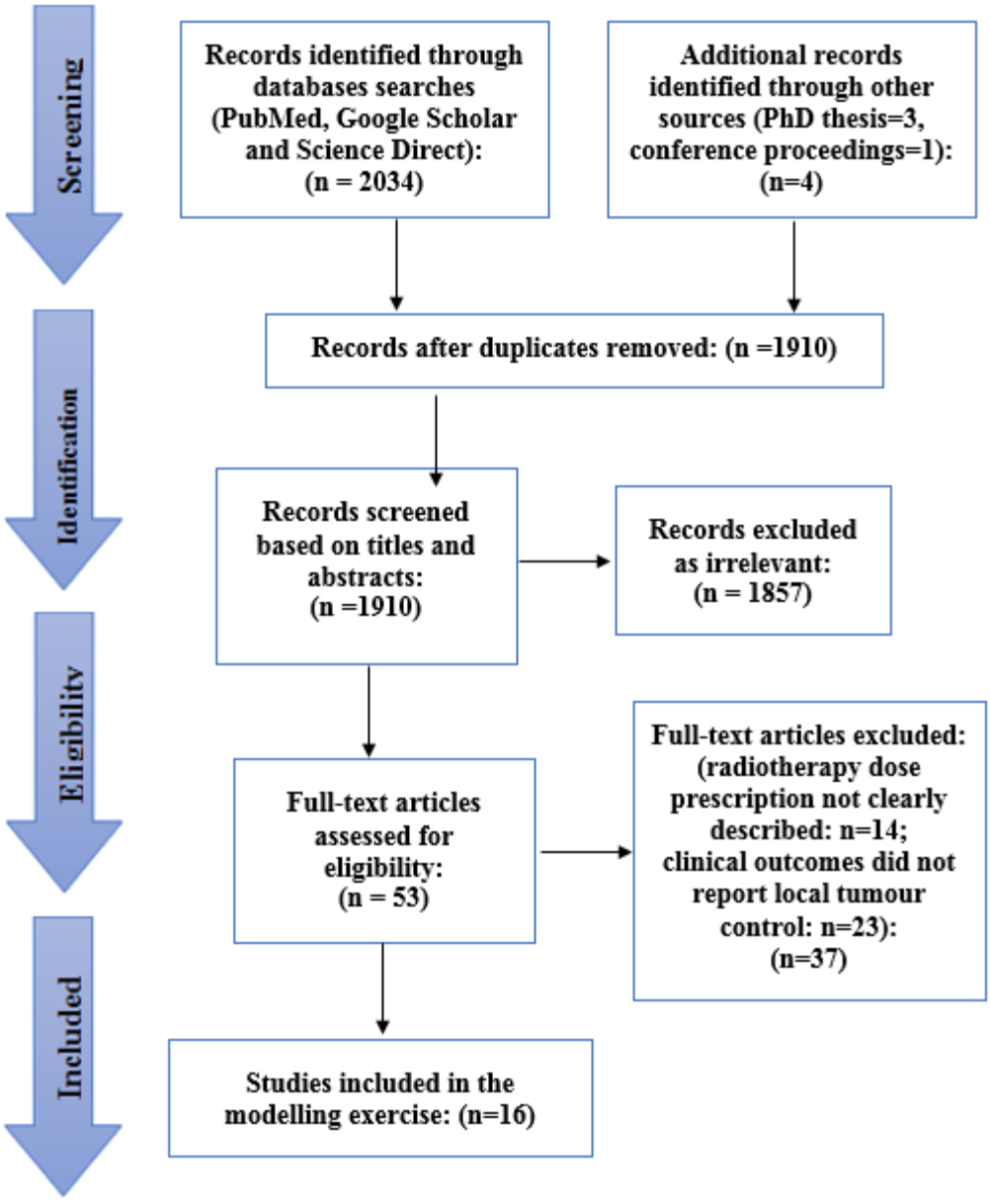

Figure 3.2: PRISMA flow diagram illustrating the various phases of the systematic review search and the study selection process.

Table 3.1:Published data on 2,713 patients with early-stage NSCLC treated by 3D-CRT, CHART or SABR, including their local tumour control rates.

RT modality	Patient cohorts	References	# of patients	d/fraction (Gy)	# of fractions	1-year tumour control (%)	2-year tumour control (%)	3-year tumour control (%)
3D-CRT	1	(Saunders et al., 1999)	225	2.0	30	35.0	13.0	7.0
3D-CRT	2	(Baumann et al., 2011)	203	2.0	33	35.0	17.0	9.0
3D-CRT	3	(Lagerwaard et al., 2002)	104	2.0	35	70.0	40.0	31.0
3D-CRT	4	(Kong et al., 2005)	56	2.1	32	44.0	34.0	29.0
3D-CRT	5	(Kong et al., 2005)	32	2.1	38	73.0	47.0	35.0
3D-CRT	6	(Kong et al., 2005)	18	2.1	46	76.0	50.0	49.0
CHART	7	(Sanganalmath et al., 2018a)	849	1.5	36	66.0	40.0	20.0
CHART	8	(Hatton et al., 2016)	23	1.5	36	65.3	39.0	20.0
CHART	9	(Baumann et al., 2011)	203	1.5	40	73.0	43.0	27.0
CHART	10	(Din et al., 2013)	583	1.5	36	63.0	31.0	20.0
SABR	11	(Andratschke et al., 2011)	92	9.0	5	89.0	83.0	83.0
SABR	12	(Takeda et al., 2009)	38	10.0	5	95.0	93.0	93.0
SABR	13	(Hamamoto et al., 2012)	128	12.0	5	96.0	89.0	84.0
SABR	14	(Dunlap et al., 2010)	40	14.0	3	90.0	88.0	85.0
SABR	15	(Kopek et al., 2009)	88	15.0	3	95.0	89.0	87.0
SABR	16	(Brown et al., 2009)	31	20.0	3	95.0	84.0	83.0

Some questions might be raised concerning the published clinical outcome data presented in Table 3.1. Is the dose escalation the central factor behind high local tumour control, or do alternative factors influence the clinical outcomes, such as patient selection and tumour size? Notably, in patients with NSCLC, recent evidence has proposed that tumour size is significantly correlated with local tumour control. (Chen et al., 2002).

For instance, Bradley et al. (2002) examined 207 inoperable NSCLC patients treated with conventionally fractionated radiotherapy to classify particular prognostic factors associated with outcomes; their multivariate and univariate statistical analysis determined that tumour size was the most notable factor for predicting local tumour control.

The research also discussed whether tumour size might be more critical than the TNM classification system (see Chapter 4), which is the standard scheme for determining operability. Moreover, additional modelling parameters, such as the radiotherapy modality, overall treatment time, radiotherapy dose prescription and dose per fraction, also influence the clinical outcome data presented in Table 3.1.

3.2.2 TCP model description

Several methods of modelling local tumour control have been previously introduced (Ruggieri et al., 2013, Ruggieri et al., 2010, Stavreva et al., 2019, Giraud et al., 2000, Chao et al., 2003, Alaswad et al., 2019b, Baker et al., 2015). One of the most popular is the LQ model combined with Poisson statistics, which proposes that local tumour control is only attained if no clonogens survive the delivered radiation dose. The LQ model in Equation 3.1 describes the surviving fraction of clonogenic cells, S(D), after exposure to a specific radiation dose D. This model has two essential features: (1) a linear component corresponding to nonrepairable single lesions produced by a single track of radiation; and (2) a quadratic component, which is produced by two separate radiation tracks, corresponding to double lesions that are repairable at low doses. The LQ model is mathematically defined by the following equation:

$$\mathbf{S(D) = exp[-\alpha nd - \beta nd^2]} \quad \textbf{(3.1)}$$

where S represents the surviving fraction, *n* is the number of fraction, *d* is the dose per fraction, D is the total dose delivered over the treatment course and α (Gy^{-1}) and β (Gy^{-2}) are the intrinsic radiosensitivity factors determining the initial slope and degree of curvature, respectively, of the fundamental cell survival curve as shown in Section 2.7.2.

It is also necessary to include the effects of incomplete sublethal lesion repair when establishing a radiobiological model to predict local tumour control. This has been addressed by introducing an additional factor (h) into Equation 3.1. Thames examined the effect of sublethal lesion repair for a fractionated treatment and recommended that the modelling process employ the following formula (Thames, 1985):

$$\mathbf{h = \left(\frac{2}{m}\right)\left(\frac{\theta}{1-\theta}\right)\left(m - \frac{1-\theta^m}{1-\theta}\right)} \quad \textbf{(3.2)}$$

where m is the number of fractions per day, $\theta = [-\tau \Delta T]$, τ is the repair half-time and ΔT is the time between fractions. Accordingly, Equation 3.1 can be rewritten as:

$$\mathbf{S(D) = exp[-\alpha nd - \beta n(1+h)\, d^2]} \quad \textbf{(3.3)}$$

Clonogenic tumour cells can repopulate during the course of fractionated radiotherapy, thereby reducing treatment effectiveness. This effect may be incorporated into the LQ model by introducing a repopulation correction factor that depends on two main parameters: the treatment duration and the clonogenic doubling time. Accordingly, Equation 3.3 can be rewritten as:

$$\mathbf{S\,(D) = e^{-n(\alpha d + G\beta d^2) + \gamma(T_0 - T_{del})}} \quad \textbf{(3.4)}$$

where T_0 is the overall radiation treatment time, T_{del} is the delay time up to the onset of accelerated proliferation and γ is the accelerated repopulation time factor. The γ factor used in this study was $0.693/T_{pot}$, with T_{pot} being the potential doubling time. The values of T_{del} and T_{pot} were 28 days and 5 days, respectively, which are consistent with the observed clinical data reported (Mehta et al., 2001, Griffin, 2006).

The idea of local tumour control evolved from an assumption that tumour control could only be attained if no clonogens survived after the radiation dose was delivered. TCP is defined by Equation 3.5, in which N_0 is the inceptive clonogen number and S(D) represents LQ cell survival:

$$\mathbf{TCP} = \mathbf{exp}\left[\left(-\mathbf{N_0 S(D)}\right)\right] \tag{3.5}$$

These TCP models were revised to include a normal distribution of the radiosensitivity parameters α, β, σ_α and σ_β for a particular population utilising a cumulative density function, which allowed the model to be determined for a Gaussian-distributed range of radiosensitivities (Walsh et al., 2016, Alaswad et al., 2019b, Walsh and Putten, 2013).

The TCP models make two assumptions: 1) that the radiosensitivity components α and β are distributed normally with standard deviations σ_α and σ_β; and 2) that the components are independent among the lung tumours that comprise the population described by the following equation:

$$\mathbf{TCP} = \frac{\mathbf{1}}{\mathbf{2\pi\sigma_\alpha\sigma_\beta}} \iint (\mathbf{exp}[-\mathbf{N_0 S(D)}]) \times \mathbf{exp}\left[\frac{-(\alpha-\bar{\alpha})^2}{2\sigma_{\alpha^2}} - \frac{(\beta-\bar{\beta})^2}{2\sigma_{\beta^2}}\right] \mathbf{d\alpha d\beta} \tag{3.6}$$

However, this integral can be estimated only through numerical methods and cannot be evaluated analytically; therefore, the present study used the following approach:

$$\mathbf{TCP} = \left(\frac{\mathbf{1}}{\mathbf{K}}\right) \sum_{\mathbf{i=1}}^{\mathbf{k}} (\mathbf{exp}[(-\mathbf{N_0 S(D)_i}] \tag{3.7}$$

where *K* represents a patient cluster with a distinctive radiosensitivity (see Figure 3.3).

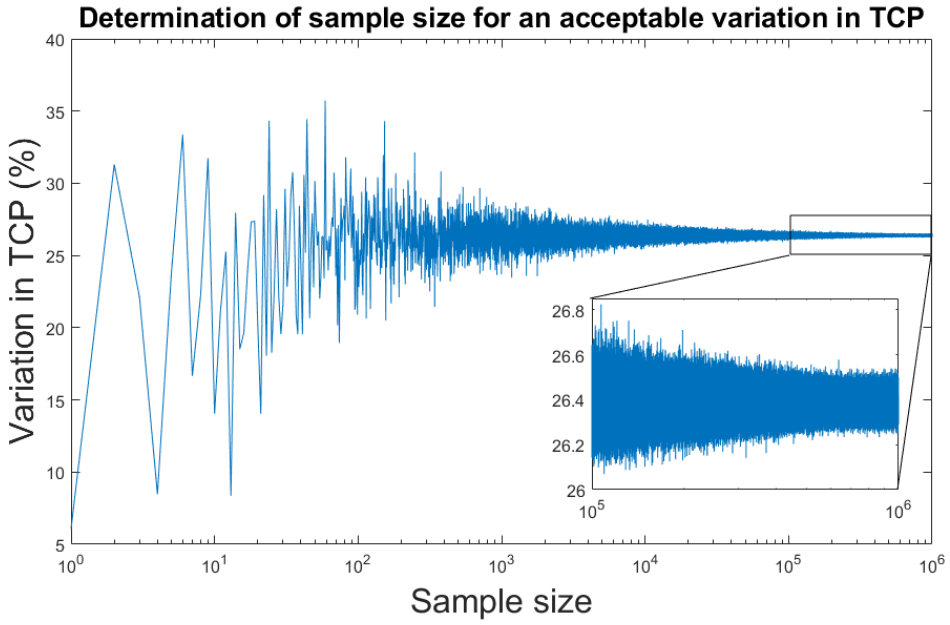

Figure 3.3: Determination of sample size: As the sample size K increases, initially the percentage difference in TCP is seen to vary substantially ($1 - 1 \times 10^2$); this fluctuation in TCP then begins to diminish considerably ($1 \times 10^3 - 1 \times 10^6$). The inset plot depicts the smallest observed fluctuation in the TCP outcomes (± 0.7). The TCP in this example was computed using Baumann et al. (2011) data, which comprised 203 patients treated with a total dose of 66 Gy, yielding a 2-year TCP of 26.4%.

Since the model was analytically intractable and the standard fitting methods were inappropriate, the TCP models were, therefore, fitted by employing the Nelder-Mead (NM) simplex algorithm (Nelder and Mead, 1965). The NM simplex algorithm is a derivative-free approach used in nonlinear continuous optimisation problems that provides a robust approach in determining a function's local minimum with various variables (Lind and Brahme, 2007).

With respect to the TCP model in this study, the variables are α, β, σα and σβ. Several initial estimates based on the known plausible ranges of radiosensitivity were used for the model simulations. These initial guesses were based on the radiosensitivity ranges that have been previously reported in the literature (Nahum, 2015, Park et al., 2008, Uzan and Nahum, 2012).

In the NM simplex algorithm, the simplex consists of a polyhedron within n + 1 vertices of the *n*-dimensional search space—that is, the number of points (vertices) is equal to one more than the number of dimensions in the search space.

For four variables (α, β, σ_α and σ_β), a simplex consists of a pentachoron with a pattern search comparing function values at the five points of the pentachoron. In each iteration, the highest objective function value (known as the worst vertex) is removed and substituted with a new vertex (known as the best vertex). This procedure produces a series of pentachorons with the function values at the points decreasing continuously.

The iterations are repeated to minimise the objective function through reflection, expansion, shrinkage and contraction. By iterating this procedure, the NM simplex algorithm determines the best solution.

Accordingly, this algorithm was used to minimise the mean squared error (MSE) that was yielded by the TCP model, which was weighted statistically to the number of patients for each dataset to avoid bias. The optimum TCP fit is that which produces the highest weighted coefficient of determination (R^2) and the lowest weighted mean squared error (wMSE).

In this part of the model, the GTV was considered to have a uniform clonogenic cell distribution. Furthermore, the clonogenic density was set at 10^7 cm^{-3} in accordance with a study reported by Webb (1994) and Baker et al. (2015), who found that this value was the best fit for the clinical data for NSCLC. Equation 3.8 was used to calculate the initial number of clonogens as proposed by Webb and Nahum (1993):

$$\mathbf{N_0 = GTV \times P_{clonogens}} \tag{3.8}$$

In addition, GTV volumes can vary between cancer stages and even between individuals in the same stage (Saunders et al., 1999). For the selected 3D-CRT and CHART studies (see Table 3.1), the majority of the patients were diagnosed with stage II or III NSCLC. Among these, one phase I randomised trial compared the clinical outcomes of patients diagnosed with stage II and III NSCLC who were treated with either 3D-CRT or CHART; it reported a mean GTV of 85 cm^3 (Hatton et al., 2016).

Accordingly, a mean GTV of 85 cm^3 was used in the present study as the input tumour size parameter for the TCP simulation for patients receiving either CHART or 3D-CRT. However, the included studies that used SABR primarily focused on stage I NSCLC with a mean GTV of 45 cm^3; this value was, therefore, used as the input tumour size parameter for the SABR TCP model in the present study (Table 3.1).

Cancer cells' response to ionising radiation depends strongly on oxygen, which mediates the indirect influences of ionising radiation and causes cell death; cells become more radioresistant under hypoxic conditions. This hypoxic effect was incorporated into the LQ model using an oxygen enhancement ratio (OER)—i.e., the ratio of doses needed to produce the same biological effect for hypoxic and oxic conditions:

$$\mathbf{S = exp\left(-\frac{\alpha}{OER}d - \frac{\beta}{OER^2}d^2\right)} \tag{3.9}$$

Within this context, the radiosensitivity parameters α and β depend on partial oxygen pressure, as determined by the OER. Typically, a tumour's OER value is 1.75; however, it has been reported as 2.8 for NSCLCs (Brown et al., 2010). Furthermore, research has established the proportion of clonogens defined as hypoxic and oxic to be 20% and 80%, respectively (Lindblom et al., 2014), and this was also incorporated into the model.

3.2.3 Modelling clonogenic cell density

Two computational radiobiological models were developed in MATLAB to study the effects of varying clonogenic density distributions on local tumour control. To the best of our knowledge, no previous study has attempted to model this effect using the new approach described in sections 3.2.3.1 and 3.2.3.2. The same 16 patient cohorts described in Table 3.1 were used to study the effects of clonogenic cell density variations on TCP. Since the central goal of this part of the study was to determine the effect of different clonogenic cell densities on TCPs, only two-year tumour control data were selected to model this effect. These proposed approaches are described in the following subsections.

3.2.3.1 Modelling clonogenic density decay in the GTV–CTV margin

This first approach sought to investigate a realistic scenario in which the clonogenic cell density inside the GTV remained constant but decreased within the GTV–CTV margins (Gahbauer et al., 2004). This approach assumed that the entire GTV had a constant and uniform clonogenic cell density of 10^7 cm^{-3}. However, the CTV was set to have a clonogenic cell density equal to 10^7 cm^{-3} at the inner edge, decaying to 10^0 cm^{-3} at the outer edge, following a Gaussian distribution (see Equation 3.10).

$$\mathbf{y} = \sum_{\mathbf{i=1}}^{\mathbf{n}} \mathbf{N_{0_i}} \mathbf{e}^{\left[-\left(\frac{\mathbf{r}-\mathbf{b_i}}{\mathbf{c_i}}\right)^2\right]} \qquad \textbf{(3.10)}$$

Here, N_0 is the clonogenic cell density, *b* is the centroid (location) and c is the decay peak width of the Gaussian decay distribution. The values used for N_0, b and c were 10^7 cm^{-3}, 0 and 0.9, respectively. In addition, *r* was the range of values (3.0–3.5 cm) that represented the GTV–CTV margin and that determined the fall-off of clonogenic cell density within the GTV–CTV margin.

For this approach, n = 40 segments were used, and additional geometric information about the value of the GTV–CTV margin was coded into the computational model, which was considered to be 5 mm, as illustrated in Figure 3.4A. The dose per fraction was also varied in the same manner as clonogenic cell density to determine the value for each segment. For instance, the prescribed radiation dose was held constant inside the GTV to match the constant clonogenic cell density and then decreased throughout the GTV–CTV margin, following the Gaussian decay (see Figure 3.4A). Equation 3.10 was also modified slightly to model the decay of the dose distribution:

$$\mathbf{y = \sum_{i=1}^{n} d_i e^{\left[-\left(\frac{r-b_i}{c_i}\right)^2\right]}} \qquad \textbf{(3.11)}$$

where d is the dose per fraction and *r* determines the radiation dose fall-off within the GTV–CTV margin. The values of the Gaussian parameters b and c were 0 and 5, respectively.

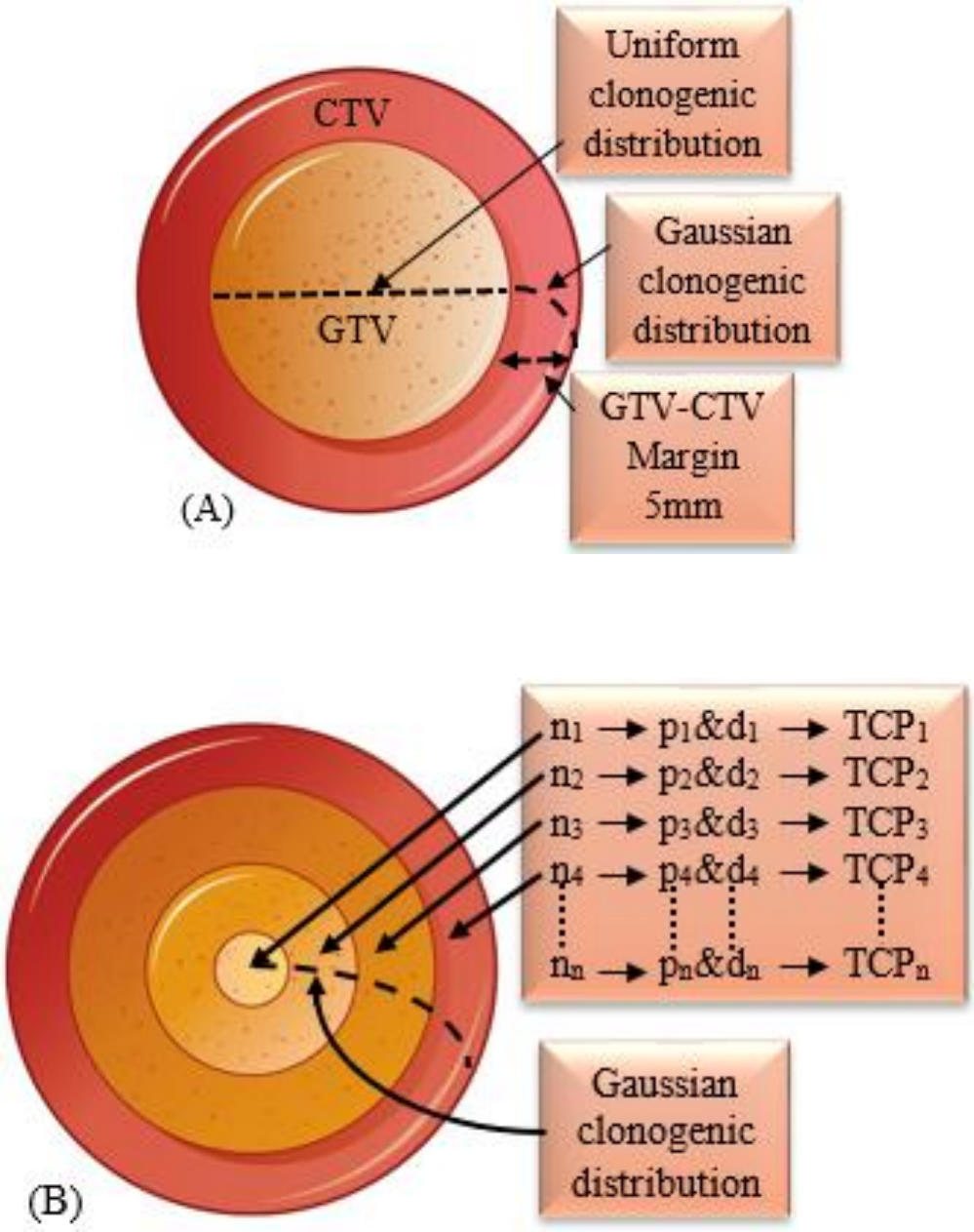

Figure 3.4:Proposed methods for modelling clonogenic cell density. (A) Illustrates the clonogenic cell density variations across the GTV and CTV. This model also introduces the concept of the GTV–CTV margin into the TCP. (B) Displays how the model functions as a numerical approximation for a nonuniform clonogenic cell density distribution and nonuniform dose-per-fraction distribution.

3.2.3.2 Modelling clonogenic density decay across whole-tumour volume

The second approach modelled a half-Gaussian clonogenic distribution from the centre of the GTV. This approach did not attempt to replicate a tumour in a practical sense; rather, its focus was solely on the computational model, and it sought to investigate the sensitivity of varying both the doses and clonogenic cell densities and their interactions in local tumour control by using both Equations 3.10 and 3.11.

The goal was to deliver a high radiation dose to areas of high clonogenic cell density and a low radiation dose to areas of low clonogenic cell density—in other words, to maximise the dose delivered to high densities and minimise the radiation to low densities. Additional geometric information (such as GTV–CTV margins) was no longer required since the distribution functions would alter clonogenic cell density, and hence, the dose per fraction across all segments, as displayed in Figure 3.4B.

3.2.4 Internal validation

To create a TCP model with an excellent reproducibility and generalization performance, one must have a sensible validation procedure. This step is crucial for the reliability and robustness of the TCP model. Diverse frameworks for validating predictive models have been proposed in the literature.

The two most common validation procedures are external and internal validations, where the former is based on test data from a different but 'plausibly related' population and the latter is based on test data from the same population (Steyerberg and Harrell, 2016, Steyerberg et al., 2003).

Jackknife, bootstrapping, split-sampling, and cross-validation methods are classified as internal validation approaches because the performance is measured using patients from the model's derivation set only (Zuo et al., 2010).

Of greater relevance is external validation, where the performance accuracy of the model is addressed and examined in independent samples to evaluate the reliability and transportability of the established model.

The historical, geographic, methodologic, spectrum, and interval methods can all be classified as external validation approaches (Labarere et al., 2014). Unfortunately, validation of a TCP model remains very uncommon and, to the best of our knowledge, measurements of TCP model performance in a systematic procedure have not yet been taken or studied in the literature.

A bootstrap resampling approach was employed to internally validate and verify the robustness of the TCP models. This approach assumed that an appropriate new dataset using the same population could be generated by randomly sampling the initial dataset and combining it with a 'replicate' bootstrap dataset (see Figure 3.5).

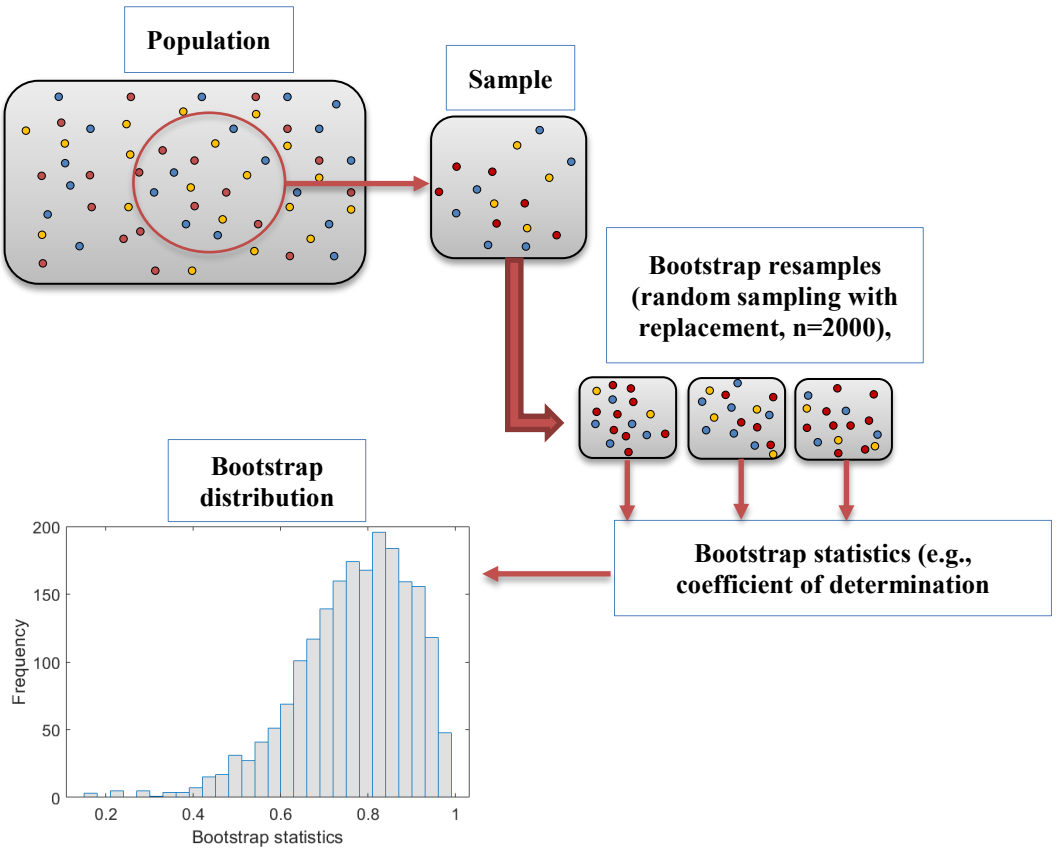

Figure 3.5: Schematic illustration describes the bootstrap validation process.

The points to be used were selected ‘with replacement’, indicating that a specific point could be selected repeatedly or not at all for a particular bootstrap sample (Efron, 1992). The internal validation procedure was performed by randomly generating 2000 bootstrap samples; each sample consisted of 16 data points, which were selected with replacement. Both R^2 and RMSE were estimated using bootstrap resampling, with their 95% confidence intervals (CIs) then determined with bias-corrected and accelerated (BCa) percentile intervals.

3.3 Results

3.3.1 Prediction of clinical outcomes: LQ-based statistical TCP model

The TCP models expressed a strong positive linear relationship between the literature's reported local tumour control and the estimated TCP outcomes. Figures 3.6A, 3.6B and 3.6C show the correlation coefficient R^2 of statistical tests between the estimated TCPs corresponding to each radiotherapy modality listed in Table 3.1 (3D-CRT, CHART and SABR). The statistical analysis resulted in tumour control rates of $R^2 = 0.96$ and wRMSE = 3.9% at the first-year follow-up, $R^2 = 0.96$ and wRMSE = 5.2% at the second-year follow-up and $R^2 = 0.97$ and wRMSE = 5.9% at the third-year follow-up; all p-values were <0.05.

Table 3.2 summarises the model's predictions of the TCPs for one-year, two-year and three-year local tumour control rates. For patients who received SABR, TCPs were as high as 98.0%, 95.9% and 93.0% at one, two- and three-year local tumour control rates, respectively, with a biologically effective dose (BED) of ≥85.5 Gy. In contrast, the best TCPs for patients in the CHART subgroup were 83.5%, 44.1% and 28.5% at the first-, second- and third-year follow-ups, respectively, with a BED of ≤69.0 Gy. Contrary to the 3D-CRT results, poor local tumour control rates—and hence, low TCPs—were produced by the TCP model (see Figures 3.6A, 3.6B, 3.6C, Table 3.1 and Table 3.2).

The results obtained from the residuals analysis of the TCP model are summarised in Figures 3.6D, 3.6E and 3.6F. This statistical test demonstrated that the TCP model yielded minimum and maximum residuals of 0.1% and -12%, respectively.

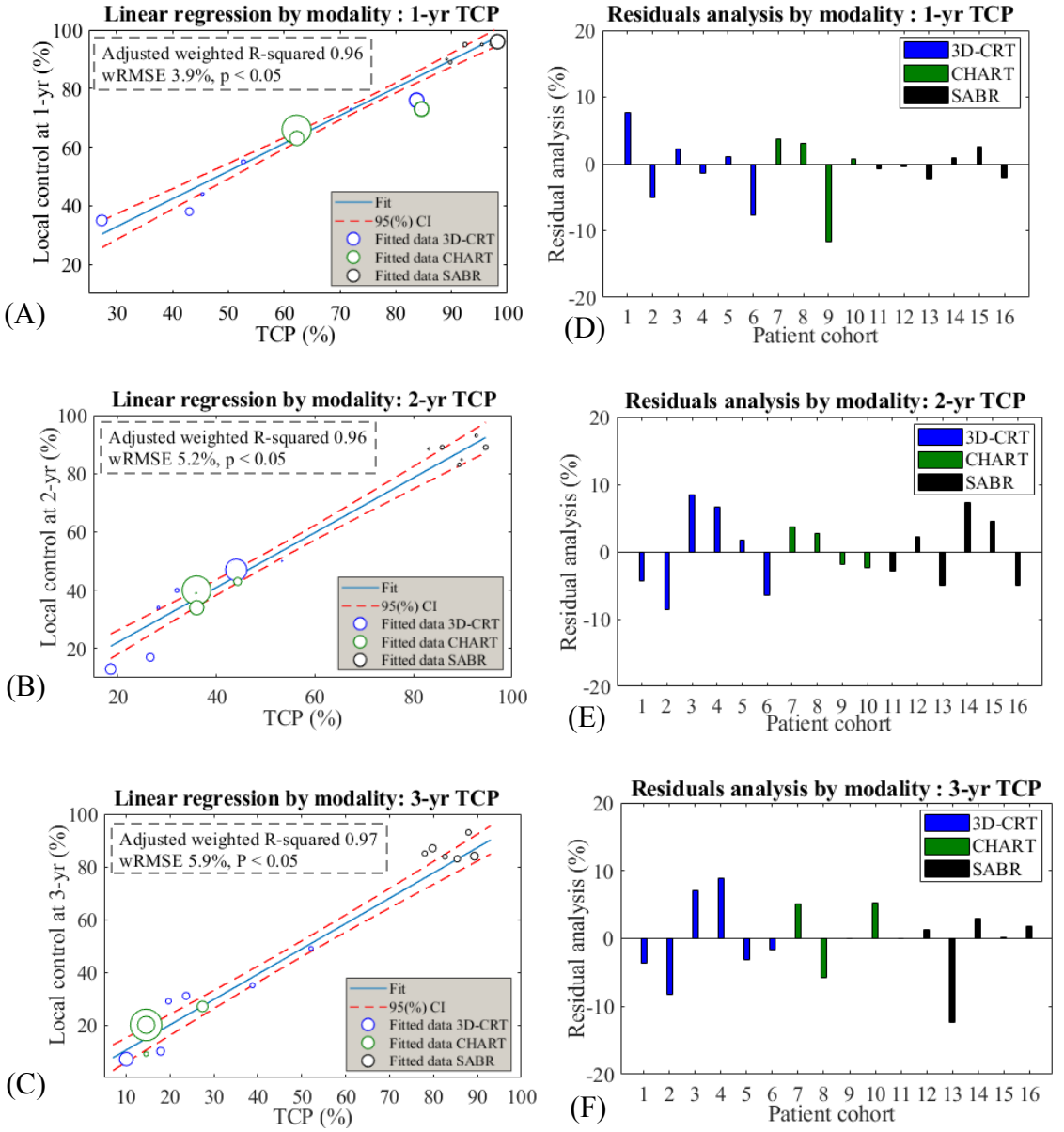

Figure 3.6: Accuracy of the TCP models. The accuracy of TCP models was quantitatively assessed by employing a residuals analysis and determining the goodness of fit. Displayed here are the linear regression (A, B & C) graphs for 3D-CRT (green circles), CHART (blue circles) and SABR (black circles), with 95% confidence bounds. Each dataset was statistically weighted and scaled based on the number of patients in each group.

Table 3.2: Summary of TCP predictions for one-year, two-year and three-year local tumour control rates for one-year, two-year and three-year local tumour control rates.

RT modality	Patient cohorts	1-year reported TCP (%)	1-year TCP (%)	Diff (%)	2-year reported TCP (%)	2-year TCP (%)	Diff (%)	3-year reported TCP (%)	3-year TCP (%)	Diff (%)
3D-CRT	1	35	29.5	5.5	13	18.2	-5.2	7	11.1	-4.1
3D-CRT	2	35	38.6	-3.6	17	26.4	-9.4	9	18.5	-9.5
3D-CRT	3	55	52.9	2.1	40	32	8	31	24	7
3D-CRT	4	44	46.3	-2.3	34	28.5	5.5	29	20.2	8.8
3D-CRT	5	73	70.1	2.9	47	44.7	2.3	35	37.5	-2.5
3D-CRT	6	76	81.2	-5.2	50	54.6	-4.6	49	49.7	-0.7
CHART	7	66	63.4	2.6	40	36	4	20	13.4	6.6
CHART	8	65.3	63.4	1.9	39	36	3	20	13.4	6.6
CHART	9	73	83.5	-10.5	43	44.1	-1.1	27	28.5	-1.5
CHART	10	63	63.4	-0.4	33	35.9	-2.9	20	13.4	6.6
SABR	11	89	89.8	-0.8	83	86.7	-3.7	83	83.7	-0.7
SABR	12	95	95.1	-0.1	93	91.4	1.6	93	90.9	2.1
SABR	13	96	98	-2	92	95.9	-3.9	84	93.3	-9.3
SABR	14	90	89.5	0.5	88	82	6	85	81.5	3.5
SABR	15	95	92.5	2.5	89	86.3	2.7	87	84	3
SABR	16	95	96.8	-1.8	86.8	93	-6.2	83.8	88.6	-4.8

Figure 3.7 displays the global minimum solution of the initial guess of the radio sensitivity components α and β and their standard deviations $\sigma_\alpha$and σ_β, as produced by the NM simplex algorithm, for the 3D-CRT, CHART and SABR clinical outcome data for early-stage NSCLC. Additionally, the derived α/β values were 11.2 Gy ± 2.5 Gy, 10.6 Gy ± 1.5 Gy and 9.2 Gy ± 2.3 Gy for the one-, two- and three-year local tumour control rates, respectively.

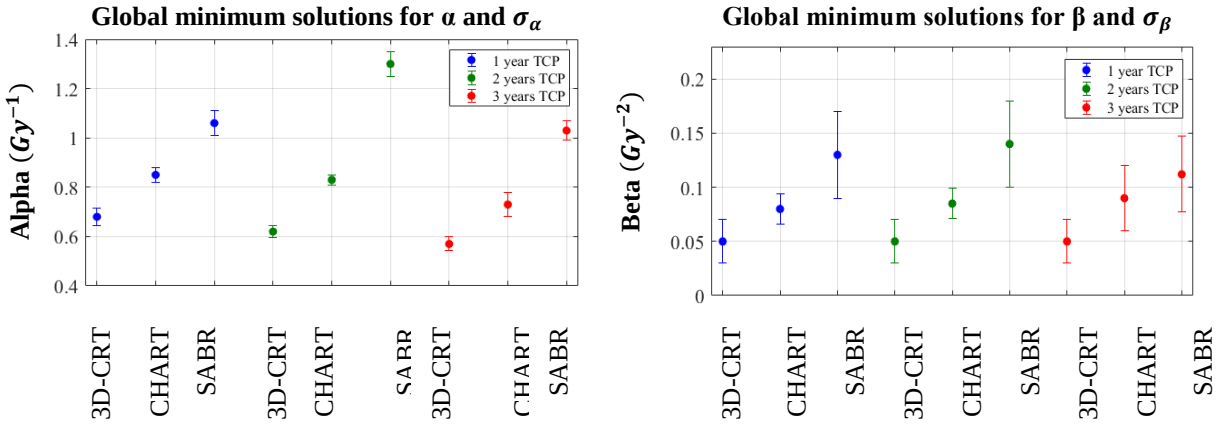

Figure 3.7: The radiosensitivity solutions produced by the NM algorithm for each dataset. The error bars represent σα and σβ.

3.3.2 Modelling clonogenic density decay in the GTV–CTV margins

Figure 3.8 shows the results of the half-Gaussian clonogenic cell density decay and half-Gaussian dose-per-fraction fall-off in the GTV–CTV margins, with constant values for the clonogenic cell density and dose per fraction in the GTV for all of the 16 patient cohorts described in Table 3.1. For the region inside the GTV, all the graphs had a constant TCP inside the GTV, which was expected since both the clonogenic cell density and dose per fraction were constant. In the GTV–CTV margins, clonogenic cell density varied from 10^7 cm^{-3} to 10^0 cm^{-3} (see Figure 3.8A).

The dose per fraction was reduced to 40% of the maximum value for all cohorts (see Figure 3.8B). Importantly, a relatively flat TCP was obtained in the GTV–CTV margin with a lower radiation dose, as displayed in Figure 3.7C.

(A)

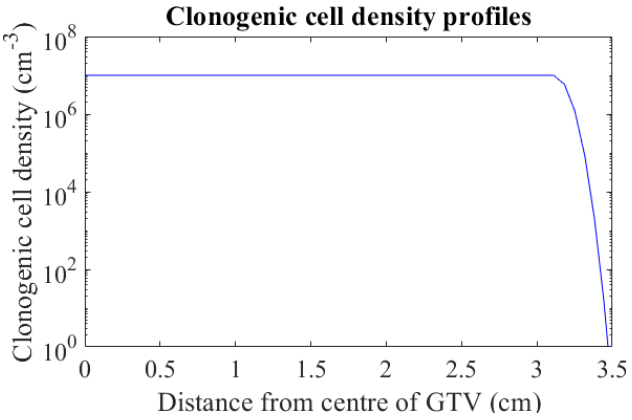

(B)

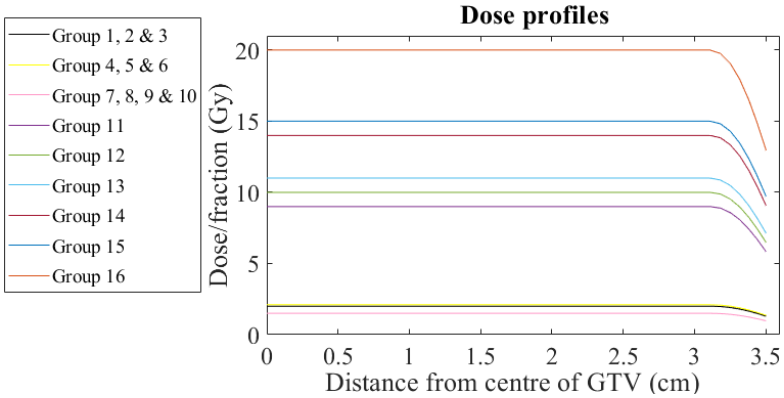

(C)

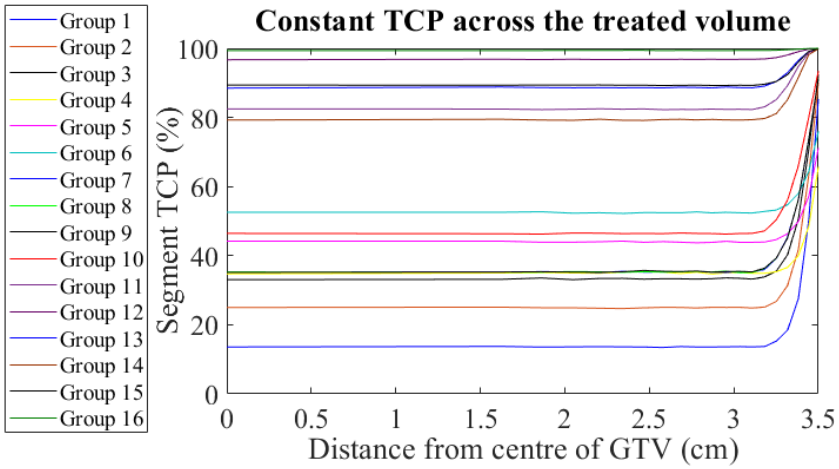

Figure 3.8: Results of clonogenic cell density variations across a GTV–CTV margin of 5 mm. Both the dose per fraction (A) and clonogenic cell density (B) were constant throughout the GTV and fell off along a half-Gaussian decay across the GTV–CTV margin. A flat TCP was achieved across the treatment volume (C).

3.3.3 Modelling clonogenic density decay across the whole-tumour volume

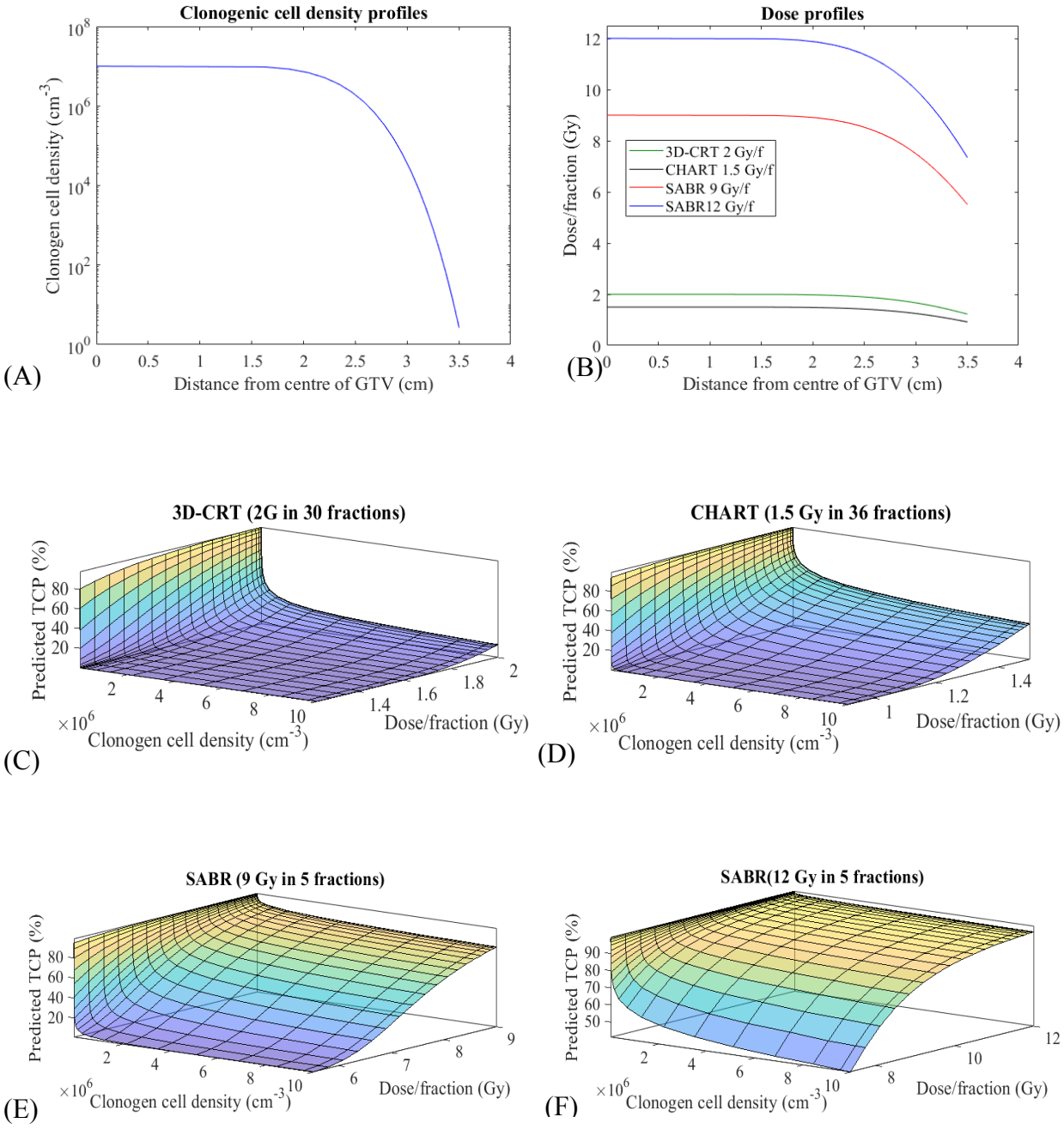

Figure 3.9: Four cohorts of patients modelled in parallel for two years post local-control treatment. Both the dose per fraction and clonogenic cell density varied along a half-Gaussian decay.

Appendix B.1 shows the results obtained using the approach described in section 3.2.3.2, as applied to the 16 patient cohorts outlined in Table 3.1 and with a clonogenic cell density distribution and dose-per-fraction distribution of a half-Gaussian decay. Figure 3.9 shows the results for four cohorts of patients: one 3D-CRT cohort, one CHART cohort and two SABR cohorts. It is immediately apparent that there is now a total of six graphs for each particular combination of cell density and dose distribution, corresponding to a graph for the dose-per-fraction profile, a graph for the clonogenic cell density profile, and separate graphs for each of the four patient cohorts. The dose per fraction was reduced to 40% of the maximum value for all cohorts, and clonogenic cell density varied from 1×10^{7} cm^{-3} to 10^{0} cm^{-3} at the outer edge of the treated volume. It is evident that values of high clonogenic cell density and low doses per fraction (the lower right side of Figures 3.9C, 3.9D, 3.9E and 3.9F) produced poorly predicted TCP values. Likewise, for the values of low clonogenic cell density and high doses per fraction (the upper left side of Figures 3.9C, 3.9D, 3.9E and 3.9F), the predicted TCP values were very high.

3.3.4 Internal validation

Figure 3.10 depicts the bootstrap results that were generated using 2,000 bootstrap resamplings of the original dataset (training set). The histogram shows the variation of the correlation coefficients (Figures 3.10A, 3.10B and 3.10C) and the RMSEs (Figures 3.10D, 3.10E and 3.10F) across all of the bootstrap samples. The mean and the 95% confidence interval (CI) of the correlation coefficients (R^2) and the RMSEs of the local TCP in these 2,000 samples with different clinical endpoints were as follows: one-year local tumour control, $R^2 = 0.98$ (95% CI = 0.93–0.99) and RMSE = 3.9 (95% CI = 2.6–6.3); two-year local tumour control, $R^2 = 0.98$ (95% CI = 0.95–0.99) and RMSE = 5.0 (95% CI = 4.0–6.3); and three-year local tumour control, $R^2 = 0.98$ (95% CI = 0.96–0.99) and RMSE = 5.5 (95% CI = 4.2–7.5).

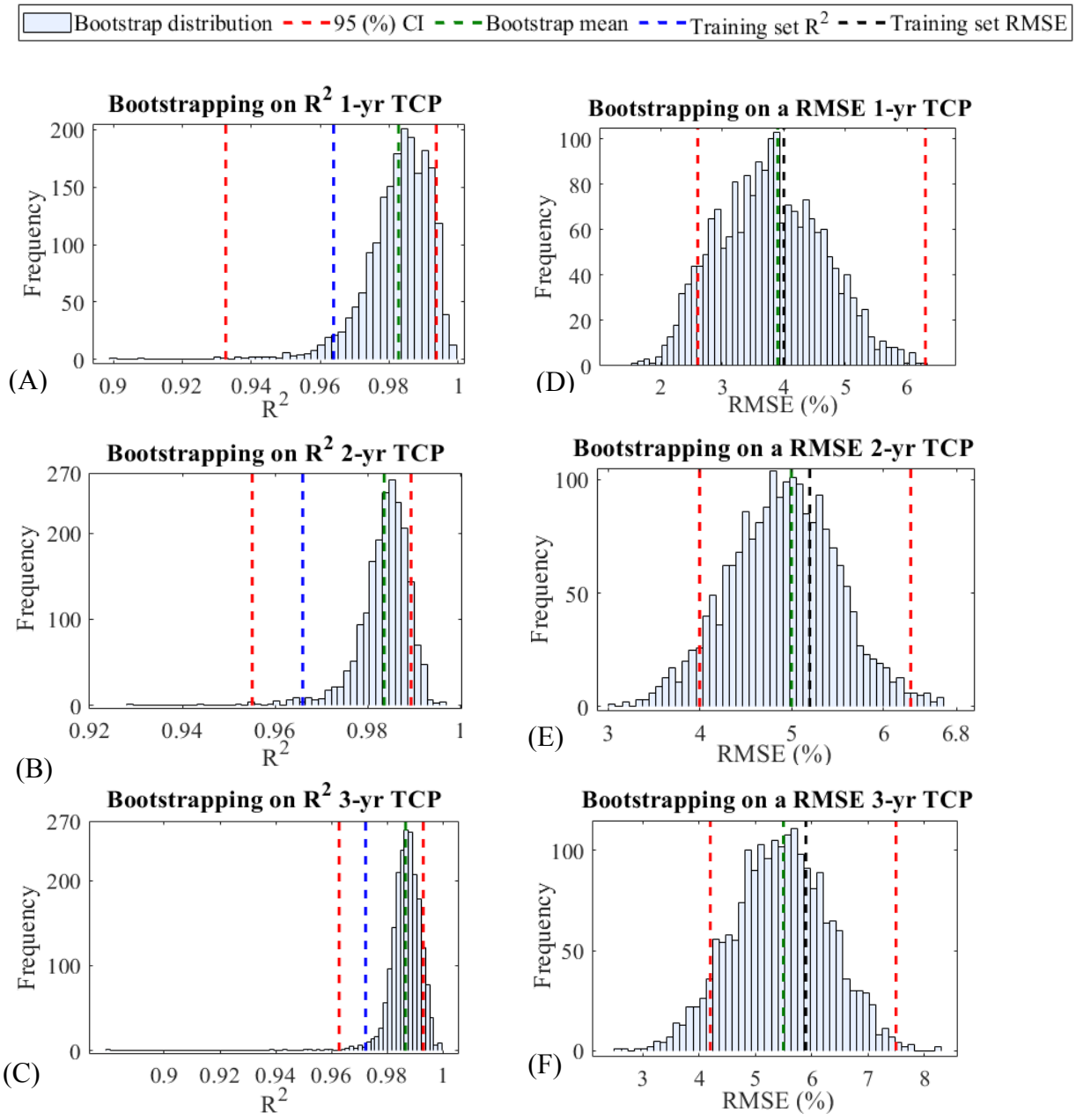

Figure 3.10: Histogram of 2,000 bootstrap samples on R^2 (A, B and C) and RMSE (D, E and F) for the one-, two- and three-year TCP model outcomes. These bootstrapping results were produced by resampling from the training set of 16 patient cohorts. The red broken vertical line indicates the boundaries of the bootstrap's 95% confidence interval, the green broken vertical line indicates the bootstrap sample mean, the blue broken vertical line indicates the R^2 value of the training set and the black broken vertical line indicates the RMSE value of the training set RMSE. The bootstrap histogram distribution of R^2 for all clinical endpoints is skewed to the left (negatively skewed histogram).

3.4 Discussion

This study used clinical data from 16 published reports on early-stage NSCLC (see Table 3.1) to establish a TCP model. An LQ-based TCP model was found to provide an adequate estimate of local tumour control for early-stage NSCLC even though the LQ model's applicability in predicting local tumour control in hypofractionated radiotherapy regimens, such as SABR, has been a controversial and much-disputed subject within the field of radiobiology. Researchers have argued that SABR is characterised by markedly different radiobiology compared to conventional dose fractionation (Brown et al., 2014, Fuks and Kolesnick, 2005).

Moreover, a number of authors have argued that LQ-based TCP modelling underestimates SABR's local tumour control because it does not take into account collateral cell death and vascular damage (Kirkpatrick et al., 2008). High-dose radiotherapy directly damages DNA and produces simultaneous indirect effects, such as out-of-field tumour responses with abscopal and bystander effects. In these situations, antitumour immunity and immune-based tumour death can be triggered by cell signals, such as apoptosis, necrosis and necroptosis (Sologuren et al., 2014).

However, no reliable evidence has been provided to support any of these arguments. In fact, previous radiobiological modelling approaches (Alaswad et al., 2018, Alaswad et al., 2019b, Baker et al., 2015), as well as the current study (Alaswad et al., 2019a), have demonstrated that local tumour control in fractionated SABR of early-stage NSCLC is adequately modelled by extending the classic LQ formula to include the effects of hypoxia, tumour repopulation and the repair of sublethal damage.

To the best of our knowledge, however, the present study is the first TCP model for early-stage NSCLC that has combined all three of these parameters. The TCP model used here accurately estimated local tumour control one, two and three years post-treatment for early-stage NSCLC patients who received either 3D-CRT, CHART or SABR.

The model's statistical analysis expressed a strong positive linear relationship between the reported local tumour control and the predicted TCP outcomes. The model's results were strongly significant in both the fitted training datasets and the validated datasets (internal validation) and therefore provide a measure of confidence in the robustness of the current radiobiological models among the wide range of fractionation schemes and treatment modalities.

Some questions might be raised about the outcomes of the TCP model's statistical analysis. Is the dose escalation the main factor behind high local tumour control, or do other factors influence TCP, such as tumour size and patient selection? In patients with NSCLC, recent evidence has suggested that GTV is significantly associated with local tumour control (Chen et al., 2002). For instance, Bradley et al. (2002) analysed 207 inoperable NSCLC patients treated with 3D-CRT to classify particular prognostic factors related to outcomes with 3D-CRT; their univariate and multivariate results indicated that GTV was the most significant factor for predicting local tumour control. The study also raised the question of whether GTV size might be more crucial than the tumour, node and metastasis (TNM) staging system (see Chapter 4), which is the conventional approach for determining operability.

In another major study, 106 patients with newly diagnosed or recurrent stage I–III NSCLC were treated with 63–103 Gy in 2.1-Gy fractions, using 3D-CRT radiotherapy; the researchers found that tumour volume had no significant influence on local tumour control (Kong et al., 2005). Moreover, when both the total radiation dose and GTV were incorporated into a Cox statistical analysis for local disease control and survival, only the total prescribed radiation doses were significant, and the treated tumour volume became less pronounced.

This suggests that radiation dose is a more robust predictor for local tumour control than GTV. In the present study, the majority of the collected patient data was related to early-stage NSCLC; therefore, patient selection and tumour size were not the main reasons for the markedly different levels of local tumour control.

A number of published studies have described the efficacy of escalating radiation doses for medically inoperable early-stage NSCLC. These studies have suggested that higher radiation doses provide better local tumour control and increase overall survival. Both TCP and clinical outcomes (Figures 3.6A, 3.6B, 3.6C, Table 3.1 and Table 3.2) have demonstrated that reducing the overall treatment time—typically an attempt to minimise the influence of the accelerated repopulation of cancer cells—played a crucial part in attaining an enhanced level of tumour control for NSCLC. In addition, increasing the treatment fractions may extend the total treatment time by more than three weeks, reaching the clonogen proliferation time zone (see Section 2.11) and ultimately causing a loss of local tumour control (Fowler, 2001).

Accordingly, CHART and SABR were superior to 3D-CRT in producing an improved level of TCP. Furthermore, fractionation schemes that were completed in fewer than 28 days showed only a small amount of repopulation, and the repopulation correction factor was therefore omitted for the subgroups of patients who received CHART or SABR. However, for treatment schemes that extended for more than 28 days, such as 3D-CRT, accelerated repopulation of the clonogenic cells is anticipated to occur for the remaining period of the treatment schedule, and this effect was therefore accounted for and modelled for the 3D-CRT data.

SABR is based on a philosophy that is distinct from other radiation therapy modalities because it utilises extremely high doses over just a few days (see Table 3.1). It is considered standard in radiotherapy that delivering focused high doses of radiation destroys the maximum number of clonogenic cells and therefore achieves optimal TCP. However, the increased probability of complications in normal tissues restricts the use of high radiation doses.

It is known that, in NSCLC, clonogenic cell density is lower at the periphery than in the centre of the GTV. However, previous studies of TCP models have not taken these variations into account, and few quantitative analyses have measured the actual number of clonogenic cells in NSCLC.

To the best of our knowledge, only one study has attempted to measure the actual number of clonogens: that of Baker and Sanger (1991), who attempted to determine the clonogenic cell density in human tumours and found it to be approximately 1.12×10^5 cm^{-3}.

The present study found that clonogenic cell density (see Figure 3.8C) exhibited a spike towards 100% TCP at the very periphery of the CTV; this is because, by definition, the CTV should have a clonogenic cell density of 0 at its outer edge. This is a good indication that the processes of clonogenic cell density segmentation and dose distribution segmentation did not adversely affect the outcomes of the model.

Moreover, the model indicated that there was a sigmoidal relationship between the dose per fraction and the predicted TCP (see Figures 3.9C, 3.9D, 3.9E and 3.9F). This can be considered a proof of concept, since it is consistent with the theory of Strigari et al. (2008) that plotting the dose per fraction against the TCP is analogous to Figures 3.9C, 3.9D, 3.9E and 3.9F, and it adds detail to the therapeutic index provided by Strigari et al. (2008).

Accurate clinical outcome predictions can offer oncologists more reliable tools to enhance their decision making when balancing predicted benefits versus expected risk. As shown in this study, the established mechanistic TCP population model can sufficiently describe the clinical outcomes of early-stage NSCLC. However, local tumour control is determined by a complicated interplay between radiation dosimetry, tumour biology, tumour microenvironment and patient-related variables. These factors present a challenge in establishing a prognostic model for routine clinical practice.

Additionally, the TCP model has only been designed to predict population-level clinical outcomes, not individual-level clinical outcomes. Although the model could, theoretically, predict both individual- and population-level clinical outcomes, the precise voxel information for each individual (e.g., dose distribution, clonogenic distribution, intratumour radiosensitivity, etc.) would be required, and this is a significant limitation of TCP models.

Another major source of uncertainty in radiobiological modelling is associated with the accurate determination of the radiosensitivity parameters α, β, σα and σβ. Data from several sources have shown high heterogeneity in reporting α and β values (Vernimmen and Slabbert, 2010, Williams et al., 2007, Datta et al., 2005, Qi et al., 2011, Pos et al., 2006), indicating that α and β values can vary considerably between tumour sites and may even fluctuate between individuals. For NSCLC, a wide range of (α/β) values (2.2–12.6) has been reported in the literature (Van Leeuwen et al., 2018, Santiago et al., 2016, Stuschke and Pöttgen, 2010).

Measurements of α, β, σ_α and σ_β can be performed in vitro in tumour cell lines or can be derived from clinical radiotherapy outcome data. In the current study, the radiosensitivity parameters were estimated by fitting the TCP to a broad spectrum of radiotherapy schedules using the NM simplex algorithm. The outcomes of the models showed that the actual values of (α/β) can vary from 7–14 Gy depending on the, clinical outcomes, radiotherapy modalities and the fractionation schedules (see Figure 3.6).

Other factors believed to influence tumour response to radiation doses (such as cell cycling, tumour spatial heterogeneity, uncertainty associated with the delivery of radiation doses and interaction with the immune system) were not taken into account in this study. These variables play a role in determining clinical outcomes and remain a challenge to quantify and address with a modelling approach.

Importantly, recent advances in radiotherapy (such as image-guided radiation therapy [IGRT], SABR, MRI-Linac and proton therapy) have improved the dosimetric uncertainties associated with treatment delivery (Yamamoto et al., 2018, Bendall et al., 2018, Gomez et al., 2018, Astaraki et al., 2019). However, such advances cannot entirely overcome the biological uncertainties. A good example of this is that the actual clonogenic density distribution of human tumours remains explicitly unknown, despite the tremendous recent developments in molecular imaging modalities.

For instance, positron emission tomography (PET) resolution is limited to 5 mm (Lazzeroni et al., 2018); microscopic diseases are considerably smaller than this, making the accurate determination of clonogenic density impossible. From a biological perspective, this issue remains one of the most significant gaps in the literature, and both physicists and radiobiologists, among other professionals in the radiation oncology community, must work together to resolve it.

In conclusion, this chapter sought to establish a mechanistic local TCP model that could describe clinical outcomes of early-stage NSCLC. The findings suggest that the TCP model is appropriate for the analysis and evaluation of radiotherapy treatment plans with respect to one-, two- and three-year local tumour control through 3D-CRT, CHART and SABR. However, the present findings are subject to several complex radiobiological and physical limitations that must be taken into account.

Chapter 4 Comparison of the T descriptor of the 7th and 8th editions of the TNM staging system for non-small-cell lung cancer after radiotherapy

4.1 Introduction

The primary factors considered in making medical oncology treatment decisions, as well as in predicting prognoses and outcome assessments, remain the disease type and extent, which are indicated by a cancer stage grouping based on the tumour, node, metastasis (TNM) classification. A large and growing body of literature has described alternative secondary prognostic determinants that might influence treatment decisions, local tumour control and overall survival; these determinants include gender, age, tumour histology and treatment type (Pinto et al., 2018, Urvay et al., 2016, Hirsch et al., 2008, Socinski et al., 2003).

Nevertheless, the TNM staging system retains greater influence and remains the most common primary indicator (Chansky et al., 2009).The TNM distribution scheme plays a vital role in standardising representations of the anatomical extent of solid malignant tumours (see Table 4.1).

Table 4.1 : Published definitions for primary tumour of NSCLC according to the T descriptors of the 7th and 8th editions (Goldstraw et al. 2016, Goldstraw et al. 2007).

Label	7th	8th
T0	No indication of primary tumour extension.	
TX	Primary tumour cannot be measured or tumour cells confirmed by bronchial washing procedure or through the presence of malignant cell in sputum, although not perceived by bronchoscopy or imaging.	
Tis	Carcinoma in situ, this is defined herein as a cluster of abnormal cells that reside in the region where they originally developed (e.g., not spread yet). These irregular cells can evolve to become cancerous and spread into adjacent healthy tissues.	
T1	Tumour 3 cm in the greatest dimension in the immediate vicinity of the lung or visceral pleura without bronchoscopic indication of invasion (i.e., no evidence of invasion to the main bronchus)	
T2	Tumour > 3 cm but ≤ 7 cm that possess either of the following particular conditions: • Involves main bronchus, ≥ 2 cm distal to the carina. • Invades visceral pleura. • Associated with atelectasis or obstructive pneumonitis that extends to the hilar region, nonetheless, does not include the entire lung.	Tumour > 3 cm but ≤ 5 cm that possess either of the following particular conditions: • Encompasses main bronchus irrespective of distance from the carina but without including the carina. • Invades visceral pleura. • Associated with atelectasis or obstructive pneumonitis that extends to the hilar region, including part or the entire lung.
T3	Tumour > 7 cm that possess either of the following particular conditions: • Invades either of the following particular organs; diaphragm, chest wall, mediastinal pleura, phrenic nerve, and parietal pericardium. • Tumour in the main bronchus < 2 cm distal to the carina but without including the carina. • Associated with atelectasis or obstructive pneumonitis of the entire lung or separate tumour nodule(s) in the same lobe.	Tumour > 5 cm but ≤ 7 cm in greatest dimension that possess either of the following particular conditions: • Invades either of the following particular organs; chest wall, phrenic nerve, and parietal pericardium. • Associated with separate tumour nodule(s) in the same lobe as the primary tumour.
T4	Tumour of any size that possess either of the following particular conditions: • Invades either of the following particular organs; mediastinum, great vessels, heart, recurrent laryngeal nerve, esophagus, trachea, carina or vertebral body. • Associated with separate tumour nodule(s) in a different ipsilateral lobe than that of the primary tumour.	Tumour >7 cm in greatest dimension that possess either of the following particular conditions: • Invades either of the following particular organs; diaphragm, mediastinum, great vessels, heart, recurrent laryngeal nerve, esophagus, carina or vertebral body. • Associated with separate tumour nodule(s) in a different ipsilateral lobe than that of the primary tumour.

In addition, the use of this scheme facilitates patient distribution into stage groups to differentiate those patients who are surgical candidates, either initially or after chemo-radiotherapy, from those who will be treated radically and from those requiring palliation. Of particular note, although the TNM classification provides guidelines for the standardisation of stage groups, it still allows for substantial variations in the overall survival and for the heterogeneity of the patient population within a single group (Goldstraw et al., 2007).

The Union for International Cancer Control (UICC) was established to update the TNM classification scheme as more data become available. Recently, major changes have occurred in the staging, diagnosis and treatment of lung cancer. The 8th edition of the TNM staging system was released in 2017 in an effort to improve the prognostic accuracy of patients with non-small cell lung cancer (NSCLC) and diminish or eliminate heterogeneity within each stage group (see Table 4.1 and Figure 4.1) (Detterbeck et al., 2017).

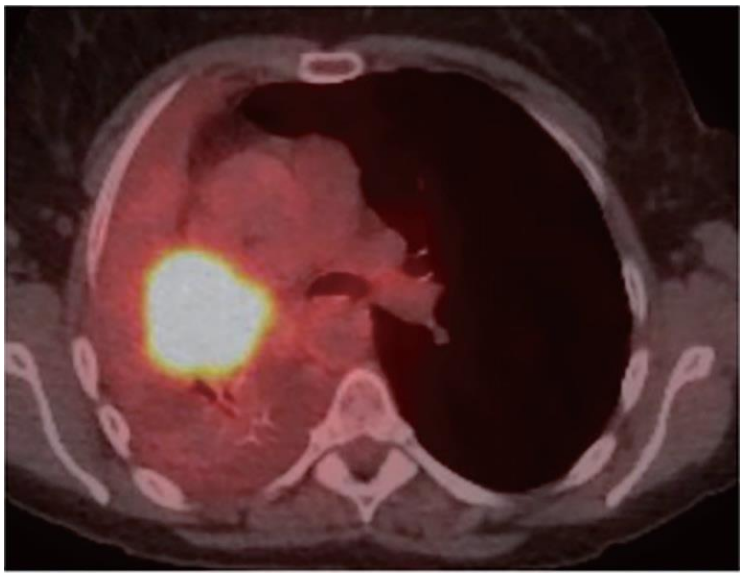

Figure 4.1: Displays a typical example of fused PET-CT image exhibiting a 5-cm obstructing tumour in the right hilum. This categorised as a T2 tumour in accordance with the newly proposed 8th edition TNM guidelines, and previously have reportedly been as a T3 in accordance with the previous 7th TNM schema (Lim et al., 2018).

The 8th TNM has analysed a total of 77,156 patients, including 70,967 (92%) NSCLC patients (Goldstraw et al., 2016). This current advanced staging system has instituted important modifications in the T category, M category and stage grouping. In relation to the T descriptor, the T1 and T2 categories now consist of subcategories differentiated by 10 mm intervals (see Figures 4.2A and 4.2B) , and the current edition relies more heavily on tumour size for classification compared with the 7th edition (Vallieres et al., 2009).

For instance, T1 is now sub-classified based on tumour size into (a) T1a (<10 mm), (b) T1b (>10 mm to 20 mm) and (c) T1c (>20 mm to 30 mm), which correspond to the three new stage subgroups in patients without lymph node involvement (stages IA1, IA2 and IA3) as exhibited in Figure 4.2A. A detailed and more in-depth analysis of the current edition can be found in (Goldstraw et al., 2016).

From a radiobiological modelling perspective, tumour size and, hence, gross tumour volumes (GTVs) are fundamental input parameters for tumour control probability (TCP) predictions. TCP models have long been used in radiotherapy to assess the probability that the treatment intentions could be attained.

Moreover, extensive efforts have been made over the last two decades to develop mathematical models that provide quantitative estimates of TCP using analytical expressions and statistical considerations. A common approach relies, fundamentally, on the assumption that all clonogenic cells are destroyed by the end of a treatment course. Thus, clonogenic cell death probability can be computed to estimate the local tumour control as described in Chapter 3.

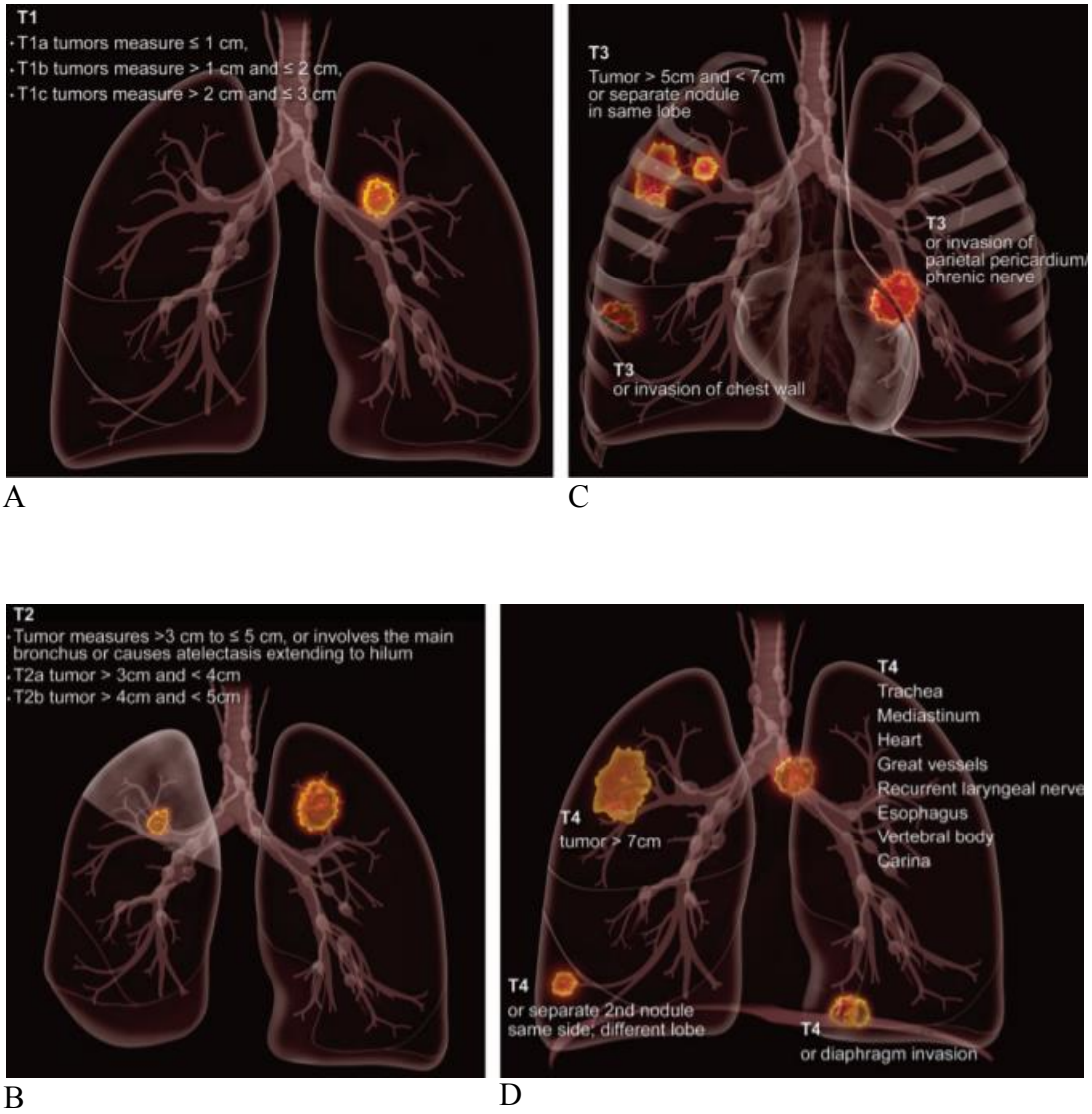

Figure 4.2: Shows an anatomic schematic drawing describing the extensions of the primary tumour of non-small cell lung cancer according to the recommendations of the newly proposed 8th TNM schema; (A) for the T1 descriptors, (B) for the T2 descriptors, (C) for the T3 descriptors and (D) for the T4 descriptors (Kandathil et al., 2018).

In recent years, there has been an increasing amount of literature emphasising the superiority of the 8th TNM over the 7th TNM (Sui et al., 2017, Chansky et al., 2017, Yang et al., 2017) in terms of clinical outcomes, albeit others disagree with this conclusion (Jung et al., 2018). In addition, no attention has been paid to quantify the discrepancy between the 7th and 8th editions of the TNM categorisation schema within the TCP modelling context.

Therefore, this chapter seeks to remedy the above-mentioned controversy in the literature by providing a conceptual TCP framework based on cancer stages. The established TCP model is based on the non-quantitative tumour descriptors T in accordance with the recommendations of the 7th and 8th editions of the TNM categorisation schema. Moreover, this study contributes new insight into the debate involving the superiority of the 8th edition over the 7th edition by investigating the TCP model outcomes of three radiotherapy modalities, namely, CHART, 3D-CRT and SABR.

4.2 Methodology

4.2.1 Patient eligibility

The TCP model was fitted, following the recommendations of the 7th and 8th TNM classification system, to a set of NSCLC patient data collected from the literature. The included studies were identified through a comprehensive systematic search of Google Scholar, Science Direct and PubMed for studies conducted between January 2007 and January 2020. Various mutable processes according to Preferred Reporting Items for Systematic Reviews and Meta-Analyses (PRISMA) were performed to determine which studies met the inclusion criteria, for the purpose of comparing the 7th and 8th editions of the TNM staging system (see Figure 4.3).

Eligible studies were identified using the following key terms: "7th TNM and 8th TNM", "T stage", "NSCLC" and "cancer stage". The following inclusion criteria were also considered in the literature search: (1) the patient's histopathology must confirm one of the three common NSCLC types: adenocarcinoma, squamous cell carcinoma or large-cell carcinoma and (2) either the tumour diameter or GTVs must have been reported.

In the first stage of the systematic review, 4,450 studies were recognised across the three electronic databases; after all duplicates were eliminated, 3,150 articles were retained. The EndNote X8.2 software (Thomson Reuters, USA) was used to manage and sort the articles. Only one study involving 354 patients met the inclusion criteria. Articles were excluded for several reasons, including but not limited to imprecise descriptions of tumour size and GTV based on the T descriptor of the 7th and 8th editions of the TNM or the lack of a detailed quantitative description of the tumour size presentation of the patient distribution based on the two editions.

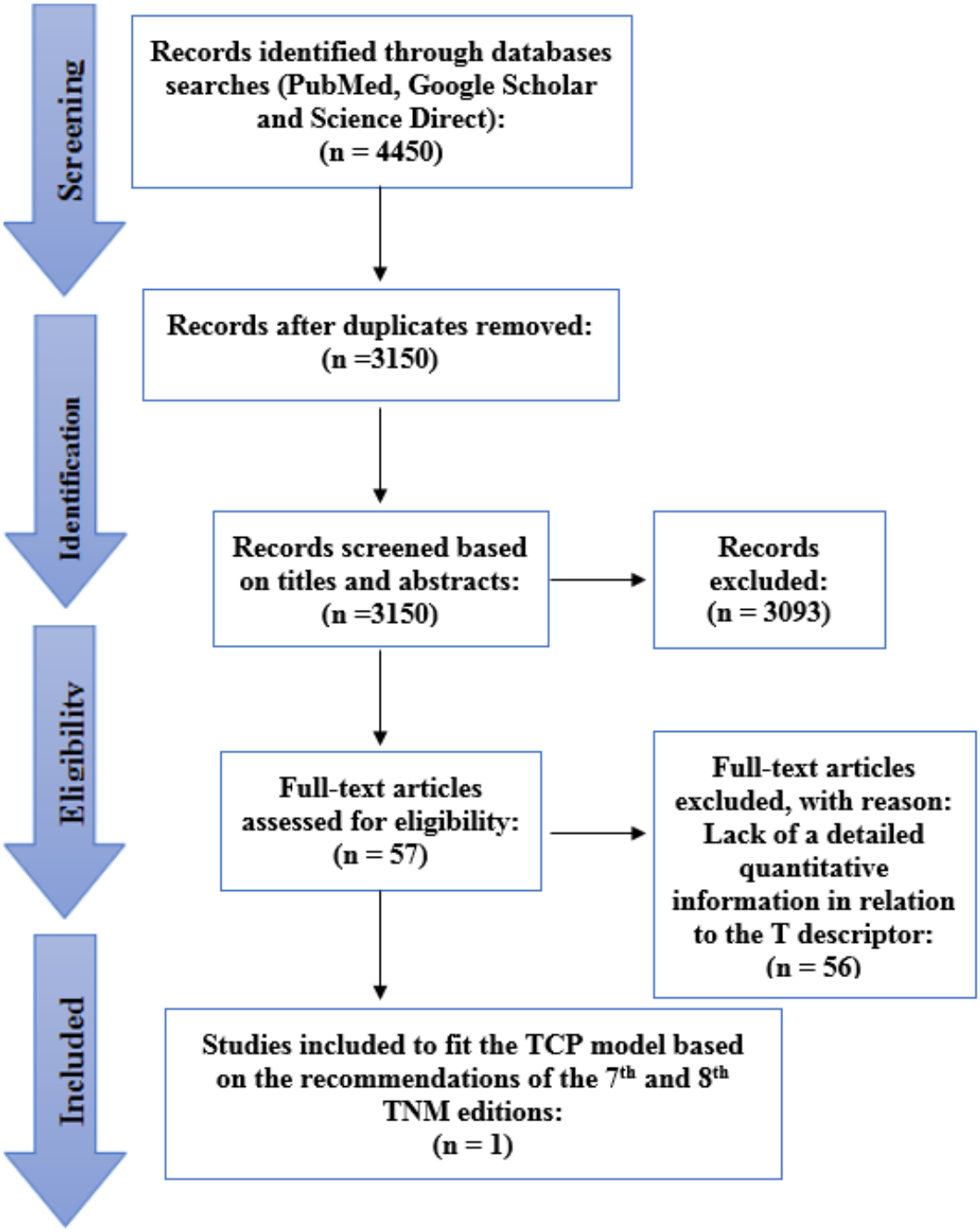

Figure 4.3: Preferred Reporting Items for Systematic Reviews and Meta-Analyses flow diagram delineating the multiple stages of the study selection and systematic review search procedure.

4.2.2 TCP based on the 7th and 8th editions of the TNM

In this part of the study, a single cohort consisting of 354 NSCLC patients was analysed to determine the impact of non-quantitative tumour descriptors T on the TCP model (Neppl et al., 2019). Notably, in the previous TCP model that was described in Chapter 3 (Alaswad et al., 2019a), a fixed GTV size was used to fit the local tumour curability model to 2,713 NSCLC cases collected from the literature. Equation 4.1 was used to compute the total initial number of clonogens (N_0). In that study, a tumour volume of 45 cm^3 was used in patients diagnosed with stage I NSCLC and treated with SABR, whereas an input value of 85 cm^3 was used in stage II and III patients treated with CHART and 3D-CRT (Alaswad et al., 2019a).

$$\mathbf{N_0 = GTV \times P_{clonogens}} \quad \textbf{(4.1)}$$

In an effort to more realistically compare and contrast the differences between the 7th and 8th editions within the TCP frameworks, tumour volume was estimated based on the T descriptor of the 7th and 8th editions of the TNM. The T descriptor represents the size of the primary tumour and indicates whether it has invaded adjacent tissues. The greatest tumour diameter (GTD) is common terminology used to characterise tumour size in NSCLC. In theory, cancers with a higher T stage are more advanced and have larger GTVs than those with lower T stages. Building on these fundamental notions, Equation 4.1 was modified accordingly as follows:

$$\mathbf{N_0 = GTV_{7^{th}TNM} \times P_{clonogens}} \quad \textbf{(4.2)}$$

$$\mathbf{N_0 = GTV_{8^{th}TNM} \times P_{clonogens}} \quad \textbf{(4.3)}$$

Here, $GTV_{7^{th}TNM}$ and $GTV_{8^{th}TNM}$ represent the estimated tumour volume based on the T descriptor of the 7th and 8th editions of the TNM, respectively. Additionally, the parameter of $P_{clonogens}$ was set at 10^7 cm^{-3} in accordance with research published by (Baker et al., 2015, Webb and Nahum, 1993, Alaswad et al., 2019b), who deduced that this value of clonogenic cell density was the best fit for NSCLC clinical outcomes.

The patients in this single cohort were stratified based on the tumour size classification described in the 7th edition. Thus, tumours measuring <20 mm were classified as T1a, whereas those measuring >20 mm to ≤30 mm were classified as T1b. T2 disease was also subdivided into T2a (>30 mm to ≤50 mm) and T2b (>50 mm to ≤70 mm). Tumours measuring >70 mm were classified as T3. It should be noted that the 7th edition uses five tumour size-based categories with cut-off points at 20, 30, 50 and 70 mm.

For comparison purposes, each patient in this single cohort was reclassified and regrouped according to the 8th edition of the TNM. As a result, the T1 and T2 categories were further subdivided according to size. T1 was sub-classified based on tumour size into (a) T1a (≤10 mm), (b) T1b (>10 mm to ≤20 mm) and (c) T1c (>20 mm to ≤30 mm), which correspond to the three subcategories of patients without lymph node involvement, namely, IA1, IA2 and IA3.

T2 stage was subdivided into T2a (>30 mm to ≤40 mm) and T2b (>40 mm to ≤50 mm). The T3 category includes tumours measuring >50 mm to ≤70 mm in diameter, whereas T4 includes tumours measuring >70 mm and invading mediastinal structures or different nodules in a different ipsilateral lobe.

In the field of radiation oncology, several studies have utilised the formula for the volume of a sphere to estimate tumour volume (Nishino et al., 2014, Piccinini et al., 2015, Faustino-Rocha et al., 2013, Ball et al., 2006). In accordance with these publications, the GTVs for the 354 patients were estimated based on the T descriptor of the TNM, as follows:

$$\mathbf{GTV_{7^{th}TNM} = (4/3)\pi \times r^{3}_{7^{th}TNM}} \quad \textbf{(4.4)}$$

$$\mathbf{GTV_{8^{th}TNM} = (4/3)\pi \times r^{3}_{8^{th}TNM}} \quad \textbf{(4.5)}$$

Here, $GTV_{7^{th}TNM}$ and $GTV_{8^{th}TNM}$ are the estimated tumour volumes based on the T descriptor of the 7th and 8th editions of the TNM, as discussed previously in this section. The $r_{7^{th}TNM}$ and $r_{8^{th}TNM}$ values characterise the tumour radius computed using the mean greatest dimension of the lesions that are displayed in Table 4.2.

The TCP model was generated following three radiotherapy fractionation schedules: 3D-CRT) SABR and CHART.

Table 4.2: Comparison of the T-descriptor and patient distribution as recommended by the 7th and 8th TNM classification systems (n = 354).

7th TNM classifications	Recommended tumour size (mm)	Published tumour size (mm) (Neppl et al., 2019)	# of patients
	Any size	91 ±27	27
	>70	72 ±2.7	80
	>50 to ≤70	59 ±8.1	54
	>30 to ≤50	39 ±8.7	113
	n/a	n/a	n/a
	>20 to ≤30	26 ±3.1	48
	<20	16 ±3.8	32

# of patients	6	26	48	69	52	81	72
Published tumour size (mm) (Neppl et al., 2019)	9.1 ±0.7	17 ±2.6	26 ±3.1	33 ±6.9	46 ±3.4	56 ±11	79 ±26
Recommended tumour size (mm)	≤10	>10 to ≤20	>20 to ≤30	>30 to ≤40	>40 to ≤50	>50 to ≤70	>70
8th TNM classifications	T1a	T1b	T1c	T2a	T2b	T3	T4

4.2.3 TCP uncertainty

In a radiotherapy procedure, the need to indicate uncertainties for the obtained results has long been recognised (Alaswad and Coleman, 2017, Alaswad and Coleman, 2019, Cai et al., 2018, Schneider et al., 2010, Ghandour et al., 2016, Bolt et al., 2017). Computationally, the accuracy of a TCP model is mainly dependent on two factors: the radiosensitivity parameters of α or β and the distribution of patients based on the 7th and 8th TNM schemes. It is presumed that the previously prescribed α and β are independent and that each has its own standard deviation, that is, σ_α and σ_β, respectively; therefore, the standard uncertainties of alpha $u(\alpha)$ and beta $u(\beta)$ were estimated as follows:

$$u_{(\alpha)} = \frac{\sigma_\alpha}{\sqrt{n}} \quad (4.6)$$

$$u_{(\beta)} = \frac{\sigma_\beta}{\sqrt{n}} \quad (4.7)$$

Here, n represents the total number of patients (n = 354) involved in the simulation process. The fractional or relative uncertainty in the $\frac{\alpha}{\beta}$ ratio was determined from the fractional uncertainties in α and β.

For instance, for alpha (α) with uncertainty u(α), the relative uncertainty is $\frac{u(\alpha)}{\alpha}$. In the same manner, for beta (β), the relative uncertainty is $\frac{u(\beta)}{\beta}$. Accordingly, the relative uncertainty of α/β is given by:

$$\frac{u\left(\alpha/\beta\right)}{\alpha/\beta} = \sqrt{\left(\frac{u(\alpha)}{\alpha}\right)^2 + \left(\frac{u(\beta)}{\beta}\right)^2} \quad \textbf{(4.8)}$$

Another source of uncertainty that should be addressed is the variation in tumour size in each stage group based on the T descriptor as recommended in the 7th and 8th editions of the TNM (see Table 4.2). Therefore, the idea of estimating the standard uncertainty as described by Equations 4.6 and 4.7 was adopted to address this issue, as follows:

$$u_{(T)} = \frac{\sigma_T}{\sqrt{n}} \quad \textbf{(4.9)}$$

Here, $u_{(T)}$ represents the standard uncertainty of the tumour size based on each T stage group (e.g. T1a) and n represents the distribution of patients in each T stage group. These two sources of uncertainties were summed up to provide the combined standard uncertainty of the TCP model u_c(TCP). To determine the expanded uncertainty of the TCP model(U_{TCP}), u_c(TCP) was multiplied by a coverage factor k, as follows:

$$U_{TCP} = k \times u_c(TCP) \quad \textbf{(4.10)}$$

A coverage factor of 2 was chosen in order to achieve a level of confidence of approximately 95%.

4.3 Results

Figure 4.4 compares the estimated GTVs based on the T descriptor as described in Tables 4.1 and 4.2. The estimated mean GTV volume was 2.3 cm^3 (0.9–3.7 cm^3) in stage T1a, 10 cm^3 (6.6–13.4 cm^3) in stage T1b, 34 cm3 (29–39 cm^3) in stage T2a, 95 cm3 (93–97 cm^3) in stage T2b, 282 cm^3 (262–302 cm^3) in stage T3 and 500 cm^3 (300–700 cm^3) in stage T4; these estimates were obtained following the recommendations of the 7th edition.

The estimated mean GTV volumes based on the guidelines provided in the 8th edition were 0.4 cm^3 (0.3–0.5 cm^3) in stage T1a, 2.7 cm3 (1.9–3.5 cm^3) in stage T1b, 10 cm^3 (6.6–13.4 cm^3) in stage T1c, 21.6 cm^3 (11.6–31.6 cm^3) in stage T2a, 53 cm^3 (41–65 cm^3) in stage T2b, 104 cm^3 (259–149 cm^3) in stage T3 and 350 cm^3 (190–510 cm^3) in stage T4. Data from the scatter graphs (see Figure 4.4) further highlight the view that cancers with higher T stage are more advanced and have larger GTV volumes than those with lower T stages.

(A)

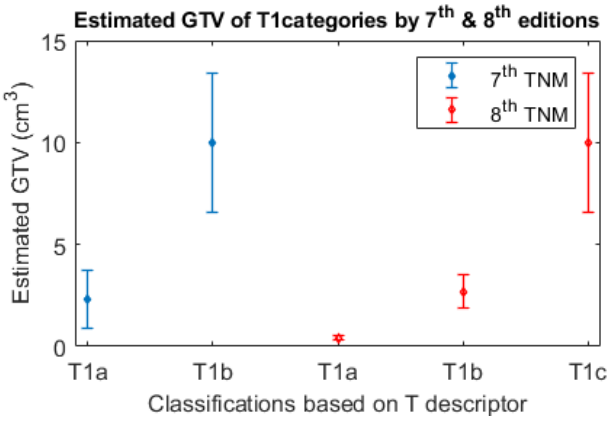

(B)

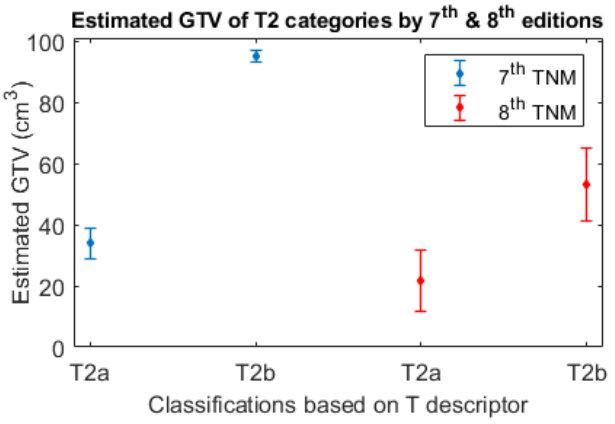

(C)

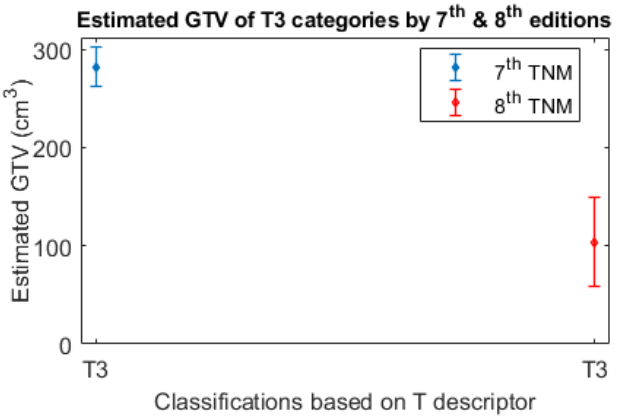

(D)

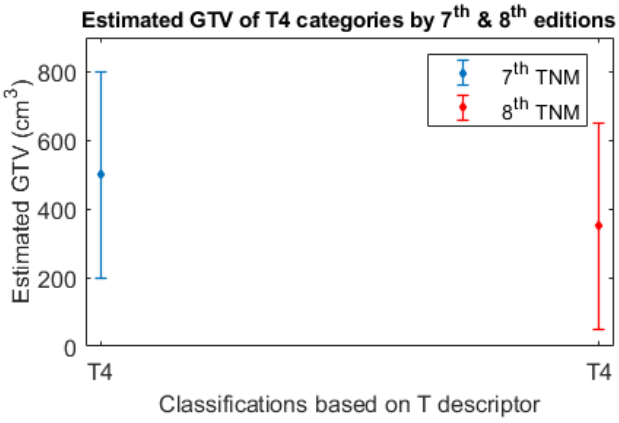

Figure 4.4: Average estimated tumour volumes based on the T descriptor of the 7th and 8th editions of the TNM staging system; (A) for T1 descriptors, (B) for T2 descriptors, (C) for T3 descriptors, and (D) for T4 descriptors. The error bars indicate the standard deviation that represents the variability of the estimated GTV in each cluster.

Figures 4.5 and 4.6 depict the variation of the TCP with the tumour size and GTV in accordance with the recommendations of the 7th and 8th TNM schema, respectively. The performance of the TCP model in the two editions of the TNM staging systems was evaluated using the coefficient of determination (R^2) and root mean square error (RMSE). Compared with the 7th edition, the 8th edition produced, to a certain degree, higher TCP predictions and an improved TCP model fit as indicated by the marginally higher R^2 values and by the marginally lower RMSE presented in Figure 4.5 and Table B.1 of Appendix B.

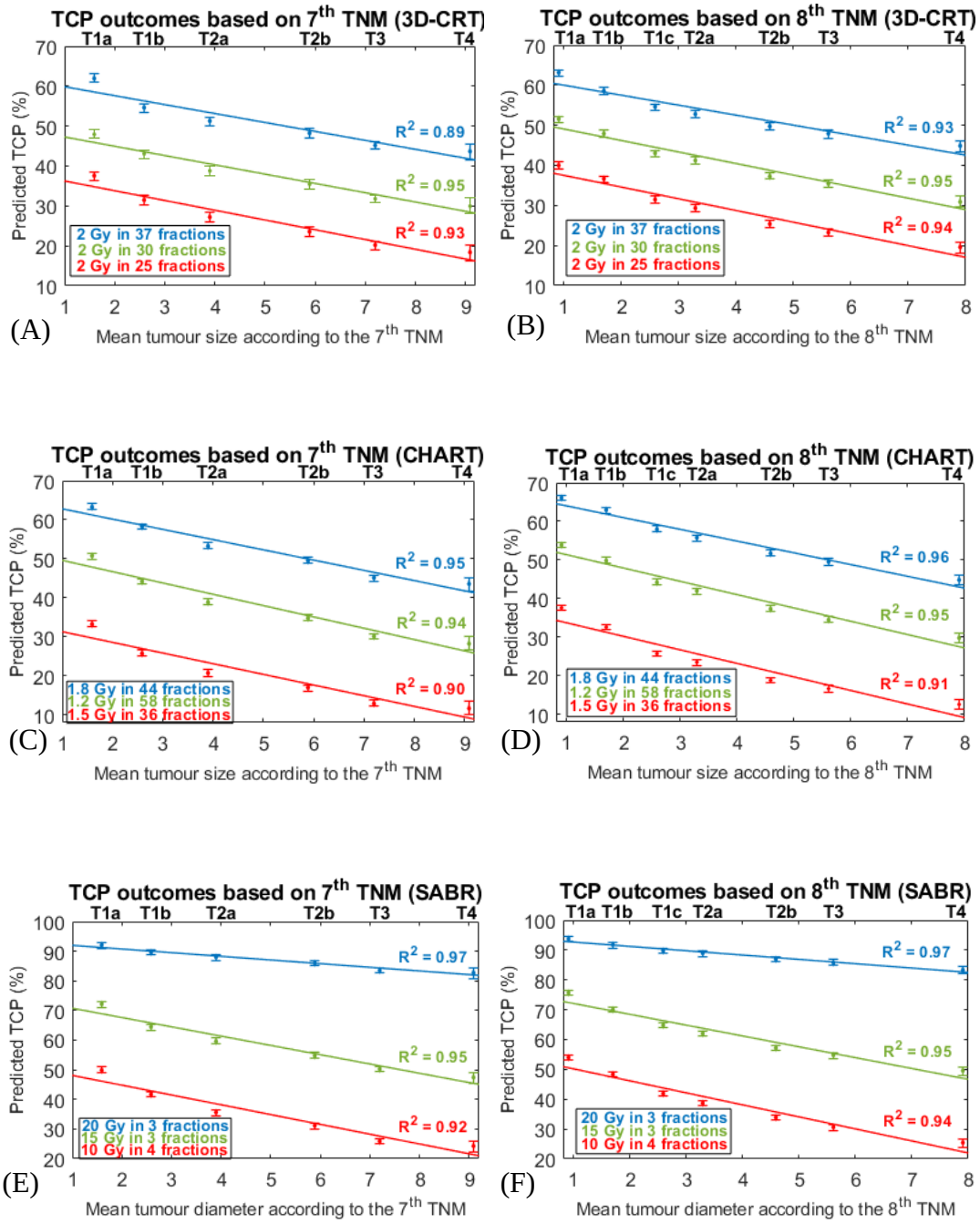

Figure 4.5: Linear regression of the TCP model outcomes as a function of the mean tumour diameter for the 354 patients, based on the T descriptor of the 7th (A, C and E) and 8th (B, D and F) editions of the TNM staging system. Comparisons were made among the three radiotherapy protocols, namely, 3D-CRT, CHART and SABR, which employ various radiotherapy dose prescriptions. The error bars represent the uncertainty budget explained in Section 4.2.3 and summarised in Table 4.5.

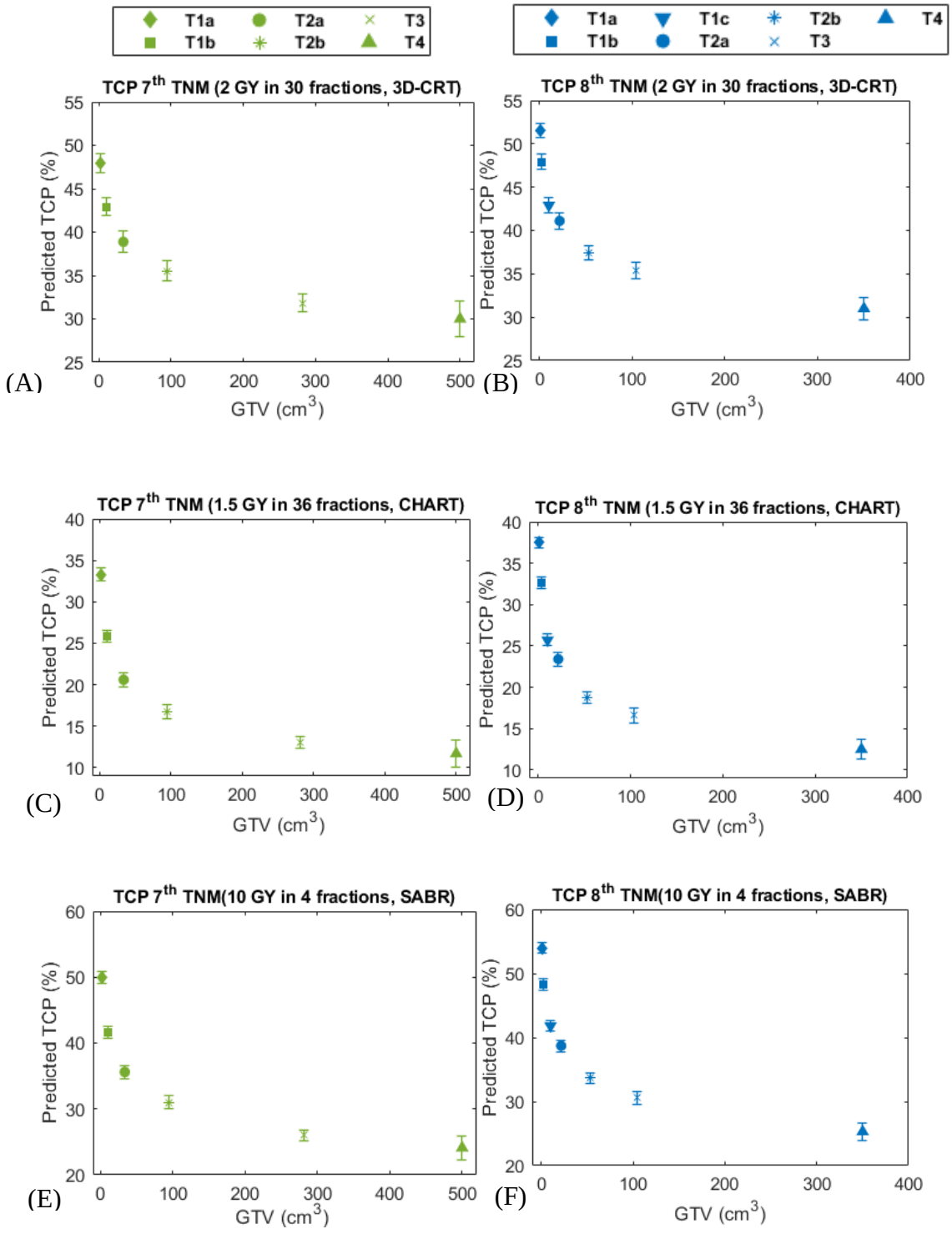

Figure 4.6: The reduction in the TCP model outcomes as a function of the GTV based on the T descriptor of the 7th (A, C and E) and 8th (B, D and F) editions of the TNM staging system. The error bars represent the uncertainty budget explained in Section 4.2.3 and summarised in Table 4.5.

The TCP curves for the three radiotherapy modalities according to the T descriptors of the 7th and 8th editions are shown in Figure 4.7. Based on the T staging criteria, the TCP curves exhibited a similar pattern in the two editions, with a distinct trend of separation in all of the T subcategories. Additionally, the TCP curves decreased as the T stage progresses to the next subgroups; this distinctive pattern was observed in all of the dose fractionation schemes implemented in the simulation process.

For example, the predicted TCP for the T stage T1a vs. T1b groups after applying 2 Gy in 30 fractions was estimated to be 48% ± 1% vs. 43% ± 1% following the 7th edition and 51.5% ± 0.8% vs. 47.8% ± 0.8% following the 8th edition. Statistical assessment based on the unpaired t-test showed that the differences in the predicted TCP between adjacent T category groups in the 8th edition were all significant.

Similar TCP findings were observed in the 7th edition, except for T3 vs. T4 (t value = −1.3, p value = 0.23) in 3D-CRT and T3 vs. T4 (t value = 1.3, p value = 0.26) in CHART; these results were not significantly different at the 95% confidence interval, as shown in Figures 4.7A and 4.7C and Tables B.2 and B.4 of Appendix B.

From the data in Figures. 4.5, 4.6 and 4.7, it is apparent that the outcomes from the TCP model also depend heavily on the fractionation scheme. The total radiotherapy dose ranges applied during the TCP simulation were 50–74 Gy, 54–79.2 Gy and 40–60 Gy for 3D-CRT, CHART and SABR, respectively. The 3 × 20 Gy SABR schedule in the 8th edition yielded the highest TCP, ranging from 93.9% to 83.3% (see Figure 4.5F), whereas the 25 × 2 Gy schedule in the 7th edition attained the lowest TCP, ranging from 37.50% to 18.35%, as shown in Figure 4.5A.

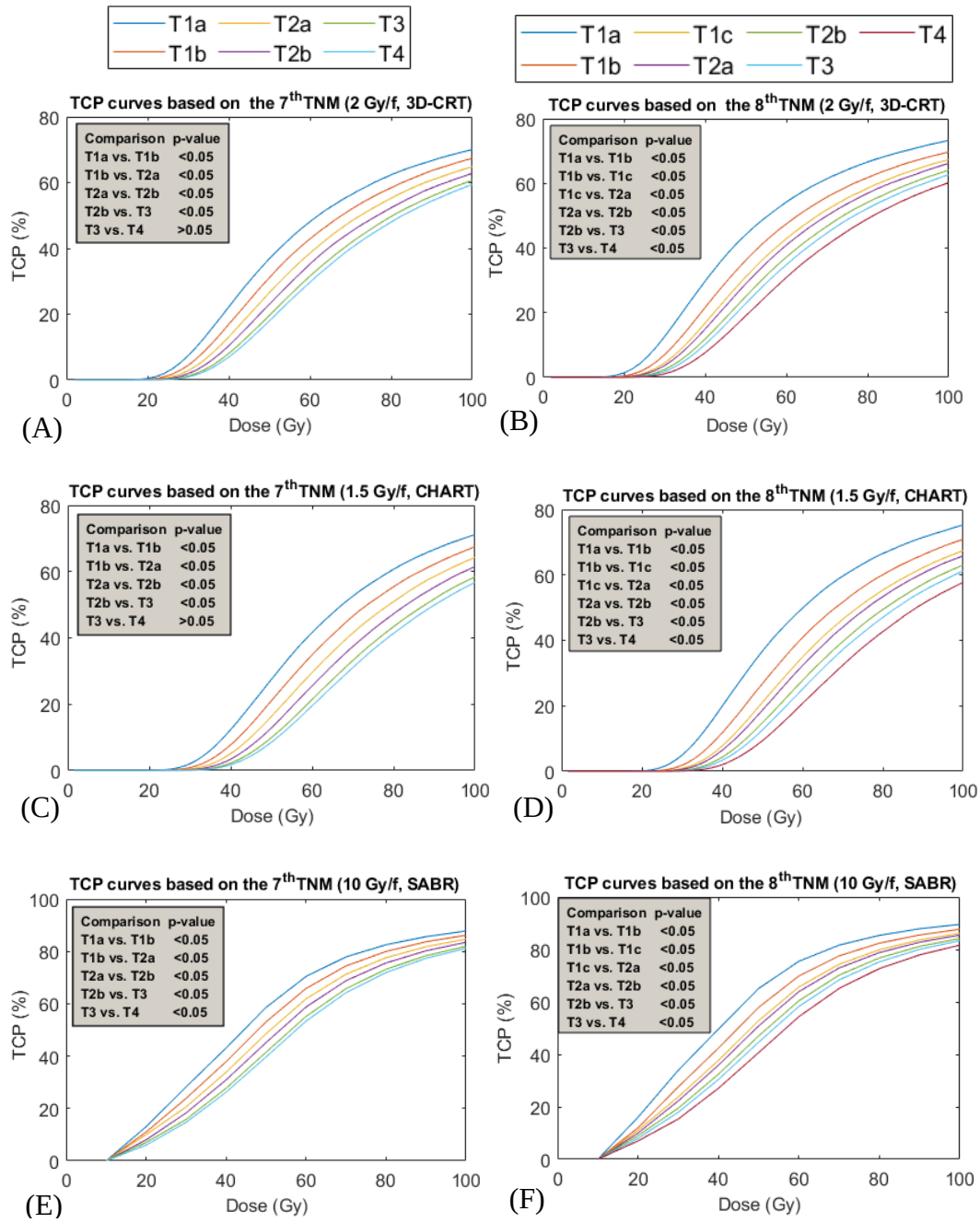

Figure 4.7: TCP curves for patients stratified by the T descriptors of the 7th and 8th TNM for 3D-CRT (A, B), CHART (C, D) and SABR (E, F).

Table 4.3: TCP-derived radiosensitivity parameters based on the NM algorithm alongside the uncertainty analysis. The units of radiosensitivity factors α and β are (Gy^{-1}) and (Gy^{-2}), respectively.

RT modality	α	β	σ_α	σ_β	$u_{(\alpha)}$	$u_{(\beta)}$	$\frac{u\left(\alpha/\beta\right)}{\alpha/\beta}$
3D-CRT	0.63	0.19	0.52	0.0053	0.30	0.003	0.48
CHART	0.61	0.13	0.36	0.018	0.18	0.01	0.30
SABR	0.61	0.12	0.55	0.0037	0.23	0.0015	0.36

Knowledge on the uncertainties in the TCP context is highly desirable for model evaluation purposes. The total TCP model uncertainties were determined in accordance with the comprehensive guidelines presented by the Guide to the Expression of Uncertainty in Measurement (GUM) (ISO and OIML, 1995). All TCP uncertainty components, specifically radiosensitivity parameters and tumour size, are summarised in Tables 4.3 and 4.4 according to the categorisation provided in the GUM. These data were used to derive the combined u_c(TCP) and expanded U_{TCP} uncertainties by the T descriptors of the 7th and 8th editions of the TNM, as indicated in Table 4.5. This statistical uncertainty demonstrated that the T4 descriptors yielded the highest expanded uncertainty of 2.0%, 1.3%, and 1.6% for the 7th edition, and 1.1%, 1.7% and 1.2% for the 8th edition as displayed in Table 4.5.

Table 4.4:Comparison of the tumour size uncertainties according to the T descriptors of the 7th and 8th TNM staging schemes.

	7th TNM			8th TNM		
T-stage	Tumour size (cm)	Standard deviation	Standard uncertainty	Tumour size (cm)	Standard deviation	Standard uncertainty
T1a	1.6	0.38	0.06	0.9	0.07	0.03
T1b	2.6	0.31	0.04	1.7	0.26	0.06
T1c	n/a	n/a	n/a	2.6	0.31	0.04
T2a	3.9	0.87	0.08	3.3	0.69	0.085
T2b	5.9	0.81	0.11	4.6	0.34	0.05
T3	7.2	0.27	0.03	5.6	1.1	0.13
T4	9.1	2.7	0.51	7.9	2.6	0.28

Table 4.5: Summary of the TCP model budget uncertainties following the T descriptors of the 7th and 8th TNM staging schemes.

	3D-CRT				CHART				SABR			
	7th TNM		8th TNM		7th TNM		8th TNM		7th TNM		8th TNM	
T-stage	u_c(TCP)	U_{TCP}	u_c(TCP)	U_{TCP}	u_c(TCP)	U_{TCP}	u_c(TCP)	U_{TCP}	u_c(TCP)	U_{TCP}	u_c(TCP)	U_{TCP}
T1a	0.54	1.09	0.40	0.80	0.36	0.73	0.33	0.65	0.43	0.87	0.39	0.79
T1b	0.52	1.05	0.43	0.85	0.34	0.68	0.36	0.71	0.41	0.82	0.42	0.85
T1c	n/a	n/a	0.41	0.82	n/a	n/a	0.34	0.68	n/a	n/a	0.41	0.82
T2a	0.56	1.12	0.45	0.90	0.38	0.76	0.39	0.77	0.45	0.89	0.45	0.90
T2b	0.60	1.17	0.42	0.83	0.40	0.81	0.35	0.69	0.48	0.96	0.40	0.81
T3	0.51	1.01	0.49	0.98	0.32	0.65	0.42	0.84	0.40	0.80	0.48	0.96
T4	1.0	2.0	0.65	1.30	0.81	1.6	0.58	1.16	0.89	1.77	0.64	1.28

4.4 Discussion

Considering that NSCLC is the leading cause of cancer-related mortality (Ferlay et al., 2015), numerous clinical approaches have been implemented to enhance patient outcomes, including the combination of two oncologic procedures such as in the promising intraoperative radiotherapy, alongside the ongoing effort to establish a novel immunotherapeutic agent for NSCLC (Neuboeck et al., 2010, Manegold et al., 2017). Additionally, clinical cancer staging has been recognised as having a major impact on the development and efficacy of radiotherapy.

The primary purpose of TNM classification is to render a reproducible and consistent characterisation of tumour extent, albeit it can also predict clinical outcomes to some extent. On that account, the TNM schema is an essential component of both patients' therapy and research frameworks. Accordingly, the current study presents further insight into how the concept of TCP correlates with cancer stage, particularly with the T descriptors of the TNM classification system.

The primary edition of the TNM staging scheme for lung cancer was first introduced in 1974 by the UICC (Yoh Watanabe, 2003), and eight editions of this TNM staging system for lung cancer have been published over the past four decades (Goldstraw, 2013, Neppl et al., 2019). These editions have emphasised that the T stage category, defined according to tumour size, is a key prognostic factor in determining disease-specific survival.

The T category was significantly updated in the 8th edition of the TNM classification system for lung cancer. For instance, in the 8th TNM edition, the T1 and T2 categories are more subdivided according to tumour size compared to 7th TNM system edition. Other than the present study, no previous TCP study has tried to quantify the difference between the 7th and 8th TNM classification scheme based on the T category.

The statistical analysis of the model outcomes revealed a strong association between tumour extent and local tumour cure probability. For instance, the T category classification according to tumour size and tumour volume generally showed that patients with T1 and T2 tumours demonstrated improved TCP outcomes compared with patients having T3 and T4 tumours, as indicated in Figures 4.5, 4.6 and 4.7. Furthermore, the regression analysis between the TCP model outcomes and mean greatest tumour sizes (see Figure 4.5) are consistent with those of other studies (Donnem et al., 2011, Ohtaki et al., 2013, Zhang et al., 2019), suggesting that both local tumour control and survival exhibited a strong negative linear reduction as a function of tumour size.

Of note, these findings further confirm the common intuition that large tumour volumes adversely affect the clinical outcomes of radiation therapy. This phenomenon may well be explained by evidence that the amount of cancer stem cells grows proportionately with the expanding tumour size and that the radiation dose required to attain local tumour curability relies on the logarithm of surviving clonogenic cells to be deactivated.

Zips (2009) observed a linear diminution of clonogenic density as radiotherapy doses increase, corroborating the results of Alaswad et al. (2019c). It is also evident that tumours become more radioresistant under hypoxic states, and hypoxia is more prevalent in large tumours than in small tumours (Salem et al., 2018, Forster et al., 2019). Clinically, a large planning target volume (PTV) frequently restricts the use of high curative radiotherapy doses due to the tolerance limit of the adjacent organs at risk. Consequently, attaining the optimum local tumour control could be adversely affected.

Within this framework, there is a large volume of retrospective studies detailing the function of tumour size as a prognostic determinant in NSCLC patients. Bradley et al. (2002) determined whether GTV volumes are a prognostic factor in 207 cases of inoperable NSCLC treated with definitive 3D-CRT.

Statistical analysis confirmed that tumour volume is highly prognostic for local tumour control and overall survival. Additionally, they suggested that tumour volume could be a fundamental basis for stratifying patients in clinical trials. Stinchcombe et al. (2006) analysed 102 cases with medically inoperable stage III NSCLC treated with concurrent chemoradiotherapy versus radiotherapy alone, and they concluded that GTV is a major critical predictor of local tumour control.

The estimated TCP for SABR, CHART and 3D-CRT in this study, as shown in Figure 4.5, concur with most of the published clinical results on this topic (Sandler et al., 1990, Socinski et al., 2008, Zehentmayr et al., 2015, Jeremic et al., 1996, Sanganalmath et al., 2018b, Kopek et al., 2009, Dunlap et al., 2010, Koto et al., 2007). For instance, the reported model outcomes for T1 and T2 in this study ranged from 94% to 89% and from 89% to 87%, respectively, corresponding to a radiation schedule of 60 Gy delivered in three fractions. These results are consistent with those of Dunlap et al. (2010) who found that the two-year local control rates were 90% and 70% for stages T1 and T2, respectively. The radiation schedule involved a total dose of 60 Gy delivered in three fractions. Moreover, they deduced that larger tumour volumes were associated with poor overall survival and local control.

Other investigators (Ohtaki et al., 2013) reported inferior outcomes for SABR modality in stage T1 (77.9%) and T2 (40%) patients treated with a total dose of 48 Gy delivered in four fractions. The above publications, alongside the TCP outcomes shown in Figure 4.5, further support the fact that higher radiotherapy doses are associated with enhanced local tumour control. When the TCP curves were analysed based on the T category of the 7th and 8th editions, an improvement in TCP curve separation was perceived in every stage, from T1a to T4, and the differences were all significant. Nevertheless, the TCP curves of the stage T3 and stage T4 patients were not significant, according to the recommendations of the 7th edition (Figures 4.7A and 4.7C). To the best of our knowledge, this study is the first to describe the impact of the inclusion of cancer stage of the 7th TNM and 8th TNM into the TCP model for NSCLC.

Additionally, the TCP model outcomes based on the T descriptors of the 8th TNM revealed an enhanced model fit, a higher R^2 and a lower RMSE compared with those of the 7th TNM, implying the superior discriminatory ability of the later edition. It seems possible that these results are due to the more fine-grained tumour size categorisation in the 8th TNM that diminish the uncertainty of the tumour volumes in the low T categories. For instance, the 1-cm cut points as described by the recently proposed 8th TNM classification systems prove that every single centimetre, from 1 cm to 5 cm, can contribute to the variations in local control probability, and thus, improve the model fit of this newly proposed edition.

Comparing the 7th and 8th editions of the TNM staging system verified the findings of many studies conducted in the discipline of radiation oncology. In an external validation study of the 8th TNM classification for lung cancer, Chansky et al. (2017) found that the discrimination by the 8th edition of stage combinations and classifications is adequately valid for clinical, pathologic and, most reliably, in stage separations for NSCLC. They further confirms the geographic transportability of this newly proposed stage grouping and its applicability to primarily nonsurgically treated cohorts.

This view was supported by Sui et al. (2017) who analysed a total of 3,599 NSCLC patients, concluding that the 8th edition yielded marginally higher discrimination compared with the 7th edition, as implied by the R^2 values of the recurrence-free survival (RFS) and the overall survival (OS) (RFS = 0.183 vs. 0.178; OS = 0.172 vs. 0.162). Similarly, Yang et al. (2017) provided an in-depth analysis of 858,909 NSCLC patients whose data were obtained from the National Cancer Database (NCDB). In this major study, Yang and his colleagues deduced that the T distribution schema of the 8th edition is more reliable than that of the 7th edition in discriminating various T subgroups, particularly in the pT1 stage. In terms of the overall performance of the two editions, the concordance index of the 7th edition in terms of pT subgrouping (0.608 ± 0.001) was slightly lower than that of the 8th edition (0.610 ± 0.001).

Moreover, they compared the cT subgrouping of the 7th edition (0.551 ± 0.001) to the cT subgrouping of the 8th edition (0.551 ± 0.001), and their results further demonstrated the superiority of the 8th edition over the 7th edition.

By contrast, in a retrospective study involving 1,316 NSCLC cases, Jung et al. (2018) remarked that the T descriptors of the 8th edition of the TNM did not yield a higher explicit predictor of prognosis than the 7th edition. This study revealed that the survival curves and the five-year survival rates based on the T descriptors of the 8th TNM classification did not significantly differ between sequential stages, more specifically for the T1a and T1b ($p = 0.752$) and T1c, T2a and T2b ($p = 0.832$) subcategories. Nevertheless, the study clarified that the 8th edition might not be inferior to the 7th edition in terms of prognostic stratification based on an analysis involving a single small cohort.

It is worth pointing out that the main limitation of the present study is that only a single-institution patient cohort was utilised to fit the TCP model. This implies that the reported TCP findings in relation to the superiority of the 8th TNM edition over 7th TNM edition should be interpreted cautiously. Therefore, further validation research with a large cohort from multiple radiotherapy centres is required to clarify whether the 8th TNM is superior to the 7th TNM within the TCP modelling perspective. It should also be noted that the idea of TCP modelling is to describe local tumour control; thus, only the T descriptor of the TNM staging system can be incorporated into the TCP model. Nonetheless, the other two descriptors – namely the N and M – can also influence the overall survival.

Chapter 5 Influence of incorporating radiotherapy and chemotherapy on the tumour control probability of patients with locally advanced non-small-cell lung cancer

5.1 Introduction

In accordance with the tumour node metastases (TNM) distribution pattern, it is estimated that one-third of patients with non-small cell lung cancer (NSCLC) will be diagnosed with locally advanced (LA) disease (e.g., IIIA or IIIB), and the majority of these patients are not eligible for surgery in light of the considerable challenge with disease extension (Puri et al., 2020). It is worth noting that the therapeutic management of inoperable LA-NSCLC requires controls of both local disease and distant micrometastasis.

Although employing radiotherapy as a sole treatment for this group of patients is potentially with curative intent, long-term survival and local tumour control rates are for the most part discouraging. For instance, the standard fractionation protocol of 60 Gy delivered in 30 sessions yields an unsatisfactory five-year local tumour control rate of just 8%, as exhibited in Figure 5.1 (Saito et al., 1997) .

Interpretations of the patterns of failure following treatment with radiotherapy alone show that the inferior clinical outcomes are correlated not only with the inability to achieve control of the primary tumour extent, but also with the occurrence of distant metastases. Therefore, it has become increasingly important to establish and assess the potential performance of other treatment modalities, including strategies combining chemotherapy and radiotherapy.

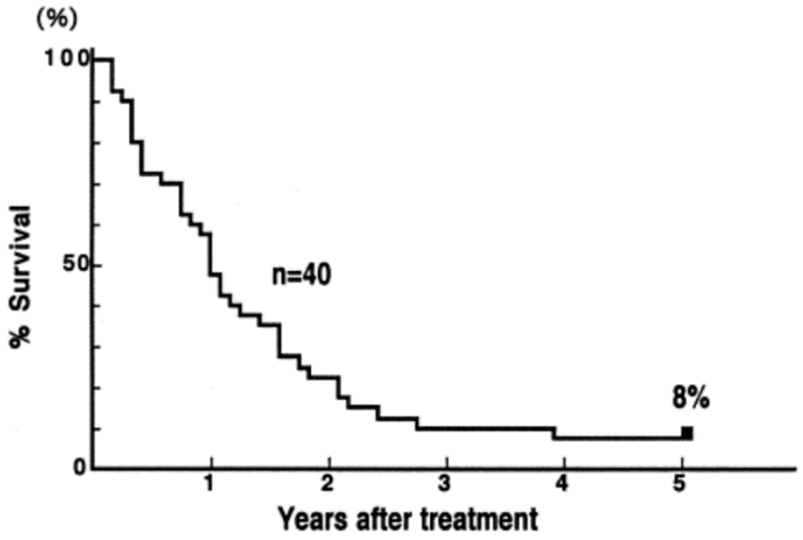

Figure 5.1: Overall survival curve for locally advanced NSCLC patients (stages IIIA and IIIB) treated with radiotherapy modality alone (Saito et al., 1997).

Within this context, a combination of systemic chemotherapy and radiation has been correlated with substantially enhanced local tumour curability and long-term survival, as depicted in Figure 5.2 (Wolski et al., 2005). Chemotherapy is aimed at eradicating cancer cells that may have metastasised (spread) to other parts of the body from the original primary tumour, shrinking primary tumours, and slowing tumour growth (Ko et al., 2018). Currently, more than 100 cytostatic chemotherapy drugs are employed in daily clinical practice (Rompelman et al., 2017).

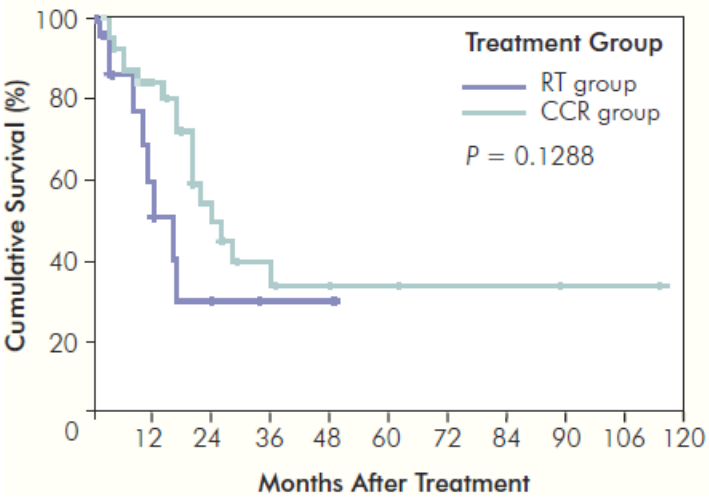

Figure 5.2: Local tumour control for locally advanced NSCLC patients treated with either concomitant chemoradiotherapy (CCR) or radical radiotherapy alone (RT) (Wolski et al., 2005).

Furthermore, a recent phase I study conducted by Higgins et al. (2017b) of Winship Cancer Institute revealed a significantly positive clinical outcome of radiotherapy concurrent with chemotherapy. In that study, 19 patients with stages IIIA and IIIB NSCLC received 44 Gy of conventionally fractionated thoracic radiation with concurrent chemotherapy, along with a dose-escalated SABR boost to the primary tumour as well as the involved mediastinal lymph nodes. The overall survival rates for the one-, two- and three-year follow-ups were 62%, 56% and 39%, respectively.

Similarly, a phase III clinical trial performed by Sause et al. (2000) investigated whether chemotherapy followed by radiotherapy could yield exceptional clinical outcomes in surgically unresectable NSCLC cases wherein patients underwent either hyperfractionated radiation or standard fractionation radiotherapy. The clinical outcomes of that study implied a trend toward an improvement in overall survival, wherein the one-year survival rate of the patients treated with radiotherapy alone was 45% and the survival rate of those treated with concurrent chemo-radiation was 60%. Nevertheless, concern persists as to whether major incidences of toxicity may occur due to the addition of chemotherapy (Chen et al., 2020).

The two fundamental oncologic treatment regimens for delivering the aforementioned combining modalities are: (a) sequential, whereby chemotherapy modality is completed prior to the initiate of the radiotherapy and (b) concurrent, according to which radiation and chemotherapy are administered simultaneously (Rajappa et al., 2019). The former approach diminished the risk of distant metastases, may also reduce the volume of the primary tumour making subsequent irradiation more effective, and may even make the tumour resectable. Nevertheless, prolonged total treatment time, postponed irradiation, and the possibility of accelerated repopulation of tumour cells (see Section 2.11) can adversely affect local tumour control.

On the other hand, the potential advantages of concurrent radiochemotherapy include – but are not limited to – sensitisation of tumour cells to radiation by the administration of chemotherapy drugs and shortening of overall treatment time compared with sequential therapy. Several studies have shown that concurrent radiochemotherapy yielded improved local control and median survival rates contrary to the sequential radiochemotherapy; one example is the noteworthy and continual effort by the NSCLC Collaborative Group., who conducted a meta-analysis of six randomised trials that evaluated the superiority of concurrent radiochemotherapy versus sequential radiochemotherapy (Aupérin et al., 2010).

Within this framework, analysis by Maguire et al. (2014) has indicated that the median progression-free survival (PFS) of concurrent radiochemotherapy was significantly enhanced in comparison with sequential radiochemotherapy (20.67 and 15.81 months, respectively), and the one- and two-year PFS rates were 55% and 34%, respectively, for the concurrent therapy arm, and 52% and 24% for the sequential therapy arm (Maguire et al., 2014). Nonetheless, sequential radiochemotherapy is associated with lower toxicity (e.g., less radiation pneumonitis and oesophageal toxicity).

Thus, concomitant radiochemotherapy is broadly employed in the UK, Ireland and other European countries as the standard treatment procedure for unresectable stage III NSCLC (Lim et al., 2010, Pallis et al., 2010, Postmus et al., 2017, Ramnath et al., 2013, Helbrow et al., 2012, Brunelli et al., 2009). Of note, the rationale behind the combined modality procedure is that cytotoxic drugs diminish micrometastatic foci and also function as radiosensitisers. Clinical data from several sources reveal that the risk of locoregional relapse and distant metastasis were less evident in concomitant radiochemotherapy compared to radiotherapy alone (see Table 5.1).

Stage III NSCLC disease can be perceived hypothetically as having two compartment regions: a loco-regional compartment in the chest and a distant compartment harbouring potential micrometastases. Thus, the paramount objective in managing this disease can be described in two aspects: eradicating the visible intrathoracic disease and diminishing the incidence of subsequent systemic intrathoracic metastases.

However, there have been few efforts to radiobiologically model these combination therapies; such modelling would facilitate patient stratification and optimisation of this combination treatment approach. Consequently, it would be practically useful if the effects of cytotoxic drugs could be expressed by radiobiological principles. Additionally, local tumour control probability (TCP) is the core radiobiological notion for NSCLC control and other cancers, as has been comprehensively investigated in various contexts of this thesis. Quantification of the chemoradiation effects by employing the TCP model can thus further yield more robust insight into the clinical implications and perspectives of this combination treatment approach.

The rationale behind the involvement of radiobiological modelling within the context of chemoradiotherapy was highlighted by Plataniotis and Dale (2008), who emphasised that clinical trial designs should include radiobiological modelling assessments that can provide an indication of how to optimally facilitate patient stratification. Nonetheless, research in the field of TCP modelling of NSCLC has tended to focus on quantifying the radiation effect alone and has not dealt with the chemotherapy principle.

Furthermore, technical advancement in dose optimisation and delivery of radiotherapy (e.g., VMAT and proton therapy) have contributed fundamentally to enhanced clinical outcomes while also diminishing the toxicities confronted during the administration of a concurrent radiochemotherapy approach. Nonetheless, several published studies were unable to reproduce that advancement in clinical outcomes and reduce toxicity for LA-NSCLC (Harris et al. 2014, Mell et al. 2003). A possible explanation for these unexpected outcomes may be due to the uncertainty in the delivered radiation dose.

The objectives of this chapter were threefold: (1) to extend the TCP model described in Chapter 3 (Alaswad et al., 2019a) in order to evaluate the feasibility of quantifying the effect of cytotoxic chemotherapy for patients diagnosed with LA-NSCLC; (2) to analyse the impact of dose variations in the overall TCP outcomes; and (3) to discuss in depth the challenges encountered during radiotherapy delivery for LA-NSCLC.

5.2 Methodology

5.2.1 Patient selection criteria

5.2.1.1 Search strategy

The clinical data employed in the TCP model fit were assembled from three electronic sources: PubMed, Google Scholar and ScienceDirect. A systematic review was performed in compliance with the Preferred Reporting Items for Systematic Reviews and Meta-Analyses (PRISMA) guidelines, in manner analogous to the searches undertaken to accomplish research demonstrated in Chapters 3 and 4 (see Figure 5.1). The search strategy for the PubMed electronic database utilised the following text words (TW) and Medical Subject Headings (MeSH): local tumour control (TW), radiotherapy alone versus chemoradiotherapy (MeSH), concurrent chemoradiotherapy (MeSH) and concomitant chemoradiotherapy (MeSH). Subsequently, the same above-mentioned keywords were diversely merged and utilised across the databases of Google Scholar and ScienceDirect. To restrict the identified clinical studies within the scope of the research question and confine the investigation to the pertinent citations, the design of the search was profoundly dependent upon the Boolean logic criteria.

5.2.1.2 Patient eligibility

Eligibility criteria required that publications examine two clusters of treatment arms comparing and analysing clinical outcomes of radiochemotherapy with radiotherapy alone in patients with histologically verified, locally advanced, nonresectable NSCLC. In an effort to provide a comprehensive overview of the available evidence for building the TCP model, all types of clinical investigations were considered, including – but not limited to – prospective studies and randomised controlled clinical trials comparing radiotherapy-alone with radiochemotherapy. A further inclusion criterion was that publications reported local tumour control details at one-, two- and three-year follow-ups.

5.2.1.3 Study selections

The preliminary comprehensive literature review search yielded a total of 951 potentially relevant articles. After excluding duplicates, 531 records were retained for further investigation. Study identification components were regulated in a three-step refinement process. During the first inclusion stage, the article titles and abstracts were comprehensively screened for the inclusion criteria, which identified 481 articles that were determined to be unrelated to the research subject. The full text of the remaining 44 citations was then systematically reviewed and analysed, which left 8 qualifying studies that met the inclusion criteria.

In the final phase of the search entailed a review of reference lists of selected papers, which yielded no additional eligible studies. Furthermore, publications that were later revised by their authors were also examined. Hence, the initial paper of the randomised and controlled phase III trial by the Japan Clinical Oncology Group (JCOG0301) (Atagi et al., 2012), which was included in the systematic review, was replaced by an updated study (Atagi et al., 2018). Nonetheless, the local tumour control outcomes reported in 2018 remained the same as reported in 2012.

5.2.1.4 Clinical data extraction

The following clinical data were extracted from each article for the purpose of modelling analysis and simulation: (1) number of patients enrolled in each treatment arm; (2) radiotherapy treatment, including the number of fractions and total dose; (3) chemotherapy agent and dosing regimen; and (4) data associated with the outcomes assessment, specifically local tumour control rates at one, two, and three years in each treatment arm. For studies whose results were exhibited only in a Kaplan-Meier curve, corresponding local control rates were extracted from the curves.

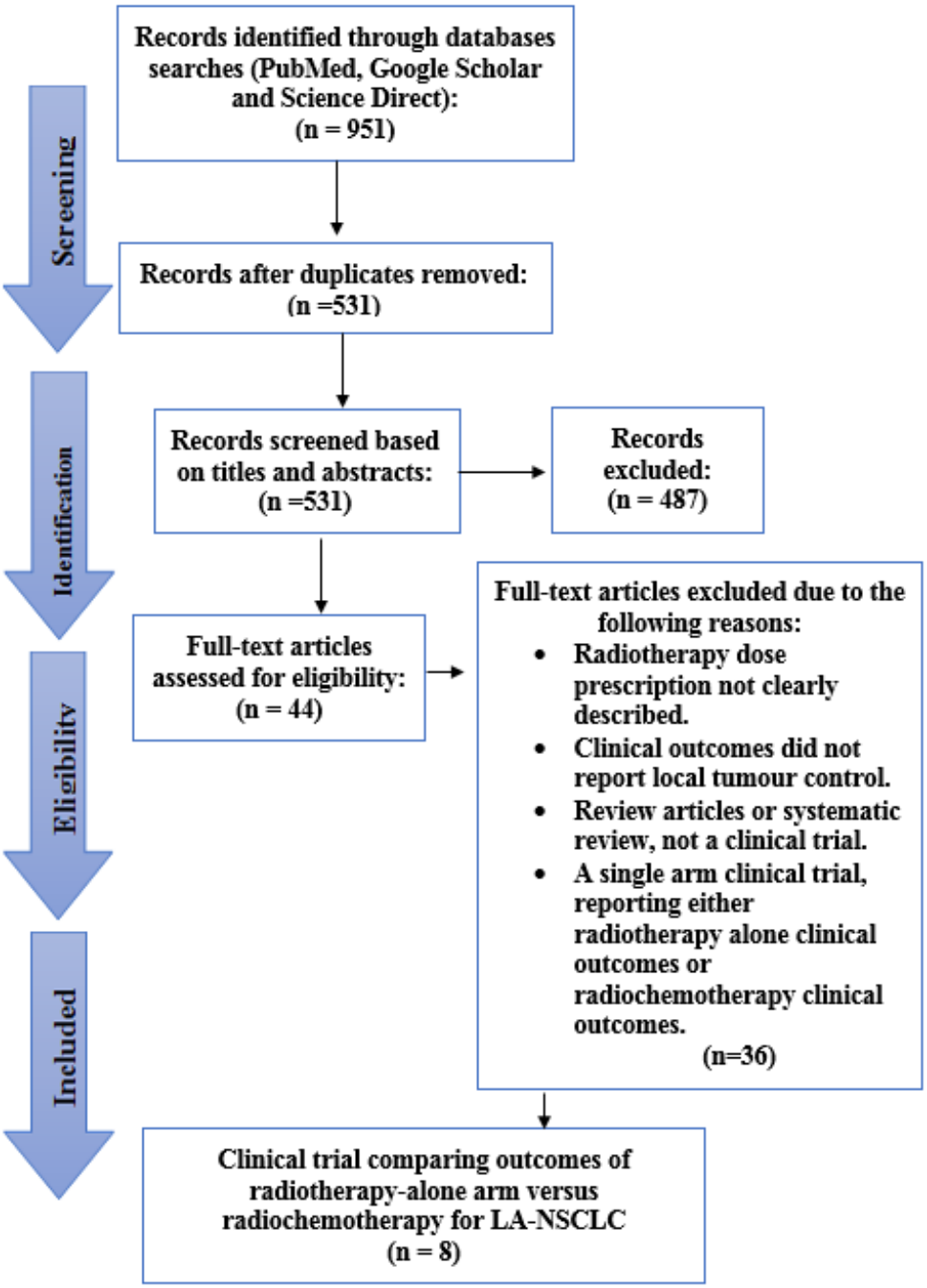

Figure 5.3: PRISMA flow diagram illustrating the various phases of the systematic review search and the study selection process.

Table 5.1: Baseline patient characteristics of the studies included in building the TCP models.

Reference	Radiation therapy alone (n = 441)						Combined chemoradiotherapy (n = 400)				
	n	TD (Gy)	d/f (Gy)	Local tumour control (%)			n	CCRT regimen	Local tumour control (%)		
				1	2	3			1	2	3
(Crino et al., 1993)	33	56	2.0	15	NA	NA	33	CIS 100 mg/m^2 and ETOP 120 mg/m^2 in addition to 56 Gy/ 28 fractions.	17	n/a	n/a
(Scagliotti et al., 2006)	46	60	2.0	20	11	NA	43	DOC 120 mg/m^2 in addition to 60 Gy/ 30 fractions	32	19	n/a
(Atagi et al., 2005, Atagi et al., 2012, Atagi et al., 2018)	23	60	2.0	18	10	8.0	23	CARB 600 mg/m^2 in addition to 60 GY/ 30 fractions	40	20	18
(Schaake-Koning et al., 1992)	114	60	3.0	35	21	9	110	CIS 120 mg/m^2 in addition to 60 Gy / 20 fractions	60	33	29
(Sarihan et al., 2004)	20	63	2.0	24	15	15	21	PAX 360 mg/m^2 in addition to 63 Gy/ 32 fractions	63	38	38
(Lee et al., 2012)	82	65	2.0	30	17	10	43	Platinum-taxol regimen in addition to 65 Gy/ 33 fractions	40	35	13
(Wolski et al., 2005)	23	70	2.0	45	30	25	45	PAX/ CARB (prescription not specified) in addition to 70 Gy/ 35 fractions	83	50	38
(Sim et al., 2001)	70	80	2.0	50	35.4	30	82	Wide range of drugs in addition to 80 Gy/ 40 fractions	56	43.1	38

No; number of patients enrolled in each arms, TD; total dose, d/f; dose per fraction, Cisplatin; CIS, etoposide; ETOP, DCO; docetaxel, CARB; carboplatin, PAX; paclitaxe

5.2.2 Radiochemotherapy model description

Exploratory radiobiological modelling may advance experience of the potential usefulness of concomitant radiochemotherapy. In this portion of the research, the TCP model described in Chapter 3 was further extended to quantify the effect of adding chemotherapy to radiotherapy. Within this framework, to quantify the therapeutic gain of radiochemotherapy in comparison to radiotherapy alone, two possible TCP models scenarios were proposed in the literature: (1) that the drug may improve tumour control probability outcomes by potentiating the local efficacy of radiotherapy (sensitisation effect), or (2) that it may have an independent effect, directly killing the tumour cells (Jones and Dale, 2005, Barazzuol et al., 2010, Plataniotis and Dale, 2008, Alaswad et al., 2020).

The dose sensitisation approach assumed that each radiotherapy dose was administered concurrently with a sensitising agent in such a way that fractional dose d became dose dc, where c was the chemotherapy-modulated radiation dose enhancement factor. The dose of chemotherapy applied in this scenario is not necessarily sufficient to cause significant cell kill. A typical value of c may range between 1.2–2, as shown in Appendix A. It is worth pointing out that the modulated radiation dose enhancement factor is not based on a specific chemotherapy prescription; rather, it is determined by trial and error. For instance, the reasonable value of this factor can be determined by inserting a set of c values within the standard TCP model equation and then evaluating whether the overall TCP is enhanced to the level observed in the clinical trial.

Remarkably, this approach may not reflect the authentic influence of chemotherapy dose prescriptions on the overall TCP outcomes (see Appendix A.8), because there are common situations in which significant doses of chemotherapy are administered simultaneously with radiotherapy, as shown in Table 5.1. For instance, carboplatin (CARB) is administered at daily doses of 30 mg/M^2 for 20 fractions in the treatment of LA-NSCLC cancer. Accordingly, the dose intensity is high and can produce meaningful cell kill and tumour regression when administered on its own. In such an

event, independent cell kills – rather than pure sensitisation – are a more realistic mechanism for quantifying the influence of synergistic cytotoxic chemotherapy with radiotherapy. Thus, it was decided that this is a more adequate approach that would be adopted in the current investigations.

The TCP-LQ model described in Equation 3.5 was amended to quantify the effect of chemotherapy prescription according to the log cell kill notion as shown in Equation 5.1. Notably, the log cell kills mechanism relies on the assumption that cytotoxic drugs eliminate a certain fraction of clonogenic cells based on the drug concentration.

$$\mathbf{TCP} = \mathbf{e}^{-\mathbf{N_0}\mathbf{e}^{-\mathbf{n}\left(\boldsymbol{\alpha}\mathbf{d}+\mathbf{G}\boldsymbol{\beta}\mathbf{d}^{\mathbf{2}}\right)+\boldsymbol{\gamma}(\mathbf{T_0}-\mathbf{T_{del}})-\mathbf{N_c}\mathbf{X}}} \quad \textbf{(5.1)}$$

Here, the chemotherapy factor can be quantified using the factor N_c, which is the number of chemotherapy cycles each with a cell kill coefficient X. Additionally, the N_cX was determined for each clinical trial described in Table 5.1 through the following two equations:

$$\mathbf{TCP_{RT}} = \mathbf{e}^{-\mathbf{N_0}\mathbf{e}^{-\mathbf{E}}} \quad \textbf{(5.2)}$$

$$\mathbf{TCP_{RT+CRT}} = \mathbf{e}^{-\mathbf{N_0}\mathbf{e}^{-\mathbf{E}-\mathbf{N_c}\mathbf{X}}} \quad \textbf{(5.3)}$$

Here, $\mathbf{TCP_{RT}}$ and $\mathbf{TCP_{RT+CRT}}$ represent local tumour control for the radiotherapy-alone and radiochemotherapy arms, respectively, which are shown in Table 5.1. By taking the natural logs and dividing both Equations 5.2 and 5.3, this leads to Equation 5.4:

$$\mathbf{N_cx} = \mathbf{ln}\left(\frac{\mathbf{ln\ TCP_{RT}}}{\mathbf{ln\ TCP_{RT+CRT}}}\right) \quad \textbf{(5.4)}$$

It is important to realise that the value of N_cx was determined for each clinical trial at different clinical end points, which were then inserted as input parameters into the original model described in Chapter 3 to quantify the influence of radio chemotherapy on the overall TCP model outcomes.

5.2.3 Impact of dose variation on TCP

It is widely recognised that radiotherapy machines are calibrated to deliver a specific radiation dose under a set of standard conditions (Eaton et al., 2020). Recent advances in radiotherapy (such as image-guided radiation therapy [IGRT], SABR, MRI-Linac and proton therapy) have reduced the dosimetric uncertainties associated with treatment delivery (Astaraki et al. 2019, Bendall et al. 2018, Gomez et al. 2018, Yamamoto et al. 2018). From that perspective, the previously recommended 5% tolerance for the absorbed-dose accuracy was substituted by more precise statistical measures. For instance, in scenarios with high radiation dose gradients (i.e., situations where dose variations greater than 20%/cm are encountered) the notion of distance to agreement (DTA) with an accuracy of 3.5 mm is strongly recommended. In contrast, in regions of low radiation dose gradients, the discrepancy between the treatment planning absorbed dose and the measured absorbed dose should be within 3.5% (Gregoire and Mackie, 2011).

Additionally, several situations may arise that result in a patient receiving a radiotherapy dose with a systematic difference to that prescribed by the radiation oncologists. The sources of radiotherapy dose uncertainty include – but are not limited to – absolute calibration of the treatment machine, modelling of radiation transport within the patient, tumour and healthy tissue delineation, patient positioning, and day-to-day patient positioning variations. These potential variations in the delivered radiotherapy dose may adversely impact the patient's clinical outcomes. Therefore, the effects of radiotherapy dose uncertainty on the TCP model were quantified. This was accomplished by varying the nominal radiation dose exhibited in Table 5.1, from -5% to +5%, with an interval of 0.5 for both radiotherapy alone and radiochemotherapy arms.

5.3 Results

Table 5.2: Computed $N_C x$ values for different clinical end points.

Clinical end point	References	TCP_{RT}	TCP_{RT+CRT}	Diff (%)	$lnTCP_{RT}$	$lnTCP_{RT+CRT}$	N_cX
1-year follow-up	(Crino et al., 1993)	0.17	0.32	14.60	-1.77	-1.15	0.43
	(Scagliotti et al., 2006)	0.23	0.42	19.00	-1.47	-0.87	0.53
	(Atagi et al., 2018)	0.23	0.44	20.50	-1.46	-0.83	0.57
	(Schaake-Koning et al., 1992)	0.25	0.53	28.60	-1.39	-0.63	0.80
	(Sarihan et al., 2004)	0.28	0.53	25.20	-1.27	-0.63	0.70
	(Lee et al., 2012)	0.31	0.52	20.60	-1.16	-0.66	0.57
	(Wolski et al., 2005)	0.39	0.67	27.80	-0.95	-0.41	0.85
	(Sim et al., 2001)	0.52	0.76	23.70	-0.66	-0.28	0.85
2-year follow-up	(Scagliotti et al., 2006)	0.127	0.26	13.3	-2.06	-1.35	0.43
	(Atagi et al., 2018)	0.126	0.266	14	-2.07	-1.32	0.45
	(Schaake-Koning et al., 1992)	0.171	0.28	10.9	-1.77	-1.27	0.33
	(Sarihan et al., 2004)	0.163	0.318	15.5	-1.81	-1.15	0.46
	(Lee et al., 2012)	0.187	0.342	15.5	-1.68	-1.07	0.45
	(Wolski et al., 2005)	0.252	0.409	15.7	-1.38	-0.89	0.43
	(Sim et al., 2001)	0.384	0.506	12.2	-0.96	-0.68	0.34
3-year follow-up	(Atagi et al., 2018)	0.078	0.2	12.2	-2.55	-1.61	0.46
	(Schaake-Koning et al., 1992)	0.12	0.307	18.7	-2.12	-1.18	0.59
	(Sarihan et al., 2004)	0.111	0.245	13.4	-2.20	-1.41	0.45
	(Lee et al., 2012)	0.134	0.251	11.7	-2.01	-1.38	0.37
	(Wolski et al., 2005)	0.196	0.314	11.8	-1.63	-1.16	0.34
	(Sim et al., 2001)	0.332	0.414	8.2	-1.10	-0.88	0.22

Table 5.2 shows the deduced chemotherapy log cell kill (i.e., $N_C x$ values) factors based on the clinical trials outcomes described in Table 5.1. The chemotherapy factor were derived for three clinical end points: one-, two- and three-year local tumour control follow-ups, which were eventually employed to quantify the effect of synergistic cytotoxic chemotherapy with radiotherapy on the overall TCP model outcomes.

The $N_C x$ values ranged from 0.43–0.85 for one-year local tumour control clinical outcomes, 0.33–0.46 for two-year local tumour control clinical outcomes, and 0.22–0.59 for three-year local tumour control clinical outcomes. From the data presented in Table 5.2, it is apparent that the $N_C x$ value for specific clinical trials depends mainly on the discrepancy between the reported local tumour controls for radiotherapy alone and radiochemotherapy arms, respectively. For instance, the greater the difference in local tumour control between the two arms, the greater the value of the $N_C x$ factor.

In agreement with previously published results (Alaswad et al., 2019a, Alaswad et al., 2019b, Alaswad et al., 2019c, Alaswad et al., 2018), the TCP model is capable of successfully fitting the clinical data of locally advanced NSCLC following the radiotherapy regimen arm (see Figure 5.4A). In this study, the TCP model quantified the synergistic cytotoxic chemotherapy with radiotherapy by incorporating the $N_C x$ factor. The TCP model outcomes revealed a strongly positive linear correlation between the predicted TCP outcomes and the local tumour control reported in the literature. Figures 5.4A and 5.4B show the correlation coefficient R^2 of statistical tests between the estimated TCPs corresponding to both arms. The statistical analysis yielded tumour control rates of $R^2 = 0.88$ and wRMSE = 0.85% for the radiotherapy alone arm, and $R^2 = 0.86$ and wRMSE = 1.3% for the radiochemotherapy arm. All p-values were < 0.05.

Consistent with the reported outcomes presented in Table 5.1, the TCP model outcomes for the radiochemotherapy arm exhibited TCPs superior to those of the radiotherapy alone arm. For the radiochemotherapy arm, TCPs were as high as 75.5%, 50.6% and 41.4% at one-, two- and three-year local tumour control rates, respectively.

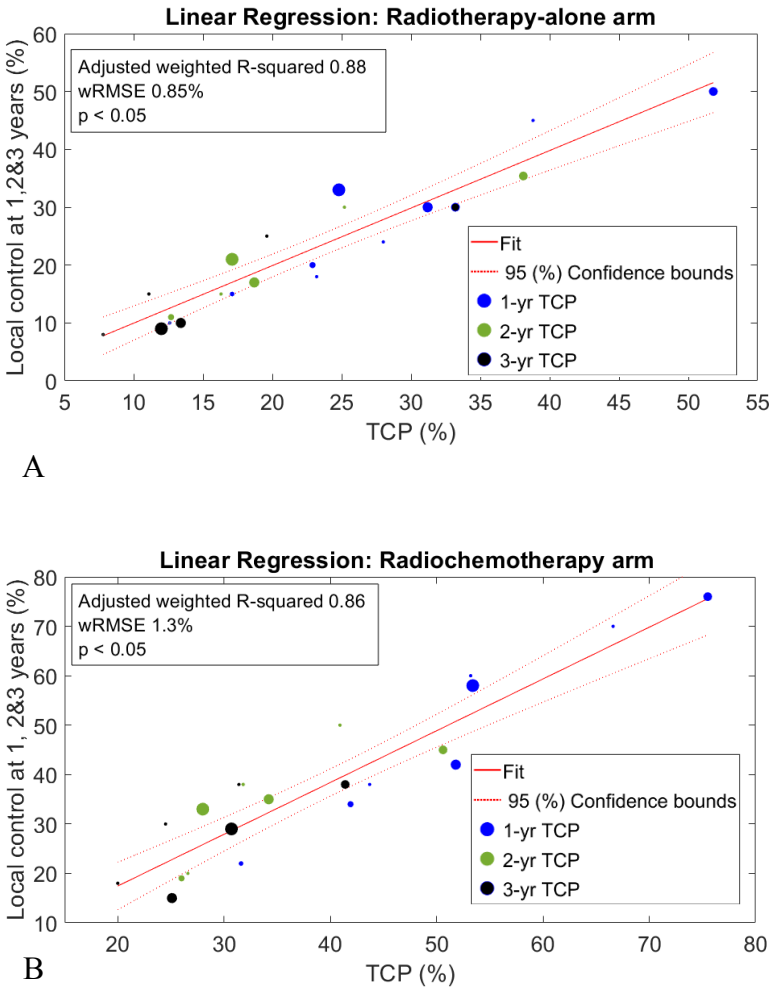

Figure 5.4: Correlation between the reported clinical outcomes and TCP model outcomes for radiotherapy alone (A) and radiochemotherapy (B) arms. The dataset was statistically weighted and scaled by incorporating the effect of the number of patients in each clinical trial.

Table 5.3 displays the global minimum solution of the initial guess of the radio sensitivity components α and β and their standard deviations σ_α and σ_β, as produced by the NM simplex algorithm, for both radiotherapy and radiochemotherapy arms.

Table 5.3: Radiosensitivity solutions produced by the NM algorithm.

RT modality	α	β	σ_α	σ_β	α/β
1-yr TCP	0.68	0.15	0.16	0.0025	4.5
2-yr TCP	0.57	0.14	0.34	0.0075	4.0
3-yr TCP	0.53	0.11	0.28	0.0018	4.8

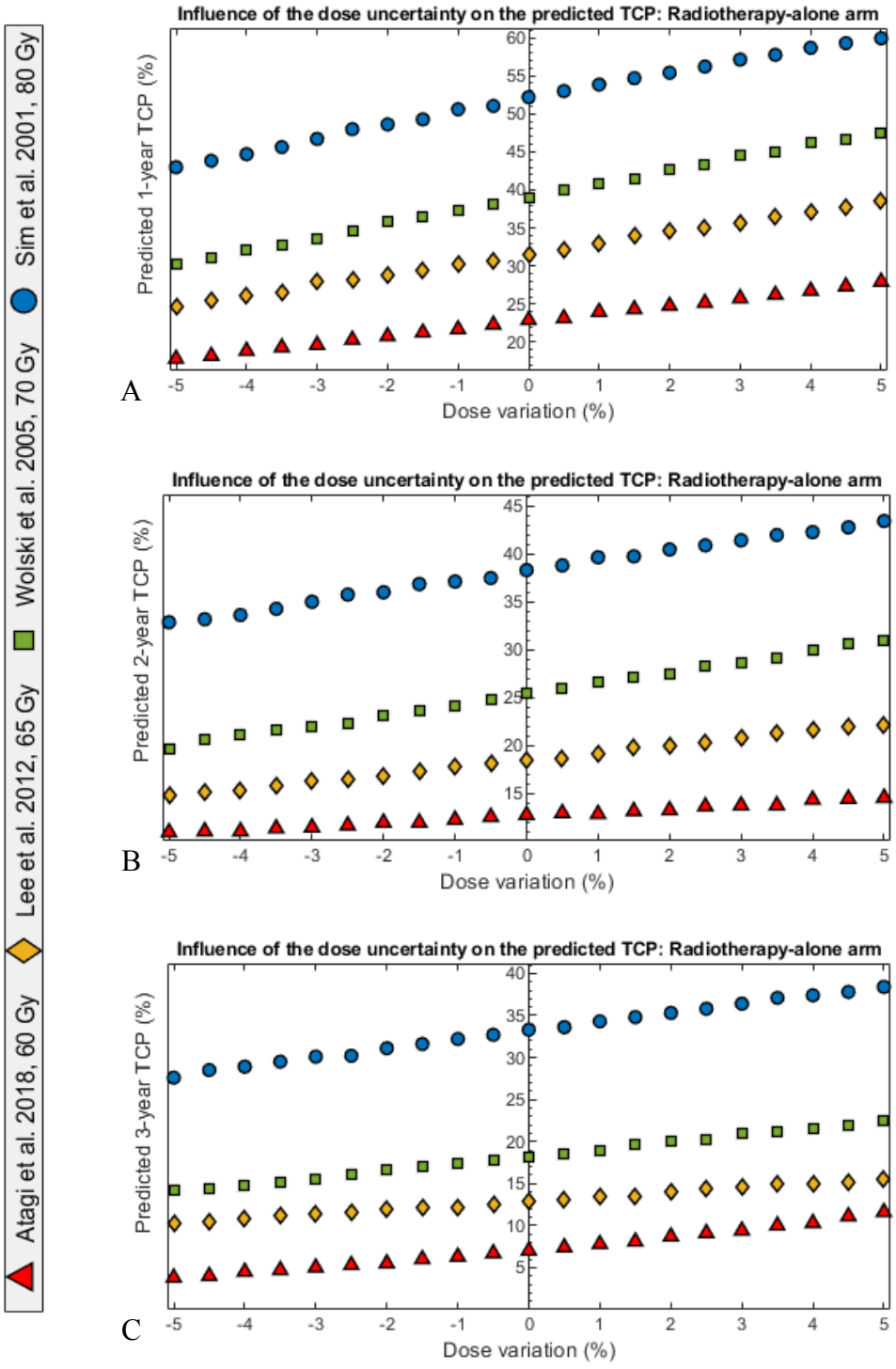

Figure 5.5: Influence of dose uncertainty on the overall TCP following radiotherapy alone arm for one-year follow-up (A), two-year follow-up (B), and three-year follow-up (C).

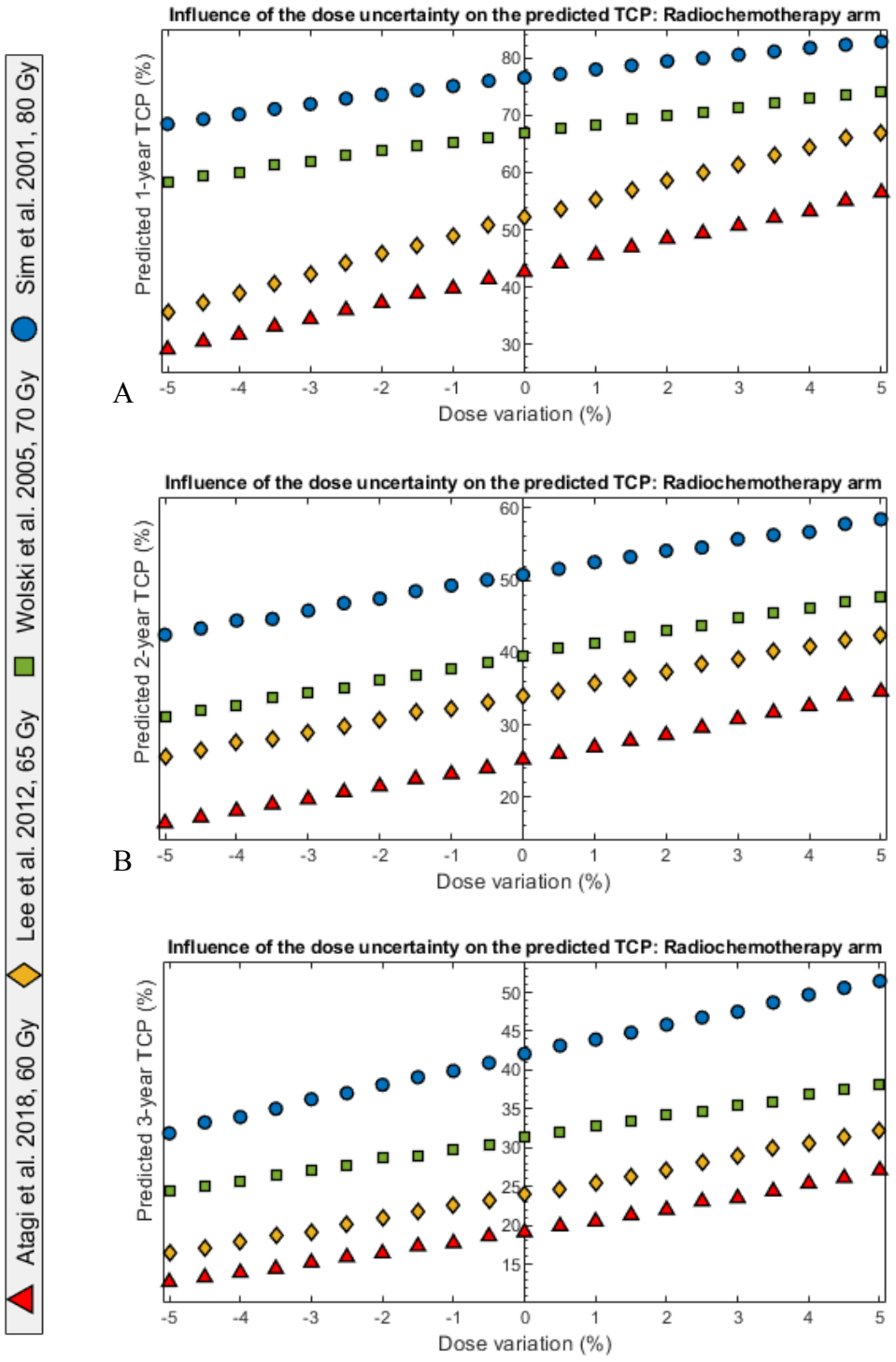

Figure 5.6: Influence of dose uncertainty on the overall TCP following radiochemotherapy arm for one-year follow-up (A), two-year follow-up (B), and three-year follow-up (C).

Figures 5.5 and 5.6 show a typical example of the variation in TCP model outcomes as a function of systematic dose shifts. The variation in the one-year TCPs for total doses of 60, 65, 70 and 80 Gy ranged between 17.8–27.9%, 24.7–38.6%, 30.3–47.4% and 42.9–59.9% for radiotherapy alone arms, and between 29.1–56.5%, 35.6–66.9%, 58.3–74.2% and 68.4–82.8% for radiochemotherapy arms, respectively (see Figures 5.5A and 5.6A). Similar variation trends were observed for the rest of the clinical end points (see Figures 5.5B, 5.5C, 5.6B and 5.6C).

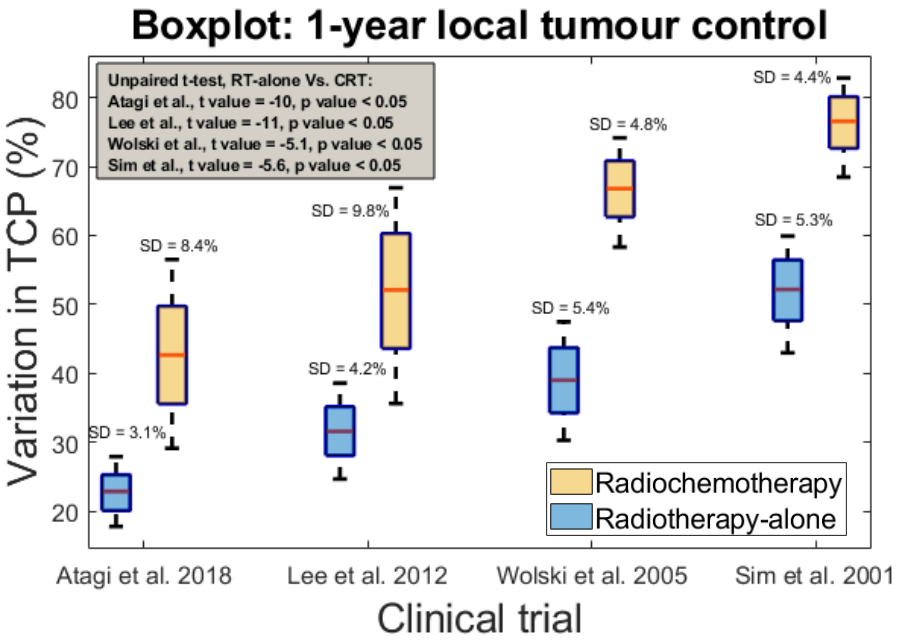

Figure 5.7: Boxplot compares the variation in TCP outcomes for radiotherapy-alone and radiochemotherapy arms due to dose uncertainty for one-year follow-up.

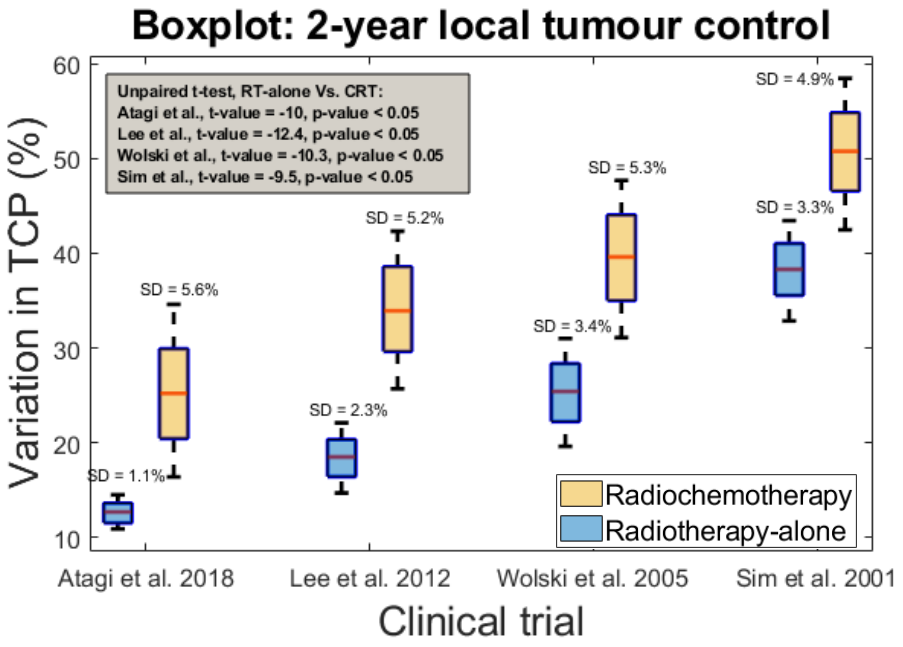

Figure 5.8: Boxplot compares the variation in TCP outcomes for radiotherapy-alone and radiochemotherapy arms due to dose uncertainty for two-year follow-up.

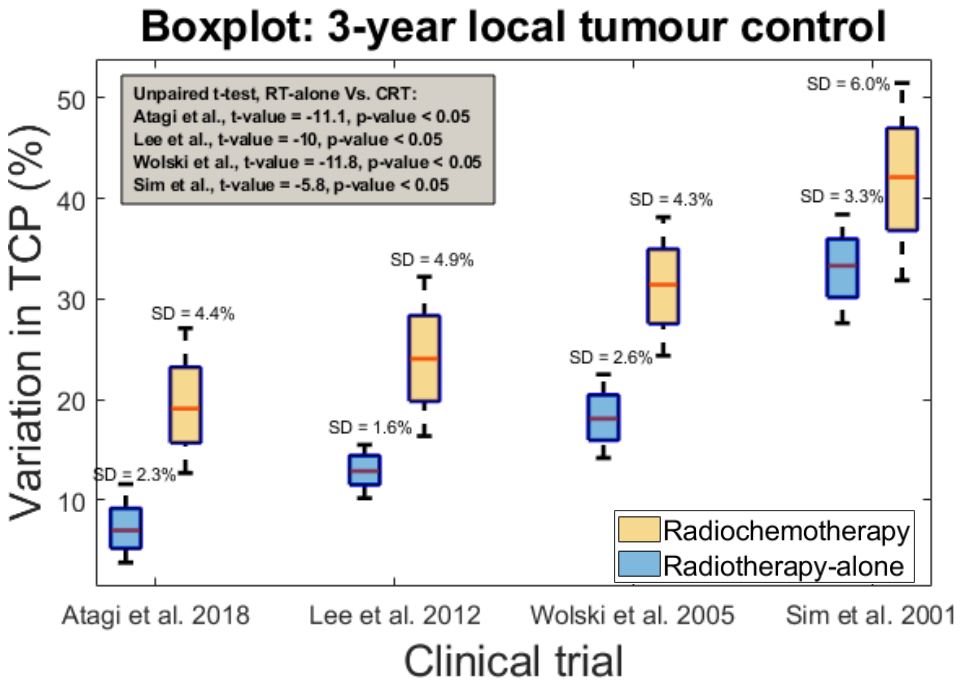

Figure 5.9: Boxplot compares the variation in TCP outcomes for radiotherapy-alone and radiochemotherapy arms due to dose uncertainty for three-year follow-up.

Additionally, in order to examine the statistical distribution of the TCP model outcomes, boxplots (also known as box-and-whisker diagrams) were employed as shown in Figures 5.7, 5.8 and 5.9. The top and bottom of the box represent the third and first quartiles of the TCP values, respectively, and the middle line indicates the median value. The statistical assessment based on the unpaired t-test showed that the differences in predicted TCP for both arms were all significant, which further highlights the enhanced model outcomes for the radiochemotherapy arm (see Figures 5.7, 5.8 and 5.9).

5.4 Discussion

LA-NSCLC is defined as stage III disease with subclassification into stages IIIA, IIIB and IIIC in accordance with the newly proposed 8th TNM. Broadly, stage III NSCLC encompasses a heterogeneous combination of tumour presentations characterised as involving locoregional spread through primary tumour extension into extrapulmonary structures (e.g., T3 or T4) or mediastinal lymph node involvement (e.g., N1, N2 or N3), but involving no evidence of distant metastases (M0). Management with radiotherapy alone for LA-NSCLC has shown undesirable clinical outcomes. The application of sequential radiochemotherapy has yielded an improvement in overall survival rates from nearly 6% to 12% at five years. With the practical experience of concomitant radiochemotherapy, this rate improved to 15% with an overall survival gain of 4.5% at five years – but at the cost of radiation pneumonitis and oesophageal toxicity (Aupérin et al., 2010).

Clinical experience of such patients with concurrent radiochemotherapy is constrained by the sensitivity of healthy lung tissues to radiation dose, which clinically may cause radiation pneumonitis and other oesophageal toxicity. Within this framework, a large volume of retrospective studies detail the clinical experience of the related toxicity following concurrent radiochemotherapy for LA-NSCLC. For instance, Tsujino et al. (2003) determined whether the percentage of pulmonary volume exposed to radiotherapy doses greater than 20 Gy (V_{20}) was associated with the incidence and grade of radiation pneumonitis in 71 patients with inoperable LA-NSCLC treated by concurrent radiochemotherapy.

Statistical analysis confirmed that radiation pneumonitis grades of 0, 1, 2, 3, and 5 were perceived in 17, 35, 16, 2, and 1 patients, respectively; the corresponding mean V_{20} values were 19%, 23.0%, 25.8%, 27.0%, and 34.5%. Thus, Tsujino and his colleagues indicated that concomitant radiochemotherapy strategy was associated with increased clinically relevant radiation pneumonitis.

In a similar vein, Graham et al. (1999) examined 99 patients with LA-NSCLC and determined that the percentage of total lung volume irradiated to 20 Gy corresponds significantly with the incidence of symptomatic radiation pneumonitis. Furthermore, a meta-analysis of sequential versus concurrent radiochemotherapy assessed six trials in 1,205 LA-NSCLC cases and indicated a substantial enhancement in the five-year rate of overall survival (11.3% to 16.2%) and a diminution in local recurrence (35% to 29%) with concomitant radiochemotherapy. Nonetheless, a significant increase in oesophageal toxicity was observed, yet no persuasive evidence of radiation pneumonitis was given in this study (Aupérin et al., 2010).

Overall, 811 patients from 8 clinical trials were used in this study, with 411 patients in the radiotherapy alone arm and 400 in the radiochemotherapy arm. The TCP simulation was developed to predict three clinical end points: one-, two- and three-year local tumour control. Table 5.1 depicts the treatment characteristics of the clinical trials included. The radiotherapy alone arm varied between the different trials in terms of dose per fraction, total radiation dose, number of daily doses and duration of overall radiotherapy course. Table 5.2 presents the exploratory calculations of the chemotherapy log cell kill factor used to fit the TCP model. Although intensive research has been conducted on the TCP modelling, no single study has quantified the influence of radiochemotherapy on the overall TCP model outcomes for NSCLC. Thus, the radiochemotherapy TCP findings in this research may be used to establish a benchmark for future studies of radiochemotherapy TCP lung modelling.

Within this context, only one TCP modelling study, conducted by Plataniotis and Dale (2008), has attempted to determine chemotherapy log cell kill (i.e., N_{CX} values). That modelling study employed clinical data from 11 clinical trials on cervical cancer to quantify synergistic cytotoxic chemotherapy with radiotherapy.

It is therefore encouraging to compare the findings shown in Table 5.2 with those reported by Plataniotis and Dale (2008), who found that the N_{CX} values for cervical cancer range between -0.275–0.838, even though they do not concur with the values presented in Table 5.2. This discrepancy may be attributable to differences in the reported clinical outcomes between cervical cancer and LA-NSCLC.

Three dominant factors make LA-NSCLC challenging to manage with radiotherapy: (1) dosimetric complications induced by the presence of tissue inhomogeneities (i.e., lung has notably low density in comparison with surrounding at-risk organs such as heart, kidneys, liver and oesophagus), (2) respiratory motion, and (3) proximity of various adjacent healthy organs with low radiation tolerances (see Section 1.5). Fundamentally, cutting-edge technologies such as 4D-CT and VMAT should yield therapeutic gains due to their capability to conform radiation doses to tumours. Nevertheless, some questions may be raised concerning the application of VMAT for thoracic cancers due to the respiratory motion involved. Additionally, in contrast to conventional 3D-CRT, VMAT irradiates only a portion of the target volume at a certain time. This creates the possibility of significant dosimetric missing of the target volume, which may, in turn, have an undesirable influence on local tumour control. This phenomenon has been recognised as 'interplay effect' (Ceberg et al., 2013, Palmer et al., 2017).

On the basis of the preceding evidence, the optimum radiotherapy technique for LA-NSCLC has been a controversial and much-disputed subject within the field of radiation oncology. Notably, no single-perspective research has been undertaken to determine the optimum radiotherapy modality for LA-NSCLC, and the published retrospective reports are contradictory. Liao et al. (2010) provided an in-depth retrospective analysis of 496 LA-NSCLC patients who were treated at MD Anderson Cancer Center between 1999 and 2006. In this major study, Liao and his colleagues compared toxicity and disease outcomes in patients treated with either 4D-CT/VMAT or 3D-CRT following concurrent radiochemotherapy regimens. The findings of this study concluded that modern technologies such as VMAT and 4D-CT are associated

with substantially improved local tumour control and survival rates, as well as a remarkable reduction in toxicity compared to 3D-CRT.

In agreement with the previous findings, a single-institution retrospective investigation has suggested that intensity-modulated radiotherapy (IMRT) can improve overall survival and reduce treatment-related pneumonitis (Bezjak et al., 2012). Nevertheless, a number of published studies were unable to reproduce that improvement in clinical outcomes and reduction in toxicity (Harris et al., 2014, Mell et al., 2003). For instance, in a major retrospective study involving 3,986 LA-NSCLC cases accumulated from the Surveillance, Epidemiology, and End Results (SEER) Medicare database, Shirvani et al. (2013) highlight the fact that clinical experience strongly encourages the adoption of VMAT in managing LA-NSCLC. Nonetheless, the study findings identified no significant differences between 3D-CRT and VMAT in the context of oesophageal, pulmonary or cardiac toxicity rates.

Some questions may be posed in relation to the inconsistency and contradictory conclusions exhibited in the literature. Is the interplay effect the major contributing factor behind such discrepancies among scholars' findings, or do other factors influence those findings, such as the dosimetric challenge in accurately delivering the VMAT plan?

Additionally, the results of the present study indicate that dosimetric uncertainty in the prescribed radiation dose could lead to undesirable clinical outcomes (see Figures 5.5 and 5.6). Similarly, in a recent analysis involving multi-radiotherapy UK centres, Bolt et al. (2017) showed that uncertainty in machine beam output measurements may result in variation of up to 10% in TCP model outcomes, which coincides with the findings listed in Figures 5.7, 5.8 and 5.9.

It is important to note that VMAT delivers the radiotherapy prescription doses by modulating photon beam intensities through the continuous variation of dose rates, gantry speeds and multileaf collimator (MLC) positions at each control point. Such a sophisticated delivery of radiation dose may introduce additional uncertainty in the mechanical operation of the Linac due to profound dependence on the application of

high numbers of small irregular field shapes, leading to discrepancies in dose distributions between computed and delivered plans. Within this framework, various quality assurance (QA) practices have been recommended to assess the dosimetric accuracy of the VMAT delivery technique.

One of the most popular tools for performing patient-specific VMAT QA techniques is the 2D dosimetric comparison between the treatment plan and the measurement. During this procedure, a measurement is obtained before the patient begins treatment. This measurement (i.e., the patient-specific QA) is evaluated using the gamma analysis concept. The accepted gamma analysis criteria of a 3% dose difference and a 3-mm distance to agreement (DTA) are the most commonly used (Mynampati et al., 2012). This step is fundamental in radiotherapy to ensure that VMAT treatment is delivered with high accuracy.

Notwithstanding the foregoing, several investigators have argued that the traditional patient-specific VMAT QA is not sensitive enough to detect dosimetric discrepancy between the treatment plan and the delivered plan. Furthermore, one drawback to the patient-specific VMAT QA technique is a weak-to-moderate correlation between clinically relevant dosimetric errors and 2D gamma analysis passing rates (Hussein et al., 2013). For instance, Mu et al. (2007) deliberately introduced random (± 1 mm and ± 2 mm) and systematic (± 0.5 mm or ± 1 mm) errors in the MLC positions to evaluate the dosimetric effect. They found no significant dosimetric variation for either PTV or OARs that were introduced by random leaf position errors, whereas clinically significant differences (8% variation in D95% and approximately 12% in D0.1 cc to critical organs) were noted by systematic leaf position errors in complex IMRT plans. Alaswad and Coleman (2019) concluded that when 2D gamma analysis is performed using a 3% dose difference and a 3-mm DTA, both QA results and the error detectability are heavily dependent on the plane chosen for measurement acquisition, and no relationship was found between the error levels in several verification planes.

Recently, log files have been established on numerous treatment machines to address concerns about traditional QA approaches in identifying both minor random and

systematic errors. One of the benefits of utilising this technique is that the log files are acquired and verified whenever the treatment plan is delivered. Hence, it can be verified during patient treatment. Furthermore, log files yield an immediate performance of VMAT plan checks and reduce the ampere-hours utilised in traditional QA techniques to a matter of minutes. However, there are still concerns about whether the log file-based QA technique offers confidence equal to that of measurements used by one of the traditional approaches.

In recent years, proton therapy has gained momentum amongst the procedures of interest due to the absence of any exit radiation dose. This distinctive feature of proton therapy may potentially enable radiotherapy dose escalation without added toxicity to healthy tissues in the vicinity of the target volume. Numerous single-arm studies have been published with promising clinical outcomes that employ concurrent chemotherapy and proton beam therapy in LA-NSCLC (Nguyen et al., 2015, Hoppe et al., 2016). In a retrospective analysis using the National Cancer Database, Higgins et al. (2017a) concluded that proton therapy yields a substantial improvement in the survival rates compared to photon therapy. However, a notable limitation of this study is the absence of toxicity data. The interest in proton therapy led to the phase II randomised trial comparing conformal passive scattering proton therapy against VMAT for LA-NSCLC. Nonetheless, this ongoing NCT00915005 phase II trial comparing passive scattering proton therapy (PSPT) against IMRT for LA-NSCLC revealed no significant difference between the two arms in terms of radiation pneumonitis or oesophageal toxicity (Liao et al., 2018). The authors have stated that proton therapy was correlated with larger high-dose lung volumes due to the application of relatively large safety margins during the PSPT treatment plans. Notably, the authors have also observed that the rate of pneumonitis for the proton arm diminished with time during the trial evaluation, and hypothesise that this may be attributable to a learning curve in proton therapy planning, as re-plans of previous patients resulted in improved dosimetry. It is worth mentioning that the management of NSCLC by employing proton therapy is still in the early developmental stages with some specific barriers, such as proton range uncertainty inside the boundaries of

moving targets, which may restrict its practical applicability in the foreseeable future.

In summary, this chapter demonstrates that the influence of radiochemotherapy can be modelled through incorporating the log cell kills concept into a TCP-LQ model and thus allow quantitative assessment of combined radiotherapy and chemotherapy modalities. Consistent with the reported outcomes presented in the extant literature, TCP model outcomes for the radiochemotherapy arm were found to be superior to those exhibited by the radiotherapy alone arm.

Chapter 6 Conclusion and future work

6.1 Conclusion

6.1.1 Optimal tumour control for early-stage non-small-cell lung cancer

This thesis makes several noteworthy contributions in the field of radiobiological modelling of NSCLC. It sought to establish a mechanistic local TCP model that could describe clinical outcomes of NSCLC. A comprehensive meta-analysis of clinical outcomes for a broad spectrum of NSCLC fractionation schemes, such as standard fractionation, hyperfractionation and hypofractionation was conducted. This outcome analysis for clinical radiotherapy of local tumour control for NSCLC has not previously been undertaken or reported by other scholars.

The findings suggest that the TCP model is appropriate for the analysis and evaluation of external beam radiation treatment plans with respect to one-, two- and three-year local tumour control through 3D-CRT, CHART and SABR.

Furthermore, this study illustrates that the TCP model can describe clinical outcomes at high doses per fraction, such as those used in SABR. Therefore, this thesis argued that LQ-based TCP modelling can adequately describe tumour control radiotherapy regimens that employ high doses per fraction.

This thesis determined that NSCLC can be adequately modelled by extending the classic LQ formula to include the effects of hypoxia, tumour repopulation and the repair of sublethal damage. To the best of our knowledge, the present study is the first TCP model for early-stage NSCLC that has combined all three of these parameters.

The variations in clonogenic cell density, with respect to TCP, were also investigated and modelled using a more practical approach to address a gap in the literature, which assumed that treated volume had a fixed quantity of clonogenic density. Within this this context, two new computational radiobiological models were developed in MATLAB to study the effects of varying both radiation dose prescription and clonogenic density distributions in local tumour control. Based on the proposed model, it was estimated that 60% of the dose was sufficient to maintain the desirable TCP after two years for the regions with lower clonogenic cell density.

It is noteworthy that the TCP model, alongside the multiple patient cohorts employed in this thesis, has been published at varying times during the PhD (Alaswad et al., 2020, Alaswad et al., 2019a, Alaswad et al., 2019b, Alaswad et al., 2019c, Alaswad et al., 2018), and has been endorsed by several scholars (Marsden, 2020, Radonic et al., 2020, Kenny et al., 2020, Inal and Duman, 2020, Matsuya et al., 2020).

Additionally, in 2020, Marsden published a paper in which he described the TCP established in this thesis as a novel and sophisticated compared with the previously published TCP models, in particular the Marsden TCP model which has been developed and published more frequently by (Uzan and Nahum, 2012).

6.1.2 Comparison of the T descriptor of the 7th and 8th editions of the TNM staging system for non-small-cell lung cancer after radiotherapy

Another core aspect of the current thesis was to assess the inclusion of cancer stages into a TCP model based on the T descriptors of the 7th and 8th editions of the TNM. The TNM staging system employs a configuration that depicts the anatomic extent of cancer, thereby enhancing the exchange of information between oncologists.

A single cohort consisting of 354 NSCLC patients was used for the model fit. The TCP findings of this study indicate that patients with earlier-stage NSCLC T subcategories, such as T1a and T1b, display an improved local tumour control compared to patients with more advanced T subcategories, such as T3 and T4.

One of the findings of this research was that the T distribution schema of the 7th edition was slightly inferior to that of the 8th edition in terms of specifying the adjacent T subcategories. To the best of our knowledge, this study is the first to describe the impact of the inclusion of cancer stage of the 7th TNM and 8th TNM into the TCP model for NSCLC. Due to the small sample size used in this study, more studies are warranted to sufficiently quantify and precisely determine the superiority of the 8th edition of the TNM classification system from the radiobiological modelling perspective.

6.1.3 Influence of incorporating radiotherapy and chemotherapy on the tumour control probability of patients with locally advanced non-small-cell lung cancer

In addition, this thesis spotlighted the tangible contribution of synergistic cytotoxic chemotherapy with radiotherapy in treating locally advanced NSCLC. Clinical trial experiences from multiple references have reported that the risk of locoregional relapse and distant metastasis was less evident for patients treated with concomitant radiochemotherapy than radiotherapy alone. Although the influence of radiotherapy alone can be adequately described by TCP model, the combined impact of concomitant chemotherapy and radiotherapy remains subject to extensive research.

Thus, the TCP-LQ model was amended to quantify the effect of chemotherapy prescription according to the log-cell kill notion. Notably, the log-cell kills mechanism relies on the assumption that cytotoxic drugs eliminate a certain fraction of clonogenic cells based on drug concentration. Overall, 811 patients from 8 clinical trials were used in this study, with 411 patients in the radiotherapy-alone arm and 400 in the radiochemotherapy arm.

The TCP simulation was developed to predict three clinical endpoints: one-, two- and three-year local tumour control. This investigation demonstrated that incorporating the log-cell kills concept into a TCP-LQ model can improve tumour cure probabilities and thus allow quantitative assessment of combined radiotherapy and chemotherapy modalities.

Furthermore, accurate clinical outcome predictions could offer oncologists more reliable tools to enhance their decision-making when balancing predicted gains versus expected risk. As previously stated, the established mechanistic TCP population model can sufficiently describe the clinical outcomes of NSCLC. Notwithstanding this, local tumour control is determined by a complex interplay between radiation dosimetry, tumour biology, tumour microenvironment and patient-related variables. Thus, this thesis argued that these factors pose a challenge in establishing a prognostic model for routine clinical practice.

6.2 Future work

6.2.1 Dose to water versus dose to medium from a radiological modelling perspective: A single institution experience

Conventional dose computations for radiotherapy treatment planning systems (TPSs) are commonly modelled to report absorbed doses to water (D_w) (assuming that the human body is largely composed of water). One possible explanation for this is that the input dosimetric data (e.g., absorbed dose, PDD, beam flatness and symmetry) used for TPS dose calculations algorithms are measured in a water phantom.

The Monte Carlo (MC) dose calculation algorithm is recognised as the gold standard from an accuracy perspective, specifically in inhomogeneous media such as the lung. The MC can accurately model the physical interactions of each electron in media, a technique that remains time-consuming despite recent progress in computational capacity. This factor may explain the difficulty in adapting this technique to use in daily clinical practice.

A recent, dramatic paradigm shift in radiotherapy occurred through reporting the prescribed radiation dose to the medium (D_m) by using the Acuros XB (AXB) dose calculation algorithm (Delbaere et al., 2019). The AXB has proved to coincide to a

large degree with the MC, even in inhomogeneous media, with the superiority of faster computation times and readily available on a commercial TPS.

Recently, this system has been implemented in the radiation oncology department of King Fahad Medical City (KFMC). Nevertheless, the issue of whether to report the dose to D_w or D_m has been a much-disputed topic within the area of radiotherapy treatment planning (Gladstone et al., 2016, Ma and Li, 2011, Walters et al., 2010, Keall, 2002, Yang et al., 2020). Thus, future work for this project will be threefold: 1) retrospectively comparing clinical outcomes for patients who were treated using D_w with D_m in KFMC, 2) comparing DVH histograms in both scenarios, and 3) establishing a radiobiological model based on both D_w and D_m TPS dose distribution.

6.2.2 Influence of radiotherapy treatment interruptions on tumour control probability: A multi-centre analysis experience

A radiotherapy treatment schedule can be disrupted for various patient- or equipment-/service-related reasons (e.g. a patient can be too ill to attend a session). However, the overall treatment time is a significant factor influencing the efficacy of a radiotherapy treatment. The accelerated repopulation of tumour clonogenic cells with increased treatment time is considered to be a major contributing cause for reduced local control without appropriate radiation dose compensation.

Thus, future work will also involve addressing and quantifying the effect of treatment gap durations as well as their temporal occurrences within a treatment on the overall tumour control of non-small cell lung cancers. The patient data will be gathered from multiple centres in Saudi Arabia. Strategies to mitigate the effect of treatment gaps, such as varying treatment fraction numbers or fraction radiation doses, will be proposed from a radiobiological modelling perspective.

6.2.3 A TCP model for proton therapy beam of non-small cell lung cancer

Proton therapy has gained in significance due to the absence of any exit radiation dose. This distinctive feature of proton therapy may potentially enable radiotherapy dose escalation without added toxicity to healthy tissues in the vicinity of the target volume. Numerous single-arm studies have been published with promising clinical outcomes that employ concurrent chemotherapy and proton beam therapy in LA-NSCLC (Nguyen et al., 2015, Hoppe et al., 2016). Recently, this therapeutic procedure has been implemented in King Fahad Medical City (KFMC) in Saudi Arabia.

Nonetheless, most radiobiological research has focused on an evolving TCP model within the context of external beam radiotherapy. Thus, it is important to develop a mechanistic TCP model that is capable of describing the response of NSCLC to proton therapy. This, in turn, can yield greater insight into the clinical implications and perspectives of this promising therapeutic procedure.

Future work for this project will therefore focus on extending the TCP-LQ model discussed in Chapter 3 (Alaswad et al., 2019a) to describe the response of NSCLC to proton therapy based on the concept of relative biological effectiveness (RBE). Notably, RBE is defined as the ratio of physical doses that cause the same biological effect and is calculated as RBE =Dcontrol ⁄Dtest. In this equation, Dcontrol is the physical dose of a reference radiation modality (X-rays) and Dtest is the physical dose of the radiation modality being investigated (protons).

6.2.4 A TCP model to improve clinical outcomes in patients with non-small cell Lung cancer: A clinical feasibility study

The quality of a radiation treatment plan is often evaluated by physical quantities such as DVH parameters. Within this context, the TCP model proposed in this thesis can be used to realise the biological consequences of the treatment. For instance, physicists can incorporate the TCP model into in-house computer programs for evaluation of treatment plans. Because the proposed TCP model can account for different fractionation regimes such as 3D-CRT, CHART, and SABR, along with modalities in combined treatment (e.g., radiochemotherapy), it provides direct estimates of outcome probabilities to accomplish optimum local tumour control. This can provide valuable clinical guidance to escalate the radiotherapy dose for NSCLC.

Additionally, physicists, along with radiation oncologists, can investigate and quantify the influence of treatment interruptions and different overall treatment time on the local tumour control. This can be accomplished by altering the clonogenic repopulation equation in the proposed TCP model. Notably, clonogenic repopulation depends on two main parameters: the treatment duration and the clonogenic doubling time.

An additional useful feature of the proposed TCP model that can be considered during plan optimization is the modelling approach of clonogenic cell density proposed in this thesis. In this method, low clonogenic cell densities can be destroyed with a relatively lower radiation dose than is usually required to eliminate tumours, while a higher radiation dose would be required to eliminate a tumour with a higher clonogenic cell density. Following these treatment plans, the optimal TCP and normal tissue complication probabilities can be attained. Notably, physicists can employ the clonogenic cell density model to achieve optimum local tumour control.

Therefore, future work for this project will focus on evaluating the feasibility of implementing the TCP-LQ model discussed in this thesis into daily clinical practice.

References

ALASWAD, M. & COLEMAN, L. 2017. Comparison of IMRT QA measurement methodology. *Physica Medica,* 42**,** 363.

ALASWAD, M. & COLEMAN, L. 2019. The sensitivity of patient-specific IMRT QA methods in detecting systematic errors: field-by-field versus single-gantry-angle composite. Journal of Physics: Conference Series. IOP Publishing, 012063.

ALASWAD, M., KLEEFELD, C. & FOLEY, M. 2019a. Optimal tumour control for early-stage non-small-cell lung cancer: A radiobiological modelling perspective. *Physica Medica,* 66**,** 55-65.

ALASWAD, M., KLEEFELD, C. & FOLEY, M. 2019b. Radiation dose intensity and local tumour control of non-small cell lung cancer: A radiobiological modelling perspective. Journal of Physics: Conference Series, 2019b. IOP Publishing, 012071.

ALASWAD, M., KLEEFELD, C. & FOLEY, M. 2019c. Radiobiological modelling of clonogen distribution, hypoxic fraction and tumour size effects on local tumour control of non-small cell lung cancer. *Physica Medica,* 67**,** 197.

ALASWAD, M., KLEEFELD, C. & FOLEY, M. 2020. Influence of incorporating radiotherapy and chemotherapy on the tumour control probability of patients with non-small cell lung cancer: A radiobiological modelling study. *Physica Medica,* Pre print.

ALASWAD, M., KLEEFELD, C., MOORE, M. & FOLEY, M. 2018. A TCP model for external beam treatment of non-small cell lung cancer. *Physica Medica,* 52**,** 172.

ANDRATSCHKE, N., ZIMMERMANN, F., BOEHM, E., SCHILL, S., SCHOENKNECHT, C., THAMM, R., MOLLS, M., NIEDER, C. & GEINITZ, H. 2011. Stereotactic radiotherapy of histologically proven inoperable stage I non-small cell lung cancer: patterns of failure. *Radiotherapy and Oncology,* 101**,** 245-249.

ASTARAKI, M., WANG, C., BUIZZA, G., TOMA-DASU, I., LAZZERONI, M. & SMEDBY, Ö. 2019. Early survival prediction in non-small cell lung cancer from PET/CT images using an intra-tumor partitioning method. *Physica Medica,* 60**,** 58-65.

ATAGI, S., KAWAHARA, M., TAMURA, T., NODA, K., WATANABE, K., YOKOYAMA, A., SUGIURA, T., SENBA, H., ISHIKURA, S. & IKEDA, H. 2005. Standard thoracic radiotherapy with or without concurrent daily low-dose carboplatin in elderly patients with locally advanced non-small cell lung cancer: a phase III trial of the Japan Clinical Oncology Group (JCOG9812). *Japanese journal of clinical oncology,* 35**,** 195-201.

ATAGI, S., KAWAHARA, M., YOKOYAMA, A., OKAMOTO, H., YAMAMOTO, N., OHE, Y., SAWA, T., ISHIKURA, S., SHIBATA, T. & FUKUDA, H. 2012. Thoracic radiotherapy with or without daily low-dose carboplatin in elderly patients with non-small-cell lung cancer: a randomised, controlled, phase 3 trial by the Japan Clinical Oncology Group (JCOG0301). *The lancet oncology,* 13**,** 671-678.

ATAGI, S., MIZUSAWA, J., ISHIKURA, S., TAKAHASHI, T., OKAMOTO, H., TANAKA, H., GOTO, K., NAKAGAWA, K., HARADA, M. & TAKEDA, Y. 2018. Chemoradiotherapy in Elderly Patients With Non–Small-Cell Lung Cancer: Long-Term Follow-Up of a Randomized Trial (JCOG0301). *Clinical lung cancer,* 19**,** e619-e627.

AUPÉRIN, A., LE PÉCHOUX, C., ROLLAND, E., CURRAN, W. J., FURUSE, K., FOURNEL, P., BELDERBOS, J., CLAMON, G., ULUTIN, H. C. & PAULUS, R. 2010. Meta-analysis of concomitant versus sequential radiochemotherapy in locally advanced non-small-cell lung cancer. *Database of Abstracts of Reviews of Effects (DARE): Quality-assessed Reviews [Internet]*. Centre for Reviews and Dissemination (UK).

BAKER, C., CARVER, A. & NAHUM, A. Local control prediction for NSCLC using a common LQ-based TCP model for both SABR and 3D-CRT fractionation. Abstract at ESTRO 3rd Forum, Barcelona, 2015. 24-28.

BAKER, F. & SANGER, L. 1991. The deensity of clonogenic cless in human solid tumors. *The International Journal of Cell Cloning,* 9**,** 155-165.

BALL, D. L., FISHER, R., BURMEISTER, B., GRAHAM, P., JOSEPH, D., PENNIMENT, M., KRAWITZ, H., WHEELER, G., POULSEN, M. & VINOD, S. 2006. Stage is not a reliable indicator of tumor volume in non-small cell lung cancer: a preliminary analysis of the Trans-Tasman Radiation Oncology Group 99-05 database. *Journal of Thoracic Oncology,* 1**,** 667-672.

BARAZZUOL, L., BURNET, N. G., JENA, R., JONES, B., JEFFERIES, S. J. & KIRKBY, N. F. 2010. A mathematical model of brain tumour response to radiotherapy and chemotherapy considering radiobiological aspects. *Journal of theoretical biology,* 262**,** 553-565.

BARENDSEN, G. W., VAN BREE, C. & FRANKEN, N. A. 2001. Importance of cell proliferative state and potentially lethal damage repair on radiation effectiveness: implications for combined tumor treatments. *International journal of oncology,* 19**,** 247-256.

BARRETT, A., MORRIS, S., DOBBS, J. & ROQUES, T. 2009. *Practical radiotherapy planning*, CRC Press.

BARRY, M. A., HUSSEIN, M. & SCHETTINO, G. 2020. Evaluating the propagation of uncertainties in biologically based treatment planning parameters. *Frontiers in oncology,* 10**,** 1058.

BARTON, M. B., FROMMER, M. & SHAFIQ, J. 2006. Role of radiotherapy in cancer control in low-income and middle-income countries. *The lancet oncology,* 7**,** 584-595.

BAUMANN, M., HERRMANN, T., KOCH, R., MATTHIESSEN, W., APPOLD, S., WAHLERS, B., KEPKA, L., MARSCHKE, G., FELTL, D. & FIETKAU, R. 2011. Final results of the randomized phase III CHARTWEL-trial (ARO 97-1) comparing hyperfractionated-accelerated versus conventionally fractionated radiotherapy in non-small cell lung cancer (NSCLC). *Radiotherapy and Oncology,* 100**,** 76-85.

BENDALL, L., PAPIEZ, B., HAWKINS, M. & FENWICK, J. 2018. Isotoxic dose escalation with real-time imaging on an MR-linac in lung radiation therapy. *International Journal of Radiation Oncology• Biology• Physics,* 102**,** S207.

BENTZEN, S. M., CONSTINE, L. S., DEASY, J. O., EISBRUCH, A., JACKSON, A., MARKS, L. B., TEN HAKEN, R. K. & YORKE, E. D. 2010. Quantitative Analyses of Normal Tissue Effects in the Clinic (QUANTEC): an introduction to the scientific issues. *International Journal of Radiation Oncology* Biology* Physics,* 76**,** S3-S9.

BENTZEN, S. M., DÖRR, W., GAHBAUER, R., HOWELL, R. W., JOINER, M. C., JONES, B., JONES, D. T., VAN DER KOGEL, A. J., WAMBERSIE, A. & WHITMORE, G. 2012. Bioeffect modeling and equieffective dose concepts in radiation oncology–terminology, quantities and units. *Radiotherapy and Oncology,* 105**,** 266-268.

BERTHELSEN, A. K., DOBBS, J., KJELLÉN, E., LANDBERG, T., MÖLLER, T. R., NILSSON, P., SPECHT, L. & WAMBERSIE, A. 2007. What's new in target volume definition for radiologists in ICRU Report 71? How can the ICRU volume definitions be integrated in clinical practice? *Cancer Imaging,* 7**,** 104.

BEZJAK, A., RUMBLE, R., RODRIGUES, G., HOPE, A., WARDE, P. & PANEL, I. I. E. 2012. Intensity-modulated radiotherapy in the treatment of lung cancer. *Clinical oncology,* 24**,** 508-520.

BOILY, G., FILION, É., RAKOVICH, G., KOPEK, N., TREMBLAY, L., SAMSON, B., GOULET, S., ROY, I. & ONCOLOGIE, C. D. L. É. D. P. E. 2015. Stereotactic ablative radiation therapy for the treatment of early-stage non–small-cell lung cancer: CEPO review and recommendations. *Journal of Thoracic Oncology,* 10**,** 872-882.

BOLT, M. A., CLARK, C. H., CHEN, T. & NISBET, A. 2017. A multi-centre analysis of radiotherapy beam output measurement. *Physics and Imaging in Radiation Oncology,* 4**,** 39-43.

BRADLEY, J. D., IEUMWANANONTHACHAI, N., PURDY, J. A., WASSERMAN, T. H., LOCKETT, M. A., GRAHAM, M. V. & PEREZ, C.

A. 2002. Gross tumor volume, critical prognostic factor in patients treated with three-dimensional conformal radiation therapy for non-small-cell lung carcinoma. *International Journal of Radiation Oncology* Biology* Physics,* 52**,** 49-57.

BRADLEY, J. D., PAULUS, R., KOMAKI, R., MASTERS, G., BLUMENSCHEIN, G., SCHILD, S., BOGART, J., HU, C., FORSTER, K. & MAGLIOCCO, A. 2015. Standard-dose versus high-dose conformal radiotherapy with concurrent and consolidation carboplatin plus paclitaxel with or without cetuximab for patients with stage IIIA or IIIB non-small-cell lung cancer (RTOG 0617): a randomised, two-by-two factorial phase 3 study. *The lancet oncology,* 16**,** 187-199.

BRENNER, D. J. 2008. The linear-quadratic model is an appropriate methodology for determining isoeffective doses at large doses per fraction. Seminars in radiation oncology, Elsevier, 234-239.

BROWN, J. M. 1999. The hypoxic cell: a target for selective cancer therapy—eighteenth Bruce F. Cain Memorial Award lecture. *Cancer research,* 59**,** 5863-5870.

BROWN, J. M., BRENNER, D. J. & CARLSON, D. J. 2013. Dose escalation, not "new biology," can account for the efficacy of stereotactic body radiation therapy with non-small cell lung cancer. *International Journal of Radiation Oncology• Biology• Physics,* 85**,** 1159-1160.

BROWN, J. M., CARLSON, D. J. & BRENNER, D. J. 2014. The tumor radiobiology of SRS and SBRT: are more than the 5 Rs involved? *International Journal of Radiation Oncology* Biology* Physics,* 88**,** 254-262.

BROWN, J. M., DIEHN, M. & LOO JR, B. W. 2010. Stereotactic ablative radiotherapy should be combined with a hypoxic cell radiosensitizer. *International Journal of Radiation Oncology* Biology* Physics,* 78**,** 323-327.

BROWN, S., BANFILL, K., AZNAR, M. C., WHITEHURST, P. & FAIVRE FINN, C. 2019. The evolving role of radiotherapy in non-small cell lung cancer. *The British journal of radiology,* 92**,** 20190524.

BROWN, W., WU, X., FAYAD, F., FOWLER, J., GARCÍA, S., MONTERROSO, M., DE LA ZERDA, A. & SCHWADE, J. 2009. Application of robotic stereotactic radiotherapy to peripheral stage I non-small cell lung cancer with curative intent. *Clinical oncology,* 21**,** 623-631.

BRUNELLI, A., CHARLOUX, A., BOLLIGER, C. T., ROCCO, G., SCULIER, J.-P., VARELA, G., LICKER, M., FERGUSON, M., FAIVRE-FINN, C. & HUBER, R. M. 2009. ERS/ESTS clinical guidelines on fitness for radical therapy in lung cancer patients (surgery and chemo-radiotherapy). *European Respiratory Journal,* 34**,** 17-41.

BUSHBERG, J. T. & BOONE, J. M. 2011. *The essential physics of medical imaging*, Lippincott Williams & Wilkins.

CAI, B., GREEN, O. L., KASHANI, R., RODRIGUEZ, V. L., MUTIC, S. & YANG, D. 2018. A practical implementation of physics quality assurance for photon adaptive radiotherapy. *Zeitschrift für Medizinische Physik,* 28**,** 211-223.

CEBERG, S., CEBERG, C., FALK, M., AF ROSENSCHÖLD, P. M. & BÄCK, S. Å. Evaluation of breathing interplay effects during VMAT by using 3D gel measurements. Journal of Physics: Conference Series, 2013. IOP Publishing, 012098.

CHANSKY, K., DETTERBECK, F. C., NICHOLSON, A. G., RUSCH, V. W., VALLIÈRES, E., GROOME, P., KENNEDY, C., KRASNIK, M., PEAKE, M. & SHEMANSKI, L. 2017. The IASLC lung cancer staging project: external validation of the revision of the TNM stage groupings in the eighth edition of the TNM classification of lung cancer. *Journal of Thoracic Oncology,* 12**,** 1109-1121.

CHANSKY, K., SCULIER, J.-P., CROWLEY, J. J., GIROUX, D., VAN MEERBEECK, J. & GOLDSTRAW, P. 2009. The International Association for the Study of Lung Cancer Staging Project: prognostic factors and pathologic TNM stage in surgically managed non-small cell lung cancer. *Journal of thoracic oncology,* 4**,** 792-801.

CHAO, K. C., BLANCO, A. I. & DEMPSEY, J. F. 2003. A conceptual model integrating spatial information to assess target volume coverage for IMRT treatment planning. *International Journal of Radiation Oncology* Biology* Physics,* 56**,** 1438-1449.

CHAPMAN, J. D. & NAHUM, A. E. 2016. *Radiotherapy treatment planning: linear-quadratic radiobiology*, CRC Press.

CHAVAUDRA, N., BOURHIS, J. & FORAY, N. 2004. Quantified relationship between cellular radiosensitivity, DNA repair defects and chromatin relaxation: a study of 19 human tumour cell lines from different origin. *Radiotherapy and oncology,* 73**,** 373-382.

CHEN, C.-Y., CHEN, K.-Y., SHIH, J.-Y. & YU, C.-J. 2020. Clinical factors associated with treatment toxicity of pemetrexed plus platinum in elderly patients with non-small cell lung cancer. *Journal of the Formosan Medical Association*.

CHEN, M., JIANG, G.-L., FU, X.-L., WANG, L.-J., QIAN, H., ZHAO, S. & LIU, T.-F. 2002. Prognostic Factors for Local Control in Non–Small-Cell Lung Cancer Treated With Definitive Radiation Therapy. *American journal of clinical oncology,* 25**,** 76-80.

CHEW, M. T., BRADLEY, D. A., SUZUKI, M., MATSUFUJI, N., MURAKAMI, T., JONES, B. & NISBET, A. 2019a. The radiobiological effects of He, C and Ne ions as a function of LET on various glioblastoma cell lines. *Journal of radiation research,* 60**,** 178-188.

CHEW, M. T., NISBET, A., SUZUKI, M., MATSUFUJI, N., MURAKAMI, T., JONES, B. & BRADLEY, D. A. 2019b. Potential lethal damage repair in

glioblastoma cells irradiated with ion beams of various types and levels of linear energy transfer. *Journal of radiation research,* 60**,** 59-68.

CHI, A., WEN, S., LIAO, Z., FOWLER, J., XU, J., NGUYEN, N. P., WELSH, J. S. & KOMAKI, R. 2007. What would be the most appropriate α/β ratio in the setting of stereotactic body. *Oncol,* 2**,** 94-100.

CRINO, L., LATINI, P., MEACCI, M., CORGNA, E., MARANZANO, E., DARWISH, S., MINOTTI, V., SANTUCCI, A. & TONATO, M. 1993. Induction chemotherapy plus high-dose radiotherapy versus radiotherapy alone in locally advanced unresectable non-small-cell lung cancer. *Annals of oncology,* 4**,** 847-851.

DATTA, N., RAJKUMAR, A. & BASU, R. 2005. Variations in clinical estimates of tumor volume regression parameters and time factor during external radiotherapy in cancer cervix: does it mimic the linear-quadratic model of cell survival? Indian Jornal of Cancer, 42, 60-70.

DELBAERE, A., YOUNES, T. & VIEILLEVIGNE, L. 2019. On the conversion from dose-to-medium to dose-to-water in heterogeneous phantoms with Acuros XB and Monte Carlo calculations. *Physics in Medicine & Biology,* 64**,** 195016.

DETTERBECK, F. C., BOFFA, D. J., KIM, A. W. & TANOUE, L. T. 2017. The eighth edition lung cancer stage classification. *Chest,* 151**,** 193-203.

DIN, O. S., HARDEN, S. V., HUDSON, E., MOHAMMED, N., PEMBERTON, L. S., LESTER, J. F., BISWAS, D., MAGEE, L., TUFAIL, A. & CARRUTHERS, R. 2013. Accelerated hypo-fractionated radiotherapy for non small cell lung cancer: results from 4 UK centres. *Radiotherapy and Oncology,* 109**,** 8-12.

DONNEM, T., ANDERSEN, S., AL-SAAD, S., AL-SHIBLI, K., BUSUND, L.-T. & BREMNES, R. M. 2011. Prognostic impact of angiogenic markers in non–small-cell lung cancer is related to tumor size. *Clinical lung cancer,* 12**,** 106-115.

DÖRR, W. 2015. Radiobiology of tissue reactions. *Annals of the ICRP,* 44**,** 58-68.

DOUGLAS, B. & FOWLER, J. 1976. The effect of multiple small doses of x rays on skin reactions in the mouse and a basic interpretation. *Radiation research,* 66**,** 401-426.

DOUGLASS, M. 2018. Eric J. Hall and Amato J. Giaccia: Radiobiology for the radiologist. Springer.

DUMA, N., SANTANA-DAVILA, R. & MOLINA, J. R. Non–small cell lung cancer: epidemiology, screening, diagnosis, and treatment. Mayo Clinic Proceedings, 2019. Elsevier, 1623-1640.

DUNLAP, N. E., LARNER, J. M., READ, P. W., KOZOWER, B. D., LAU, C. L., SHENG, K. & JONES, D. R. 2010. Size matters: a comparison of T1 and T2 peripheral non–small-cell lung cancers treated with stereotactic body radiation therapy (SBRT). *The Journal of thoracic and cardiovascular surgery,* 140**,** 583-589.

DURANTE, M. & FLANZ, J. Charged particle beams to cure cancer: strengths and challenges. Seminars in oncology, 2019. Elsevier, 219-225.

EATON, D. J., BASS, G., BOOKER, P., BYRNE, J., DUANE, S., FRAME, J., GRATTAN, M., THOMAS, R. A., THORP, N. & NISBET, A. 2020. IPEM code of practice for high-energy photon therapy dosimetry based on the NPL absorbed dose calibration service. *Physics in Medicine & Biology,* 65**,** 195006.

EFRON, B. 1992. Bootstrap methods: another look at the jackknife. *Breakthroughs in statistics*. Springer.

EMAMI, B., LYMAN, J., BROWN, A., COLA, L., GOITEIN, M., MUNZENRIDER, J., SHANK, B., SOLIN, L. & WESSON, M. 1991. Tolerance of normal tissue to therapeutic irradiation. *International Journal of Radiation Oncology* Biology* Physics,* 21**,** 109-122.

FAUSTINO-ROCHA, A., OLIVEIRA, P. A., PINHO-OLIVEIRA, J., TEIXEIRA-GUEDES, C., SOARES-MAIA, R., DA COSTA, R. G., COLACO, B., PIRES, M. J., COLACO, J. & FERREIRA, R. 2013. Estimation of rat mammary tumor volume using caliper and ultrasonography measurements. *Lab animal,* 42**,** 217-224.

FERLAY, J., SOERJOMATARAM, I., DIKSHIT, R., ESER, S., MATHERS, C., REBELO, M., PARKIN, D. M., FORMAN, D. & BRAY, F. 2015. Cancer incidence and mortality worldwide: sources, methods and major patterns in GLOBOCAN 2012. *International journal of cancer,* 136**,** E359-E386.

FORSTER, J. C., MARCU, L. G. & BEZAK, E. 2019. Approaches to combat hypoxia in cancer therapy and the potential for in silico models in their evaluation. *Physica Medica,* 64**,** 145-156.

FOWLER, J. 1984. Fractionated radiation therapy after Strandqvist. *Acta Radiologica: Oncology,* 23**,** 209-216.

FOWLER, J. F. 1989. The linear-quadratic formula and progress in fractionated radiotherapy. *The British journal of radiology,* 62**,** 679-694.

FOWLER, J. F. 2001. Biological factors influencing optimum fractionation in radiation therapy. *Acta oncologica,* 40**,** 712-717.

FUKS, Z. & KOLESNICK, R. 2005. Engaging the vascular component of the tumor response. *Cancer cell,* 8**,** 89-91.

GAHBAUER, R., LANDBERG, T., CHAVAUDRA, J., DOBBS, J., GUPTA, N., HANKS, G., HORIOT, J.-C., JOHANSSON, K.-A., MÖLLER, T. & NAUDY, S. 2004. Prescribing, recording, and reporting electron beam therapy. *Journal of the ICRU,* 4**,** 1-2.

GHANDOUR, S., COSINSCHI, A., MAZOUNI, Z., PACHOUD, M. & MATZINGER, O. 2016. Optimization of stereotactic body radiotherapy treatment planning using a multicriteria optimization algorithm. *Zeitschrift für Medizinische Physik,* 26**,** 362-370.

GIRAUD, P., ANTOINE, M., LARROUY, A., MILLERON, B., CALLARD, P., DE RYCKE, Y., CARETTE, M.-F., ROSENWALD, J.-C., COSSET, J.-M. & HOUSSET, M. 2000. Evaluation of microscopic tumor extension in non–small-cell lung cancer for three-dimensional conformal radiotherapy planning. *International Journal of Radiation Oncology* Biology* Physics,* 48**,** 1015-1024.

GLADSTONE, D. J., KRY, S. F., XIAO, Y. & CHETTY, I. J. 2016. Dose specification for NRG radiation therapy trials. *International journal of radiation oncology, biology, physics,* 95**,** 1344.

GLIDE-HURST, C. K. & CHETTY, I. J. 2014. Improving radiotherapy planning, delivery accuracy, and normal tissue sparing using cutting edge technologies. *Journal of thoracic disease,* 6**,** 303.

GOLDSTRAW, P. 2013. New TNM classification: achievements and hurdles. *Translational lung cancer research,* 2**,** 264.

GOLDSTRAW, P., CHANSKY, K., CROWLEY, J., RAMI-PORTA, R., ASAMURA, H., EBERHARDT, W. E., NICHOLSON, A. G., GROOME, P., MITCHELL, A. & BOLEJACK, V. 2016. The IASLC lung cancer staging project: proposals for revision of the TNM stage groupings in the forthcoming (eighth) edition of the TNM classification for lung cancer. *Journal of Thoracic Oncology,* 11**,** 39-51.

GOLDSTRAW, P., CROWLEY, J., CHANSKY, K., GIROUX, D. J., GROOME, P. A., RAMI-PORTA, R., POSTMUS, P. E., RUSCH, V., SOBIN, L. & COMMITTEE, I. A. F. T. S. O. L. C. I. S. 2007. The IASLC Lung Cancer Staging Project: proposals for the revision of the TNM stage groupings in the forthcoming (seventh) edition of the TNM Classification of malignant tumours. *Journal of thoracic oncology,* 2**,** 706-714.

GOMEZ, D. R., LI, H. & CHANG, J. Y. 2018. Proton therapy for early-stage non-small cell lung cancer (NSCLC). *Translational Lung Cancer Research,* 7**,** 199.

GRAHAM, M. V., PURDY, J. A., EMAMI, B., HARMS, W., BOSCH, W., LOCKETT, M. A. & PEREZ, C. A. 1999. Clinical dose–volume histogram analysis for pneumonitis after 3D treatment for non-small cell lung cancer (NSCLC). *International Journal of Radiation Oncology* Biology* Physics,* 45**,** 323-329.

GREENE, D. & WILLIAMS, P. C. 1997. *Linear accelerators for radiation therapy*, CRC Press.

GREGOIRE, V. & MACKIE, T. R. 2011. Dose prescription, reporting and recording in intensity-modulated radiation therapy: a digest of the ICRU Report 83. *Imaging in Medicine,* 3**,** 367.

GRIFFIN, R. J. 2006. Radiobiology for the Radiologist, 6th Edition. International Journal of Radiation Oncology • Biology • Physics, 66, 627.

GUCKENBERGER, M., KLEMENT, R. J., ALLGÄUER, M., ANDRATSCHKE, N., BLANCK, O., BODA-HEGGEMANN, J., DIECKMANN, K., DUMA,

M., ERNST, I. & GANSWINDT, U. 2016. Local tumor control probability modeling of primary and secondary lung tumors in stereotactic body radiotherapy. *Radiotherapy and Oncology,* 118**,** 485-491.

GUIRADO, D., RUIZ-ARREBOLA, S., TORNERO-LÓPEZ, A. M., DE LA VEGA, J. M., PRADA, P. J. & LALLENA, A. M. 2020. A radiobiological study of the schemes with a low number of fractions in high-dose-rate brachytherapy as monotherapy for prostate cancer. *Journal of Contemporary Brachytherapy,* 12**,** 193.

GUNDERSON, L. L. & TEPPER, J. E. 2015. *Clinical radiation oncology*, Elsevier Health Sciences.

HALL, E. & GIACCIA, A. 2012. Radiobiology for the Radiologist 7th edn, Vol. II 432-447. Wolters Kluwer Health/Lippincott Williams & Wilkins.

HALPERIN, E. C., PEREZ, C. A. & BRADY, L. W. 2020. Perez and Brady's principles and practice of radiation oncology.

HAMAMOTO, Y., KATAOKA, M., YAMASHITA, M., NOGAMI, N., SUGAWARA, Y., KOZUKI, T., SAWADA, S., SUEHISA, H., SHINOHARA, S. & NAKAJIMA, N. 2012. Factors affecting the local control of stereotactic body radiotherapy for lung tumors including primary lung cancer and metastatic lung tumors. *Japanese journal of radiology,* 30**,** 430-434.

HARO, G. J., SHEU, B., COOK, N. R., WOODARD, G. A., MANN, M. J. & KRATZ, J. R. 2019. Comparison of conventional TNM and novel TNMB staging systems for non–small cell lung cancer. *JAMA Network Open,* 2**,** e1917062-e1917062.

HARRIS, J. P., MURPHY, J. D., HANLON, A. L., LE, Q.-T., LOO JR, B. W. & DIEHN, M. 2014. A population-based comparative effectiveness study of radiation therapy techniques in stage III non-small cell lung cancer. *International Journal of Radiation Oncology* Biology* Physics,* 88**,** 872-884.

HATTON, M. Q. F., HILL, R., FENWICK, J. D., MORGAN, S. A., WILSON, P. C., ATHERTON, P. J., DICKSON, J., MURRAY, K. E. & PAUL, J. 2016. Continuous hyperfractionated accelerated radiotherapy–Escalated dose (CHART-ED): A phase I study. *Radiotherapy and Oncology,* 118**,** 471-477.

HELBROW, J., MACNICOLL, F., BAYMAN, N. & FAIVRE-FINN, C. 2012. Concurrent chemoradiotherapy for locally advanced, unresectable non-small cell lung cancer: a UK survey of current practice. *Clinical oncology,* 24**,** e127.

HENK, J., WHITELOCKE, R., WARRINGTON, A. & BESSELL, E. 1993. Radiation dose to the lens and cataract formation. *International Journal of Radiation Oncology* Biology* Physics,* 25**,** 815-820.

HIGGINS, K. A., O'CONNELL, K., LIU, Y., GILLESPIE, T. W., MCDONALD, M. W., PILLAI, R. N., PATEL, K. R., PATEL, P. R., ROBINSON, C. G. & SIMONE II, C. B. 2017a. National Cancer Database analysis of proton

versus photon radiation therapy in non-small cell lung cancer. *International Journal of Radiation Oncology* Biology* Physics,* 97**,** 128-137.

HIGGINS, K. A., PILLAI, R. N., CHEN, Z., TIAN, S., ZHANG, C., PATEL, P., PAKKALA, S., SHELTON, J., FORCE, S. D. & FERNANDEZ, F. G. 2017b. Concomitant Chemotherapy and Radiotherapy with SBRT Boost for Unresectable Stage III Non–Small Cell Lung Cancer: A Phase I Study. *Journal of Thoracic Oncology,* 12**,** 1687-1695.

HIRSCH, F. R., SPREAFICO, A., NOVELLO, S., WOOD, M. D., SIMMS, L. & PAPOTTI, M. 2008. The prognostic and predictive role of histology in advanced non-small cell lung cancer: a literature review. *Journal of Thoracic Oncology,* 3**,** 1468-1481.

HOF, H., RHEIN, B., HAERING, P., KOPP-SCHNEIDER, A., DEBUS, J. & HERFARTH, K. 2009. 4D-CT-based target volume definition in stereotactic radiotherapy of lung tumours: comparison with a conventional technique using individual margins. *Radiotherapy and Oncology,* 93**,** 419-423.

HONG, B.-J., KIM, J., JEONG, H., BOK, S., KIM, Y.-E. & AHN, G.-O. 2016. Tumor hypoxia and reoxygenation: the yin and yang for radiotherapy. *Radiation Oncology Journal,* 34**,** 239.

HOPPE, B. S., HENDERSON, R., PHAM, D., CURY, J. D., BAJWA, A., MORRIS, C. G., D'AGOSTINO JR, H., FLAMPOURI, S., HUH, S. & LI, Z. 2016. A phase 2 trial of concurrent chemotherapy and proton therapy for stage III non-small cell lung cancer: results and reflections following early closure of a single-institution study. *International Journal of Radiation Oncology* Biology* Physics,* 95**,** 517-522.

HUSSEIN, M., ROWSHANFARZAD, P., EBERT, M. A., NISBET, A. & CLARK, C. H. 2013. A comparison of the gamma index analysis in various commercial IMRT/VMAT QA systems. *Radiotherapy and Oncology,* 109**,** 370-376.

INAL, A. & DUMAN, E. 2020. Adaptive time management for patients who have non-small cell lung cancer and underwent definitive radiotherapy: a dosimetric study of different gap duration scenarios. *International Journal of Radiation Biology***,** 1-15.

ISO, I. & OIML, B. 1995. Guide to the Expression of Uncertainty in Measurement. *Geneva, Switzerland,* 122.

JEREMIC, B., SHIBAMOTO, Y., ACIMOVIC, L. & MILISAVLJEVIC, S. 1996. Hyperfractionated radiation therapy with or without concurrent low-dose daily carboplatin/etoposide for stage III non-small-cell lung cancer: a randomized study. *Journal of Clinical Oncology,* 14**,** 1065-1070.

JONES, B. 1999. Mathematical models of tumour and normal tissue response. *Acta oncologica,* 38**,** 883-893.

JONES, B. & DALE, R. 2005. The potential for mathematical modelling in the assessment of the radiation dose equivalent of cytotoxic chemotherapy given

concomitantly with radiotherapy. *The British journal of radiology,* 78**,** 939-944.

JUNG, H. S., LEE, J. G., LEE, C. Y., KIM, D. J. & CHUNG, K. Y. 2018. Validation of the T descriptor in the new 8th TNM classification for non-small cell lung cancer. *Journal of thoracic disease,* 10**,** 162.

KANDATHIL, A., KAY, F. U., BUTT, Y. M., WACHSMANN, J. W. & SUBRAMANIAM, R. M. 2018. Role of FDG PET/CT in the eighth edition of TNM staging of non–small cell lung cancer. *RadioGraphics,* 38**,** 2134-2149.

KASTELIJN, E. A., EL SHAROUNI, S. Y., HOFMAN, F. N., VAN PUTTE, B. P., MONNINKHOF, E. M., VAN VULPEN, M. & SCHRAMEL, F. M. 2015. Clinical outcomes in early-stage NSCLC treated with stereotactic body radiotherapy versus surgical resection. *Anticancer research,* 35**,** 5607-5614.

KEALL, P. 2002. Dm rather than Dw should be used in Monte Carlo treatment planning. Against the proposition. *Medical physics,* 29**,** 923-924.

KENNY, E., LAVIN, D., COLGAN, N., MCCLEAN, B. & COURNANE, S. 2020. The 10th Annual scientific Meeting of the Irish Association of physicists in medicine (IAPM ASM 2019). Elsevier.

KHAN, F. M. & GIBBONS, J. P. 2014. *Khan's the physics of radiation therapy*, Lippincott Williams & Wilkins.

KIRKPATRICK, J. P., MEYER, J. J. & MARKS, L. B. The linear-quadratic model is inappropriate to model high dose per fraction effects in radiosurgery. Seminars in radiation oncology, 2008. Elsevier, 240-243.

KO, E. C., RABEN, D. & FORMENTI, S. C. 2018. The integration of radiotherapy with immunotherapy for the treatment of non–small cell lung cancer. *Clinical Cancer Research,* 24**,** 5792-5806.

KOCHER, M., TREUER, H., VOGES, J., HOEVELS, M., STURM, V. & MÜLLER, R.-P. 2000. Computer simulation of cytotoxic and vascular effects of radiosurgery in solid and necrotic brain metastases. *Radiotherapy and Oncology,* 54**,** 149-156.

KONG, F.-M., TEN HAKEN, R. K., SCHIPPER, M. J., SULLIVAN, M. A., CHEN, M., LOPEZ, C., KALEMKERIAN, G. P. & HAYMAN, J. A. 2005. High-dose radiation improved local tumor control and overall survival in patients with inoperable/unresectable non–small-cell lung cancer: Long-term results of a radiation dose escalation study. *International Journal of Radiation Oncology* Biology* Physics,* 63**,** 324-333.

KOPEK, N., PALUDAN, M., PETERSEN, J., HANSEN, A. T., GRAU, C. & HØYER, M. 2009. Co-morbidity index predicts for mortality after stereotactic body radiotherapy for medically inoperable early-stage non-small cell lung cancer. *Radiotherapy and Oncology,* 93**,** 402-407.

KOTO, M., TAKAI, Y., OGAWA, Y., MATSUSHITA, H., TAKEDA, K., TAKAHASHI, C., BRITTON, K. R., JINGU, K.-I., TAKAI, K. &

MITSUYA, M. 2007. A phase II study on stereotactic body radiotherapy for stage I non-small cell lung cancer. *Radiotherapy and Oncology,* 85**,** 429-434.

KOYI, H., JOHANSSON, L., FROM, J. & NYRÉN, S. 2015. Biopsy testing in an inoperable, non-small cell lung cancer population—a retrospective, real-life study in Sweden. *Journal of thoracic disease,* 7**,** 2226.

LABARERE, J., BERTRAND, R. & FINE, M. J. 2014. How to derive and validate clinical prediction models for use in intensive care medicine. *Intensive care medicine,* 40**,** 513-527.

LAGERWAARD, F. J., SENAN, S., VAN MEERBEECK, J. P., GRAVELAND, W. J. & GROUP, R. O. T. S. 2002. Has 3-D conformal radiotherapy (3D CRT) improved the local tumour control for stage I non-small cell lung cancer? *Radiotherapy and oncology,* 63**,** 151-157.

LAZZERONI, M., UHRDIN, J., CARVALHO, S., VAN ELMPT, W., LAMBIN, P., DASU, A., WERSÄLL, P. & TOMA-DASU, I. 2018. Evaluation of third treatment week as temporal window for assessing responsiveness on repeated FDG-PET-CT scans in Non-Small Cell Lung Cancer patients. *Physica Medica,* 46**,** 45-51.

LEE, J. H., WU, H.-G., KIM, H. J., KIM, D.-W., LEE, S.-H., KIM, T. M., KIM, Y. W. & HEO, D. S. 2012. Influence of comorbidities on the efficacy of radiotherapy with or without chemotherapy in elderly stage III non-small cell lung cancer patients. *Cancer research and treatment: official journal of Korean Cancer Association,* 44**,** 242.

LIAO, Z., LEE, J. J., KOMAKI, R., GOMEZ, D. R., O'REILLY, M. S., FOSSELLA, F. V., BLUMENSCHEIN JR, G. R., HEYMACH, J. V., VAPORCIYAN, A. A. & SWISHER, S. G. 2018. Bayesian adaptive randomization trial of passive scattering proton therapy and intensity-modulated photon radiotherapy for locally advanced non–small-cell lung cancer. *Journal of Clinical Oncology,* 36**,** 1813.

LIAO, Z. X., KOMAKI, R. R., THAMES JR, H. D., LIU, H. H., TUCKER, S. L., MOHAN, R., MARTEL, M. K., WEI, X., YANG, K. & KIM, E. S. 2010. Influence of technologic advances on outcomes in patients with unresectable, locally advanced non–small-cell lung cancer receiving concomitant chemoradiotherapy. *International Journal of Radiation Oncology* Biology* Physics,* 76**,** 775-781.

LIM, E., BALDWIN, D., BECKLES, M., DUFFY, J., ENTWISLE, J., FAIVRE-FINN, C., KERR, K., MACFIE, A., MCGUIGAN, J. & PADLEY, S. 2010. Guidelines on the radical management of patients with lung cancer. *Thorax,* 65**,** iii1-iii27.

LIM, W., RIDGE, C. A., NICHOLSON, A. G. & MIRSADRAEE, S. 2018. The 8th lung cancer TNM classification and clinical staging system: review of the changes and clinical implications. *Quantitative imaging in medicine and surgery,* 8**,** 709.

LIND, B. K. & BRAHME, A. 2007. The radiation response of heterogeneous tumors. *Physica Medica,* 23**,** 91-99.

LINDBLOM, E., ANTONOVIC, L., DASU, A., LAX, I., WERSÄLL, P. & TOMA-DASU, I. 2014. Treatment fractionation for stereotactic radiotherapy of lung tumours: a modelling study of the influence of chronic and acute hypoxia on tumour control probability. *Radiation Oncology,* 9**,** 149.

LITTLE, J. B. 1968. Cellular effects of ionizing radiation. *New England Journal of Medicine,* 278**,** 308-315.

MA, C. & LI, J. 2011. Dose specification for radiation therapy: dose to water or dose to medium? *Physics in Medicine & Biology,* 56**,** 3073.

MAGUIRE, J., KHAN, I., MCMENEMIN, R., O'ROURKE, N., MCNEE, S., KELLY, V., PEEDELL, C. & SNEE, M. 2014. SOCCAR: A randomised phase II trial comparing sequential versus concurrent chemotherapy and radical hypofractionated radiotherapy in patients with inoperable stage III Non-Small Cell Lung Cancer and good performance status. *European journal of cancer,* 50**,** 2939-2949.

MANEGOLD, C., DINGEMANS, A.-M. C., GRAY, J. E., NAKAGAWA, K., NICOLSON, M., PETERS, S., RECK, M., WU, Y.-L., BRUSTUGUN, O. T. & CRINÒ, L. 2017. The potential of combined immunotherapy and antiangiogenesis for the synergistic treatment of advanced NSCLC. *Journal of Thoracic Oncology,* 12**,** 194-207.

MARKS, L. B., YORKE, E. D., JACKSON, A., TEN HAKEN, R. K., CONSTINE, L. S., EISBRUCH, A., BENTZEN, S. M., NAM, J. & DEASY, J. O. 2010. Use of normal tissue complication probability models in the clinic. *International Journal of Radiation Oncology* Biology* Physics,* 76**,** S10-S19.

MARSDEN, J. 2020. Tumour control probability of a UK cohort of lung SABR patients. *Journal of Radiotherapy in Practice***,** 1-3.

MATSUYA, Y., SATO, T., NAKAMURA, R., NAIJO, S. & DATE, H. 2020. A theoretical cell-killing model to evaluate oxygen enhancement ratios at DNA damage and cell survival endpoints in radiation therapy. *Physics in Medicine & Biology,* 65**,** 095006.

MCCLELLAN, R. O. 2019. Biomarkers of Exposure and Responses to Ionizing Radiation. *Biomarkers in Toxicology.* Elsevier.

MEHTA, M., SCRIMGER, R., MACKIE, R., PALIWAL, B., CHAPPELL, R. & FOWLER, J. 2001. A new approach to dose escalation in non–small-cell lung cancer. *International Journal of Radiation Oncology*Biology*Physics,* 49**,** 23-33.

MELL, L. K., ROESKE, J. C. & MUNDT, A. J. 2003. A survey of intensity-modulated radiation therapy use in the United States. *Cancer,* 98**,** 204-211.

MOHER, D., LIBERATI, A., TETZLAFF, J. & ALTMAN, D. G. 2010. Preferred reporting items for systematic reviews and meta-analyses: the PRISMA statement. *Int J Surg,* 8**,** 336-341.

MOLINA, J. R., YANG, P., CASSIVI, S. D., SCHILD, S. E. & ADJEI, A. A. Non-small cell lung cancer: epidemiology, risk factors, treatment, and survivorship. Mayo Clinic Proceedings, 2008. Elsevier, 584-594.

MU, G., LUDLUM, E. & XIA, P. 2007. Impact of MLC leaf position errors on simple and complex IMRT plans for head and neck cancer. *Physics in medicine & biology,* 53**,** 77.

MUNSHI, A., HOBBS, M. & MEYN, R. E. 2005. Clonogenic cell survival assay. *Chemosensitivity.* Springer.

MURSHED, H. 2019. *Fundamentals of Radiation Oncology: Physical, Biological, and Clinical Aspects*, Academic Press.

MYNAMPATI, D. K., YAPARPALVI, R., HONG, L., KUO, H. C. & MAH, D. 2012. Application of AAPM TG 119 to volumetric arc therapy (VMAT). *Journal of applied clinical medical physics,* 13**,** 108-116.

NAHUM, A. E. 2015. The radiobiology of hypofractionation. *Clinical oncology,* 27**,** 260-269.

NAHUM, A. E., MOVSAS, B., HORWITZ, E. M., STOBBE, C. C. & CHAPMAN, J. D. 2003. Incorporating clinical measurements of hypoxia into tumor local control modeling of prostate cancer: implications for the α/β ratio. *International Journal of Radiation Oncology* Biology* Physics,* 57**,** 391-401.

NELDER, J. A. & MEAD, R. 1965. A simplex method for function minimization. *The computer journal,* 7**,** 308-313.

NEPPL, C., KELLER, M. D., SCHERZ, A., DORN, P., SCHMID, R. A., ZLOBEC, I. & BEREZOWSKA, S. 2019. Comparison of the 7th and 8th edition of the UICC/AJCC TNM staging system in primary resected squamous cell carcinomas of the lung–a single center analysis of 354 cases. *Frontiers in medicine,* 6**,** 196.

NEUBOECK, N., LINDENMANN, J., MATZI, V., JAKSE, G., OECHS, A., KAPP, S., MAIER, A. & SMOLLE-JÜTTNER, F.-M. 2010. Intraoperative radiotherapy (IORT)–alternative treatment in functionally nonresectable nonsmall cell lung cancer (NSCLC). *European Surgery,* 42**,** 209-213.

NGUYEN, Q.-N., LY, N. B., KOMAKI, R., LEVY, L. B., GOMEZ, D. R., CHANG, J. Y., ALLEN, P. K., MEHRAN, R. J., LU, C. & GILLIN, M. 2015. Long-term outcomes after proton therapy, with concurrent chemotherapy, for stage II–III inoperable non-small cell lung cancer. *Radiotherapy and Oncology,* 115**,** 367-372.

NISHINO, M., JACKMAN, D., DIPIRO, P., HATABU, H., JÄNNE, P. & JOHNSON, B. 2014. Revisiting the relationship between tumour volume and diameter in advanced NSCLC patients: an exercise to maximize the utility of each measure to assess response to therapy. *Clinical radiology,* 69**,** 841-848.

NOMIYA, T. 2013. Discussions on target theory: past and present. *Journal of radiation research,* 54**,** 1161-1163.

OHTAKI, Y., HISHIDA, T., YOSHIDA, J., ISHII, G., KAWASE, A., AOKAGE, K., NISHIMURA, M. & NAGAI, K. 2013. The clinical outcome of non-small cell lung cancer patients with adjacent lobe invasion: the optimal classification according to the status of the interlobar pleura at the invasion point. *European Journal of Cardio-Thoracic Surgery,* 43**,** 302-309.

OTTER, S. J., STEWART, A. J. & DEVLIN, P. M. 2019. Modern brachytherapy. *Hematology/Oncology Clinics,* 33**,** 1011-1025.

PALLIS, A., GRIDELLI, C., VAN MEERBEECK, J., GREILLIER, L., WEDDING, U., LACOMBE, D., WELCH, J., BELANI, C. & AAPRO, M. 2010. EORTC Elderly Task Force and Lung Cancer Group and International Society for Geriatric Oncology (SIOG) experts' opinion for the treatment of non-small-cell lung cancer in an elderly population. *Annals of oncology,* 21**,** 692-706.

PALMER, A. L., NASH, D., KEARTON, J. R., JAFARI, S. M. & MUSCAT, S. 2017. A multicentre 'end to end'dosimetry audit of motion management (4DCT-defined motion envelope) in radiotherapy. *Radiotherapy and Oncology,* 125**,** 453-458.

PANAWALA, L. 2019. *What is the Difference Between G1 and G2 Phase of Cell Cycle.*

PARK, C., PAPIEZ, L., ZHANG, S., STORY, M. & TIMMERMAN, R. D. 2008. Universal survival curve and single fraction equivalent dose: useful tools in understanding potency of ablative radiotherapy. *International Journal of Radiation Oncology* Biology* Physics,* 70**,** 847-852.

PARK, H. J., GRIFFIN, R. J., HUI, S., LEVITT, S. H. & SONG, C. W. 2012. Radiation-induced vascular damage in tumors: implications of vascular damage in ablative hypofractionated radiotherapy (SBRT and SRS). *Radiation research,* 177**,** 311-327.

PICCININI, F., TESEI, A., ARIENTI, C. & BEVILACQUA, A. 2015. Cancer multicellular spheroids: volume assessment from a single 2D projection. *Computer methods and programs in biomedicine,* 118**,** 95-106.

PINTO, J. A., VALLEJOS, C. S., RAEZ, L. E., MAS, L. A., RUIZ, R., TORRES-ROMAN, J. S., MORANTE, Z., ARAUJO, J. M., GÓMEZ, H. L. & AGUILAR, A. 2018. Gender and outcomes in non-small cell lung cancer: an old prognostic variable comes back for targeted therapy and immunotherapy? *ESMO open,* 3.

PLATANIOTIS, G. A. & DALE, R. G. 2008. Use of concept of chemotherapy-equivalent biologically effective dose to provide quantitative evaluation of contribution of chemotherapy to local tumor control in chemoradiotherapy cervical cancer trials. *International Journal of Radiation Oncology* Biology* Physics,* 72**,** 1538-1543.

POS, F. J., HART, G., SCHNEIDER, C. & SMINIA, P. 2006. Radical radiotherapy for invasive bladder cancer: What dose and fractionation schedule to choose? *International Journal of Radiation Oncology* Biology* Physics,* 64**,** 1168-1173.

POSTMUS, P., KERR, K., OUDKERK, M., SENAN, S., WALLER, D., VANSTEENKISTE, J., ESCRIU, C. & PETERS, S. 2017. Early and locally advanced non-small-cell lung cancer (NSCLC): ESMO Clinical Practice Guidelines for diagnosis, treatment and follow-up. *Annals of Oncology,* 28**,** iv1-iv21.

POWERS, E. 1962. Considerations of survival curves and target theory. *Phys. in Med. Biol.,* 7.

PURANDARE, N. C. & RANGARAJAN, V. 2015. Imaging of lung cancer: implications on staging and management. *The Indian journal of radiology & imaging,* 25**,** 109.

PURI, S., SALTOS, A., PEREZ, B., LE, X. & GRAY, J. E. 2020. Locally advanced, unresectable non-small cell lung cancer. *Current oncology reports,* 22**,** 1-10.

QI, X. S., WHITE, J. & LI, X. A. 2011. Is α/β for breast cancer really low? *Radiotherapy and Oncology,* 100**,** 282-288.

QIU, B., LI, Q. W., AI, X. L., WANG, B., HUAN, J., ZHU, Z. F., YU, G. H., JI, M., JIANG, H. H. & LI, C. 2020. Investigating the loco-regional control of simultaneous integrated boost intensity-modulated radiotherapy with different radiation fraction sizes for locally advanced non-small-cell lung cancer: clinical outcomes and the application of an extended LQ/TCP model. *Radiation Oncology,* 15**,** 1-10.

RADONIC, S., BESSERER, J., MEIER, V., BLEY, C. R. & SCHNEIDER, U. 2020. A novel analytical population TCP model includes cell density and volume variations: application to canine brain tumor. *arXiv preprint arXiv:2010.08348*.

RAJAPPA, S., SHARMA, S. & PRASAD, K. 2019. Unmet clinical need in the management of locally advanced unresectable lung cancer: Treatment strategies to improve patient outcomes. *Advances in Therapy,* 36**,** 563-578.

RAMNATH, N., DILLING, T. J., HARRIS, L. J., KIM, A. W., MICHAUD, G. C., BALEKIAN, A. A., DIEKEMPER, R., DETTERBECK, F. C. & ARENBERG, D. A. 2013. Treatment of stage III non-small cell lung cancer: Diagnosis and management of lung cancer: American College of Chest Physicians evidence-based clinical practice guidelines. *Chest,* 143**,** e314S-e340S.

ROMPELMAN, F. M., SMIT, A. A., FRANSSEN, E. J. & CRUL, M. 2017. Drug–drug interactions of cytostatics with regular medicines in lung cancer patients. *Journal of Oncology Pharmacy Practice,* 23**,** 483-490.

ROS. 2020. *Linear Accelerator (LINAC) Price Guide & Costs* [Online]. Available: https://www.oncologysystems.com/resources/linear-accelerator-guides/used-linac-price#:~:text=Linear%20accelerators%20that%20can%20be%20purchased%20for%20%24750%2C000%20to%20%241.5,Varian%20TrueBeam [Accessed 18/01/ 2021].

RUGGIERI, R., NACCARATO, S. & NAHUM, A. E. 2010. Severe hypofractionation: non-homogeneous tumour dose delivery can counteract tumour hypoxia. *Acta Oncologica,* 49**,** 1304-1314.

RUGGIERI, R., STAVREVA, N., NACCARATO, S. & STAVREV, P. 2013. Computed 88% TCP dose for SBRT of NSCLC from tumour hypoxia modelling. *Physics in Medicine & Biology,* 58**,** 4611.

SAITO, Y., HAYAKAWA, K., NAKAYAMA, Y., KATANO, S., FURUTA, M., ISHIKAWA, H., NASU, S., MITSUHASHI, N. & NIIBE, H. 1997. Radiation therapy for stage III non-small cell lung cancer invading chest wall. *Lung cancer,* 18**,** 171-178.

SALEM, A., ASSELIN, M.-C., REYMEN, B., JACKSON, A., LAMBIN, P., WEST, C. M., O'CONNOR, J. P. & FAIVRE-FINN, C. 2018. Targeting hypoxia to improve non–small cell lung cancer outcome. *JNCI: Journal of the National Cancer Institute,* 110**,** 14-30.

SANDLER, H. M., CURRAN JR, W. J. & TURRISI III, A. T. 1990. The influence of tumor size and pre-treatment staging on outcome following radiation therapy alone for stage I non-small cell lung cancer. *International Journal of Radiation Oncology* Biology* Physics,* 19**,** 9-13.

SANGANALMATH, P., LESTER, J., BRADSHAW, A., DAS, T., ESLER, C., ROY, A., TOY, E., LESTER, J., BUTTON, M. & WILSON, P. 2018a. Continuous Hyperfractionated Accelerated Radiotherapy (CHART) for Non-small Cell Lung Cancer (NSCLC): 7 Years' Experience From Nine UK Centres. *Clinical Oncology,* 30**,** 144-150.

SANGANALMATH, P., LESTER, J. E., BRADSHAW, A. G., DAS, T., ESLER, C., ROY, A. E. F., TOY, E., LESTER, J. F., BUTTON, M., WILSON, P., COMINS, C., ATHERTON, P., PICKLES, R., FOWERAKER, K., WALKER, G. A., KENI, M. & HATTON, M. Q. 2018b. Continuous Hyperfractionated Accelerated Radiotherapy (CHART) for Non-small Cell Lung Cancer (NSCLC): 7 Years' Experience From Nine UK Centres. *Clin Oncol (R Coll Radiol),* 30**,** 144-150.

SANTIAGO, A., BARCZYK, S., JELEN, U., ENGENHART-CABILLIC, R. & WITTIG, A. 2016. Challenges in radiobiological modeling: can we decide between LQ and LQ-L models based on reviewed clinical NSCLC treatment outcome data? *Radiation Oncology,* 11**,** 67.

SARIHAN, S., KAYISOGULLARI, U., ERCAN, I. & ENGIN, K. 2004. Randomized phase 2 study of radiotherapy alone versus radiotherapy with paclitaxel in non-small cell lung cancer. *Journal of international medical research,* 32**,** 375-383.

SAUNDERS, M., DISCHE, S., BARRETT, A., HARVEY, A., GRIFFITHS, G. & PARMAR, M. 1999. Continuous, hyperfractionated, accelerated radiotherapy (CHART) versus conventional radiotherapy in non-small cell lung cancer: mature data from the randomised multicentre trial. *Radiotherapy and oncology,* 52**,** 137-148.

SAUSE, W., KOLESAR, P., TAYLOR IV, S., JOHNSON, D., LIVINGSTON, R., KOMAKI, R., EMAMI, B., CURRAN JR, W., BYHARDT, R. & DAR, A. R. 2000. Final results of phase III trial in regionally advanced unresectable non-small cell lung cancer: Radiation Therapy Oncology Group, Eastern Cooperative Oncology Group, and Southwest Oncology Group. *Chest,* 117**,** 358-364.

SCAGLIOTTI, G. V., SZCZESNA, A., RAMLAU, R., CARDENAL, F., MATTSON, K., VAN ZANDWIJK, N., PRICE, A., LEBEAU, B., DEBUS, J. & MANEGOLD, C. 2006. Docetaxel-based induction therapy prior to radiotherapy with or without docetaxel for non-small-cell lung cancer. *British journal of cancer,* 94**,** 1375-1382.

SCHAAKE-KONING, C., VAN DEN BOGAERT, W., DALESIO, O., FESTEN, J., HOOGENHOUT, J., VAN HOUTTE, P., KIRKPATRICK, A., KOOLEN, M., MAAT, B. & NIJS, A. 1992. Effects of concomitant cisplatin and radiotherapy on inoperable non-small-cell lung cancer. *New England Journal of Medicine,* 326**,** 524-530.

SCHAUE, D. & MCBRIDE, W. H. 2015. Opportunities and challenges of radiotherapy for treating cancer. *Nature reviews Clinical oncology,* 12**,** 527.

SCHEENSTRA, A. E., ROSSI, M. M., BELDERBOS, J. S., DAMEN, E. M., LEBESQUE, J. V. & SONKE, J.-J. 2014. Alpha/beta ratio for normal lung tissue as estimated from lung cancer patients treated with stereotactic body and conventionally fractionated radiation therapy. *International Journal of Radiation Oncology* Biology* Physics,* 88**,** 224-228.

SCHNEIDER, U., STIPPER, A. & BESSERER, J. 2010. Dose-response relationship for lung cancer induction at radiotherapy dose. *Zeitschrift für Medizinische Physik,* 20**,** 206-214.

SHANNON, A. M., BOUCHIER-HAYES, D. J., CONDRON, C. M. & TOOMEY, D. 2003. Tumour hypoxia, chemotherapeutic resistance and hypoxia-related therapies. *Cancer treatment reviews,* 29**,** 297-307.

SHIMOHIGASHI, Y., ARAKI, F., MARUYAMA, M., NAKATO, K., NAKAGUCHI, Y. & KAI, Y. 2016. Evaluation of target localization accuracy for image-guided radiation therapy by 3D and 4D cone-beam CT in the presence of respiratory motion: a phantom study. *Biomedical Physics & Engineering Express,* 2**,** 025008.

SHIRVANI, S. M., JIANG, J., GOMEZ, D. R., CHANG, J. Y., BUCHHOLZ, T. A. & SMITH, B. D. 2013. Intensity modulated radiotherapy for stage III non-small cell lung cancer in the United States: predictors of use and association with toxicities. *Lung cancer,* 82**,** 252-259.

SIM, S., ROSENZWEIG, K. E., SCHINDELHEIM, R., NG, K. K. & LEIBEL, S. A. 2001. Induction chemotherapy plus three-dimensional conformal radiation therapy in the definitive treatment of locally advanced non-small-cell lung cancer. *International Journal of Radiation Oncology* Biology* Physics,* 51**,** 660-665.

SOCINSKI, M. A., BLACKSTOCK, A. W., BOGART, J. A., WANG, X., MUNLEY, M., ROSENMAN, J., GU, L., MASTERS, G. A., UNGARO, P. & SLEEPER, A. 2008. Randomized phase II trial of induction chemotherapy followed by concurrent chemotherapy and dose-escalated thoracic conformal radiotherapy (74 Gy) in stage III non–small-cell lung cancer: CALGB 30105. *Journal of clinical oncology,* 26**,** 2457-2463.

SOCINSKI, M. A., MORRIS, D. E., MASTERS, G. A. & LILENBAUM, R. 2003. Chemotherapeutic management of stage IV non-small cell lung cancer. *Chest,* 123**,** 226S-243S.

SOLOGUREN, I., RODRÍGUEZ-GALLEGO, C. & LARA, P. C. 2014. Immune effects of high dose radiation treatment: implications of ionizing radiation on the development of bystander and abscopal effects. *Translational Cancer Research*.

SONG, S. Y., CHOI, W., SHIN, S. S., LEE, S.-W., DO AHN, S., KIM, J. H., JE, H. U., PARK, C. I., LEE, J. S. & CHOI, E. K. 2009. Fractionated stereotactic body radiation therapy for medically inoperable stage I lung cancer adjacent to central large bronchus. *Lung cancer,* 66**,** 89-93.

STAVREVA, N., STAVREV, P., BALABANOVA, A., NAHUM, A., RUGGIERI, R. & PRESSYANOV, D. 2019. Modelling the effect of spread in radiosensitivity parameters and repopulation rate on the probability of tumour control. *Physica Medica,* 63**,** 79-86.

STEWART, R. D., YU, V. K., GEORGAKILAS, A. G., KOUMENIS, C., PARK, J. H. & CARLSON, D. J. 2011. Effects of radiation quality and oxygen on clustered DNA lesions and cell death. *Radiation research,* 176**,** 587-602.

STEYERBERG, E. W., BLEEKER, S. E., MOLL, H. A., GROBBEE, D. E. & MOONS, K. G. 2003. Internal and external validation of predictive models: a simulation study of bias and precision in small samples. *Journal of clinical epidemiology,* 56**,** 441-447.

STEYERBERG, E. W. & HARRELL, F. E. 2016. Prediction models need appropriate internal, internal–external, and external validation. *Journal of clinical epidemiology,* 69**,** 245-247.

STINCHCOMBE, T. E., MORRIS, D. E., MOORE, D. T., BECHTEL, J. H., HALLE, J. S., MEARS, A., DESCHESNE, K., ROSENMAN, J. G. & SOCINSKI, M. A. 2006. Post-chemotherapy gross tumor volume is predictive of survival in patients with stage III non-small cell lung cancer treated with combined modality therapy. *Lung cancer,* 52**,** 67-74.

STRIGARI, L., D'ANDREA, M., ABATE, A. & BENASSI, M. 2008. A heterogeneous dose distribution in simultaneous integrated boost: the role of the clonogenic cell density on the tumor control probability. *Physics in Medicine & Biology,* 53**,** 5257.

STROOM, J. C. & HEIJMEN, B. J. 2002. Geometrical uncertainties, radiotherapy planning margins, and the ICRU-62 report. *Radiotherapy and oncology,* 64**,** 75-83.

STUSCHKE, M. & PÖTTGEN, C. 2010. Altered fractionation schemes in radiotherapy. *Controversies in the Treatment of Lung Cancer.* Karger Publishers.

SUI, X., JIANG, W., CHEN, H., YANG, F., WANG, J. & WANG, Q. 2017. Validation of the stage groupings in the eighth edition of the TNM classification for lung cancer. *Journal of Thoracic Oncology,* 12**,** 1679-1686.

TAKEDA, A., SANUKI, N., KUNIEDA, E., OHASHI, T., OKU, Y., TAKEDA, T., SHIGEMATSU, N. & KUBO, A. 2009. Stereotactic body radiotherapy for primary lung cancer at a dose of 50 Gy total in five fractions to the periphery of the planning target volume calculated using a superposition algorithm. *International Journal of Radiation Oncology* Biology* Physics,* 73**,** 442-448.

TAREMI, M., HOPE, A., DAHELE, M., PEARSON, S., FUNG, S., PURDIE, T., BRADE, A., CHO, J., SUN, A. & BISSONNETTE, J.-P. 2012. Stereotactic body radiotherapy for medically inoperable lung cancer: prospective, single-center study of 108 consecutive patients. *International Journal of Radiation Oncology* Biology* Physics,* 82**,** 967-973.

TEOH, M., CLARK, C., WOOD, K., WHITAKER, S. & NISBET, A. 2011. Volumetric modulated arc therapy: a review of current literature and clinical use in practice. *The British journal of radiology,* 84**,** 967-996.

THAMES, H. D. 1985. An 'incomplete-repair'model for survival after fractionated and continuous irradiations. *International Journal of Radiation Biology and Related Studies in Physics, Chemistry and Medicine,* 47**,** 319-339.

TIMMERMAN, R. D., PAULUS, R., PASS, H. I., GORE, E., EDELMAN, M. J., GALVIN, J. M., CHOY, H., STRAUBE, W., NEDZI, L. A. & MCGARRY, R. 2013. RTOG 0618: Stereotactic body radiation therapy (SBRT) to treat operable early-stage lung cancer patients. American Society of Clinical Oncology.

TSUJINO, K., HIROTA, S., ENDO, M., OBAYASHI, K., KOTANI, Y., SATOUCHI, M., KADO, T. & TAKADA, Y. 2003. Predictive value of dose-volume histogram parameters for predicting radiation pneumonitis after concurrent chemoradiation for lung cancer. *International Journal of Radiation Oncology* Biology* Physics,* 55**,** 110-115.

TURNER, S., LOCHRIN, C., DISCHE, S., SAUNDERS, M. & MAHER, E. 1995. Continuous hyperfractionated accelerated radiotherapy in the treatment of carcinoma of the columella and vestibule of the nose. *European Journal of Cancer Part B: Oral Oncology,* 31**,** 368-372.

URVAY, S. E., YUCEL, B., ERDIS, E. & TURAN, N. 2016. Prognostic factors in stage III non-small-cell lung cancer patients. *Asian Pacific Journal of Cancer Prevention: APJCP,* 17**,** 4693.

UZAN, J. & NAHUM, A. 2012. Radiobiologically guided optimisation of the prescription dose and fractionation scheme in radiotherapy using BioSuite. *The British journal of radiology,* 85**,** 1279-1286.

VALLIERES, E., SHEPHERD, F. A., CROWLEY, J., VAN HOUTTE, P., POSTMUS, P. E., CARNEY, D., CHANSKY, K., SHAIKH, Z. & GOLDSTRAW, P. 2009. The IASLC Lung Cancer Staging Project: proposals regarding the relevance of TNM in the pathologic staging of small cell lung cancer in the forthcoming (seventh) edition of the TNM classification for lung cancer. *Journal of Thoracic Oncology,* 4**,** 1049-1059.

VAN LEEUWEN, C., OEI, A., CREZEE, J., BEL, A., FRANKEN, N., STALPERS, L. & KOK, H. 2018. The alfa and beta of tumours: a review of parameters of the linear-quadratic model, derived from clinical radiotherapy studies. *Radiation oncology,* 13**,** 1-11.

VERNIMMEN, F. J. & SLABBERT, J. P. 2010. Assessment of the α/ß ratios for arteriovenous malformations, meningiomas, acoustic neuromas, and the optic chiasma. *International journal of radiation biology,* 86**,** 486-498.

WALSH, S. & PUTTEN, W. 2013. *A TCP model for external beam treatment of intermediate-risk prostate cancer*.

WALSH, S., ROELOFS, E., KUESS, P., LAMBIN, P., JONES, B., GEORG, D. & VERHAEGEN, F. 2016. A validated tumor control probability model based on a meta- analysis of low, intermediate, and high- risk prostate cancer patients treated by photon, proton, or carbon- ion radiotherapy. *Medical physics,* 43**,** 734-747.

WALTERS, B., KRAMER, R. & KAWRAKOW, I. 2010. Dose to medium versus dose to water as an estimator of dose to sensitive skeletal tissue. *Physics in Medicine & Biology,* 55**,** 4535.

WAMBERSIE, A., LANDBERG, T., CHAVAUDRA, J., DOBBS, J., HANKS, G., JOHANSSON, K., MOLLER, T., PURDY, J., AKANUMA, A. & GERARD, J. 1992. Prescribing, recording, and reporting photon beam therapy presentation of the ICRU report# 50. *Journal of Medical Physics,* 17**,** 5.

WANG, X., YIN, C., SU, S., LI, X., WANG, C., ZHANG, C. & LIU, M. 2018. Long-term effects of neoadjuvant radiotherapy, adjuvant radiotherapy, and chemotherapy-only on survival of locally advanced non-small cell lung Cancer undergoing surgery: a propensity-matched analysis. *BMC cancer,* 18**,** 1067.

WEBB, S. 1994. Optimum parameters in a model for tumour control probability including interpatient heterogeneity. *Physics in Medicine & Biology,* 39**,** 1895.

WEBB, S. & NAHUM, A. 1993. A model for calculating tumour control probability in radiotherapy including the effects of inhomogeneous distributions of dose and clonogenic cell density. *Physics in Medicine & Biology,* 38**,** 653.

WEST, C. M. & SLEVIN, F. 2019. Tumour hypoxia. Clinical Oncology, 31, 595-555.

WHO. 2020. *Cancer fact sheets* [Online]. International Agency for Research on Cancer. Available: https://gco.iarc.fr/today/fact-sheets-cancers [Accessed 08/01/ 2021].

WILLERS, H., DAHM-DAPHI, J. & POWELL, S. 2004. Repair of radiation damage to DNA. *British journal of cancer,* 90**,** 1297-1301.

WILLIAMS, J. 2019. Basic clinical radiobiology. Taylor & Francis.

WILLIAMS, S. G., TAYLOR, J. M., LIU, N., TRA, Y., DUCHESNE, G. M., KESTIN, L. L., MARTINEZ, A., PRATT, G. R. & SANDLER, H. 2007. Use of individual fraction size data from 3756 patients to directly determine the α/β ratio of prostate cancer. *International Journal of Radiation Oncology* Biology* Physics,* 68**,** 24-33.

WITHERS, H., TAYLOR, J. & MACIEJEWSKI, B. 1988. The hazard of accelerated tumor clonogen repopulation during radiotherapy. *Acta oncologica,* 27**,** 131-146.

WOLSKI, M. J., BHATNAGAR, A., FLICKINGER, J. C., BELANI, C. P., RAMALINGAM, S. & GREENBERGER, J. S. 2005. Multivariate Analysis of Survival, Local Control, and Time to Distant Metastases in Patients with Unresectable Non–Small-Cell Lung Carcinoma Treated with 3-Dimensional Conformal Radiation Therapy with or Without Concurrent Chemotherapy. *Clinical lung cancer,* 7**,** 100-106.

YAMAMOTO, T., KABUS, S., BAL, M., BZDUSEK, K., KEALL, P. J., WRIGHT, C., BENEDICT, S. H. & DALY, M. E. 2018. Changes in regional ventilation during treatment and dosimetric advantages of CT ventilation image guided radiation therapy for locally advanced lung cancer. *International Journal of Radiation Oncology* Biology* Physics,* 102**,** 1366-1373.

YANG, L., WANG, S., ZHOU, Y., LAI, S., XIAO, G., GAZDAR, A. & XIE, Y. 2017. Evaluation of the 7th and 8th editions of the AJCC/UICC TNM staging systems for lung cancer in a large North American cohort. *Oncotarget,* 8**,** 66784.

YANG, X., CAO, Y., SHAO, Q., LI, S., LEI, M. & YANG, Z. 2020. Improving the accuracy of converting dose to medium to dose to water algorithms in small megavoltage photon fields in dose to medium based treatment planning systems. *Physica Medica,* 71**,** 62-70.

YOH WATANABE, M. 2003. TNM classification for lung cancer. *Ann Thorac Cardiovasc Surg,* 9.

ZAPPA, C. & MOUSA, S. A. 2016. Non-small cell lung cancer: current treatment and future advances. *Translational lung cancer research,* 5**,** 288.

ZEHENTMAYR, F., WURSTBAUER, K., DEUTSCHMANN, H., FUSSL, C., KOPP, P., DAGN, K., FASTNER, G., PORSCH, P., STUDNICKA, M. & SEDLMAYER, F. 2015. DART-bid: dose-differentiated accelerated radiation therapy, 1.8 Gy twice daily. *Strahlentherapie und Onkologie,* 191**,** 256-263.

ZHANG, T., ZHANG, J.-T., LI, W.-F., LIN, J.-T., LIU, S.-Y., YAN, H.-H., YANG, J.-J., YANG, X.-N., WU, Y.-L. & NIE, Q. 2019. Visceral pleural invasion in T1 tumors (≤ 3 cm), particularly T1a, in the eighth tumor-node-metastasis classification system for non-small cell lung cancer: a population-based study. *Journal of thoracic disease,* 11**,** 2754.

ZHENG, X., SCHIPPER, M., KIDWELL, K., LIN, J., REDDY, R., REN, Y., CHANG, A., LV, F., ORRINGER, M. & KONG, F.-M. S. 2014. Survival outcome after stereotactic body radiation therapy and surgery for stage I non-small cell lung cancer: a meta-analysis. *International Journal of Radiation Oncology* Biology* Physics,* 90**,** 603-611.

ZIPS, D. 2009. Tumour growth and response to radiation. *Basic clinical radiobiology,* 4**,** 78-101.

ZUGAZAGOITIA, J., GUEDES, C., PONCE, S., FERRER, I., MOLINA-PINELO, S. & PAZ-ARES, L. 2016. Current challenges in cancer treatment. *Clinical therapeutics,* 38**,** 1551-1566.

ZUO, G., XU, Z., YU, H. & HAO, B. 2010. Jackknife and bootstrap tests of the composition vector trees. *Genomics, proteomics & bioinformatics,* 8**,** 262-267.

Appendix A Dissemination of Research

A.1 Optimal tumour control for early-stage non-small-cell lung cancer: A radiobiological modelling perspective

- DOI: 10.1016/j.ejmp.2019.09.074

Physica Medica 66 (2019) 55–65

Contents lists available at ScienceDirect

Physica Medica

journal homepage: www.elsevier.com/locate/ejmp

Original paper

Optimal tumour control for early-stage non-small-cell lung cancer: A radiobiological modelling perspective

Mohammed Alaswad[a,b,*], Christoph Kleefeld[a], Mark Foley[a]

[a] School of Physics, National University of Ireland Galway, Galway, Ireland
[b] Comprehensive Cancer Centre, Radiation Oncology, King Fahad Medical City, Riyadh 11525, Saudi Arabia

ARTICLE INFO

Keywords:
NSCLC
TCP
Clonogenic cell density distribution
GTV–CTV margin

ABSTRACT

A fully heterogeneous population tumour control probability (TCP) model, based on the linear-quadratic (LQ) cell survival concept combined with the Poisson statistic, was established to predict local tumour control after one, two and three years. This TCP model was created using data from 16 publications that reported on early-stage non-small-cell lung cancer (NSCLC) treated using either three-dimensional conformal radiation therapy (3D-CRT), continuous hyperfractionated accelerated radiotherapy (CHART) or stereotactic ablative body radiotherapy (SABR). The TCP model was fitted to the clinical outcome data using optimized radiosensitivity values produced by the Nelder-Mead simplex algorithm. The statistical analysis resulted in R^2 values of 0.96, 0.96 and 0.97 and wRMSE values of 3.9%, 5.2% and 5.9% for one-, two- and three-year local tumour control rates, respectively. The TCP models for one, two and three years were internally validated using a bootstrap resampling approach. The mean R^2 and 95% CI for the bootstrap samples were 0.98 (0.93–0.99), 0.98 (0.95–0.99) and 0.98 (0.96–0.99) for the one-, two- and three-year local tumour control rates, respectively. Variations in the TCP with clonogenic density were then further investigated by introducing a new mathematical model to vary the clonogenic cell and radiation dose distribution across the treated volume. Based on the above model, it was estimated that 60% of the dose was sufficient to maintain the TCP after two years for the areas with lower clonogenic cell density. If externally validated, this lower-dose treatment plan could have beneficial effects on the surrounding healthy tissue without negatively affecting tumour control.

1. Introduction

Lung cancer remains the most common cause of cancer mortality, with approximately 1.81 million patients diagnosed with the disease in 2012 [1]. The two main categories of lung cancer are non-small-cell lung cancer (NSCLC), which includes 80% of all lung cancers, and small-cell lung cancer (SCLC), which accounts for the remaining 20% [2]. Radical surgery remains a treatment mainstay for early-stage NSCLC; however, many patients with NSCLC are not candidates for surgery due to comorbidities, such as cardiopulmonary dysfunction, stage I, II or chronic obstructive pulmonary disease or tumour size during stages III and IV [3], or because they refuse surgery altogether. Consequently, curative external-beam radiotherapy is commonly regarded as an alternative therapeutic procedure for early-stage NSCLC [4].

The conventional fractionation (CF) radiotherapy schedule, as proposed by the Radiation Therapy Oncology Group (RTOG) [5], is 45–70 Gy and includes one treatment per day of 1.8–2.5 Gy per fraction over 6–8 weeks. Notably, CF radiotherapy has historically been associated with poor local tumour control (35%, 17% and 9% at one-, two- and three-year follow-ups, respectively) [6]. Another fractionation scheme suggested by some institutions in the United Kingdom is continuous hyperfractionated accelerated radiotherapy (CHART), which prescribes radiation doses of 54 Gy via 1.5 Gy per fraction delivered 3 times per day. In the United Kingdom, CHART is recommended as the standard of care for patients undergoing a radiotherapy course for NSCLC [7]. This fractionation scheme has the potential to improve local tumour control up to 66%, 40% and 20% at one-, two- and three-year follow-ups, respectively [7].

In addition, improved survival and local tumour control can be attained using stereotactic ablative radiotherapy (SABR), a state-of-the-art technique that is considered the optimal treatment for patients with early-stage NSCLC for whom surgical procedures are not appropriate. Several studies and prospective phase II trials have confirmed that the

* Corresponding author at: School of Physics, National University of Ireland Galway, Galway, Ireland and Comprehensive Cancer Centre, Radiation Oncology, King Fahad Medical City, Riyadh, Saudi Arabia.
E-mail address: medphy00@gmail.com (M. Alaswad).

https://doi.org/10.1016/j.ejmp.2019.09.074
Received 1 July 2019; Received in revised form 6 September 2019; Accepted 8 September 2019
Available online 24 September 2019

A.2 Radiation dose intensity and local tumour control of non-small cell lung cancer: A radiobiological modelling perspective

- DOI: 10.1088/1742-6596/1248/1/012071

A.3 A TCP model for external beam treatment of non-small cell lung cancer

- DOI: 10.1016/j.ejmp.2018.06.037

Physica Medica
Volume 52, August 2018, Page 172

Poster Session – For consideration for Imaging Equipment Ltd. Bursary P4

A TCP model for external beam treatment of non-small cell lung cancer

Mohammed Alaswad [a] ✉, Christoph Kleefeld [a], Margaret Moore [b], Mark Foley [c]

Show more

+ Add to Mendeley Share Cite

https://doi.org/10.1016/j.ejmp.2018.06.037

Radiobiology has progressed sufficiently to provide suitable understanding of the radiation response of a wide spectrum of cell lines, and this principal provides a degree of certainty in the capability to describe this radiation response using mathematical models. The focus of this project was to examine the ability of a mechanistic Tumor Control Probability (TCP) model to predict treatment outcomes for a wide range of treatment strategies for Non-Small Cell Lung Cancer (NSCLC), such as hypo-fractionation, standard fractionation, and hyper-fractionation. A fully heterogeneous population-averaged TCP model was fit to clinical outcome data accumulated from the literature for NSCLC using optimized radiosensitivity values produced by the simplex algorithm. The clinical data reported the two-year local tumor control rate for Stage I–II NSCLC for dose prescription varies between 1.5–15 Gy per fraction. The biological parameters α, β, $\sigma\alpha$, and $\sigma\beta$ were obtained with the simplex algorithm's search of the radiosensitivity solution space of the outcome data described above. These values were obtained through a robust fitting procedure using the simplex algorithm based on the best available clinical data for dose response, total initial clonogen number, clonogen density, clonogen distribution, and hypoxia status of the average in NSCLC patients. The TCP model achieves an excellent level of fit, R^2value of 0.92, and RMSE of 2.4% for the clinical outcome data for hyper, standard, and hypofractionated treatments using realistic values for biological input parameters. Residuals $\leqslant$3% are produced by the TCP model when compared to clinical outcome data for both standard fractionation and SABR.

A.4 Radiobiological modelling of clonogen distribution, hypoxic fraction and tumour size effects on local tumour control of non-small cell lung cancer

- DOI: 10.1016/j.ejmp.2019.09.185

Download PDF

Physica Medica

Volume 67, November 2019, Page 197

Radiobiological modelling of clonogen distribution, hypoxic fraction and tumour size effects on local tumour control of non-small cell lung cancer

Mohammad Alaswad, Christoph Kleefeld, Mark Foley

Show more

+ Add to Mendeley Share Cite

https://doi.org/10.1016/j.ejmp.2019.09.185 Get rights and content

Previous article in issue Next article in issue

Published clinical data show that hypoxia in human lung tumours can impede the establishment of optimum local tumour control. However, the overall effect of hypoxia on the tumour control probability (TCP) model is not clear. The focus of this project was to assess the influence of radiobiological parameters (the number of clonogens and the hypoxic fraction), as well as some treatment parameters (i.e., the tumour size), on local tumour control of early stage non-small cell lung cancer (NSCLC). A TCP model, based on LQ cell survival concept combined with the Poisson statistic, was established to predict one, two and three years of local tumour control. This TCP model was created using data from seventeen publications of early-stage NSCLC treated using one of the three radiotherapy modalities: three-dimensional conformal radiation therapy (3D-CRT), continuous hyperfractionated accelerated radiotherapy (CHART) or stereotactic ablative body radiotherapy (SABR). The variations in the TCP with the gross tumour volume (GTV) size, clonogen number and hypoxic fraction were then investigated. This issue was approached by varying the clonogen densities values (between 101 and 107 cm̂3), the GTV volume (20–140 cc) and the hypoxic fraction (20–90%). The optimum values used to compute the TCP model were a clonogen density of 107 cm̂3 and a hypoxic fraction of 20%, which were consistent with the clinical outcome values reported in the literature for NSCLC. This radiobiological model has demonstrated the proof of concept that poor local tumour control is strongly associated with the hypoxic fraction and large tumours.

A.5 Comparison of the T descriptor of the 7th and 8th editions of the TNM staging system for non-small cell lung cancer after radiotherapy: An analysis from the TCP modelling perspective

- Manuscript ID: RPOR-D-20-00295

Reports of Practical Oncology & Radiotherapy

Comparison of the T descriptor of the 7th and 8th editions of the TNM staging system for non-small cell lung cancer after radiotherapy: An analysis from the TCP modelling perspective

--Manuscript Draft--

Manuscript Number:	
Article Type:	Original research article
Keywords:	Tumour control probability; 7th TNM classification; 8th TNM classification; Non-small cell lung cancer
Corresponding Author:	Mohammed Alaswad National University of Ireland Galway Galway, IRELAND
First Author:	Mohammed Alaswad
Order of Authors:	Mohammed Alaswad
	Christoph Kleefeld
	Mark Foley
Abstract:	Aim This study aims to incorporate the T descriptor of the 7th and 8th editions of the TNM categorisation schema into a tumour control probability (TCP) model. Background The tumour, node, metastasis (TNM) staging system employs a configuration that depicts the anatomic extent of cancer, thereby enhancing the exchange of information between oncologists. Materials and methods A mechanistic TCP model based on the linear-quadratic concept combined with the Poisson statistic was developed to assess variations in local tumour control according to the 7th and 8th editions of the TNM classification system. The simulation involved a single cohort of 354 patients with non-small cell lung cancer (NSCLC). Results The estimated mean gross tumour volumes (GTV) were 2.3–500 cm3 and 0.4–350 cm3 in accordance with the recommendations of the 7th and 8th editions, respectively. The predicted TCP for the T1a vs. T1b group after applying 2 Gy in 30 fractions was 48% ± 1.09% vs. 43% ± 1.05% according to the 7th edition and 51.5% ± 0.80% vs. 47.8% ± 0.85% according to the 8th edition. Conclusion: The differences in the predicted TCP between the adjacent T category groups in the 8th edition were all significant. Similar findings were observed in the 7th edition, except for the T3 vs. T4 stage. The TCP model outcomes based on the T descriptors of the 8th TNM revealed an enhanced model fit, a higher R2 and a lower RMSE compared with those of the 7th TNM, implying the superior discriminatory ability of the later edition.

A.6 Internal and external validation of a tumour control probability model for non-small cell lung cancer

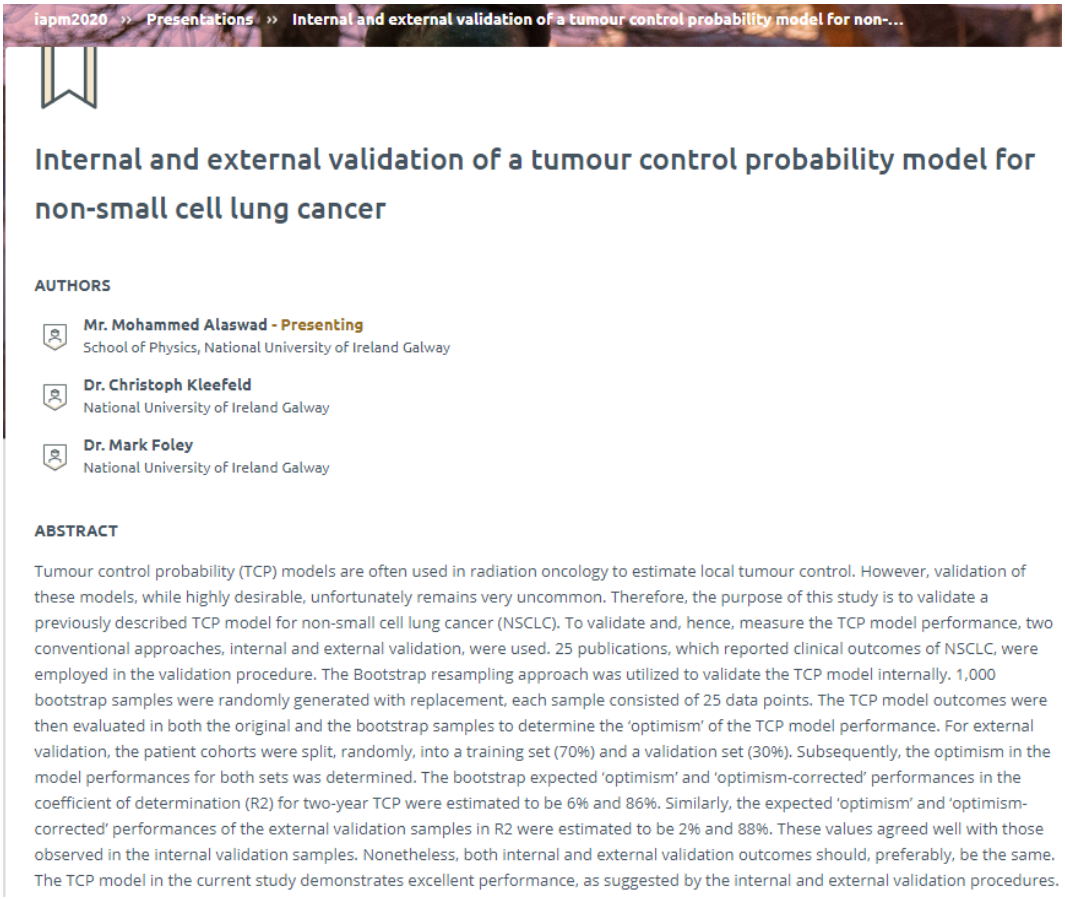

iapm2020 ›› Presentations ›› Internal and external validation of a tumour control probability model for non-...

Internal and external validation of a tumour control probability model for non-small cell lung cancer

AUTHORS

Mr. Mohammed Alaswad - Presenting
School of Physics, National University of Ireland Galway

Dr. Christoph Kleefeld
National University of Ireland Galway

Dr. Mark Foley
National University of Ireland Galway

ABSTRACT

Tumour control probability (TCP) models are often used in radiation oncology to estimate local tumour control. However, validation of these models, while highly desirable, unfortunately remains very uncommon. Therefore, the purpose of this study is to validate a previously described TCP model for non-small cell lung cancer (NSCLC). To validate and, hence, measure the TCP model performance, two conventional approaches, internal and external validation, were used. 25 publications, which reported clinical outcomes of NSCLC, were employed in the validation procedure. The Bootstrap resampling approach was utilized to validate the TCP model internally. 1,000 bootstrap samples were randomly generated with replacement, each sample consisted of 25 data points. The TCP model outcomes were then evaluated in both the original and the bootstrap samples to determine the 'optimism' of the TCP model performance. For external validation, the patient cohorts were split, randomly, into a training set (70%) and a validation set (30%). Subsequently, the optimism in the model performances for both sets was determined. The bootstrap expected 'optimism' and 'optimism-corrected' performances in the coefficient of determination (R2) for two-year TCP were estimated to be 6% and 86%. Similarly, the expected 'optimism' and 'optimism-corrected' performances of the external validation samples in R2 were estimated to be 2% and 88%. These values agreed well with those observed in the internal validation samples. Nonetheless, both internal and external validation outcomes should, preferably, be the same. The TCP model in the current study demonstrates excellent performance, as suggested by the internal and external validation procedures.

A.7 Comparison of the T descriptor of the 7th and 8th editions of the TNM staging system for non-small cell lung cancer after radiotherapy: An analysis from the TCP modelling perspective

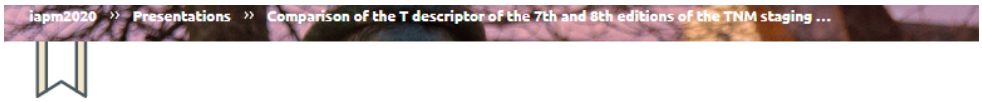

Comparison of the T descriptor of the 7th and 8th editions of the TNM staging system for non-small cell lung cancer after radiotherapy: An analysis from the TCP modelling perspective

AUTHORS

Mr. Mohammed Alaswad - Presenting
School of Physics, National University of Ireland Galway

Dr. Christoph Kleefeld
National University of Ireland Galway

Dr. Mark Foley
National University of Ireland Galway

ABSTRACT

The tumour, node, metastasis (TNM) staging system employs a configuration that depicts the anatomic extent of cancer, thereby enhancing the exchange of information between oncologists. This study aims to incorporate the T descriptor of the TNM classification system into a tumour control probability (TCP) model. A mechanistic TCP model based on the linear-quadratic concept combined with the Poisson statistic was developed to assess variations in local tumour control according to the 7^{th} and 8^{th} editions of the TNM classification system. The simulation involved a single cohort of 354 patients with non-small cell lung cancer (NSCLC). The estimated mean gross tumour volumes (GTV) were 2.3–500 cm^3 and 0.4–350 cm^3 in accordance with the recommendations of the 7^{th} and 8^{th} editions, respectively. The predicted TCP for the T1a vs. T1b group after applying 2 Gy in 30 fractions was 48% ± 1.09% vs. 43% ± 1.05% according to the 7^{th} edition and 51.5% ± 0.80% vs. 47.8% ± 0.85% according to the 8^{th} edition. The differences in the predicted TCP between the adjacent T category groups in the 8^{th} edition were all significant. Similar findings were observed in the 7^{th} edition, except for the T3 vs. T4 stage. The TCP model outcomes based on the T descriptors of the 8^{th} TNM revealed an enhanced model fit, a higher R^2 and a lower RMSE compared with those of the 7^{th} TNM, implying the superior discriminatory ability of the later edition.

A.8 Influence of radiotherapy and chemotherapy on tumour control probability in patients with non-small cell lung cancer: A radiobiological modelling study

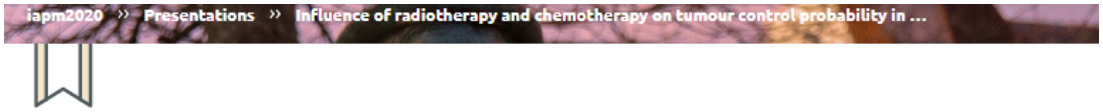

Influence of radiotherapy and chemotherapy on tumour control probability in patients with non-small cell lung cancer: A radiobiological modelling study

AUTHORS

Mr. Mohammed Alaswad - Presenting
School of Physics, National University of Ireland Galway

Dr. Christoph Kleefeld
National University of Ireland Galway

Dr. Mark Foley
National University of Ireland Galway

ABSTRACT

Currently, synergistic cytotoxic chemotherapy with radiotherapy is being increasingly applied to treat locally advanced non-small cell lung cancer (NSCLC). This approach is believed to offer superior local tumour control, although concerns remain as to whether major incidences of toxicity may occur. While the effect of radiotherapy-alone can be well described by the tumour control probability (TCP) model, the combined effect of concomitant chemotherapy and radiotherapy is still subject to intensive research. Therefore, a previously developed mechanistic TCP model, was further extended to assess the impact of the chemotherapy factor on the TCP model. Data from four patient cohorts, accumulated from the literature, were selected for this modelling study. The dose sensitisation approach was employed to investigate and quantify the effect of chemotherapy on the estimated TCP. This approach assumed that each radiotherapy dose was given concurrently with a sensitising agent in such a way that fractional dose 'd' became dose 'dc', where 'c' was the chemotherapy-modulated radiation dose enhancement factor (c). The following values for c were used during the TCP simulation: 1.2, 1.4, 1.8, and 2. Accordingly, patients receiving concurrent chemotherapy had significantly enhanced TCPs compared to those treated with radiotherapy-alone. The estimated 2-year TCP rates in the 'radiation-alone' and the 'radiation combined with chemotherapy' groups were 23.0% and 39%, 39% and 48.9%, 25.7% and 40.7% and 32.9% and 45.2%, respectively. Therefore, this study demonstrates that incorporating sensitising agents into a TCP model can improve tumour cure probabilities and, thus, allow quantitative assessment of combined radiotherapy and chemotherapy modalities.

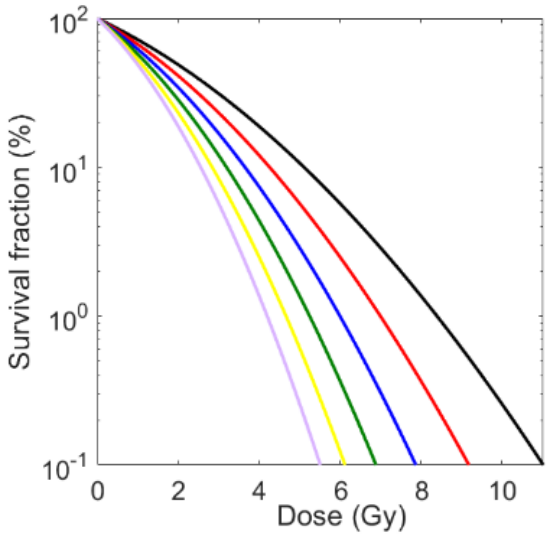

Figure A.1: Survival fractionation. Comparison between radiation-alone or chemo-radiation. Radiation-alone is represented by the black line, chemo-radiation (c=1.2) is represented by the red line, chemo-radiation (c=1.4) is represented by the blue line, chemo-radiation (c=1.6) is represented by the green line, chemo-radiation (c=1.8) is represented by the yellow line and chemo-radiation (c=2) is represented by the purple line.

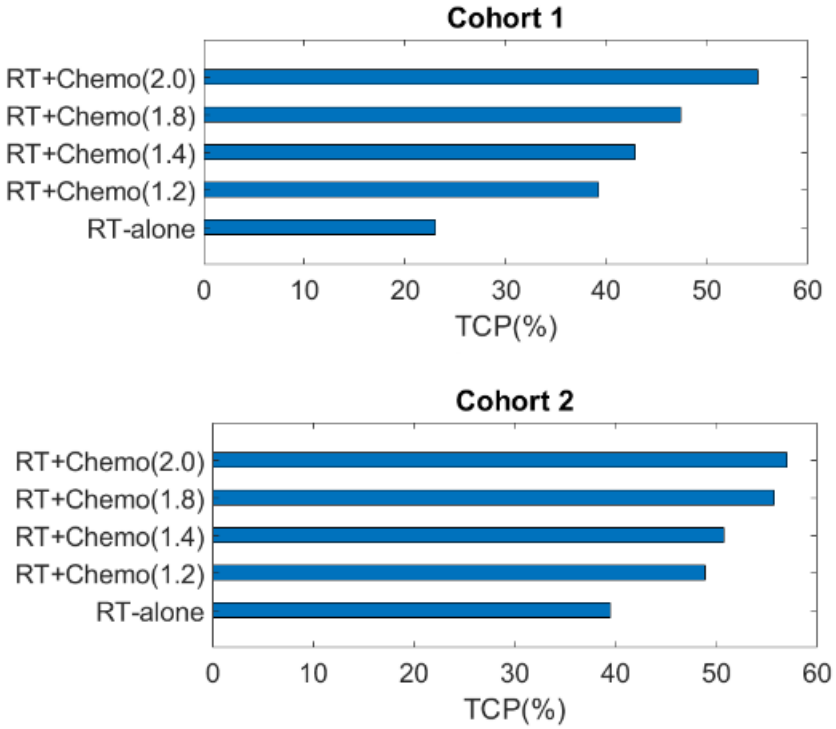

Figure A.2: Variations in tumour cure probabilities with different values of the chemotherapy-modulated radiation dose enhancement factor.

A.9 Radiobiological modelling of concomitant radiochemotherapy for patients with locally advanced non-small cell lung cancer: A tumour control probability perspective

Radiobiological modelling of concomitant radiochemotherapy for patients with locally advanced non-small cell lung cancer: A tumour control probability perspective.

M. Alaswad[1,2], C. Kleefeld[1 1], M. Foley[1].
(1) National University of Ireland Galway, (2) King Fahad Medical City

Purpose: Locally advanced non-small cell lung cancer (LA-NSCLC) is characterised as a stage III disease with subdivisions into stages IIIA, IIIB and IIIC in accordance with the newly proposed 8th tumour-node-metastasis (TNM) framework. Currently, synergistic cytotoxic chemotherapy with radiotherapy is most prevalent in treating LA-NSCLC. Clinical trial experience from multiple references has reported that the risk of locoregional relapse and distant metastasis was less evident for patients treated with concomitant radiochemotherapy than radiotherapy alone. Although the influence of radiotherapy alone can be adequately described by the tumour control probability (TCP) model, the combined impact of concomitant chemotherapy and radiotherapy is still subject to extensive research. Therefore, the paramount purpose of this study is to develop a TCP model that can describe the effect of synergistic chemotherapy with radiotherapy for locally advanced NSCLC patients.

Materials and Method: A fully heterogeneous population TCP model, based on the linear-quadratic (LQ) cell survival notion combined with the Poisson statistic, was established to predict local tumour control for LA-NSCLC following two therapeutic approaches: radiotherapy alone and radiochemotherapy. The TCP-LQ model was amended to quantify the effect of chemotherapy prescription according to the log-cell kill notion. Notably, the log-cell kills mechanism relies on the assumption that cytotoxic drugs eliminate a certain fraction of clonogenic cells based on the drug concentration. Overall, 811 patients from 8 clinical trials were enrolled in this study, with 411 patients in the radiotherapy-alone arm and 400 in the radiochemotherapy arm. The TCP simulation was developed to predict three clinical endpoints: one-, two- and three-year local tumour control. The TCP model was fitted to the clinical outcome data using optimised radiosensitivity values (e.g., alpha and beta values) produced by the Nelder-Mead simplex algorithm.

Results: The TCP model outcomes revealed a strong positive linear correlation between the predicted TCP outcomes and the literature's reported local tumour control. Consistent with the reported outcomes presented in the literature, the TCP model outcomes for the radiochemotherapy arm exhibited superior TCPs than the radiotherapy-alone arm. For the radiochemotherapy arm, TCPs were as high as 75.5%, 50.6% and 41.4% at one-, two- and three-year local tumour control rates, respectively. In contrast to the radiotherapy-alone arm results, the TCP model yielded undesirable local tumour control rates.

Conclusions: This study demonstrates that incorporating the log-cell kills concept into a TCP-LQ model can improve tumour cure probabilities and thus allow quantitative assessment of combined radiotherapy and chemotherapy modalities.

Keywords: tumour control probability, locally advanced non-small cell lung cancer, radiotherapy, chemotherapy, radiochemotherapy.

Dear MOHAMMED ALASWAD

with reference to the 3rd European Congress of Medical Physics, organized by EFOMP and hosted by AIFM to be held in Torino, Italy on June 16-19, 2021, please find here below all the relevant information about the abstract you submitted via the online submission system.

Abstract ID	474	**Please refer to this ID number for any communication related to your abstract**
Title	Radiobiological modelling of concomitant radiochemotherapy for patients with locally advanced non-small cell lung cancer: A tumour control probability perspective.	
Topic	1 - Radiotherapy (RT)	

Should you wish to update or modify your submitted abstract, kindly upload the new version on the online submission system and send a mail to ecmp2020@symposium.it to inform us.
We remain at your complete disposal for any further clarification you may need.

Best regards
The Organizing Secretariat

Symposium srl
via Gozzano 14
10073 Ciriè, Torino
Italy
Tel. +39 011 9211467
Fax +39 011 9224992
www.symposium.it

A.10 Influence of radiotherapy dose uncertainty on local tumour control for locally advanced non-small cell lung cancer

Influence of radiotherapy dose uncertainty on local tumour control for locally advanced non-small cell lung cancer

M. Alaswad[1,2], C. Kleefeld[1 1], M. Foley[1].
(1) National University of Ireland Galway, (2) King Fahad Medical City

Purpose: It is widely recognised that radiotherapy machines are calibrated to deliver a specific radiation dose under a set of standard conditions. However, certain clinical situations may arise which result in a patient receiving a radiotherapy dose that is systematically different to the dose prescribed by radiation oncologists. The sources of radiotherapy dose uncertainty include – but are not limited to – absolute calibration of the treatment machine, modelling of radiation transport within the patient, delineation of tumour and healthy tissues, patient positioning, and day-to-day patient positioning variations. These potential variations in the radiotherapy dose delivered may adversely impact patients' clinical outcomes. Thus, the purpose of this study is to quantify the influence of radiotherapy dose uncertainty on overall tumour control probability (TCP).

Materials and Method: A one-year TCP model was established based on the linear-quadratic cell concept combined with Poisson statistics. The TCP model was fitted to a series of locally advanced non-small cell lung cancer (LA-NSCLC) patients drawn from the literature, who were treated with either radiotherapy alone or radiochemotherapy. The TCP-LQ model was extended to quantify the effect of chemotherapy prescription according to the log-cell kill notion. The TCP simulation was performed by delivering prescription radiation doses of 60, 65, 70 and 80 Gy via 3D-conformal radiation therapy (3D-CRT). In order to study the impact of radiotherapy dose uncertainty on TCP outcomes, the nominal radiation dose was varied from -5% to +5% with an interval of 0.5 for the radiotherapy-alone and radiochemotherapy arms.

Results: The variations in local tumour control probability for total radiation doses of 60, 65, 70 and 80 Gy ranged between 17.8–27.9%, 24.7–38.6%, 30.3–47.4% and 42.9–59.9% for the radiotherapy-alone arms, and between 29.1–56.5, 35.6–66.9, 58.3–74.2 and 68.4–82.8 for the radiochemotherapy arms.

Conclusions: This study sought to evolve a TCP model that could interpret the clinical outcomes of LA-NSCLC. One of the more significant findings of this research is that radiotherapy dose uncertainty can adversely impact local tumour control in LA-NSCLC cases.

Keywords: radiotherapy, uncertainty, tumour control probability, locally advanced non-small cell lung cancer.

Dear MOHAMMED ALASWAD

with reference to the 3rd European Congress of Medical Physics, organized by EFOMP and hosted by AIFM to be held in Torino, Italy on June 16-19, 2021, please find here below all the relevant information about the abstract you submitted via the online submission system.

Abstract ID	477	**Please refer to this ID number for any communication related to your abstract**
Title	Influence of radiotherapy dose uncertainty on local tumour control for locally advanced non-small cell lung cancer.	
Topic	1 - Radiotherapy (RT)	

Should you wish to update or modify your submitted abstract, kindly upload the new version on the online submission system and send a mail to ecmp2020@symposium.it to inform us.
We remain at your complete disposal for any further clarification you may need.

Best regards
The Organizing Secretariat

Symposium srl
via Gozzano 14
10073 Ciriè, Torino
Italy
Tel. +39 011 9211467
Fax +39 011 9224992
www.symposium.it

A.11 The sensitivity of patient-specific IMRT QA methods in detecting systematic errors: field-by-field versus single-gantry-angle composite

- DOI: 10.1088/1742-6596/1248/1/012063

Journal of Physics: Conference Series

PAPER • OPEN ACCESS

The sensitivity of patient-specific IMRT QA methods in detecting systematic errors: field-by-field versus single-gantry-angle composite

To cite this article: M Alaswad and L Coleman 2019 *J. Phys.: Conf. Ser.* **1248** 012063

A.12 Comparison of IMRT QA measurement methodology

- DOI: doi.org/10.1016/j.ejmp.2017.05.074

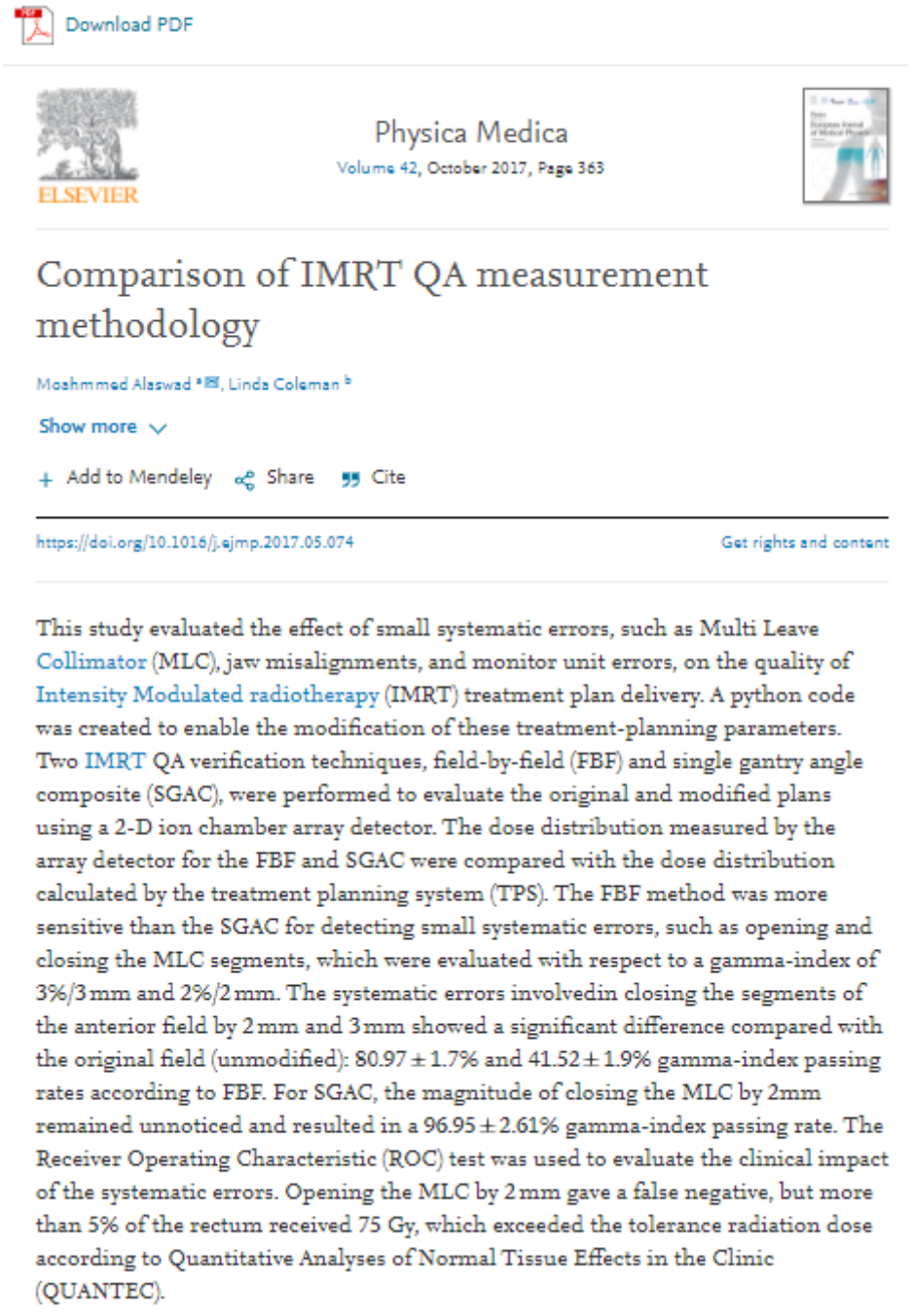

Download PDF

ELSEVIER

Physica Medica

Volume 42, October 2017, Page 363

Comparison of IMRT QA measurement methodology

Moahmmed Alaswad [a], Linda Coleman [b]

Show more

+ Add to Mendeley Share Cite

https://doi.org/10.1016/j.ejmp.2017.05.074

Get rights and content

This study evaluated the effect of small systematic errors, such as Multi Leave Collimator (MLC), jaw misalignments, and monitor unit errors, on the quality of Intensity Modulated radiotherapy (IMRT) treatment plan delivery. A python code was created to enable the modification of these treatment-planning parameters. Two IMRT QA verification techniques, field-by-field (FBF) and single gantry angle composite (SGAC), were performed to evaluate the original and modified plans using a 2-D ion chamber array detector. The dose distribution measured by the array detector for the FBF and SGAC were compared with the dose distribution calculated by the treatment planning system (TPS). The FBF method was more sensitive than the SGAC for detecting small systematic errors, such as opening and closing the MLC segments, which were evaluated with respect to a gamma-index of 3%/3 mm and 2%/2 mm. The systematic errors involvedin closing the segments of the anterior field by 2 mm and 3 mm showed a significant difference compared with the original field (unmodified): 80.97 ± 1.7% and 41.52 ± 1.9% gamma-index passing rates according to FBF. For SGAC, the magnitude of closing the MLC by 2mm remained unnoticed and resulted in a 96.95 ± 2.61% gamma-index passing rate. The Receiver Operating Characteristic (ROC) test was used to evaluate the clinical impact of the systematic errors. Opening the MLC by 2 mm gave a false negative, but more than 5% of the rectum received 75 Gy, which exceeded the tolerance radiation dose according to Quantitative Analyses of Normal Tissue Effects in the Clinic (QUANTEC).

Appendix B Additional results

B.1 Optimal tumour control for early-stage non-small-cell lung cancer: A radiobiological modelling perspective

- DOI: 10.1016/j.ejmp.2019.09.074

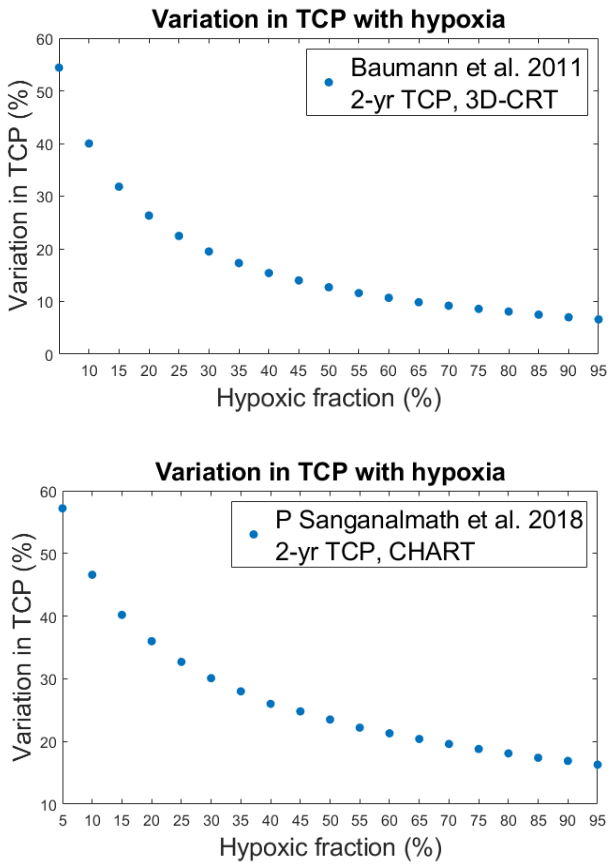

Figure B.1: Analysis of variation in TCP as a function of hypoxic using: A) Baumann et al. (2011) data that comprised of 203 patients, treated using a total dose of 66 Gy, yielding a 2-year TCP of 26.4 %; (B) Sanganalmath et al. (2018a) data that comprised of 849 patients, treated using a total dose of 54 Gy, yielding a 2-year TCP of 36 %.

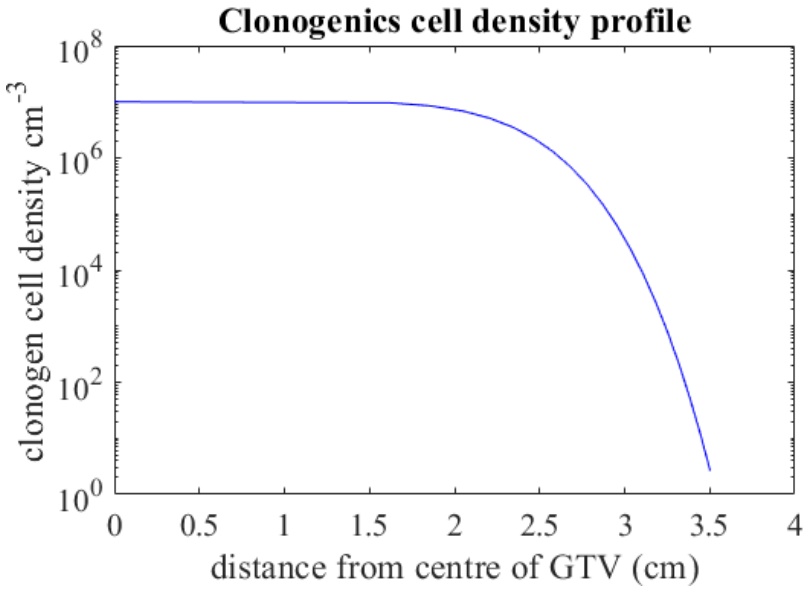
Clonogenics cell density profile
clonogen cell density cm-3
10^8
10^6
10^4
10^2
10^0
0
0.5
1
1.5
2
2.5
3
3.5
4
distance from centre of GTV (cm)

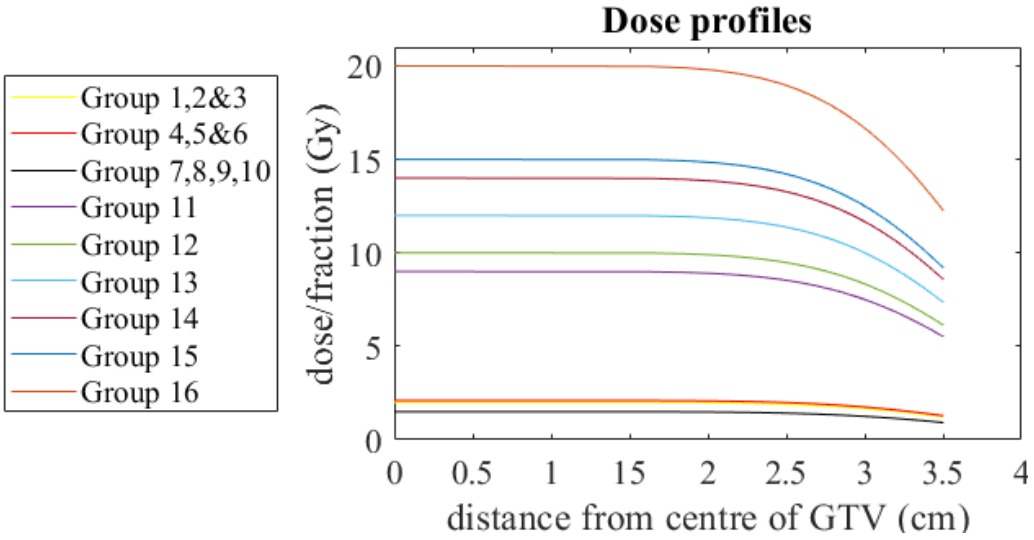
Dose profiles
Group 1,2&3
Group 4,5&6
Group 7,8,9,10
Group 11
Group 12
Group 13
Group 14
Group 15
Group 16
dose/fraction (Gy)
20
15
10
5
0
0
0.5
1
15
2
2.5
3
3.5
4
distance from centre of GTV (cm)

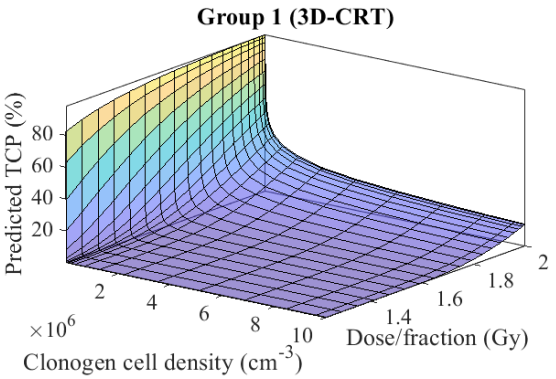
Group 1 (3D-CRT)
Predicted TCP (%)
80
60
40
20
2
4
6
8
10
×10^6
Clonogen cell density (cm^-3)
1.4
1.6
1.8
2
Dose/fraction (Gy)

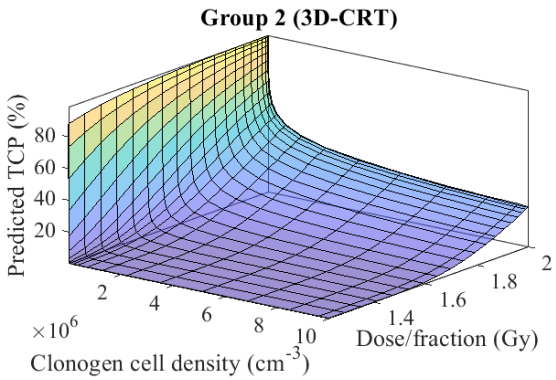
Group 2 (3D-CRT)
Predicted TCP (%)
80
60
40
20
2
4
6
8
10
×10^6
Clonogen cell density (cm^-3)
1.4
1.6
1.8
2
Dose/fraction (Gy)

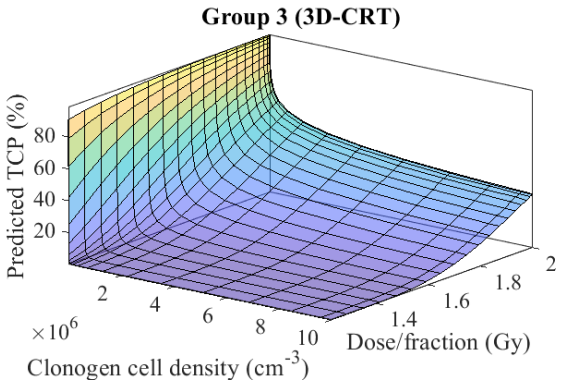
Group 3 (3D-CRT)
Predicted TCP (%)
80
60
40
20
2
4
6
8
10
×10^6
Clonogen cell density (cm^-3)
1.4
1.6
1.8
2
Dose/fraction (Gy)

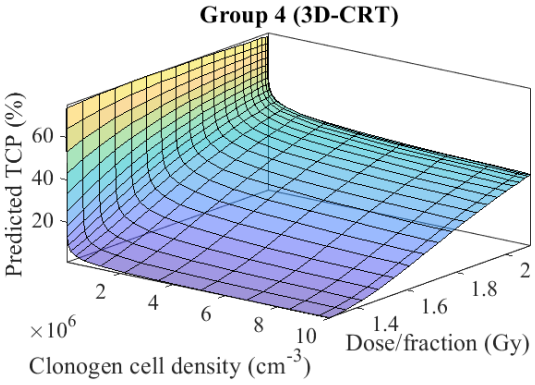
Group 4 (3D-CRT)
Predicted TCP (%)
60
40
20
2
4
6
8
10
×10^6
Clonogen cell density (cm^-3)
1.4
1.6
1.8
2
Dose/fraction (Gy)

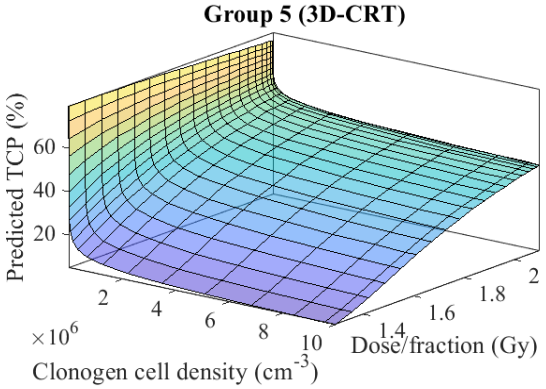
Group 5 (3D-CRT)
Predicted TCP (%)
60
40
20
2
4
6
8
10
×10^6
Clonogen cell density (cm^-3)
1.4
1.6
1.8
2
Dose/fraction (Gy)

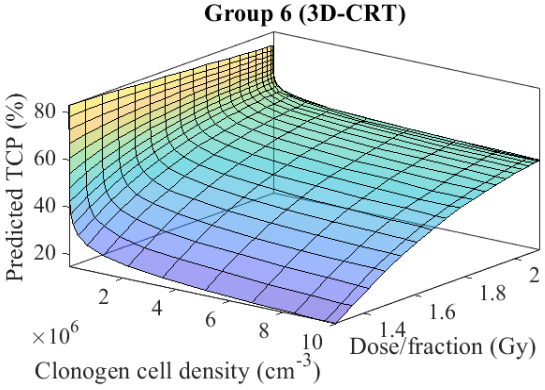
Group 6 (3D-CRT)
Predicted TCP (%)
80
60
40
20
2
4
6
8
10
×10^6
Clonogen cell density (cm^-3)
1.4
1.6
1.8
2
Dose/fraction (Gy)

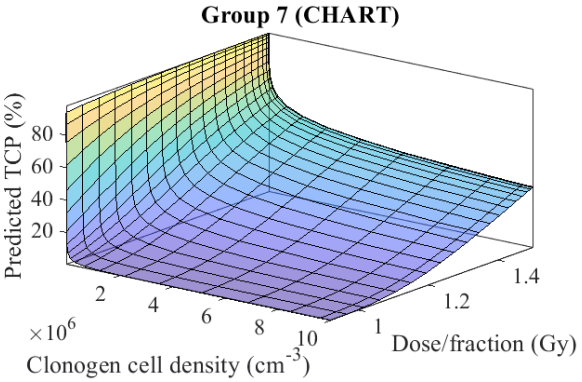
Group 7 (CHART)
Predicted TCP (%)
80
60
40
20
2
4
6
8
10
×10^6
Clonogen cell density (cm^-3)
1
1.2
1.4
Dose/fraction (Gy)

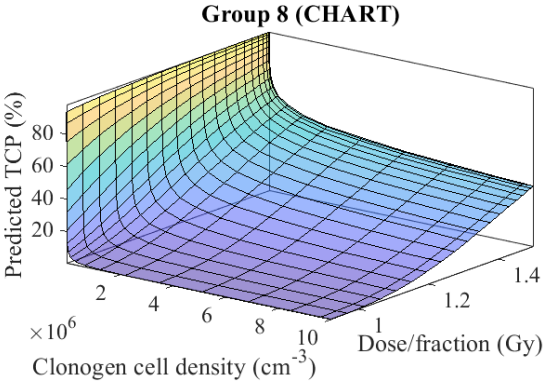
Group 8 (CHART)
Predicted TCP (%)
80
60
40
20
2
4
6
8
10
×10^6
Clonogen cell density (cm^-3)
1
1.2
1.4
Dose/fraction (Gy)

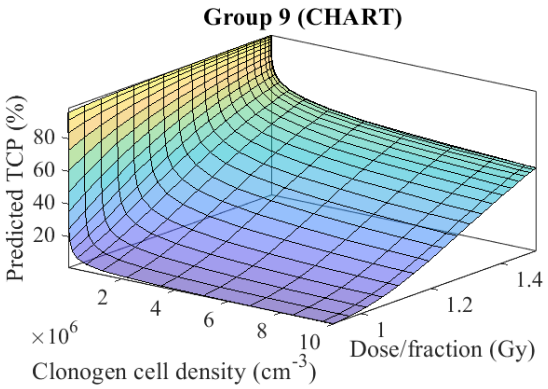
Group 9 (CHART)
Predicted TCP (%)
80
60
40
20
2
4
6
8
10
×10^6
Clonogen cell density (cm^-3)
1
1.2
1.4
Dose/fraction (Gy)

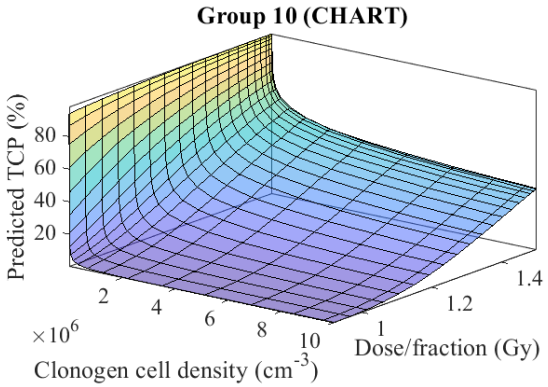
Group 10 (CHART)
Predicted TCP (%)
80
60
40
20
2
4
6
8
10
×10^6
Clonogen cell density (cm^-3)
1
1.2
1.4
Dose/fraction (Gy)

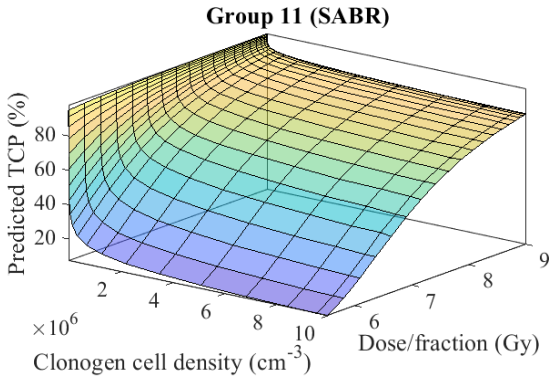
Group 11 (SABR)
Predicted TCP (%)
80
60
40
20
2
4
6
8
10
×10^6
Clonogen cell density (cm^-3)
6
7
8
9
Dose/fraction (Gy)

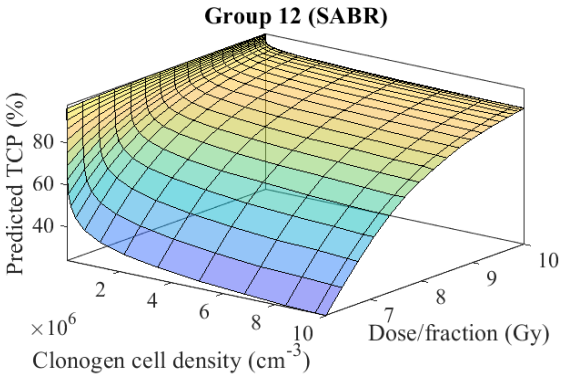
Group 12 (SABR)
Predicted TCP (%)
80
60
40
2
4
6
8
10
×10^6
Clonogen cell density (cm^-3)
7
8
9
10
Dose/fraction (Gy)

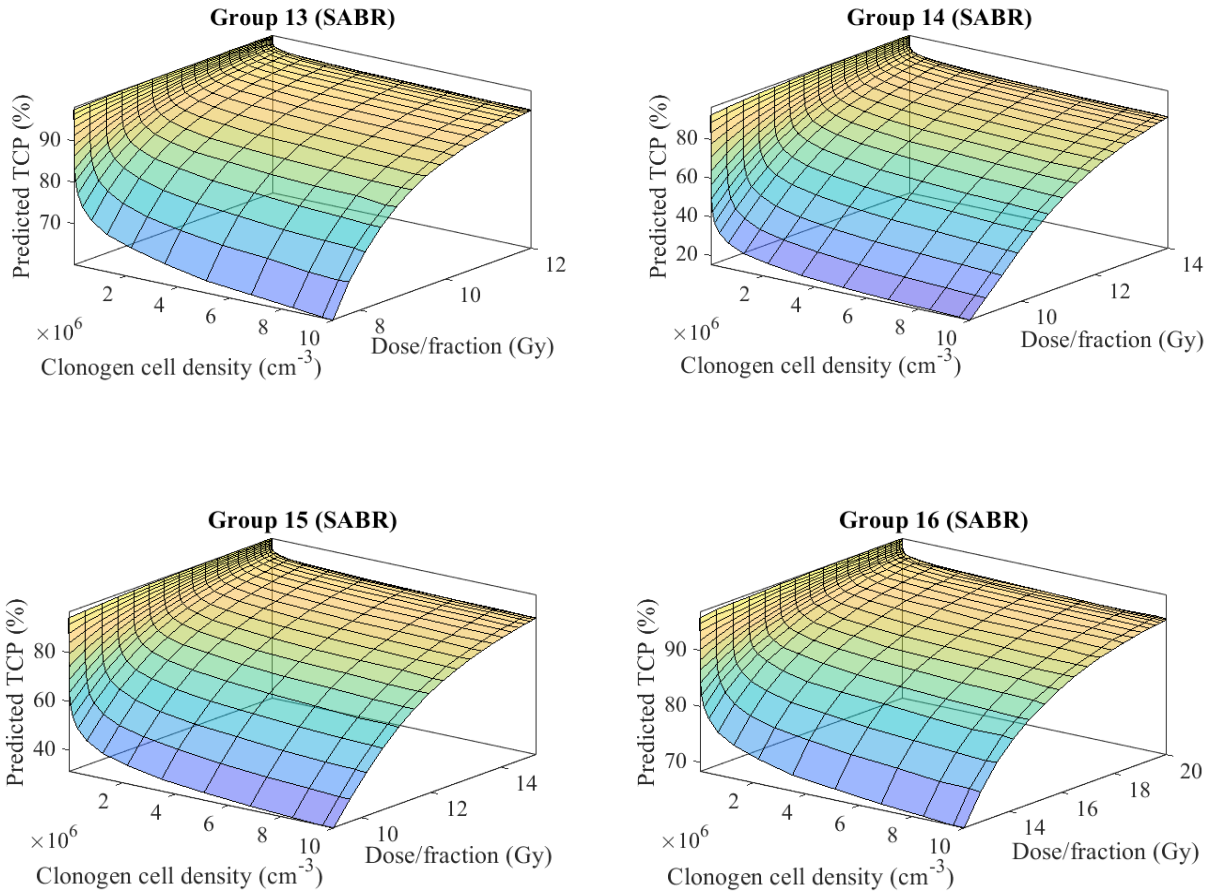

Figure B.2: Shows the results obtained using the approach described in Section 3.2.3, as applied to the 16 patient cohorts outlined in Table 3.1 and with a clonogenic cell density distribution and dose-per-fraction distribution of a half-Gaussian decay.

B.2 Comparison of the T descriptor of the 7th and 8th editions of the TNM staging system for non-small cell lung cancer after radiotherapy: An analysis from the TCP modelling perspective

Table B.1: Comparison of the TCP model performance according to the T descriptors of the 7th and 8th TNM staging scheme.

Radiotherapy modality	Fractionation schedule	7th TNM		8th TNM	
		R^2	RMSE	R^2	RMSE
3D-CRT	2 Gy in 25 fractions	0.93	2.07	0.94	0.93
	2 Gy in 30 fractions	0.95	1.68	0.95	0.94
	2 Gy in 37 fractions	0.89	2.47	0.93	1.91
CHART	1.5 Gy in 36 fractions	0.90	2.82	0.91	2.53
	1.2 Gy in 58 fractions	0.94	2.27	0.95	1.94
	1.8 Gy in 44 fractions	0.95	1.84	0.96	1.53
SABR	10 Gy in 4 fractions	0.92	3.01	0.94	2.65
	15 Gy in 3 fractions	0.95	2.29	0.95	2.19
	20 Gy in 3 fractions	0.97	0.91	0.97	0.68

Table B.2: Statistical assessment based on the unpaired t-test for 7th TNM (3D-CRT, 2 Gy in 30 fractions).

T-descriptor	TCP outcomes	Comparison	t-value	p-value
T1a	48.00 ±1.09	T1a vs. T1b	-5.9	P < 0.05
T1b	43.00 ±1.05	T1b vs. T2a	4.5	P < 0.05
T2a	38.88 ±1.12	T2a vs. T2b	-3.5	P < 0.05
T2b	35.53 ±1.17	T2b vs. T3	4.1	P < 0.05
T3	31.80 ±1.01	T3 vs. T4	-1.3	0.23
T4	30.01 ±2.0	n/a	n/a	n/a

Table B.3: Statistical assessment based on the unpaired t-test for 8th TNM (3D-CRT, 2 Gy in 30 fractions).

T-descriptor	TCP outcomes	Comparison	t-value	p-value
T1a	51.5 ±0.80	T1a vs. T1b	5.3	P < 0.05
T1b	478 ±0.85	T1b vs. T1c	-7.4	P < 0.05
T1c	42.9 ±0.82	T1c vs. T2a	2.9	P < 0.05
T2a	41.1 ±0.90	T2a vs. T2b	-5.3	P < 0.05
T2b	37.4 ±0.83	T2b vs. T3	3.39	P < 0.05
T3	35.0 ±0.98	T3 vs. T4	-4.8	P < 0.05
T4	31.0 ±1.30	n/a	n/a	n/a

Table B.4: Statistical assessment based on the unpaired t-test for 7th TNM (CHART, 1.5 Gy in 36 fractions).

T-descriptor	TCP outcomes	Comparison	t-value	p-value
T1a	33.3 ±0.73	T1a vs. T1b	13.0	P < 0.05
T1b	25.8 ±0.68	T1b vs. T2a	-8.9	P < 0.05
T2a	20.6 ±0.76	T2a vs. T2b	6.0	P < 0.05
T2b	16.8 ±0.81	T2b vs. T3	-6.3	P < 0.05
T3	13.0 ±0.65	T3 vs. T4	1.3	0.26
T4	11.7 ±1.6	n/a	n/a	n/a

Table B.5: Statistical assessment based on the unpaired t-test for 8th TNM (CHART, 1.5 Gy in 36 fractions).

T-descriptor	TCP outcomes	Comparison	t-value	p-value
T1a	37.5 ±0.65	T1a vs. T1b	8.8	P < 0.05
T1b	32.6 ±0.71	T1b vs. T1c	-12.1	P < 0.05
T1c	25.7 ±0.68	T1c vs. T2a	3.9	P < 0.05
T2a	23.4 ±0.77	T2a vs. T2b	-7.7	P < 0.05
T2b	18.8 ±0.69	T2b vs. T3	3.5	P < 0.05
T3	16.6 ±0.84	T3 vs. T4	-5.0	P < 0.05
T4	12.5 ±1.16	n/a	n/a	n/a

Table B.6: Statistical assessment based on the unpaired t-test for 7th TNM (SABR, 10 Gy in 4 fractions).

T-descriptor	TCP outcomes	Comparison	t-value	p-value
T1a	50.0 ±0.43	T1a vs. T1b	24.4	P < 0.05
T1b	41.6 ±0.41	T1b vs. T2a	-17.0	P < 0.05
T2a	35.6 ±0.45	T2a vs. T2b	12.1	P < 0.05
T2b	31.0 ±0.48	T2b vs. T3	-13.8	P < 0.05
T3	26.0 ±0.40	T3 vs. T4	3.34	P < 0.05
T4	24.1 ±0.90	n/a	n/a	n/a

Table B.7: Statistical assessment based on the unpaired t-test for 8th TNM (SABR, 10 Gy in 10 fractions).

T-descriptor	TCP outcomes	Comparison	t-value	p-value
T1a	54.0 ±0.79	T1a vs. T1b	7.45	P < 0.05
T1b	48.3 ±0.85	T1b vs. T1c	-8.7	P < 0.05
T1c	41.8 ±0.82	T1c vs. T2a	4.5	P < 0.05
T2a	38.7 ±0.90	T2a vs. T2b	-7.1	P < 0.05
T2b	33.7 ±0.81	T2b vs. T3	4.2	P < 0.05
T3	30.6 ±0.96	T3 vs. T4	-5.7	P < 0.05
T4	25.3 ±1.28	n/a	n/a	n/a